

**MOBILE PHASE MODIFIER EFFECTS AND
ELECTROCHEMICAL DETECTION
IN SUPERCRITICAL FLUID CHROMATOGRAPHY**

by

Marie Di Maso

A thesis submitted to the Faculty of Graduate Studies and Research in partial
fulfilment of the requirements for the degree of Doctor of Philosophy.

Department of Chemistry
McGill University
Montréal, Québec, Canada

July 1990

(c) Marie Di Maso 1990

To Mom and Dad

and

Robert,

**MOBILE PHASE MODIFIER EFFECTS AND
ELECTROCHEMICAL DETECTION
IN SUPERCRITICAL FLUID CHROMATOGRAPHY**

The role of mobile phase modifiers in supercritical fluid chromatography (SFC) and their effect on the separation process were investigated. A study of the influence of temperature and density on chromatographic behaviour in supercritical carbon dioxide and four modified carbon dioxide mobile phases demonstrates the importance of both density and mobile phase composition in controlling retention characteristics. The information gained from these studies was used to develop methodology for the separation and detection of a series of phenothiazinone compounds and an assay for L-615,919, 4-chloro-3H-phenothiazin-3-one, in plasma. The development of an analytical method for the analysis of sorbitan trioleate in pharmaceutical formulations demonstrates a unique application of SFC with flame ionization detection (FID) that is not possible by other chromatographic techniques

The feasibility of an electrochemical detection system for SFC has been demonstrated. The design and construction of an electrochemical detector with a platinum ultramicro working electrode and factors influencing its performance are described.

LES EFFETS D'UN MODIFICATEUR DE LA PHASE SUPERCRITIQUE ET DETECTION ELECTROCHIMIQUE EN CHROMATOGRAPHIE EN PHASE SUPERCRITIQUE

Le rôle du modificateur de la phase supercritique dans la chromatographie en phase supercritique (CPS) et ses effets sur le processus de la séparation chromatographique ont été investigés. Une étude de l'influence de la température et de la densité sur le comportement chromatographique démontre l'importance de la densité et de la composition de la phase supercritique pour le contrôle de la rétention. L'information obtenu de cettés études a été utilisé pour le développement d'une méthodologie pour la séparation et la détection d'une serie de composé de phénothiazinone et une méthode analytique pour L615,919, 4-chloro-3H-phénothiazin-3-one, dans plasma. Le développement d'une méthode pour l'analyse de sorbitan trioléate dans les formulations pharmaceutiques démontre une application unique de la CPS pour la détection par ionisation de flamme qui n'est pas possible avec les autres techniques chromatographiques.

La possibilité d'utilisé la détection électrochimique pour la chromatographie en phase supercritique a été démontrée. La conception et la construction d'un détecteur électrochimique qui utilise une micro-électrode de platine et les facteurs qui influencent sa performance sont décrits.

Acknowledgements

I would like to express my gratitude to Professor William C. Purdy for his guidance and encouragement in pursuing my research interests. His support in the joint research with Merck Frosst Centre for Therapeutic Research is most appreciated.

I would like to thank Dr. Meredith L. Cotton for the unique opportunity to pursue my research goals in the department of pharmaceutical research and development at Merck Frosst.

I am most grateful for the assistance and support of many people at both the chemistry department at McGill University and Merck Frosst Centre for Therapeutic Research:

Pierre Lamarche, for his expertise in developing a technique for modifying supercritical fluids and many helpful discussions;

Dr. Elizabeth Kwong, for her assistance in planning and executing the plasma studies;

Dr. C.K. Lau and Dr. Yves Girard, for providing the phenothiazinone compounds;

George Kopp for preparing the microelectrodes and Fred Kluck for constructing a support for the electrochemical detector;

And the pharmaceutical research and development group at Merck Frosst.

The support, countless discussions and friendship of Alexis Carpenter and Jeff McCarthy are very much appreciated.

I most indebted to Dr. Sam A. McClintock, foremost, for co-directing this research work and for having created a most unique opportunity to carry out this research. Most of all, I would like to thank Sam for his guidance, many helpful discussions and suggestions, encouragement and patience throughout the course of this research and beyond.

The unselfish support and understanding throughout the pursuit of my educational goals from my parents, Anna and Luigi; the eternal patience and encouragement from my husband, Robert; and support from my brother, Peter, have made this all possible.

Finally, I would like to thank the department of chemistry at McGill University for demonstrator assistantships, Natural Science and Engineering Research Council of Canada and Merck Frosst Centre for Therapeutic Research for financial support throughout the course of this work.

Table of Contents

Acknowledgements	- i -
Table of Contents	- ii -
List of Figures	- vi -
List of Tables	- xiii -

Chapter 1

Supercritical Mobile Phases in Chromatographic Separations	- 1 -
1.1 Introduction	- 1 -
1.2 Dense gas chromatography	- 2 -
1.3 Recent developments in supercritical fluid chromatography ..	- 7 -
1.4 Retention processes in binary mobile phases and electrochemical detection in supercritical fluid chromatography.	- 13 -
1.5 References	- 16 -

Chapter 2

Instrumental Aspects of Supercritical Fluid Chromatography and Experimental Procedures	- 18 -
2.1 Instrumental considerations	- 18 -
2.1.1 Solvent Delivery	- 18 -
2.1.2 Sample Introduction	- 18 -
2.1.3 Column technology	- 20 -
2.1.4 Restrictors	- 21 -
2.1.5 Mobile Phases	- 23 -
2.1.6 Programming Methods	- 24 -
2.1.7 Mobile phase modifiers	- 24 -
2.1.8 Detection Strategies	- 25 -
2.2 Experimental procedures	- 25 -
2.2.1 Instrumental	- 25 -
2.2.2 The role of modifiers in chromatographic separations.	- 26 -
2.2.2.1 Chromatographic system	- 26 -

2.2.2.2	Chemicals	- 26 -
2.2.2.3	Technique to modify supercritical mobile phases	- 27 -
2.2.2.4	Isothermal studies	- 27 -
2.2.2.5	Isodense studies	- 27 -
2.2.3	Analysis of phenothiazinones in plasma by packed column SFC.	- 29 -
2.2.3.1	Chromatographic system	- 29 -
2.2.3.2	Chemicals	- 29 -
2.2.3.3	Calibration curve	- 29 -
2.2.3.4	Preparation of dosing solution	- 30 -
2.2.3.5	Dosing regime	- 30 -
2.2.3.6	Plasma samples	- 30 -
2.2.3.7	Cyclic voltammetry of phenothiazinones	- 30 -
2.2.4	An electrochemical detection system for SFC	- 31 -
2.2.4.1	Chemicals	- 31 -
2.2.4.2	Electrochemical Cell	- 31 -
2.2.5	Determination of sorbitan trioleate in metered-dose inhalers by SFC.	- 33 -
2.2.5.1	Chromatographic system	- 33 -
2.2.5.2	Sample preparation	- 33 -
2.3	References	- 34 -

Chapter 3

	The Role of Modifiers in Chromatographic Separations	- 35 -
3.1	Introduction	- 35 -
3.2	Experimental	- 37 -
3.3	Results and Discussion	- 37 -
3.3.1	Chromatographic parameters	- 37 -
3.3.2	Isothermal and isodense studies	- 39 -
3.3.2.1	Supercritical carbon dioxide mobile phase	- 39 -
3.3.2.2	Critical parameters in binary and tertiary mobile phases	- 42 -
3.3.2.3	Formic acid modified carbon dioxide	- 48 -
3.3.2.4	Dichloromethane/formic acid modified carbon dioxide	- 58 -
3.3.2.5	Acetonitrile modified carbon dioxide	- 58 -

3.3.3	Modifier effects.	- 60 -
3.3.3.1	Effects on retention times	- 60 -
3.3.3.2	Effects on enthalpy of transfer between mobile and stationary phases	- 72 -
3.4	Conclusion	- 82 -
3.5	References	- 83 -

Chapter 4

	Analysis of Phenothiazinones in Plasma by Packed Column SFC . .	- 84 -
4.1	Introduction	- 84 -
4.2	Experimental conditions	- 87 -
4.3	Results and Discussion	- 87 -
4.3.1	Retention behaviour in supercritical carbon dioxide.	- 87 -
4.3.2	Effect of modifiers on retention characteristics. .	- 90 -
4.3.3	Separation of phenothiazinone analogs.	- 93 -
4.3.4	Assay for L615,919 in plasma.	- 102 -
4.3.5	Electrochemical investigation	- 109 -
4.4	Conclusions	- 109 -
4.5	References	- 114 -

Chapter 5

	An Electrochemical Detection System for Supercritical Fluid Chromatography	- 115 -
5.1	Introduction	- 115 -
5.1.1	Diffusion characteristics	- 117 -
5.1.1.1	Diffusion to a spherical electrode.	- 120 -
5.1.1.2	Shape of voltammogram at a spherical electrode.	- 123 -
5.1.1.3	Diffusion to a disc electrode.	- 125 -
5.1.1.4	Shape of voltammogram at a disc electrode	- 128 -
5.1.2	Ohmic drop at ultramicroelectrodes.	- 129 -
5.1.3	Cell time constant.	- 131 -
5.1.4	Capacitive current at ultramicroelectrodes . . .	- 133 -
5.1.5	Small size advantage of ultramicroelectrodes . .	- 134 -
5.1.6	Steady state current response.	- 135 -

5.1.7	Ultramicroelectrodes in hydrodynamic systems.	- 136 -
5.1.8	Electrochemical measurements in supercritical fluids.	- 137 -
5.2	Experimental	- 137 -
5.3	Results and Discussion	- 138 -
5.3.1	High pressure conditions.	- 138 -
5.3.2	Flow rate dependency.	- 138 -
5.3.3	Design of electrochemical cell.	- 138 -
5.3.4	Characterization of electrochemical cell.	- 139 -
5.3.5	Hydrodynamic performance of cell.	- 141 -
5.4	Conclusion	- 149 -
5.5	References	- 150 -

Chapter 6

Determination of Sorbitan Trioleate in Metered-dose Inhalers by Supercritical Fluid Chromatography

6.1	Introduction	- 153 -
6.2	Experimental	- 157 -
6.3	Results and Discussion	- 157 -
6.3.1	Restrictor placement	- 157 -
6.3.2	Chromatographic separation	- 161 -
6.3.3	Concentration of SPAN 85 in each formulation	- 161 -
6.4	Conclusion	- 164 -
6.5	References	- 168 -

Contributions to Original Knowledge.	- 169 -
Appendix A.	- 170 -
Appendix B.	- 177 -

List of Figures

Chapter 1

- Figure 1.1 Phase diagram for carbon dioxide. - 2 -
- Figure 1.2 Pressure-density isotherms for carbon dioxide. Figure reproduced from reference 9. - 5 -

Chapter 2

- Figure 2.1 Schematic of supercritical fluid chromatograph. - 19 -
- Figure 2.2 Restrictor models for SFC. See text for description. - 22 -
- Figure 2.3 Apparatus for the addition of organic solvents to supercritical fluids. - 28 -
- Figure 2.4 High pressure electrochemical cell. - 32 -

Chapter 3

- Figure 3.1 Peak width (a) and capacity ratio (b) as a function of temperature at constant density (0.7g/ml). Mobile phase: supercritical carbon dioxide. - 40 -
- Figure 3.2 $\ln(k')$ (a) and efficiency (b) as a function of temperature at a constant of 0.7 g/ml. Mobile phase: supercritical carbon dioxide. - 41 -
- Figure 3.3 Selectivity (a) and resolution (b) as a function of temperature at a constant density of 0.7 g/ml. Mobile phase: supercritical carbon dioxide. - 43 -
- Figure 3.4 Peak width (a) and capacity ratio (b) as a function of density at constant temperature (60°C). Mobile phase: supercritical carbon dioxide. - 44 -

Figure 3.5	Selectivity (a) and resolution (b) as a function of density at constant temperature (60°C). Mobile phase: supercritical carbon dioxide.	- 45 -
Figure 3.6	Chromatograms of model compounds at constant temperature (70°C) for various densities. Supercritical carbon dioxide mobile phase.	- 46 -
Figure 3.7	Peak widths (a) and capacity ratios (b) as a function of temperature at constant density (0.7g/ml). Mobile phase: formic acid (0.25 mole%) in carbon dioxide.	- 50 -
Figure 3.8	Selectivity (a) and Resolution (b) plotted against temperature at constant density (0.7 g/ml). Mobile phase: formic acid (0.25 mole%) in carbon dioxide.	- 51 -
Figure 3.9	Peak widths (a) and capacity ratios (b) plotted against density at constant temperature (60°C). Mobile phase: formic acid (0.25 mole%) in carbon dioxide.	- 52 -
Figure 3.10	$\ln(k')$ (a) and efficiency (b) as a function of density at constant temperature (60°C).	- 53 -
Figure 3.11	Selectivity (a) and resolution (b) as a function of density at 60°C.	- 54 -
Figure 3.12	Capacity ratio (a) and efficiency (b) as a function of temperature at constant density (0.7 g/ml). Mobile phase: formic acid (1.26 mole%) in carbon dioxide.	- 55 -
Figure 3.13	Selectivity (a) and resolution (b) as a function of temperature at constant density (0.7 g/ml). Mobile phase: formic acid (1.26 mole%) in carbon dioxide.	- 56 -
Figure 3.14	Peak widths (a) and capacity ratios (b) as a function of density at constant temperature (60°C). Mobile phase: formic acid (1.26 mole%) in carbon dioxide.	- 57 -
Figure 3.15	Selectivity (a) and resolution (b) as a function of density at constant temperature (60°C). Mobile phase: formic acid (1.26 mole%) in carbon dioxide.	- 59 -

Figure 3.16	k' as a function of density at constant temperature (60°C) and k' as a function of temperature at constant density (0.7g/ml) Mobile phase: 0.87 mole% dichloromethane/0.16 mole% formic acid/carbon dioxide. - 61 -
Figure 3.17	Selectivity (a) and resolution (b) as a function of density at constant temperature (60°C). Mobile phase : 0.87 mole % dichloromethane/0.16 mole% formic acid/carbon dioxide. - 62 -
Figure 3.18	Peak widths (a) and capacity ratios (b) plotted against temperature at constant density (0.7 g/ml). Mobile phase: 0.8 mole% acetonitrile in carbon dioxide. - 63 -
Figure 3.19	Selectivity (a) and resolution (b) as a function of temperature at constant density (0.7 g/ml). Mobile phase 0.8 mole% acetonitrile in carbon dioxide. - 64 -
Figure 3.20	Peak widths (a) and capacity ratios (b) as a function of density at 60°C. Mobile phase: 0.8 mole% acetonitrile in carbon dioxide. - 65 -
Figure 3.21	Selectivity (a) and resolution (b) as a function of density at constant temperature (60°C). Mobile phase: 0.8 mole% acetonitrile in carbon dioxide. - 66 -
Figure 3.22	Plot of k' versus temperature at constant density (0.7 g/ml) (a) and versus density at constant temperature (60°C) (b) for anthraquinone in simple carbon dioxide and three modified CO ₂ phases. - 68 -
Figure 3.23	Plot of k' versus temperature at constant density (0.7 g/ml) (a) and versus density at constant temperature (60°C) (b) for anthracene in simple carbon dioxide and three modified CO ₂ phases. - 69 -
Figure 3.24	Plot of k' versus temperature at constant density (0.7 g/ml) (a) and versus density at constant temperature (60°C) (b) for pyrene in simple carbon dioxide and three modified CO ₂ phases. - 70 -
Figure 3.25	Chromatograms of model compounds in three modified and simple carbon dioxide mobile phases at constant temperature (60°C) and equivalent densities (0.7 g/ml). - 71 -
Figure 3.26	van't Hoff plot for anthraquinone in supercritical carbon dioxide. - 73 -
Figure 3.27	van't Hoff plot for anthraquinone in (a) 0.25 mole% and (b) 1.26 mole% formic acid in carbon dioxide. - 74 -

Figure 3.28	van't Hoff plot for anthraquinone in (a) 0.87 mole% CH_2Cl_2 /0.16 mole% $\text{CHO}_2\text{H}/\text{CO}_2$ and (b) 0.8 mole% acetonitrile in carbon dioxide.	- 75 -
Figure 3.29	Enthalpy as a function of density for anthraquinone for each mobile phase investigated.	- 77 -
Figure 3.30	Enthalpy as a function of density for anthracene for each mobile phase investigated.	- 79 -
Figure 3.31	Enthalpy as a function of density for pyrene for each mobile phase investigated.	- 80 -
Figure 3.32	Enthalpy as a function of mobile phase composition at a density of 0.7 g/ml.	- 81 -
Chapter 4		
Figure 4.1	Cyclo-oxygenase and 5-lipoxygenase pathways.	- 85 -
Figure 4.2	Structure of phenothiazinone compounds.	- 89 -
Figure 4.3	Chromatograms of phenothiazinone analogs at 80°C and 4500 psi in supercritical carbon dioxide.	- 91 -
Figure 4.4	Chromatograms of phenothiazinone analogs at 80°C and 4500 psi in supercritical carbon dioxide.	- 92 -
Figure 4.5	Capacity ratios (a) and peak widths (b) as a function of temperature at a density of 0.7 g/ml. Mobile phase: 0.25 mole% formic acid.	- 94 -
Figure 4.6	Capacity ratios (a) and peak widths (b) as a function of temperature at a density of 0.9 g/ml. Mobile phase: 0.25 mole% formic acid.	- 95 -
Figure 4.7	Comparison of three phenothiazinone analogs in (A) 0.25 mole% formic acid and (B) 0.87 mole% dichloromethane/0.16 mole% formic acid in carbon dioxide at 80°C and 0.8 g/ml.	- 97 -
Figure 4.8	Capacity ratios (a) and peak widths (b) as a function acetonitrile concentration in mobile phase. Temperature: 40°C.	- 98 -

Figure 4.9	Resolution as a function of percent modifier. Temperature: 40°C.	- 99 -
Figure 4.10	Chromatograms of phenothiazinone mixture at 40°C in (a) 0.8 mole% acetonitrile and (b) 1.6 mole% acetonitrile in carbon dioxide. 1. L615,919; 2. L649,991; 3. L649,927; 4. L651,392.	- 100 -
Figure 4.11	Capacity ratios (a) and Peak widths (b) as function of modifier (acetonitrile) concentration at 80°C.	- 101 -
Figure 4.12	Comparison of chromatograms for the phenothiazinone mixture at equivalent density programs and same temperature (40°C) in (a) 0.8 mole% acetonitrile/carbon dioxide and (b) simple carbon dioxide. -	103 -
Figure 4.13	Chromatogram of drug (L615,919) <u>2</u> and internal standard (L649,927) <u>1</u> (a) standard solution and (b) rat plasma.	- 104 -
Figure 4.14	Calibration curve for study 1 for an average of 3 injections. (a) full concentration range and (b) low concentration range.	- 105 -
Figure 4.15	Plasma profile for one rat in study 1.	- 106 -
Figure 4.16	Calibration curve for study 2	- 107 -
Figure 4.17	Plasma profile study 2	- 108 -
Figure 4.18	Plasma profile for three rodents in a simultaneous study.	- 110 -
Figure 4.19	Cyclic voltammogram of (a) L615,919 and (b) L649,927 in CH ₃ CN/0.1M TBA TFB. Pt-wire auxiliary and Ag/AgCl reference electrodes and platinum ultramicroelectrode as the working electrode.	- 111 -
Figure 4.20	Cyclic voltammogram of (a) L653,849 and (b) L651,392 in CH ₃ CN/0.1M TBA TFB. Pt-wire auxiliary and Ag/AgCl reference electrodes and platinum ultramicroelectrode as the working electrode.	- 112 -
 Chapter 5		
Figure 5.1	Semi-infinite linear diffusion at a macroelectrode.	- 118 -

Figure 5.2	Peak-shaped voltammogram at a macroelectrode.	- 118 -
Figure 5.3	Radial diffusion at a microelectrode.	- 119 -
Figure 5.4	Sigmoidal-shaped voltammogram at a microelectrode.	- 119 -
Figure 5.5	High pressure electrochemical cell.	- 140 -
Figure 5.6	Platinum Microelectrode.	- 142 -
Figure 5.7	Cyclic voltammogram of ferrocene (5mM) in CH ₃ CN/0.1M TBA TFB in three-electrode cell. Reference electrode: Ag/AgCl. Auxiliary electrode: platinum wire.	- 142 -
Figure 5.8	Cyclic voltammogram of ferrocene (5mM) in CH ₃ CN/0.1M TBA TFB in electrochemical cell. Stainless steel quasi-reference electrode.	- 143 -
Figure 5.9	Cyclic voltammogram of ferrocene (5 mM) in CH ₃ CN/0.1M TBA TFB in electrochemical cell pressurized to 2000 psi with CO ₂ . Stainless steel quasi-reference electrode.	- 143 -
Figure 5.10	Schematic of complete SFC/ECD system.	- 144 -
Figure 5.11	Response of electrochemical detector for the solvent (acetonitrile) injected on column. Applied potential set at 0.8 volts. Isobaric at 2200 psi and 40°C.	- 146 -
Figure 5.12	Response of electrochemical detector for 10 µg of ferrocene injected on column. Applied potential set at 0.8 volts. Isobaric at 2200 psi and 40°C.	- 146 -
Figure 5.13	Hydrodynamic voltammogram for ferrocene, average of three injections.	- 147 -
 Chapter 6		
Figure 6.1	Schematic of a metered-dose inhaler.	- 154 -
Figure 6.2	Structure of sorbitan trioleate.	- 156 -
Figure 6.3	Effect of SPAN 85 concentration on aerosol plumes.	- 157 -

Figure 6.4	Schematic of flame-ionization detector.	- 159 -
Figure 6.5	Chromatogram of sorbitan trioleate standard (3.2 μg). Column: 2.1x100 mm ODS (5 μm). Mobile phase: supercritical CO_2 . Isobaric at 2400 psi, 40°C.	- 162 -
Figure 6.6	Calibration curve for sorbitan trioleate with pyrene as the internal standard.	- 163 -
Figure 6.7	Chromatogram of Medihaler ISO® sample (0.95 μg). See Figure 6.6 for chromatographic conditions.	- 165 -
Figure 6.8	Chromatogram of Medihaler EPI® sample (1.5 μg). See Figure 6.6 for chromatographic conditions.	- 165 -
Figure 6.9	Chromatogram of Duo-Medihaler® sample (3.1 μg). See Figure 6.6 for chromatographic conditions.	- 166 -
Figure 6.10	Chromatogram of Alupent® sample (2.0 μg). See Figure 6.6 for chromatographic conditions.	- 166 -
Figure 6.11	Chromatogram of in-house formulation (0.40 μg). See Figure 6.6 for chromatographic conditions.	- 167 -

List of Tables

Chapter 2

Table 2.1 Physical Properties of Certain Supercritical Fluids - 23 -

Chapter 3

Table 3.1 Linear regression of van't Hoff plots - 76 -

Chapter 5

Table 5.1 Microelectrode Geometries - 116 -

Chapter 6

Table 6.1 Effect of Restrictor Position - 160 -

Table 6.2 SPAN 85 in Drug Products. - 164 -

Chapter 1

Supercritical Mobile Phases in Chromatographic Separations

1.1 Introduction

Supercritical fluid chromatography (SFC) has recently received increased attention as a complimentary technique to both high performance liquid chromatography (HPLC) and gas chromatography (GC). Supercritical fluid chromatography is essentially modified gas chromatography, where the mobile phase is a highly compressed gas operated at or above its critical temperature and pressure, where it exists as a supercritical fluid. The intrinsic properties of supercritical fluids offer unique chromatographic advantages for the separation and detection of a wide range of compounds. Above the critical temperature, the vapour and liquid have the same density and the fluid cannot be liquified by increasing the pressure. A supercritical fluid is obtained from a liquid by increasing the temperature at constant pressure (greater than the critical pressure) or from a gas by increasing the pressure at constant temperature (greater than the critical temperature). The phase diagram for carbon dioxide (Figure 1.1) depicts the critical region as a shaded area with dashed lines as the boundary since no phase change occurs. In the supercritical state the physical properties of the fluid are intermediate between those of liquids and gases at ambient conditions. Specifically, the density of a supercritical fluid approaches that of a liquid, while its viscosity is comparable to that of a gas. The density of a supercritical fluid, which can be easily controlled by a change in pressure, influences the solubility and chromatographic retention of solutes. The low viscosity of a supercritical fluid leads to lower pressure drops across a chromatographic column for a

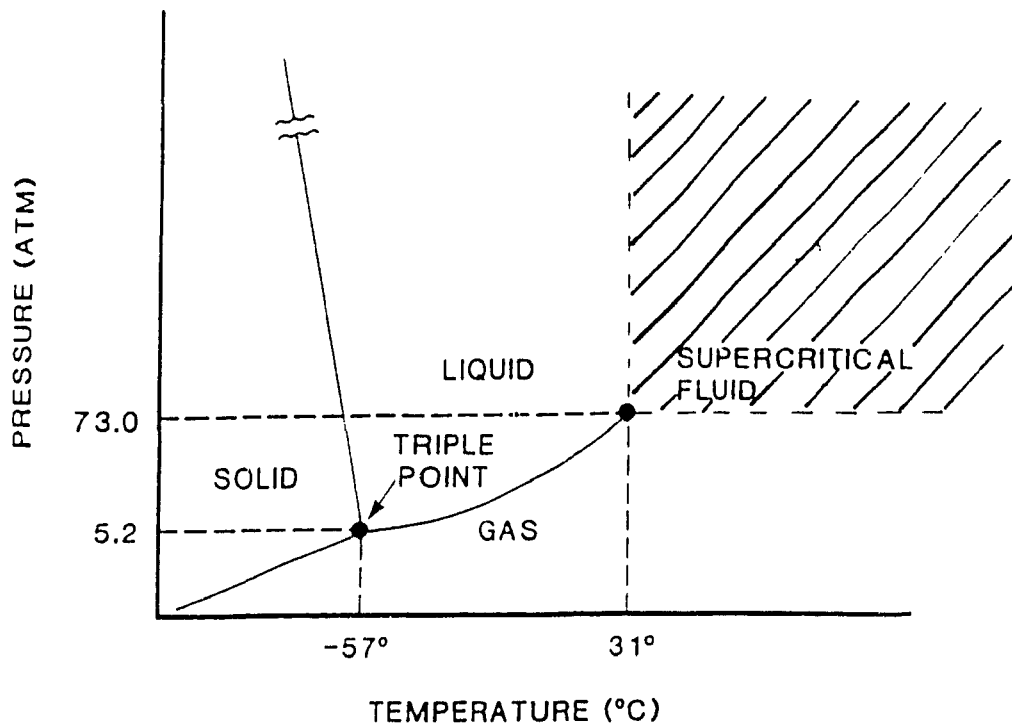


Figure 1.1 Phase diagram for carbon dioxide.

given flow rate. Low pressure drops result in more theoretical plates per metre and improved efficiency. The diffusivity in a supercritical fluid is between that of a liquid and a gas. Higher solute diffusion coefficients in supercritical fluids, as compared to liquids, produce higher efficiencies for SFC systems than comparable HPLC system [1]. Supercritical fluids can dissolve a variety of solutes, including high molecular weight and non-volatile compounds and have unique chemical and physical properties which make them useful as chromatographic mobile phases.

1.2 Dense gas chromatography

Supercritical fluid technology can be traced back to 1822 when the critical phenomenon was first observed [2]. Baron Cagnard de la Tour described the disappearance of the vapour-liquid interface when pressurizing certain liquids and recorded values for the critical temperature and pressure for these solvents. Hannay and Hogarth [3] studied the solvent properties of carbonic acid in its critical state.

They reasoned that in going from the liquid state to the critical state, a solution of solvent and nonvolatile solid would precipitate the solid, since the ability to dissolve solids is a property of liquids, not gases. Experiments with various solvents and solids indicated that solids were soluble in gases under high pressure and there is no discontinuity in passing from the liquid to the gaseous (critical) state. Measurements of critical parameters of several fluids compared well with those recorded by Baron Cagnaird de la Tour. Further investigations showed that the critical point of the fluid is raised by the presence of a small quantity of dissolved salt [4]. The solvating ability of supercritical fluids is due to 'molecular closeness' achieved by the high pressure as opposed to 'internal attraction' as in liquids [3].

In 1958, Lovelock [5] proposed the use of solvents in their critical state as the chromatographic mobile phases in order to extend the scope of gas chromatography to include ionic compounds which are otherwise nonvolatile. However, it was Klesper, Corwin and Turner [6] who first put "dense gas" chromatography to practice in 1962. Halogenated methanes (freons) were used as mobile phases for the elution of nickel porphyrin isomers. The authors suggested that the increased mobility observed with increasing mobile phase pressure should permit the analysis of high molecular weight compounds at lower temperatures.

Giddings [7,8] developed a theoretical basis for the effect of pressure increase in gas chromatography. At very high pressures, gas and liquid chromatography converge and the intermolecular forces become large enough to induce migration of nonvolatile analytes. There is no theoretical limit to the size of analytes that will migrate since, above the critical point, compression of the fluid can yield any desired density. The author also mathematically described the phenomena of differential equilibrium shifts at high pressures. With increasing pressure, the intermolecular distances decrease to reduce the volume, while the molecular volumes tend to increase. This can result in equilibrium shifts depending upon the nature of the solute mobile phase interactions and upon changes in the stationary phase structure induced by the increased pressure. Since the solvent power of the mobile phase is a function of pressure it can be quickly and precisely varied throughout a

chromatographic run by mechanical means. The relatively low viscosity and high diffusivity of dense gases theoretically leads to enhanced speeds of separation. Giddings also suggested that the solvent power of a dense gas depends on both its 'physical effect', as described by its pressure and temperature, and its 'chemical effect' described by its polarity, acid-base properties and hydrogen-bonding abilities. In a subsequent paper [9] the authors developed mathematical equations using the Hildebrand solubility parameter to describe the magnitude of the solubility of solutes in compressed gases from gas to liquid densities.

$$\delta = 1.25 P_c^{1/2} \left(\frac{\rho_R}{\rho_{Rl}} \right) \quad (1.1)$$

δ	=	Hildebrand solubility parameter
P_c	=	critical pressure
ρ_R	=	reduced critical density
ρ_{Rl}	=	reduced density of corresponding liquid

The physical effect is given by the (ρ_R/ρ_{Rl}) while the chemical effect is described by $1.25 P_c^{1/2}$. To a first approximation, an elutropic series may be prepared by including only the chemical effect term. As solute molecules become larger and more complex, the magnitude of δ must increase as the volatility of the solute decreases.

Sie et al. [10,11] described a theoretical basis for the significance of intermolecular forces between mobile phase molecules and solute molecules. Fluid-liquid (FLC) [12] and fluid-solid (FSC) [13] chromatography were compared to gas-liquid (GLC), liquid-liquid (LLC), and liquid-solid (LSC) chromatography. At the high pressures, solute volatility increases with decreased temperature due to the increased intermolecular interactions at the greater density accompanying the lower temperatures. The enhancement of volatility is more pronounced for heavier substances, consequently the separation of members of a series is more difficult at higher pressures. Selectivity between low and high molecular weight compounds dominate at low pressures and elution order is as in GLC. At higher pressures,

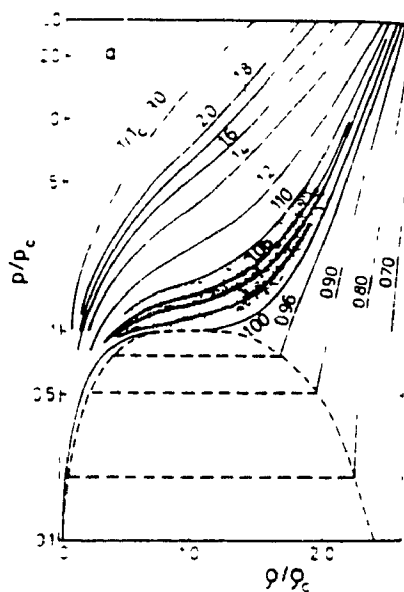


Figure 1.2 Pressure-density isotherms for carbon dioxide. Figure reproduced from reference 9.

selectivity according to type predominates and elution is as would be for LLC. Temperature change near the critical point has the greatest effect, where a small change in temperature results in a large change in fluid density [Figure 1.2]. In FLC the phase of the same or different polarity can be combined unlike in GLC where the stationary phases are limited by their thermal stability and in LLC where the two phases must be immiscible. With a polar stationary liquid on a non-polar mobile fluid the effects of volatility and polarity tend to cancel each other and conditions are favourable for the separation of different compound types. When both the stationary liquid and the mobile phase are polar, the effects of solute volatility and polarity reinforce each other such that a series of analogs can be separated. With a supercritical mobile phase, as compared to a gaseous mobile phase, there is an increased solubility of the analyte molecules in the mobile phase and retention on the stationary phase is reduced because of the competition between analyte molecules and mobile phase molecules for active sites on the silica support.

Jentoft and Gouw [14] introduced programming techniques for the separation of materials with a large range of molecular weights. An increasing pressure program

results in lower k' values of solutes, making it ideally suited for the analysis of mixtures with wide molecular weight ranges. Temperature programming is used in a limited number of applications in SFC since capacity ratio (k') values of a solute can increase, decrease or remain constant with increasing temperature.

Use of supercritical mobile phases with low critical temperatures, such as carbon dioxide, have many advantages. Jentoft and Gouw [15] proposed that the lower operating temperatures permit (i) the analysis of thermally labile compounds, (ii) the use of a stationary phase of limited thermal stability, and (iii) the possibility of simple solvent elimination from collected samples. These authors also presented the first paper on the separation of polyaromatic hydrocarbons (PAH) from automobile exhaust by SFC with a supercritical carbon dioxide mobile phase [16]. Using a polymer chemically bonded to porous microbeads as the stationary phase in a packed column, the PAH's were separated according to ring type. An octadecyl phase bonded to porous silica particles separated the PAH's according to molecular weight.

Novotny et al. [17] studied the effects of temperature and pressure in SFC on model compounds in the vicinity of the critical point. A gradual decrease in k' with increasing pressure was obtained at various temperatures. Plots of k' as a function of temperature show a maximum, the value of which is dependent on the mobile phase. A change in stationary phase results in a change in the absolute values of the k' but the shape of the k' versus temperature curves remain the same. k' values of solutes can also be decreased by the addition of a second component (modifier) to the mobile phase. The authors speculated that both pressure and inverse temperature programming might be useful in SFC.

Klesper and Hartmann [18] reported a systematic study of the influence of operating temperature, rate of linear pressure programming and mobile phase composition on the separation of polystyrene oligomers. Better resolution was observed for slower pressure programs, higher isothermal operating temperatures and the addition of a methanol modifier to the supercritical n-pentane mobile phase. The authors were the first to suggest that the methanol might be covering up active sites on the silica support in the Porasil A packed column.

1.3 Recent developments in supercritical fluid chromatography

Although the future of SFC seemed promising, the rapid development of HPLC during the same period overshadowed that of SFC. The lack of commercial SFC instrumentation and practical problems encountered with using supercritical fluids also contributed to the slow growth of the technique. Renewed interest in supercritical fluid chromatography occurred in the early 1980's. This was in part a result of: (i) the introduction of capillary SFC in 1981; (ii) commercial availability of packed-column instrumentation in 1982 and, (iii) the introduction of capillary instrumentation in 1985.

Novotny et al. [19] examined the potential advantages of capillary SFC over both capillary GC and capillary LC. Capillary GC is restricted by the volatility and thermal stability of the solutes. The lower diffusion coefficients in liquids as compared to gases require very small diameter columns (10-30 microns) in capillary LC, placing strict requirements on the instrumentation. Solute diffusion coefficients are at least an order of magnitude greater in supercritical fluids than in liquids, therefore larger diameter columns (50-100 microns) can be used. Much lower pressure drops occur over capillary columns as compared to packed columns in SFC, thus reducing negative density gradients along the length of the column. The authors later described the instrumentation needed for open-tubular SFC with particular emphasis on sample introduction and detection systems [20]. Methods and principles of SFC were later published by Peadar and Lee [21], where the importance of mobile phase density on solute retention as opposed to pressure was discussed. An equation was presented predicting that the $\log k'$ versus \log of fluid density for a solute should be linear.

During the same period an instrument company introduced a commercial packed-column SFC system [22] and Gere et al. [23] discussed the merits of small particle diameter columns packed with 3, 5 and 10 micron particles, coated with an octadecylsilane layer. Although some workers believed the small particles would have deleterious effects on the pressure drop along the column, pressure differences between the column inlet and outlet of 25% caused no observable changes in

chromatographic performance. Essentially the theoretical plate height improved with smaller diameter particle packings. Resolution per unit time was 5-10 times better in SFC than in HPLC with the same columns. Gere [24] first reported on the need of modifiers in supercritical mobile phases to elute some polar solutes. Log k' of various phthalates were measured as a function of weight percent of various modifiers (hexane, THF, iso-propanol and methanol) in supercritical carbon dioxide. The effect of each modifier was found to depend on its ability to form hydrogen bonds. The rapid development of SFC from 1981 to the present has produced a growing body of work on many aspects of the technique both from a theoretical standpoint and instrumental point of view. Early instrumentation for packed column SFC provided only one mode of operation, ignoring the advantages gained by pressure or density programming. These instruments were also unable to interface with ionization detectors. Consequently for the first half of 1980's more work was carried out with capillary SFC.

The technique of capillary SFC is highly suited to the analysis of complex mixtures, since the increased permeability of capillary columns over packed columns leads to high separation efficiencies. Density programming in SFC is most effective at pressures near the critical pressure since small changes in pressure result in large density changes. Large pressure drops along the length of the column which may result in a rapid loss of resolution during the density programming are not encountered with capillary columns [25]. Many different programming techniques have been used including linear pressure, linear density and asymptotic density [26]. Since most solvent delivery systems provide for pressure control, density programming is achieved by the use of algorithms to convert density into pressure.

Although the development of instrumentation was important, growth of SFC as an analytical technique was due mainly to a better understanding of retention processes through the development of thermodynamic models. Solute retention as a function of pressure or density at constant temperature was first described by van Wassen and Schneider [27] and is given by,

$$\left(\frac{\partial \ln k'}{\partial P}\right)_T = \frac{[v_1^{m,\infty} - v_1^{s,\infty}]}{RT} - K \quad (1.2)$$

where

k'	=	capacity ratio
R	=	gas constant
P	=	pressure
T	=	temperature
$v_1^{m,\infty}$	=	solute partial molar volume in the mobile phase at infinite dilution
$v_1^{s,\infty}$	=	solute partial molar volume in the stationary phase at infinite dilution
K	=	isothermal compressibility of fluid solution ($1/V[\partial V/\partial P]$)

The partial molar volume of the solute in the mobile phase at infinite dilution is a measure of the solvent-solute interactions and can be expressed as follows [28],

$$v_1^{m,\infty} = K_2 V_2 \left[\left(\frac{\partial P}{\partial n_1} \right)_{T, V, n_2} \right] \quad (1.3)$$

where

K_2	=	isothermal compressibility of the pure solvent
V_2	=	molar volume of pure solvent

Combining equations 1.2 and 1.3 yields an expression for the slope of solute retention as a function of pressure at constant temperature;

$$\left(\frac{\partial \ln k'}{\partial P}\right)_T = \frac{K_2 V_2 \left[\left(\frac{\partial P}{\partial n_1} \right)_{T, V, n_2} \right] - v_1^{s,\infty}}{RT} - K \quad (1.4)$$

The solute retention dependence on density at constant temperature is given by,

$$\left(\frac{\partial \ln k'}{\partial \rho}\right)_T = \left(\frac{\partial \ln k'}{\partial P}\right)_T \left(\frac{\partial P}{\partial \rho}\right)_T \quad (1.5)$$

where $\left(\frac{\partial P}{\partial \rho}\right)_T =$ the slope of pressure versus density as described by an equation of state

The Peng-Robinson equation of state [29], a relatively simple two parameter cubic equation, can be used to evaluate (i) the partial molar volume of solute in the mobile phase; (ii) the isothermal compressibility of the fluid solution and the pure solvent; and (iii) the pressure relationship on density at constant pressure. The Peng-Robinson equation of state has the following form,

$$P = \frac{RT}{V-b} - \frac{a(T)}{V(V+b) + b(V-b)} \quad (1.6)$$

where $V =$ molar volume (M/ ρ)
 $a, b =$ constants

The pressure is expressed as a function of the molar volume and two constants (a) which is a measure of the intermolecular attraction force, and (b) which is related to the size of the (spherical) molecules.

$$a = a(T_c) \times \alpha(T, \omega) = 0.45724 \frac{R^2 T_c^2}{P_c} \quad (1.7)$$

$$b = b(T_c) = 0.07780 \frac{RT_c}{P_c} \quad (1.8)$$

The term $\alpha(T_r, \omega)$ is a function of the reduced temperature and the acentric factor (ω); at the critical point it equals unity.

$$\alpha = [1 + \kappa (1 - T_r^{1/2})]^2 \quad (1.9)$$

κ is a constant characteristic of the solvent and is related to the acentric factor of the solvent, by the following equation,

$$\kappa = 0.37464 + 1.54226 \omega - 0.26992 \omega^2 \quad (1.10)$$

All the terms of equations 1.4 and 1.5, except for the partial molar volume of the solute in the stationary phase (which can be estimated), can be evaluated as a function of pressure or density at constant temperature.

If infinite dilution during retention in SFC is assumed, the solute distribution coefficient (K_D) can be related to the Gibbs free energy of solute transfer from the mobile phase to the stationary phase by [30],

$$\Delta G = -RT \ln K_D \quad (1.11)$$

The thermodynamic relationship between the solute distribution coefficient and the temperature is

$$\ln K_D = -\frac{\Delta H}{RT} + \frac{\Delta S}{R} \quad (1.12)$$

where ΔH = change in enthalpy of solute transfer
between the mobile and stationary phases
 ΔS = change in entropy of solute transfer
between the mobile and stationary phases

The solute distribution coefficient is related to the solute retention by the following,

$$K_D = \frac{C_s}{C_m} = k' \frac{V_m}{V_s} = k' \phi \quad (1.13)$$

where

C_s	=	solute concentration in stationary phase
C_m	=	solute concentration in mobile phase
V_m	=	volume of mobile phase
V_s	=	volume of stationary phase
ϕ	=	phase ratio

Substituting equation 1.13 into equation 1.12 gives an expression for the capacity ratio in terms of entropy and enthalpy,

$$\ln k' = -\frac{\Delta H}{RT} + \frac{\Delta S}{R} - \ln \phi \quad (1.14)$$

The slope of a plot of $\ln k'$ against the inverse of temperature at constant pressure is,

$$\left(\frac{\partial \ln k'}{\partial T^{-1}} \right)_P = -\frac{\Delta H}{R} \quad (1.15)$$

While the slope of $\ln k'$ versus T^{-1} at constant density is calculated as follows,

$$\left(\frac{\partial \ln k'}{\partial T^{-1}} \right)_\rho = \left(\frac{\partial \ln k'}{\partial P} \right)_T \left(\frac{\partial P}{\partial T^{-1}} \right)_\rho + \left(\frac{\partial \ln k'}{\partial T^{-1}} \right)_P \quad (1.16)$$

The effective enthalpy of solute transfer (ΔH_T) between the mobile phase and the stationary phase can be determined at constant density;

$$\left(\frac{\partial \ln k'}{\partial T^{-1}}\right)_\rho = \delta + \Delta H - \Delta H_T \quad (1.17)$$

where $\delta =$ correction term containing a thermal expansivity term and $(\partial \ln k' / \partial P)_T (\partial \ln k' / \partial T^{-1})_\rho$

In high pressure liquid chromatography, where pressure has a negligible effect on solvent density, and in gas chromatography, where the pressure is held constant, δ is zero.

The effective enthalpy of solute transfer in SFC is obtained by determining solute retention as a function of temperature at various densities. A plot of ΔH_T as a function of density for different stationary phases gives an indication of the solute stationary phase interactions. A linear dependence, where the greatest solvation occurs at higher density (less negative ΔH_T values), is indicative of a partition-like mechanism. An asymptotic curvature at higher densities is attributed to solvation or swelling of the bonded phase particularly for capillary columns.

The equations developed above by Yonker and Smith [31] provide a simple thermodynamic model permitting the study of the effects of macroscopic thermodynamic parameters and their role in retention. The thermodynamic studies of retention as a function of temperature at constant density provides a method to study SFC retention from gas-like to liquid-like densities, permitting comparison with GC and HPLC, respectively.

1.4 Retention processes in binary mobile phases and electrochemical detection in supercritical fluid chromatography.

The acceptance of SFC as an alternate analytical technique to GC and HPLC lies in understanding the effects of the many variables that can be controlled and the

development of applications that are unique to this technique. As indicated by the increasing number of publications and conference proceedings [32], supercritical fluid chromatography shows great potential as a separation technique. However, this potential will only be realized through the further development of fundamental theoretical approaches and the application of SFC to problems of analytical importance. This work has concentrated on two main aspects of SFC: (i) the study of retention processes with binary and tertiary mobile phases and (ii) the development of an electrochemical detection (ECD) system.

The solvating power of common supercritical mobile phases can be continuously varied and controlled by density programming. This approach has obvious limitations and appropriate solvent strengths which provide reasonable separations are not always available from a homogeneous mobile phase. The addition of small quantities of organic solvents to the supercritical fluid alters retention behaviour for many compounds. At the time this work was started, the exact role of modifiers in the chromatographic process was unknown and therefore the first experiments were designed to identify the role of modifiers and their effect on the separation process (Chapter 3). The information gained from these studies was used to develop methodology for the separation and detection of a series of phenothiazinone analogs and an assay method for one of the analogs in plasma (Chapter 4).

An important advantage of SFC lies in the analysis of compounds not amenable to either GC or HPLC. The liquid-like solvating abilities of supercritical fluids and the simple task of interfacing with GC-like detection systems makes it highly suited for the analysis of thermally labile, high molecular weight compounds. In chapter 6, the analysis of sorbitan trioleate, a high molecular weight surfactant, demonstrates a unique application of SFC that is not possible by other chromatographic techniques.

A second aspect of this work was to determine the feasibility of electrochemical detection for SFC. Electrochemical detection systems for HPLC have become a valuable tool for trace organic analysis, mainly due to their selectivity and high sensitivity. Electrochemical measurements in supercritical fluids have the

potential for improving these detection limits since diffusion coefficients are an order of magnitude greater than those found in liquids. A two-electrode amperometric detection system using a platinum ultramicroelectrode was designed and built and factors influencing its performance discussed in Chapter 5.

1.5 References

1. D.R. Gere, Hewlett-Packard Publication No. 43-5953-1695 (1983) 1.
2. Cagnaird de la Tour, Baron, *Ann. Chim. Phys.*, **21** (1822) 127.
3. J. B. Hannay and J. Hogarth, *Proc. R. Soc. London*, **30** (1880) 178.
4. J.P. Hannay, *Proc. R. Soc. London*, **30** (1880) 178.
5. J.E. Lovelock, Critical State Chromatography, notarized document, State of Connecticut, County of New Haven, Mary G. DeCosta (notary), October 23, 1958, witnessed by: S.R. Lipsky and R. Landowne.
6. E. Klesper, A.H. Corwin and D.A. Turner, *J. Org. Chem.*, **27** (1962) 700.
7. J.C. Giddings, *Sep. Sci.*, **1** (1966) 73.
8. J.C. Giddings, W.A. Manwaring and M.N. Myers, *Science*, **154** (1966) 146.
9. J.C. Giddings, M.N. Myers and J.W. King, *J. Chromatogr. Sci.*, **7** (1969) 276.
10. S.T. Sie, W. van Beersum and G.W.A. Rijnders, *Sep. Sci.*, **1** (1966) 459.
11. S.T. Sie and G.W.A. Rijnders, *Sep. Sci.*, **2** (1967) 699.
12. S.T. Sie and G.W.A. Rijnders, *Sep. Sci.*, **2** (1967) 729.
13. S.T. Sie and G.W.A. Rijnders, *Sep. Sci.*, **2** (1967) 755.
14. R.E. Jentoft and T.H. Gouw, *J. Chromatogr. Sci.*, **8** (1970) 138.
15. R.E. Jentoft and T.H. Gouw, *Anal. Chem.*, **44** (1972) 681.
16. R.E. Jentoft and T.H. Gouw, *Anal. Chem.*, **48** (1976) 2196.
17. M. Novotny, W. Bertsch and A. Zlatkis, *J. Chromatogr.*, **61** (1971) 17.
18. E. Klesper and W. Hartmann, *J. Polym. Sci. Polym. Let. Ed.*, **15** (1977) 707.
19. M. Novotny, S.R. Springston, P.A. Peaden, J.C. Fjeldsted and M.L. Lee, *Anal. Chem.*, **53** (1981) 407.
20. P.A. Peaden, J.C. Fjeldsted, M.L. Lee, S.R. Springston and M. Novotny, *Anal. Chem.*, **54** (1982) 736.

21. P.A. Peaden and M.L. Lee, *J. Liq. Chromatogr.*, **5** (1982) 179.
22. Chemical and Engineering News (March 22), (1982) 45.
23. D.R. Gere, R. Board and D. McManigill, *Anal. Chem.*, **54** (1982) 736.
24. D.R. Gere, *Science*, **222** (1983) 253.
25. P.A. Peaden and M.L. Lee, *J. Chromatogr.*, **259** (1983) 1.
26. J.C. Fjeldsted, W.P. Jackson, P.A. Peaden, and M.L. Lee, *J. Chromatogr. Sci.*, **21** (1983) 222.
27. U. van Wasen and G.M. Schneider, *Chromatographia*, **8** (1975) 274.
28. P.C. Wu and P. Ehrlich, *AIChE J*, **19** (1973) 533.
29. D-Y. Peng and D.B. Robinson, *Ind. Eng. Chem. Fundam.*, **15** (1976) 59.
30. M.A. McHugh and V.J. Krukonis, *Supercritical Fluid Extraction: Principles and Practice*, Butterworths, Boston (1986) Chapter 11.
31. C.R. Yonker and R.D. Smith, *Supercritical Fluid Extraction and Chromatography*, ACS Symposium Series, (1988) Chapter 9 , p162.
32. T.L. Chester and J.D. Pinkston, *Anal. Chem.*, **62** (1990) 394R.

Chapter 2

Instrumental Aspects of Supercritical Fluid Chromatography and Experimental Procedures

2.1 Instrumental considerations

2.1.1 Solvent Delivery

Instrumentation for SFC is essentially borrowed from both GC and microbore HPLC with slight modifications (Figure 2.1). Supercritical fluids require strict control of the pressure as opposed to the flow rate, therefore pulseless fluid delivery systems are essential. Syringe pumps are commonly used, some of which provide cooling of the pump head for delivery of liquid mobile phases. The pumping system must also allow for pressure or density programming. Pressure is typically programmed from 1800-6000 psi in either a linear or asymptotic mode. Density programming is usually achieved by relating the mobile phase temperature and pressure to the density by the use of computer algorithms.

2.1.2 Sample Introduction

Fixed volume injection valves originally designed for microbore HPLC make effective injectors for SFC. For packed columns injection volumes are between 0.1 and 1.0 μl ; capillary columns require injection volumes below 0.1 μl which is achieved by installing a splitter between the injector and the column. Slight changes in the column temperature can cause unwanted density gradients along the length of the column, therefore precise temperature control is achieved with conventional gas chromatograph ovens.

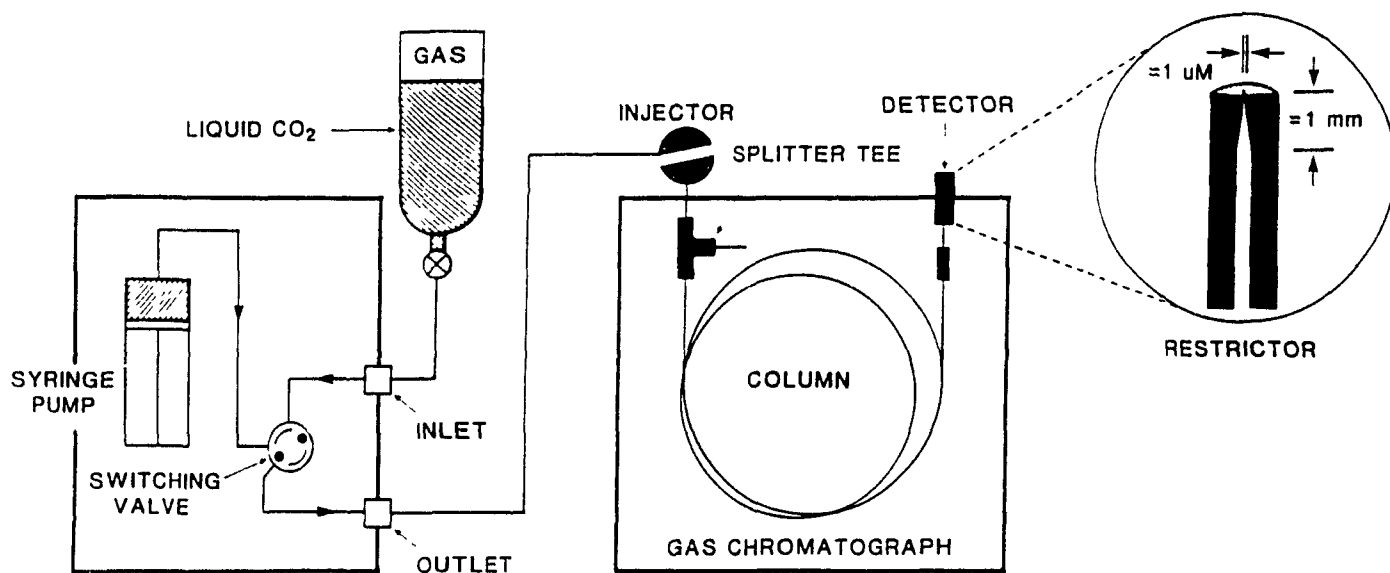


Figure 2.1 Schematic of supercritical fluid chromatograph.

2.1.3 Column technology

The small diameter capillary columns (<100 micron i.d.) necessary to obtain high efficiencies in reasonable analysis times for SFC place strict requirements on the preparation of the columns and on instrumentation. The solvating power of many supercritical fluids is sufficient to dissolve common stationary phases, therefore extensive crosslinking is necessary to stabilize the surface [1]. Modification of common stationary phase coating techniques have been reported in the literature [2,3,4].

The low sample capacity of capillary columns places stringent requirements on the sample introduction technique. For typical SFC capillary columns of 50 micron i.d., injection volumes less than 100 nl are necessary. This has been achieved with high pressure internal sample loop valve injectors, used in microbore HPLC, connected to a flow splitting device [5]. The split ratios are determined by both the detection device and the sample concentration. Both fused silica capillary columns and packed columns are used in SFC, the choice is dependent on the analytical problem. Open tubular columns are made of narrow fused silica tubing, in which a film of a stationary phase is coated on the inside wall. The stationary phase is typically a polymeric film which is immobilized by extensive cross-linking. The diameter of the column affects the mobile phase flow through the column, the sample loadability, the permissible injections and detection volumes and the pressure drop across the column [6]. Capillary columns for SFC are of smaller internal diameter, typically 10-50 μm , than those used for GC due to the lower diffusion coefficients in supercritical fluids. Greater efficiencies can be obtained with capillary columns since they can be made very long producing a large number of theoretical plates. Low mobile phase flow rates associated with capillary columns allow easy interfacing with both GC-type and microbore HPLC-type detectors.

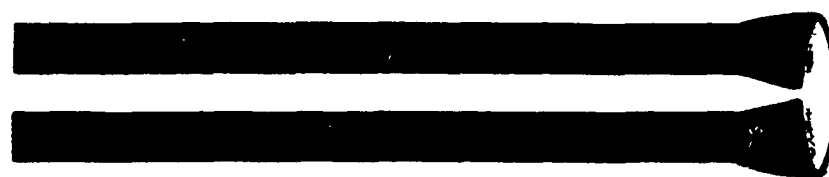
Microbore columns originally developed for microbore LC are typically used for packed-column SFC. The types of packing are similar to those used for LC, while the lengths and internal diameters of SFC packed columns are more limited due to pressure drop considerations and upper flow limitations of some commonly used

detectors. Particle diameters range between 5 and 20 μm and column lengths are between 10 and 25 cm. Typical reversed-phase materials containing long-chain hydrocarbon groups (C_8 or C_{18}) have been used as well as phases containing cyano, amino or diol groups bonded to silica particles. Insufficient shielding of residual silanol groups on the silica support favours strong interactions with polar solute molecules resulting in broad tailing peaks. Two methods can be used to minimize this problem: (i) use of homogeneous polymer bonded stationary phases or, (ii) use of modifiers in the mobile phase to compete with solute molecules for these active sites. Packed columns have higher sample loading capacity, which can result in lower detection limits. Higher flow rates lead to faster analyses and greater efficiency per unit length. Packed columns have been used for all studies in this work.

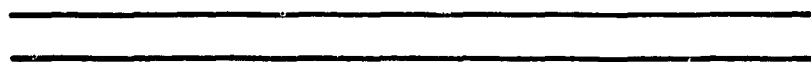
2.1.4 Restrictors

Restrictors are used to (i) maintain the operating pressure throughout the chromatographic system by providing a back pressure and (ii) reduce the system pressure to atmospheric pressure in a smooth, rapid decompression step. Placement and requirements of the restrictor differ according to the detection system used. For LC-type detectors, where measurements are made in the supercritical state, the restrictor is placed after the detector [7]. The restrictor is placed at the inlet of the detection system when using GC-type detectors so that the eluent is decompressed to atmospheric pressure and measurements are made in the gaseous state. Ideally the restriction device for SFC should: (i) provide uniform flow; (ii) provide resistance to plugging; (iii) provide variable flow rate capabilities; and (iv) allow for complete transfer of labile or non-volatile solutes to the detector without pyrolysis or precipitation of analyte particles. Although a variety of designs are available, the ideal restrictor has yet to be developed. To avoid solute precipitation and erratic detector response, the restrictor should be short and made of a heat conducting material. Fused silica tubing is typically used.

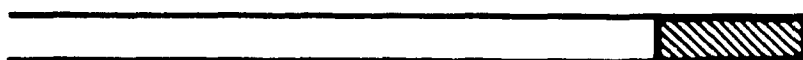
There are various types of restrictors available (Figure 2.2). The integral type restrictor is fabricated by sealing the tip of a fused silica capillary and polishing it



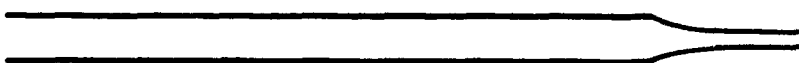
INTEGRAL



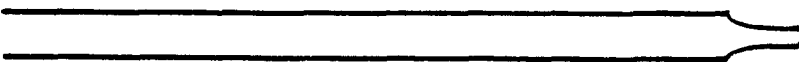
FUSED SILICA CAPILLARY



CERAMIC FRIT



ROBOT-PULLED



CRIMPED

Figure 2.2

Restrictor models for SFC. See text for description.

until a small orifice giving the desired flow rate is obtained. Decompression occurs only at this orifice, therefore minimizing problems of precipitation and erratic response of the detector. These restrictors are most commonly used for both capillary and packed columns. Linear restrictors are lengths of narrow bore fused silica (5-10 μm), the length determines the flow rate. Since decompression occurs throughout the length of the column, problems with spiking have been encountered. Ceramic frit restrictors have a 2 cm frit at the end of narrow bore fused silica tubing; these work well with open tubular columns but have problems with clogging when used with packed columns. The most sturdy restrictors are the crimped-type made of platinum, but reproducibility of the crimped orifice size is very low. Integral-type restrictors which can be fabricated in the laboratory are reliable and were used for all experiments.

2.1.5 Mobile Phases

Table 2.1 Physical Properties of Certain Supercritical Fluids

Fluid	Critical Temperature (°C)	Critical Pressure (atm)	Critical Density (g ml ⁻¹)
CO ₂	31.3	72.9	0.47
N ₂ O	36.5	72.5	0.45
NH ₃	132.5	112.5	0.24
n-C ₄	152.0	37.5	0.23
n-C ₅	196.6	33.3	0.23
SF ₆	45.5	37.1	0.74
Xe	16.6	58.4	1.10
CCl ₂ F ₂	111.8	40.7	0.56
CHF ₃	25.9	46.9	0.52

Typical mobile phases include carbon dioxide, nitrous oxide, ammonia, sulphur hexafluoride, and chlorofluorocarbons (Table 2.1). To analyze thermally labile substrates an eluent is chosen with a low critical temperature. To a first approximation the value of the critical pressure is a measure of solvent strength, therefore high critical pressures are preferred, although practical considerations place limitations on this value. Supercritical carbon dioxide is most commonly used as a mobile phase in SFC because of its low critical temperature (31.8°C) and high critical pressure (72.2 atm). Carbon dioxide is also non-toxic, non-explosive, inexpensive and has a minimal background response in flame-based and spectroscopic detection systems. The most obvious disadvantage of supercritical carbon dioxide is its low polarity.

2.1.6 Programming Methods

The most evident advantage of SFC over both GC and LC is the variety of methods available to control solute retention. SFC offers both temperature programming (as in GC) and mobile phase composition programming (as in LC) plus density programming. The ability to alter solvent strength with density is a primary advantage of SFC over other chromatographic techniques. Dual control of temperature and pressure is used to influence mobile phase density. Generally capacity ratios decrease exponentially with an increase in density, indicating greater solvation at the higher density. In developing a method for the separation of a number of species a density gradient is used to optimize resolution.

2.1.7 Mobile phase modifiers

For some polar compounds the range in solvent strength offered by density programming of the mobile phase may not be adequate to elute the compound or provide reasonable separation. Addition of a second component (modifier) to the mobile phase can greatly extend the power of density programming.

2.1.8 Detection Strategies

Both LC-type and GC-type detectors have been used for SFC. Fluorescence and ultraviolet absorption detection systems for SFC use high pressure cell able to withstand pressures up to 6000 psi. These are most commonly used for packed column SFC with modified supercritical mobile phases. Some flow cell configurations for capillary SFC use on column detection, where the polyimide coating is removed from the end of the column which is then placed in the light path of a UV detector.

Flame-ionization detection is most popular with capillary SFC; the higher flow rates associated with packed-columns poses some problems with keeping the flame lit and maintaining ionization efficiency. Flame ionization detection (FID) and nitrogen phosphorous thermionic detection (NPD) have been used in SFC by decompressing the fluid at the detector inlet [8].

Fourier Transform Infrared spectrometers (FT-IR) have been utilized for measurements in both the supercritical state, using small volume, high pressure cells, and after fluid decompression, using solvent evaporation/deposition techniques.

Interfacing SFC and mass spectrometers has proven to be a simpler task than interfacing HPLC-MS systems because of the reduced amount of solvents. The low flow rates associated with capillary SFC permit the entire effluent to be accommodated by existing GC-MS pumping systems. The major problems are the placement of the restrictor and heating of the capillary interface. Typically temperature regulated interfaces are used which place the restrictor at the end of a nozzle directed into the ion source region [9,10]. Both thermospray and solvent elimination techniques have also been used for packed column SFC.

2.2 Experimental procedures

2.2.1 Instrumental

A model 5890 gas chromatograph (Hewlett-Packard, Palo Alto, CA) was

equipped with a Microgradient System Syringe Pump (Applied Biosystems Inc., Santa Clara, CA) to pressurize and pump the supercritical fluid mobile phase. Samples were introduced onto the column via a Rheodyne injection valve with a 0.5 or 1.0 μl sample rotor. Separations were performed on a Rexchrom 300Å C-18, 5 μm , 100 X 2.1 mm ID column (Chromatographic Sciences Company, St. Laurent, Québec, Canada). Fused silica integral restrictors, constructed in-house, maintained the supercritical conditions. Retention times, peak heights and areas and peak widths at half height were recorded by a Hewlett-Packard 3390 integrator. Unless otherwise stated this chromatographic system was used for all experiments in this work.

2.2.2 The role of modifiers in chromatographic separations.

Results from the investigation of the role of several modifiers (formic acid, dichloromethane, and acetonitrile) in supercritical mobile phases are discussed in chapter 3.

2.2.2.1 Chromatographic system

A Kratos model 773 UV-Absorbance detector (Applied Biosystems Inc., Santa Clara, CA, USA) set at 250 nm served as the detection system. A 1.0 μl loop was used for the Rheodyne injection valve.

2.2.2.2 Chemicals

Isobutyl benzene, phenyl acetic acid, anthracene, anthraquinone and pyrene were obtained from Aldrich (Milwaukee, Wisconsin, USA) and used as received. Dichloromethane and formic acid were obtained from BDH (Toronto, Ontario, Canada). The acetonitrile-doped and simple supercritical carbon dioxide were obtained from Scott Specialty Gases (Plumsteadville, Pennsylvania, USA). Other modified phases were prepared in-house according to the following technique.

2.2.2.3 Technique to modify supercritical mobile phases

A glass vacuum manifold constructed from stock components (see Figure 2.3) was connected via a trap immersed in liquid nitrogen to a laboratory vacuum pump and the system was evacuated. A known amount of modifier was poured into a clean aluminum gas cylinder which was then immersed in liquid nitrogen for a sufficient time to allow the modifier to freeze. The target cylinder is then connected to the manifold and the system evacuated again. The supply cylinder containing SFC grade CO₂ was connected to the manifold and the rate of gas flow from the supply cylinder to the target cylinder was controlled with a fine control regulator. Throughout the filling process the vacuum was monitored with a mercury manometer. The length of time necessary to fill the cylinder was dependent not only on the flow rate of the gas but the rate at which it freezes, requiring its weight to be determined at regular intervals, 25-30 minutes for a final weight of 300 grams. Care must be taken not to overfill the cylinder. It should be allowed to reach room temperature under ambient conditions before use. Although exactly predetermined modifier/gas ratios are difficult to attain, the final concentrations are readily calculated. The method described provided a useful in-house technique for making binary and tertiary mobile phases.

2.2.2.4 Isothermal studies

Isobutyl benzene, phenyl acetic acid, anthracene, anthraquinone and pyrene were dissolved in dichloromethane at a concentration of 100 µg/ml and were injected (1.0 µl) under conditions of constant temperature and changing density. Four injections were averaged for each density setting (0.5 -0.9 g/ml). The process was repeated for each change in temperature (40 -100°C) and each mobile phase. The operating pressure to obtain the desired density for a given temperature was calculated using a computer algorithm. For details see Appendix A.

2.2.2.5 Isodense studies

Isobutyl benzene, phenyl acetic acid, anthracene, anthraquinone and pyrene were dissolved in dichloromethane at a concentration of 100 µg/ml and were injected

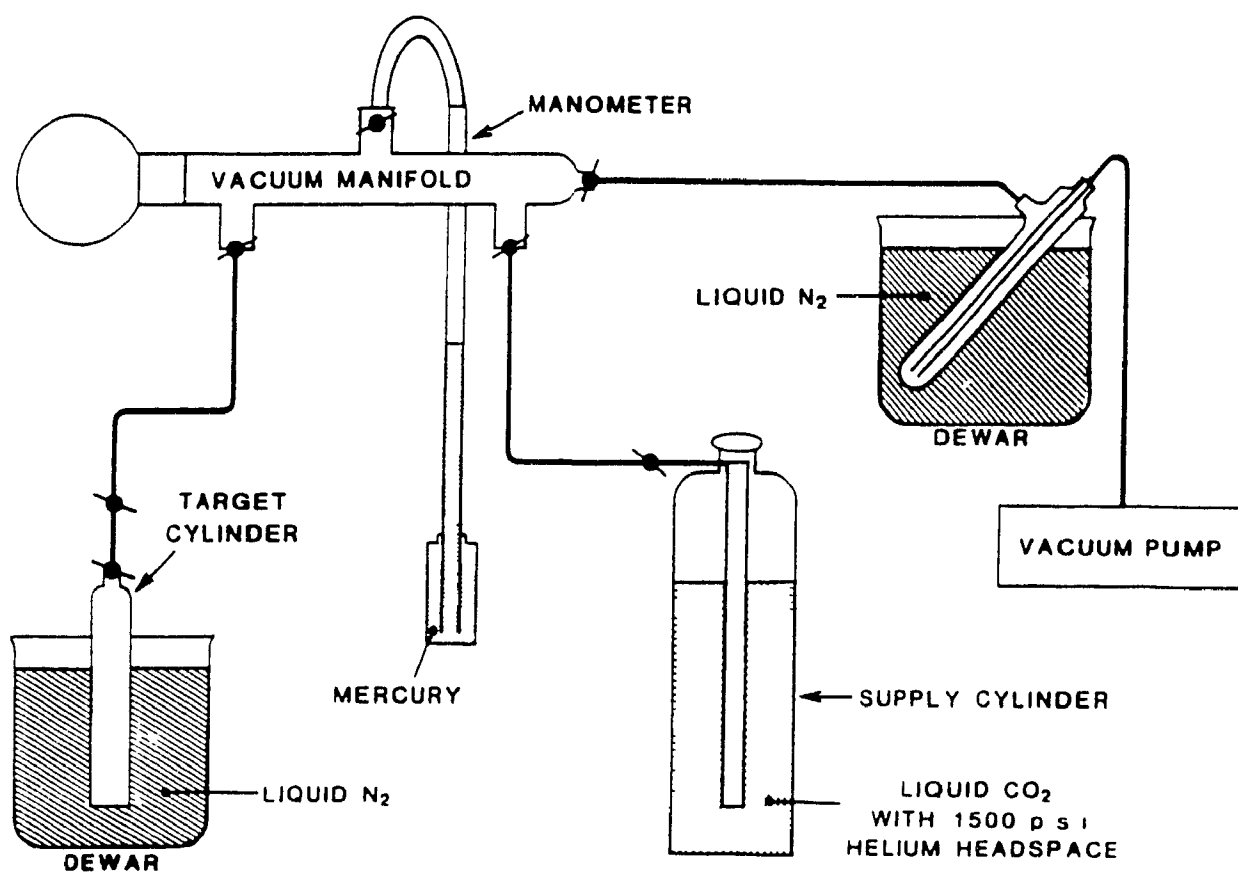


Figure 2.3 Apparatus for the addition of organic solvents to supercritical fluids.

(1.0 μ l) under conditions of constant density and changing temperature. Four injections were made for each a range of temperatures (40 -100°C) at a given density. The process was repeated for densities between 0.5 - 0.9 g/ml and for each mobile phase. For both the isothermal and isodense studies, the peak heights, peak widths at half height and retention times were recorded as an average of four injections.

2.2.3 Analysis of phenothiazinones in plasma by packed column SFC.

The separation of a series of phenothiazinone analogs and an assay for one analog in plasma are described in chapter 4.

2.2.3.1 Chromatographic system

A Kratos model 773 UV-Absorbance detector (Applied Biosystems Inc., Santa Clara, CA, USA) set at 250 nm served as the detection system. A 1.0 μ l loop was used for the Rheodyne injection valve.

2.2.3.2 Chemicals

Dichloromethane and acetonitrile were obtained from BDH (Toronto, Ontario, Canada). The acetonitrile-doped and simple supercritical carbon dioxide were obtained from Scott Specialty Gases (Plumsteadville, Pennsylvania, USA). Phenothiazinone analogs were synthesized by the medicinal chemistry group at Merck Frosst Centre for Therapeutic Research.

2.2.3.3 Calibration curve

A stock solution of L615,919 (4-chloro-3H-phenothiazin-3-one) was prepared by dissolving 10 mg of the drug in 10 ml of dichloromethane. A stock solution of the internal standard L649,927 (benzo(a)-phenothiazin-3-one) was also prepared with a concentration of 1 mg/ml. Ten standard solutions were prepared with a concentration range between 2 and 900 μ g/ml each containing 100 μ l of the internal standard for a final concentration of 0.1 mg/ml. A calibration curve was obtained by plotting the average peak height ratio of five injections of each standard solution against the

concentration.

2.2.3.4 Preparation of dosing solution

A 20 mg/ml suspension was prepared by grinding the drug to a fine powder using a mortar and pestle. A 1% Methocel solution was added to the powdered drug and ground to obtain a homogeneous suspension.

2.2.3.5 Dosing regime

Rats ranging from 300 to 400 g weight were used for these studies. The animals were fasted overnight before the study and fed six hours after dosing. Water was allowed *ad libitum*. On the day of the study, the animals were weighed and dosed 150 mg of drug per 1 kg weight of the rodent orally via gastric intubation. Under ether anaesthesia, serial blood samples were withdrawn from the jugular vein of the animal at various times. Plasma samples were separated by centrifugation and stored at -20°C until analysis.

2.2.3.6 Plasma samples

To each 400 µl sample of plasma 50 µl of 0.1 mg/ml solution of L649,927 (internal standard) and 200 µl of 0.1 N HCl was added. The mixture was agitated on a vortex mixer for two minutes. Ethyl acetate (1 ml) was added and the mixture was again vortexed for four minutes and then centrifuged for 15 minute at 12000 rpm. The ethyl acetate layer was collected and evaporated to dryness under a stream of nitrogen. The aqueous layer was extracted a second time with 1 ml of ethyl acetate. The organic layer was combined with the first evaporated extract and evaporated to dryness. Each sample was redissolved in 50 µl of dichloromethane and 1.0 µl was injected on column.

2.2.3.7 Cyclic voltammetry of phenothiazinones

The phenothiazinone compounds (1 mg/ml) were dissolved in acetonitrile containing 0.1M tetrabutyl ammonium tetrafluoroborate (TBA TFB) as the supporting

electrolyte. A platinum ultramicroelectrode served as the working electrode, a silver/silver chloride electrode as the reference and a platinum wire as the auxiliary electrode. All scans were recorded at 100 mV/sec. Cyclic voltammograms were recorded with a BAS CV 27 voltammograph (BioAnalytical Systems, West Lafayette, Indiana, USA) and a HP7090A plotter (Hewlett-Packard, Palo Alto, CA, USA).

2.2.4 An electrochemical detection system for SFC

The design and performance of an electrochemical detection system for SFC is described in chapter 5.

2.2.4.1 Chemicals

Ferrocene and tetrabutylammonium tetrafluoroborate (Aldrich, Milwaukee, Wisconsin, USA) were used as received. The acetonitrile and tetrabutylammonium tetrafluoroborate/acetonitrile-doped supercritical carbon dioxide were obtained from Scott Specialty Gases (Plumsteadville, Pennsylvania, USA). The solubility of the salt in the carbon dioxide/acetonitrile mixture was verified before shipping.

2.2.4.2 Electrochemical Cell

An ultramicroelectrode made from 10- μ m diameter platinum wire sealed in narrow-bore glass capillary was obtained from BioAnalytical Systems Inc. (West Lafayette, Indiana, USA). The glass capillary was of narrower diameter (3.2 μ m) than those commercially available. The electrode body was filled with epoxy resin to provide mechanical support. Two centimetres of the electrode body were ground to accommodate the cell compartment and to provide a rough surface for sealing. The preliminary design uses a high pressure stainless steel tee-union as the electrochemical cell (Figure 2.4). The inlet and outlet ports are 1/16 inch diameter with a 1/8 inch diameter third port for the working electrode. The column eluent enters the cell through a fused silica capillary threaded into the swagelok union positioned directly above the working electrode in a wall-jet geometry. The restrictor, placed through the

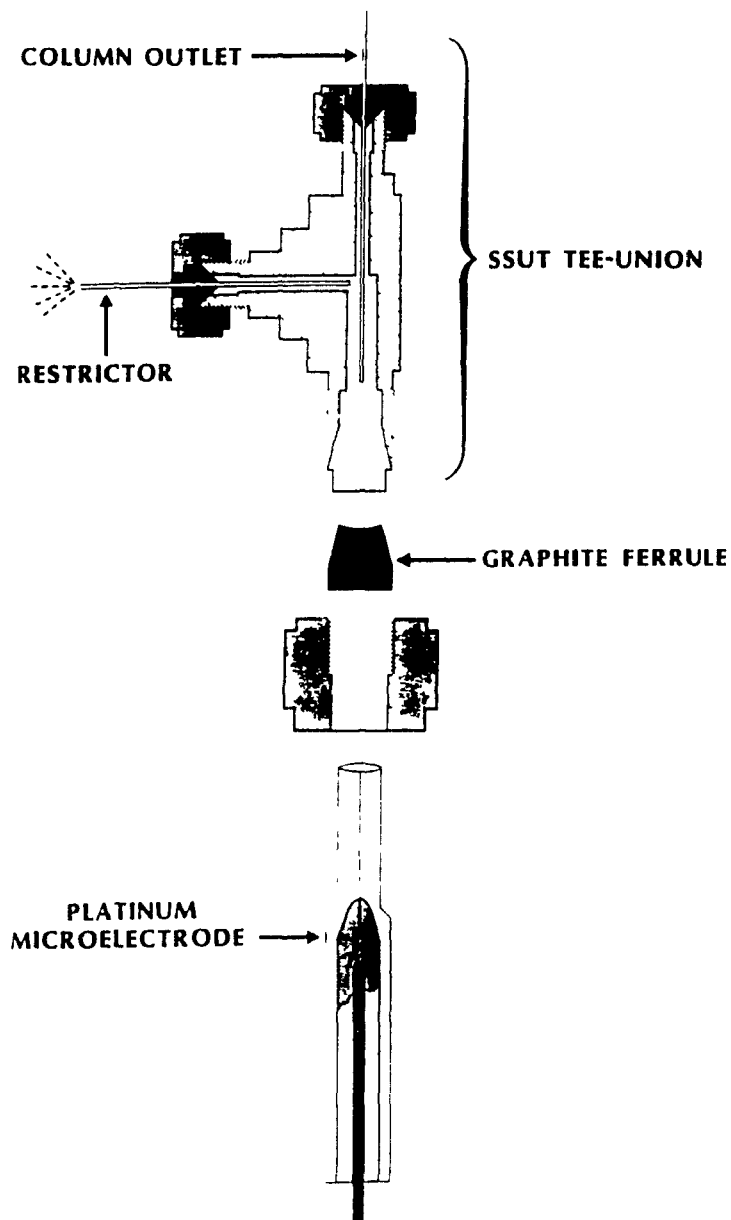


Figure 2.4 High pressure electrochemical cell.

side arm, is well removed from the working electrode to avoid decompression near the electrode which may cause precipitation of either the analyte or electrolyte modifier [11]. Graphite ferrules were used to swage all components. The cell body served as the quasi-reference electrode.

Cyclic voltammograms were recorded with a BAS CV 27 voltammograph and an HP7090A plotter. For the hydrodynamic studies, the potential was controlled by a BAS amperometric detector LC-4 and the current was recorded on a HP3390 integrator. The cell was housed in a BAS Faraday cage.

2.2.5 Determination of sorbitan trioleate in metered-dose inhalers by SFC.

A method for the analysis of sorbitan trioleate in aerosol formulations has been developed and is described in chapter 6.

2.2.5.1 Chromatographic system

Eluents were monitored with a flame-ionization detector set at 350°C. All experiments were run at constant pressure (2400 psi) and temperature (40°C). Solvents were all HPLC grade and were used as received. Sorbitan trioleate was obtained from ATLAS Chemicals (lot #A17297).

2.2.5.2 Sample preparation

Each aerosol canister was immersed in liquid nitrogen for twenty minutes to liquefy the contents. The canister was opened with a pipe cutter and the contents poured into a beaker. After all the propellant evaporates, the dry residue was vortexed with a known quantity of dichloromethane to dissolve the sorbitan trioleate. The sample was then centrifuged at 12000 rpm for 15 minutes and the supernatant filtered through a 0.45 µm filter prior to injection. A calibration curve was prepared by dissolving appropriate amounts of sorbitan trioleate and an internal standard (pyrene 0.2 mg/ml) in dichloromethane.

2.3 References

1. L. McLaren, M.N. Myers and J.C. Giddings, *Science*, **159** (1968) 197.
2. B.W. Wright, P.A. Peaden, M.L. Lee and T. Stark, *J. Chromatogr.*, **248** (1982) 17.
3. R.C. Kong and M.L. Lee, *J. High Resolut. Chromatogr. Chromatogr. Commun.*, **6** (1983) 319.
4. B.E. Richter, J.C. Kuei, J.I. Shelton, L.W. Castle, J.S. Bradshaw and M.L. Lee, *J. Chromatogr.*, **279** (1983) 21.
5. P.A. Peaden, J.C. Fjeldsted, M.L. Lee, S.R. Springston and M. Novotny, *Anal. Chem.*, **54** (1982) 1090.
6. P.J. Schoenmakers, in *Supercritical Fluid Chromatography*, RSC Chromatography Monographs, London, (1988), Chapter 4, p102.
7. J.C. Fjeldsted, B.E. Richter, W.P. Jackson and M.L. Lee, *J. Chromatogr.*, **279** (1983) 423.
8. J.C. Fjeldsted, R.C. Kong, and M.L. Lee, *J. Chromatogr.*, **279** (1983) 449.
9. R.D. Smith, W.D. Felix, J.C. Fjeldsted and M.L. Lee, *Anal. Chem.*, **54** (1982) 1883.
10. R.D. Smith, J.C. Fjeldsted and M.L. Lee, *J. Chromatogr.*, **247** (1982) 231.
11. A.C. Michael and R.M. Wightman, *Anal. Chem.*, **61** (1989) 2193.

Chapter 3

The Role of Modifiers in Chromatographic Separations

3.1 Introduction

A key feature of SFC is that a chromatographic separation can be optimized for a given stationary phase by varying temperature, as in GC, mobile phase composition, as in HPLC, plus the additional option of varying pressure and density. Since the solvent strength of a supercritical fluid is closely related to its density, pressure or density gradients can be used in the development of a separation [1]. The solubility parameter of the supercritical mobile phase is influenced both by its critical temperature and the operating density. To solubilize a solute, the solubility parameters of the solute and the solvent should be nearly equal. To a first approximation, the value of the critical pressure is a measure of a supercritical fluid's solvent strength, but practical limitations of presently available instrumentation do not permit the use of fluids with high critical pressures. Increasing the density of the supercritical mobile phase also increases the solubility parameter and consequently affects the solutes. Enhancing the solvent strength by increasing density is limited by both practical constraints of the solvent delivery system and the low compressibility of the fluid as it reaches liquid-like densities [2].

Supercritical carbon dioxide is the most commonly used SFC mobile phase due to its low critical temperature and moderate critical pressure, which permits the elution of thermally labile compounds while operating within practical pressure limits of current instrumentation. Carbon dioxide is non-toxic, inexpensive, non-flammable and has minimal response in flame ionization detectors. Under typical SFC operating conditions (40-120°C, 1200-5500 psi) supercritical carbon dioxide's solvent strength,

as measured by the Hildebrand solubility parameter, overlaps those of several common organic solvents such as hexane, pentane, dichloromethane, toluene, THF and isopropyl alcohol [3]. This suggests that migration in supercritical CO₂ will occur if the compound is soluble in any of these organic solvents. A problem occurs because of the limited solvating ability of supercritical carbon dioxide for many polar substrates. Increased solvent strength can be achieved by the addition of organic solvents, in which the solute is soluble, to the supercritical CO₂ mobile phase. Addition of a polar modifier typically results in decreased capacity ratios as compared to the single component mobile phase. Retention in a chromatographic process is controlled by several interactions: (i) the solubility of the solute in the mobile phase, as determined by the solute-solvent interactions; (ii) the affinity of the solute for the stationary phase; and (iii) interaction of the mobile phase molecules with the stationary phase. With bonded stationary phases interactions can occur with both the bonded phase and the support material, typically silica. To influence retention the modifier must alter one or more of the above mentioned mechanisms.

The successful development of SFC requires a more complete understanding of fluid properties, their dependence on physical parameters, temperature, density and composition, and their influence on retention behaviour. When this work was started there was no clear understanding or consensus by those working in the area as to the exact role of mobile phase modifiers. It was suspected that mobile phases could be tailored for a specific application but little information was available on which to base the selection of a mobile phase composition for a given application. Although thermodynamic models existed to describe retention and selectivity they were unable to account for stationary phase interactions and were not useful for predictive purposes in developing a separation strategy for a given series of compounds. Therefore a systematic study of the influence of temperature, density and mobile phase composition on chromatographic parameters for several compounds on a reversed phase column was undertaken. The practical problem in delivering mixed supercritical phases was overcome by adopting a common technique for subdividing gases to modify commercially available supercritical fluids. This permitted the study of the

influence of density and temperature on model compounds in binary and tertiary eluent mixtures and helped define the importance and role of modifiers generally.

3.2 Experimental

For experimental details see section 2.2.2.1 - 2.2.2.4 in chapter 2.

3.3 Results and Discussion

Several investigators [4,5,6] have suggested possible roles for modifiers in supercritical mobile phases. Polar additives can act as surfactants decreasing the interfacial tension between the mobile and stationary phases. They can also provide competition between solute and mobile phase molecules for active sites on the chromatographic column. Co-solvent molecules may interact with functional groups on the solutes and/or increase the fluid's dielectric constant, introduce hydrogen bonding capabilities, and alter mass transfer characteristics and solvent viscosity. The addition of a less volatile solvent has the added effect of increasing the critical temperature and pressure of the mobile phase and thus the density or solvating power of the fluid [7].

3.3.1 Chromatographic parameters

Solute affinity for the mobile and stationary phases in SFC is dependent on the composition of each, as well as on the mobile phase density and temperature. Initial studies were designed to investigate the influence of density and temperature on the chromatographic behaviour of a set of model compounds for a given mobile phase and stationary phase.

The chromatographic parameters investigated included peak width at half height, capacity ratio, effective plate number, selectivity and resolution. The capacity factor (k') is the ratio of the number of moles of solute in the stationary phase over

the number of moles in the mobile phase and is related to the retention time of the solute according to the following equation,

$$k' = \frac{t_R - t_0}{t_0} \quad (3.1)$$

where t_0 = retention time of an unretained species
 t_R = retention time of species of interest

The separation factor or selectivity (α) is the ratio of capacity factors for two adjacent peaks,

$$\alpha = \frac{k_2}{k_1} \quad (3.2)$$

where k_1 = capacity ratio of earlier eluting analyte
 k_2 = capacity ratio of adjacent analyte

Selectivity is varied by changing the composition of the mobile and/or stationary phase. Both selectivity and capacity factor are a measure of the peak position.

Column efficiency (N) is the relative ability of a given column to provide narrow bands of solute.

$$N = 5.54 \left(\frac{t_R}{t_{w0.5}} \right)^2 \quad (3.3)$$

where $t_{w0.5}$ = peak width at half height

The value of N is constant for different solutes for a given column, mobile phase, temperature and linear velocity. Therefore an increase in retention time results in an increased peak width. The separation efficiency is controlled by changing the column length or the solvent velocity.

The resolution is a measure of the relative resolution achieved for a given sample mixture. The resolution between two adjacent peaks is equal to the distance

between the two peak centres divided by the average peak width. Resolution can be expressed in terms of experimental parameters such as k' , N and α :

$$R = \left(\frac{1}{4}\right) (\alpha - 1) \sqrt{N} \left(\frac{k'}{1 + k'}\right) \quad (3.4)$$

Both the separation efficiency and the resolution are a measure of the peak distortion developed throughout the length of the column.

The availability of solubility data for various organic solvents in supercritical carbon dioxide, provides a means for preparing homogeneous binary and tertiary mobile phases. Packed columns designed for HPLC are routinely used for SFC. C-18 bonded phase packed columns have shown versatility for the separation of a large variety of compounds in HPLC and seemed an appropriate candidate for SFC.

3.3.2 Isothermal and isodense studies

3.3.2.1 Supercritical carbon dioxide mobile phase

A series of model compounds (iso-butyl benzene, phenyl acetic acid, anthraquinone, anthracene and pyrene) was selected to demonstrate substituent and molecular size effects under various conditions. Chromatograms were obtained for four injections of the test mixture at each temperature and density (see appendix B for table of data). Chromatographic parameters were plotted under conditions of constant density as a function of temperature. Generally capacity ratios and peak widths decreased in a non-linear fashion with increasing temperature at constant density (Figure 3.1). The shape of the k' versus temperature curve for the individual compounds remained the same for each density studied, but the values of the capacity ratios decreased with increasing density. The greatest change in capacity ratio was obtained for pyrene, the largest molecule of the mixture, indicating that its solubility in the mobile phase is increased at the higher temperature. A plot of $\ln(k')$ as a function of temperature shows a linear dependence for each solute (Figure 3.2a). The

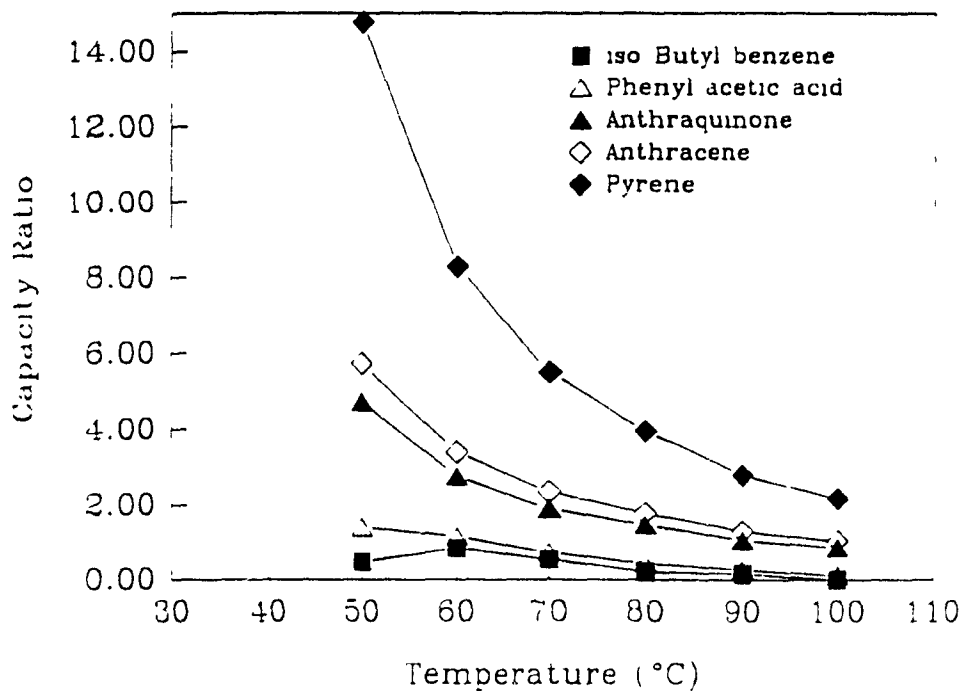
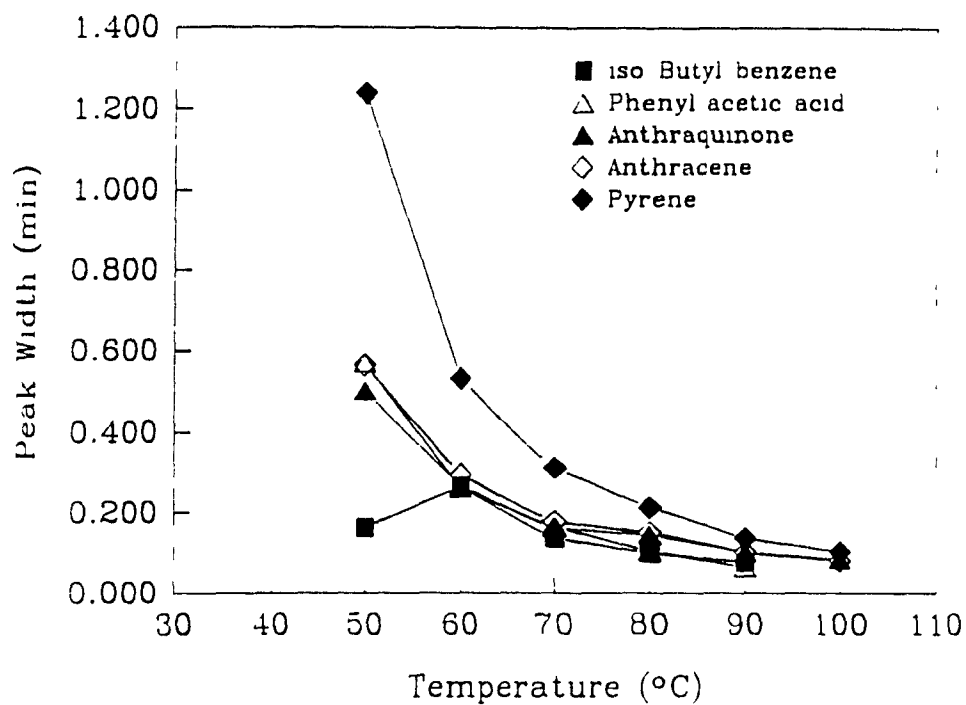


Figure 3.1 Peak width (a) and capacity ratio (b) as a function of temperature at constant density (0.7g/ml). Mobile phase: supercritical carbon dioxide.

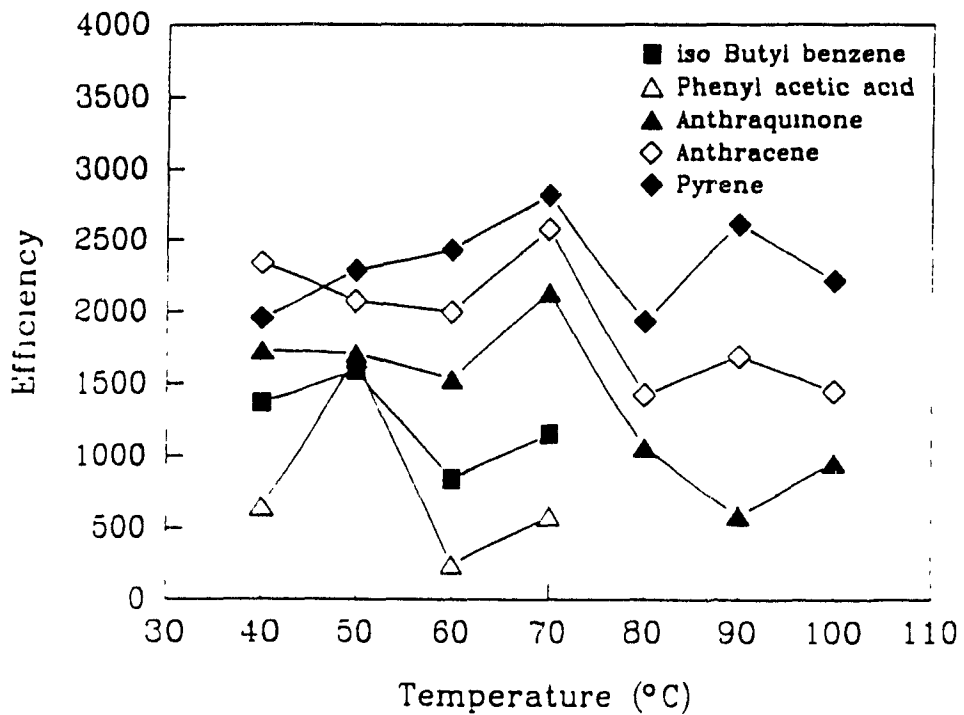
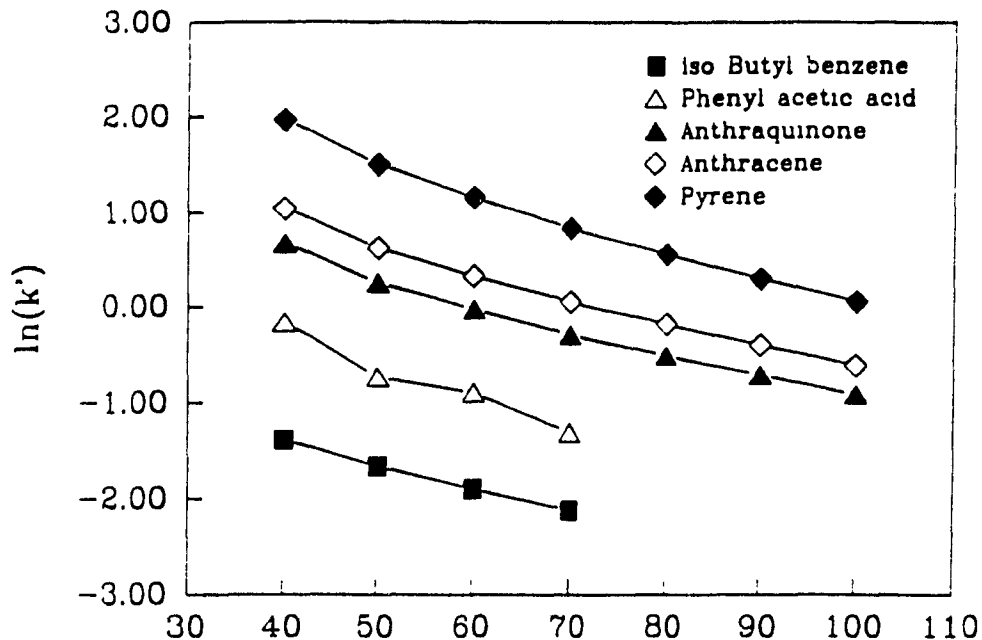


Figure 3.2 $\ln(k')$ (a) and efficiency (b) as a function of temperature at a constant of 0.7 g/ml. Mobile phase: supercritical carbon dioxide.

dependence of efficiency on temperature shows a maximum at 70°C for anthraquinone, anthracene, and pyrene, while the smaller compounds have a maximum value at 50°C; this is true for all densities investigated (Figure 3.2b). Selectivity between anthraquinone and anthracene remains constant for the temperature range studied, while selectivity for anthracene and pyrene decreases slightly with increasing temperature (Figure 3.3a). The greatest change occurs for the resolution between anthracene and pyrene, which decreases rapidly with increasing temperature. This is a direct result of the large retention time change for pyrene with temperature (Figure 3.3b).

At constant temperature, capacity ratios decrease with increasing density much more rapidly, than at constant density with increasing temperature. Again the curve is asymptotic, and the shape dependent on the analyte at each temperature (Figure 3.4b). The capacity ratio values are higher at the lower temperature. Resolution between anthracene and anthraquinone, which differ in polarity, remains constant, while the resolution between anthracene and pyrene decreases rapidly with increasing density (Figure 3.5b). This suggests that the effect of density is greater on the larger molecule, due to its increased solubility in the mobile phase.

At constant temperature, changes in density greatly influences the chromatographic separation. The control density exerts on retention behaviour is best seen by comparing chromatograms obtained for the test mixture at constant temperature and different densities. A decrease in analysis times by a factor of ten was obtained by increasing the density from 0.5 to 0.7 g/ml (Figure 3.6). However, the increased speed of analysis is at the cost of resolution. The smaller molecules are better resolved at the lower densities, while the larger solutes, anthraquinone, pyrene and anthracene, have better peak shape at intermediate densities. In order to separate such a mixture a density gradient must be used.

3.3.2.2 Critical parameters in binary and tertiary mobile phases

Binary mobile phases are being used in SFC due to the ability of the second component to chemically alter the properties of the mobile phase. Problems occur

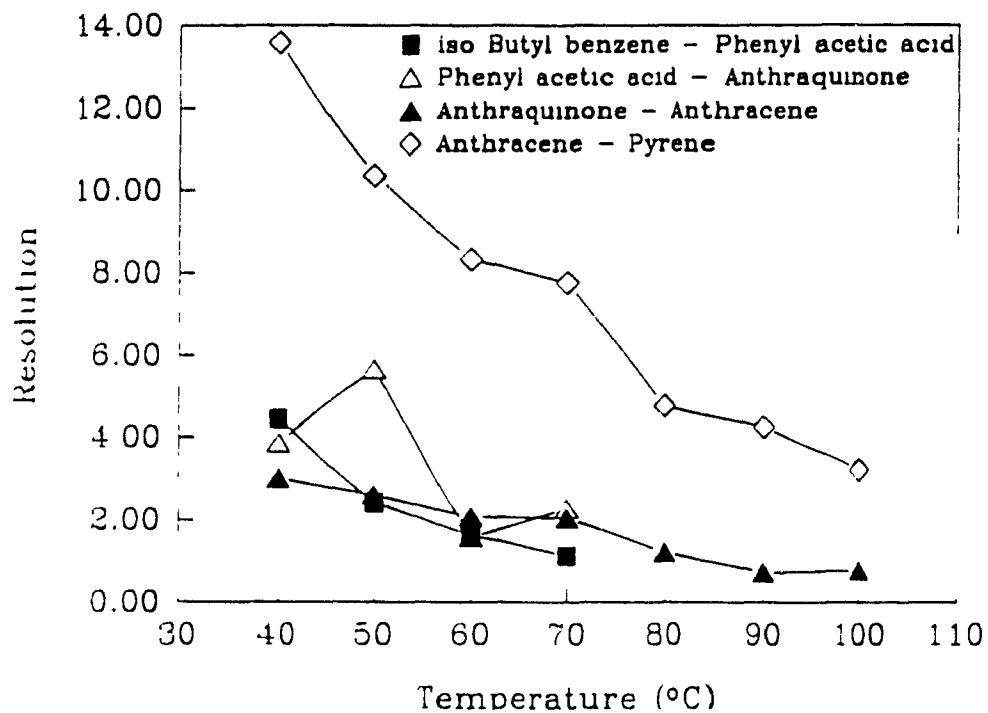
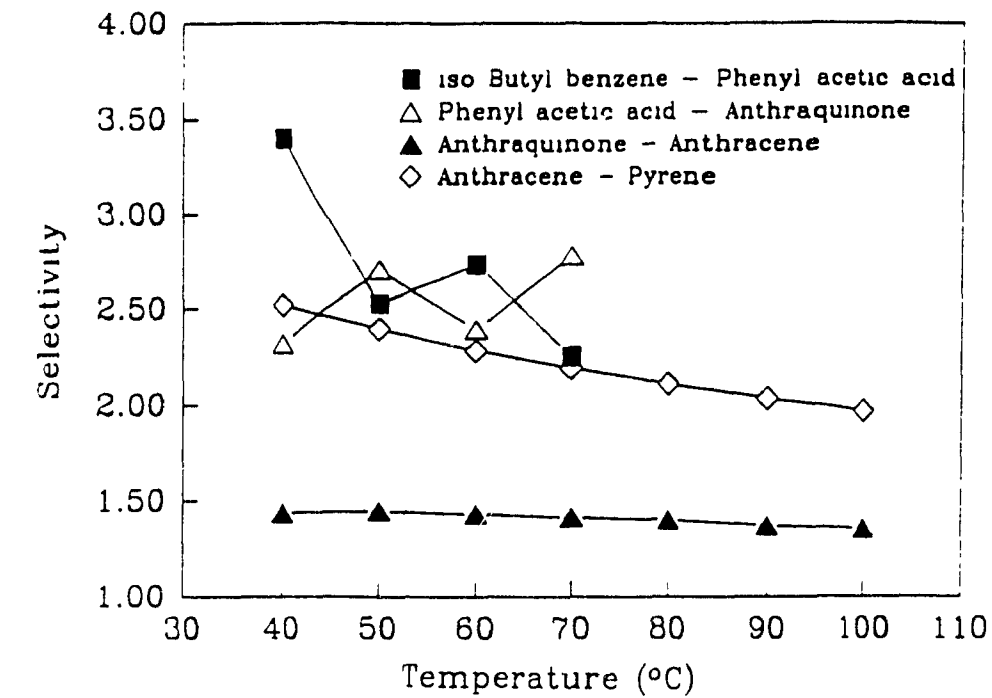


Figure 3.3

Selectivity (a) and resolution (b) as a function of temperature at a constant density of 0.7 g/ml. Mobile phase: supercritical carbon dioxide.

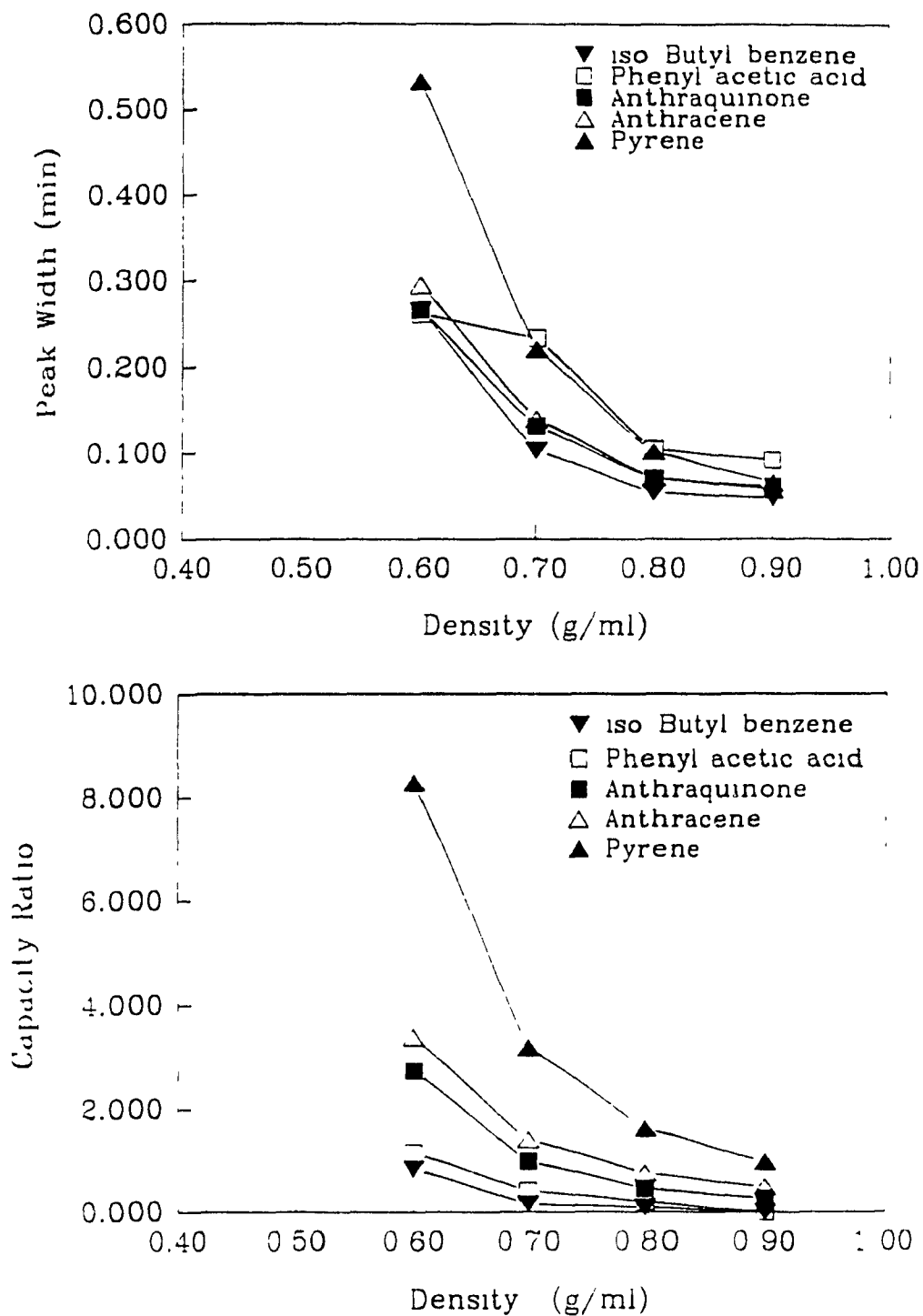


Figure 3.4

Peak width (a) and capacity ratio (b) as a function of density at constant temperature (60°C). Mobile phase: supercritical carbon dioxide.

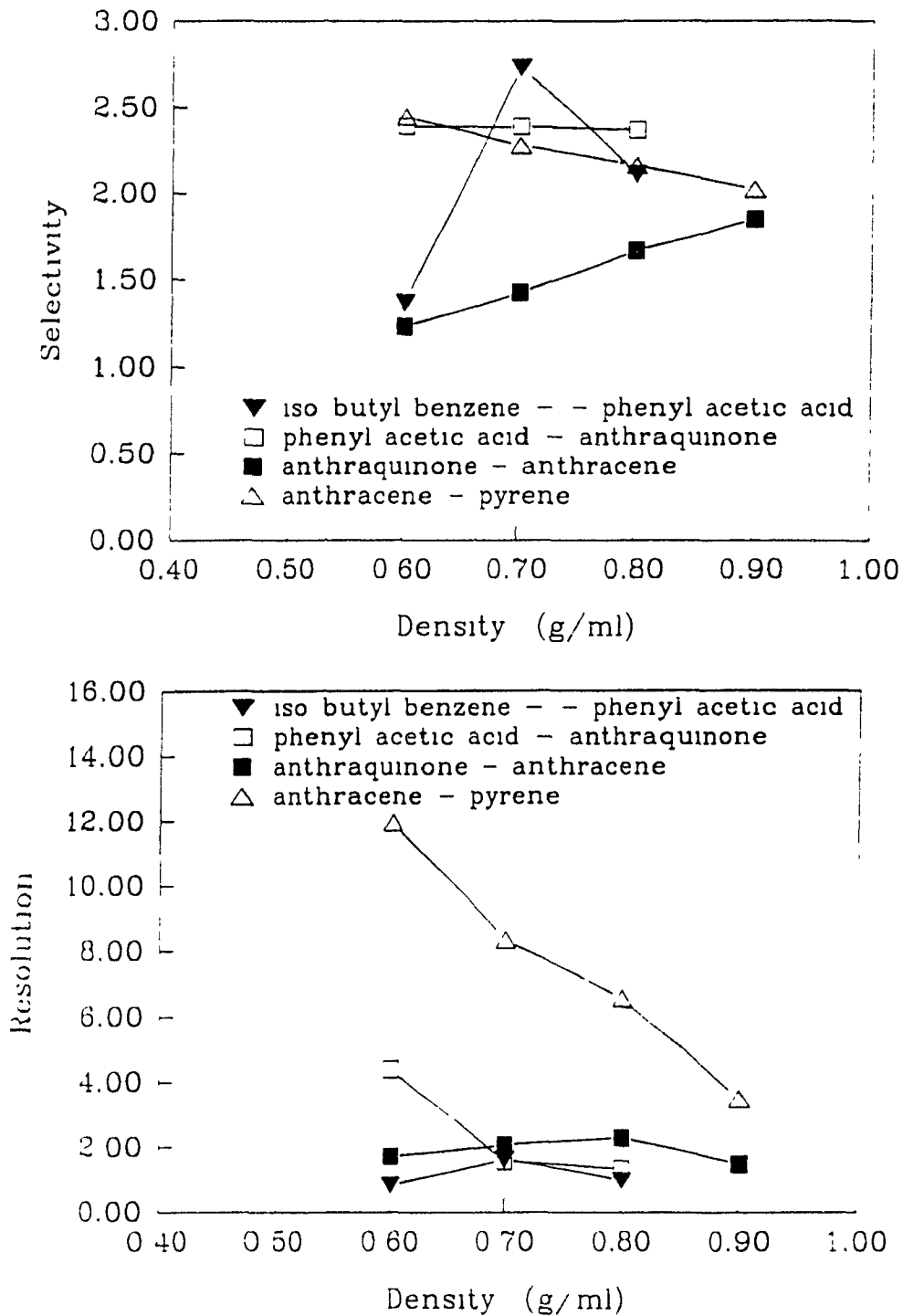
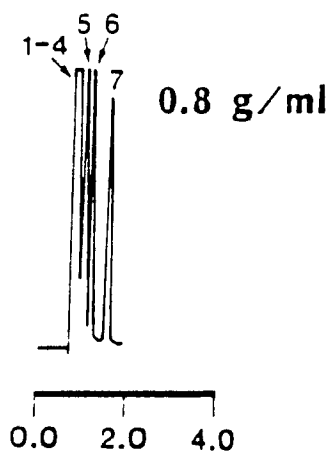
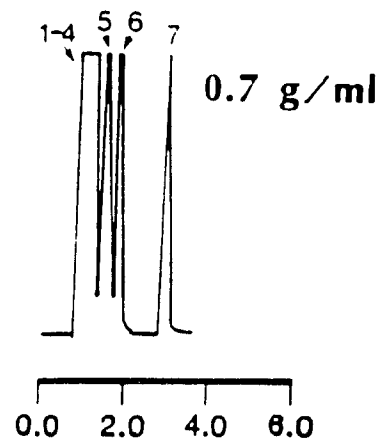
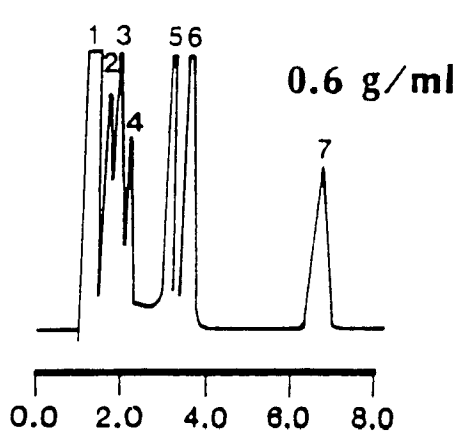
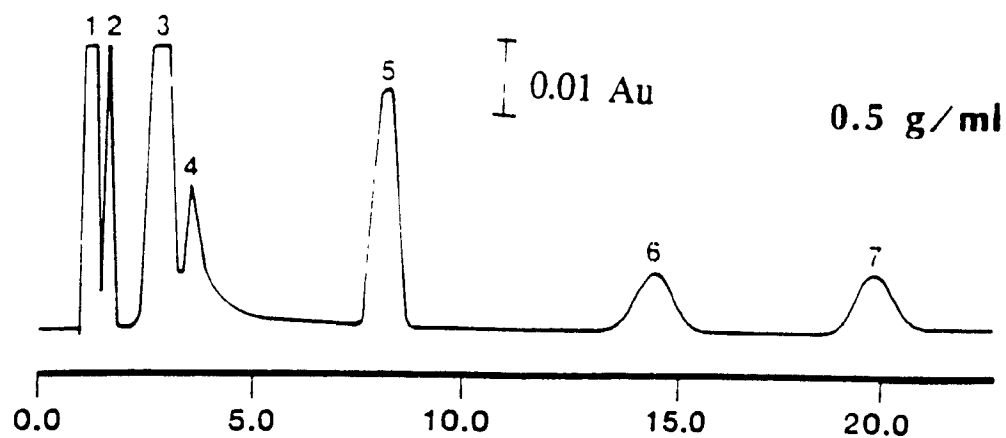


Figure 3.5 Selectivity (a) and resolution (b) as a function of density at constant temperature (60°C). Mobile phase: supercritical carbon dioxide.



- 1 Methylene Chloride
- 2 Isobutyl Benzene
- 3 Phenylacetic Acid
- 4 Ibuprofen
- 5 Anthraquinone
- 6 Anthracene
- 7 Pyrene

Figure 3.6 Chromatograms of model compounds at constant temperature (70°C) for various densities. Supercritical carbon dioxide mobile phase.

when using modifiers in supercritical mobile phases due to the non-linear relationship between the critical parameters of a binary mixture of eluents and the eluent composition. Critical parameters for mixed phases have not been experimentally determined, therefore the critical temperature and pressure are estimated on a theoretical basis using equations of state. The Peng-Robinson equation of state was chosen for the calculation of critical parameters and for the determination of pressure and density values since: (i) it is a simple two-parameter cubic equation with solvable roots and (ii) it is commonly used, therefore providing a means for comparison with other data in the literature. Generally semi-empirical equations of state express pressure as the sum of a repulsion pressure (term I) and an attraction pressure (term II). The Peng-Robinson equation of state has modified the attractive pressure term of the van der Waals equation (term II).

$$P = \underbrace{\frac{RT}{V-b}}_I - \underbrace{\frac{a(T)}{V(V+b) + b(V-b)}}_{II} \quad (3.5)$$

Other equations of state have been developed [8,9] but most require solution by numerical methods. The density of a supercritical fluid changes rapidly near the critical point and therefore an equation of state with more parameters would best describe the change in density with pressure and temperature. However, since most of the following studies were conducted at conditions well above the critical point, the Peng-Robinson equation of state provided a good estimate of the critical parameters.

The density of the binary and tertiary fluids was determined by addition parameters as described by the Peng-Robinson equation.

$$a = \sum_i \sum_j x_i x_j a_{ij} \quad (3.6)$$

$$a_{ij} = (1 - \delta_{ij})a_i^{1/2}a_j^{1/2} \quad (3.7)$$

$$b = \sum_i x_i b_i \quad (3.8)$$

The two constants for the equation were calculated for each component of the mobile phase and were added according to the mixing rules describe by Peng and Robinson before being used in the equation of state. A computer program was written to calculate the density and critical parameters of various mixtures of organic solvents with carbon dioxide (see Appendix A for a listing of the program). For a given temperature and density, the Peng-Robinson equation gave the operating pressure for the particular mobile phase.

3.3.2.3 Formic acid modified carbon dioxide

Coverage of the silica support on common HPLC bonded-phase columns is usually less than 30%, leaving many silanol groups bare. Peak tailing of polar solutes may occur as a result of adsorption of the solute onto bare sites on the silica support. In HPLC trifluoroacetic, phosphoric or formic acid is typically added to the mobile phase to compete with the solute molecules for the bare silica sites. This produces a more uniform stationary phase surface, therefore considerably reducing peak tailing. It was hoped that similar effects could be achieved by the addition of formic acid to supercritical CO₂ mobile phase. At the time of these studies only single component mobile phases were available commercially, therefore the binary and tertiary phase were prepared in the laboratory by adapting a technique commonly used for subdividing gases (section 2.2.2.3).

Formic acid was chosen because of its solubility in supercritical carbon dioxide and its compatibility with both FID and UV absorption detection. Addition of the formic acid (0.25%) initially decreased retention times for all the compounds. Capacity ratio curves for anthraquinone, anthracene, and pyrene decrease

asymptotically with temperature at constant density (Figure 3.7), the shape of the curves are similar to those obtained with simple CO₂, while the k' values are lower for the same density in the formic acid modified phase. Selectivity and resolution curves (Figure 3.8) for anthraquinone/anthracene and anthracene/pyrene are very similar indicating that the resolution of these compounds in this system is governed by its selectivity. Resolution of two compounds takes into account the capacity ratios of each solute, the selectivity ratio and efficiency and therefore a plot of these individual components would indicate the predominate factor.

Capacity ratios and peak widths for isobutyl benzene remained constant for increasing density, suggesting no change in solute-solvent interaction (Figure 3.9). At constant temperature both the capacity ratios and peak widths decrease in a non-linear fashion with increasing density, indicating that the increase in density increases the solubility of the solutes in the mobile phase as well as the solute-stationary phase interaction. Efficiency for anthraquinone, anthracene and pyrene reach maxima at 0.8 g/ml (Figure 3.10b). Selectivity and resolution for anthraquinone/anthracene reach minima at a density of 0.8 g/ml (Figure 3.11). Selectivity of anthracene over pyrene steadily increases with density, while the resolution between the two increases only slightly.

The amount of formic acid in the mobile phase was then increased to 1.26 mole%. Plots of capacity ratio as a function of temperature at constant density have similar shapes to those recorded for the lower formic acid concentration, but the values of k' at lower temperatures for pyrene are slightly higher (Figure 3.12a). Efficiency for anthraquinone, anthracene and pyrene reach a maximum at 50°C and a minimum at 80°C (Figure 3.12b). Selectivity for anthraquinone and anthracene is constant for the temperature range investigated, while the anthracene/pyrene selectivity decreases slightly with increasing temperature (Figure 3.13). The resolution of both pairs is influenced by both the selectivity and capacity ratios.

At constant temperature the peak width curves are similar to the capacity ratio curves, indicating higher solvation of each solute with increasing density (Figure 3.14). Selectivity for anthraquinone/anthracene increases with density and the resolution

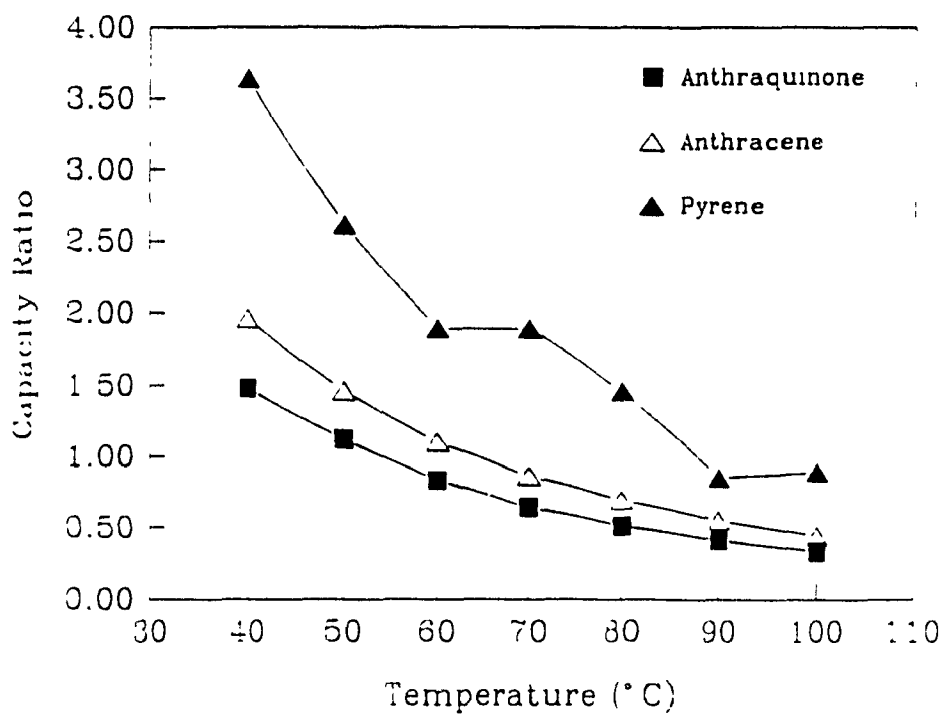
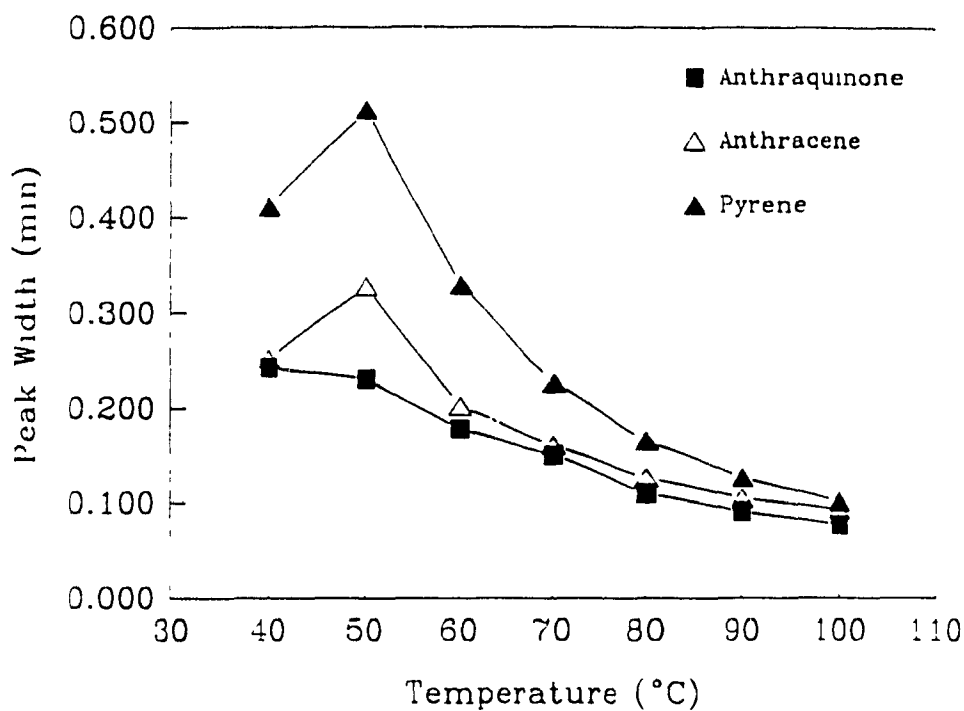


Figure 3.7 Peak widths (a) and capacity ratios (b) as a function of temperature at constant density (0.7g/ml). Mobile phase: formic acid (0.25 mole%) in carbon dioxide.

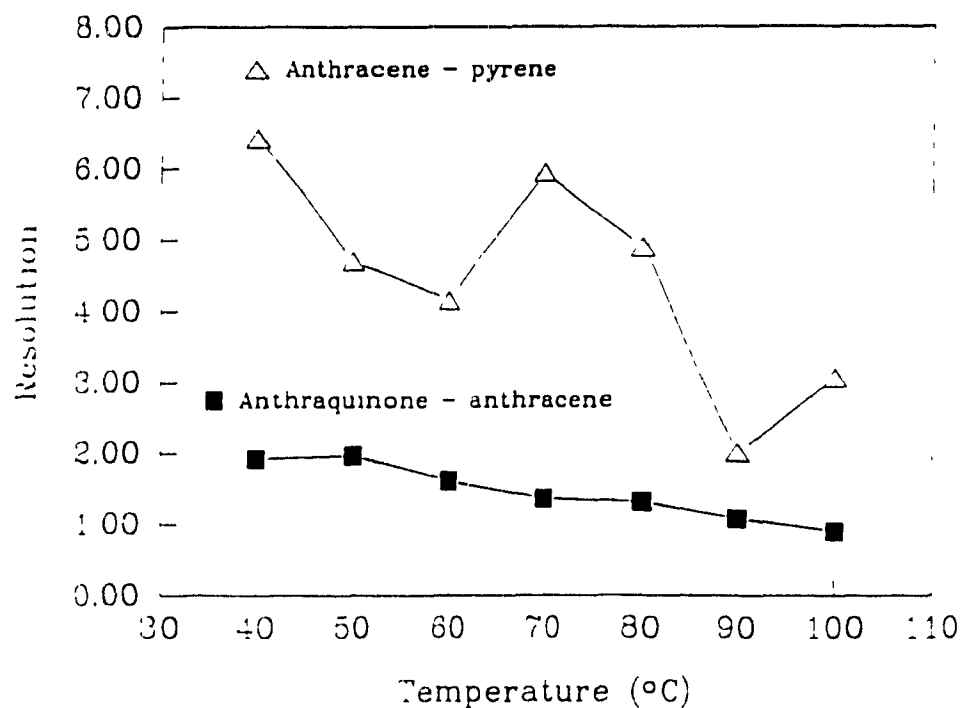
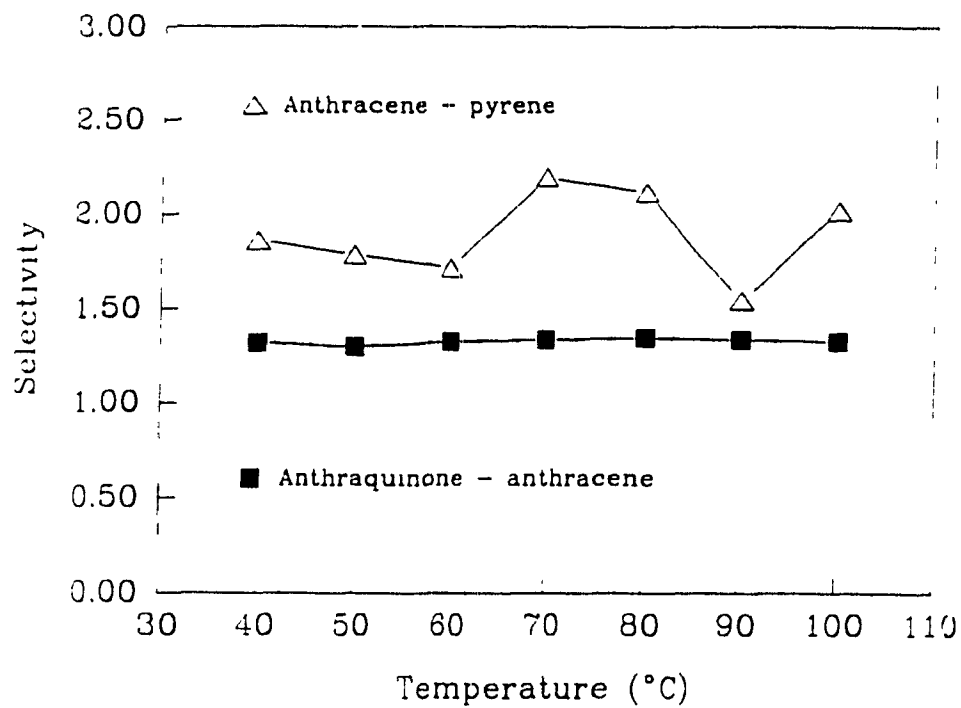


Figure 3.8

Selectivity (a) and Resolution (b) plotted against temperature at constant density (0.7 g/ml). Mobile phase: formic acid (0.25 mole%) in carbon dioxide.

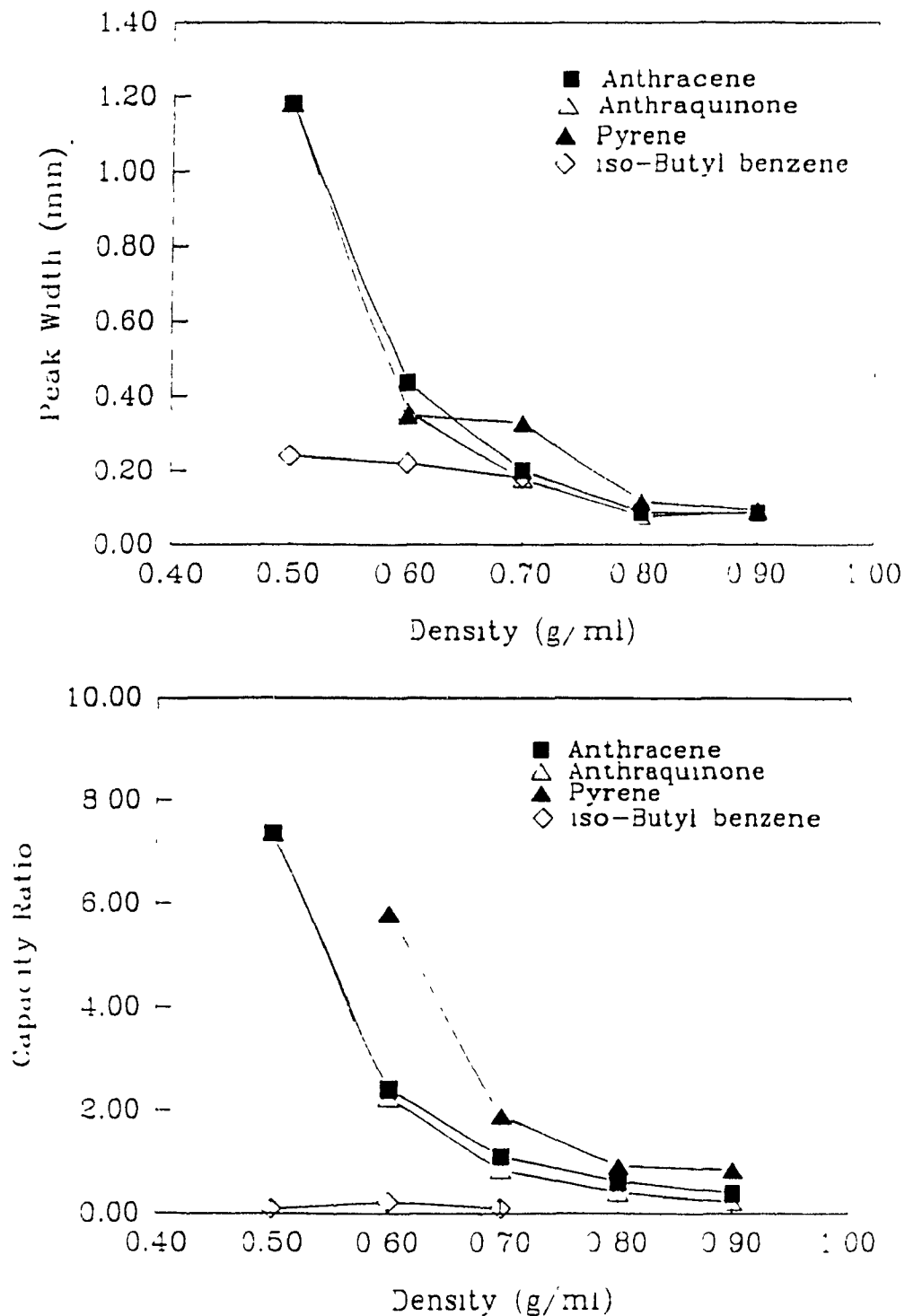


Figure 3.9

Peak widths (a) and capacity ratios (b) plotted against density at constant temperature (60°C). Mobile phase: formic acid (0.25 mole%) in carbon dioxide.

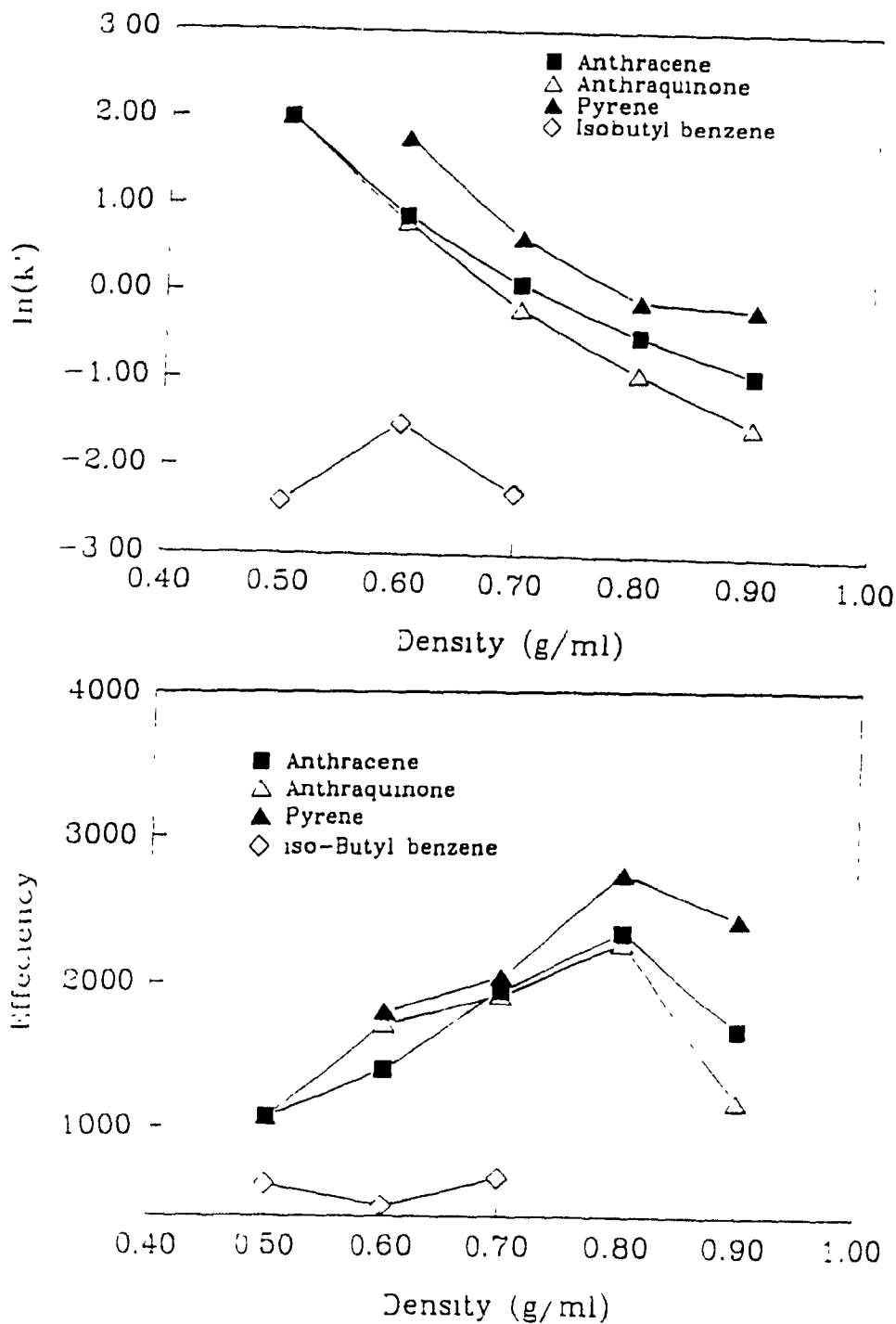


Figure 3.10 $\ln(k')$ (a) and efficiency (b) as a function of density at constant temperature (60°C).

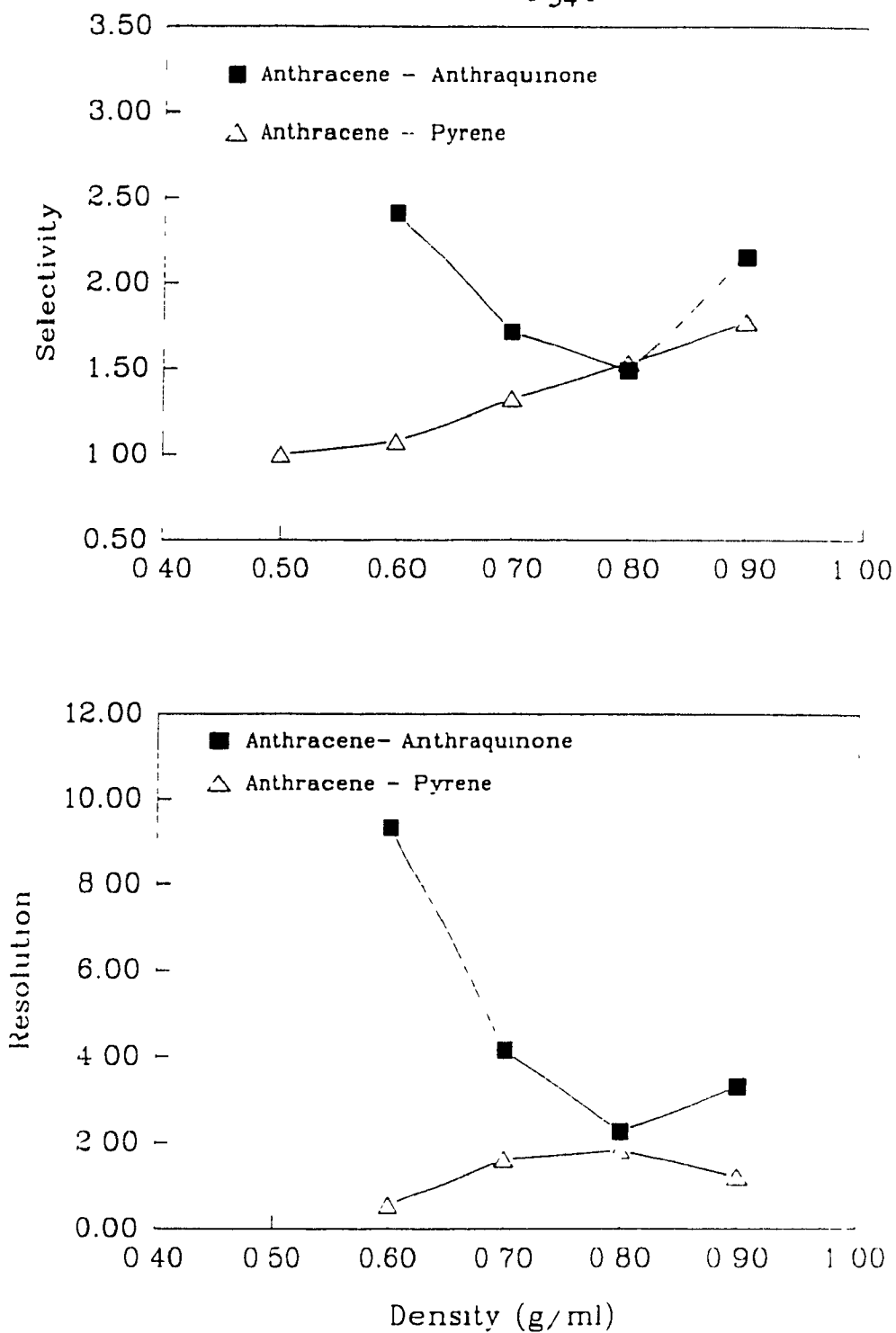


Figure 3.11 Selectivity (a) and resolution (b) as a function of density at 60°C.

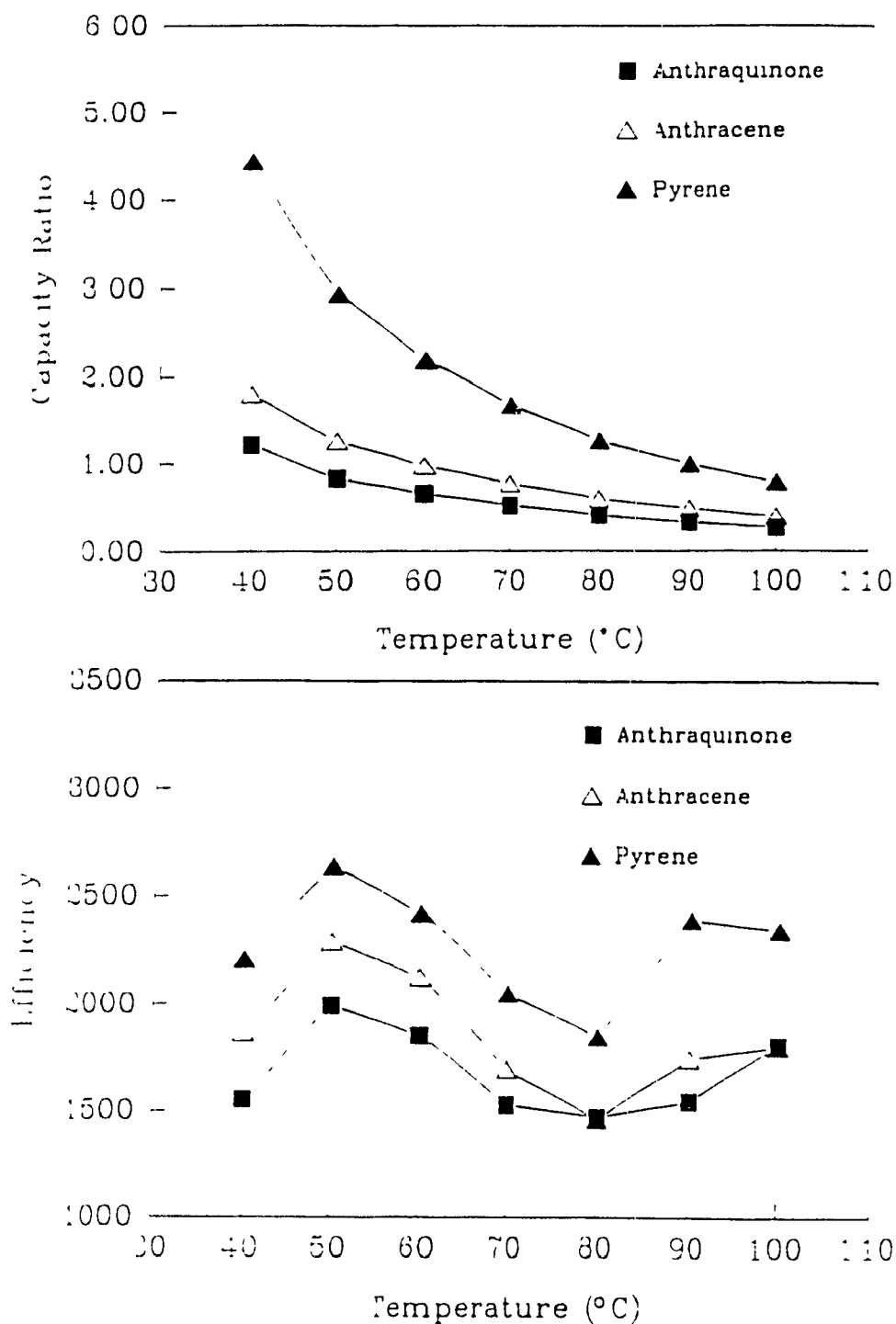


Figure 3.12 Capacity ratio (a) and efficiency (b) as a function of temperature at constant density (0.7 g/ml). Mobile phase: formic acid (1.26 mole%) in carbon dioxide.

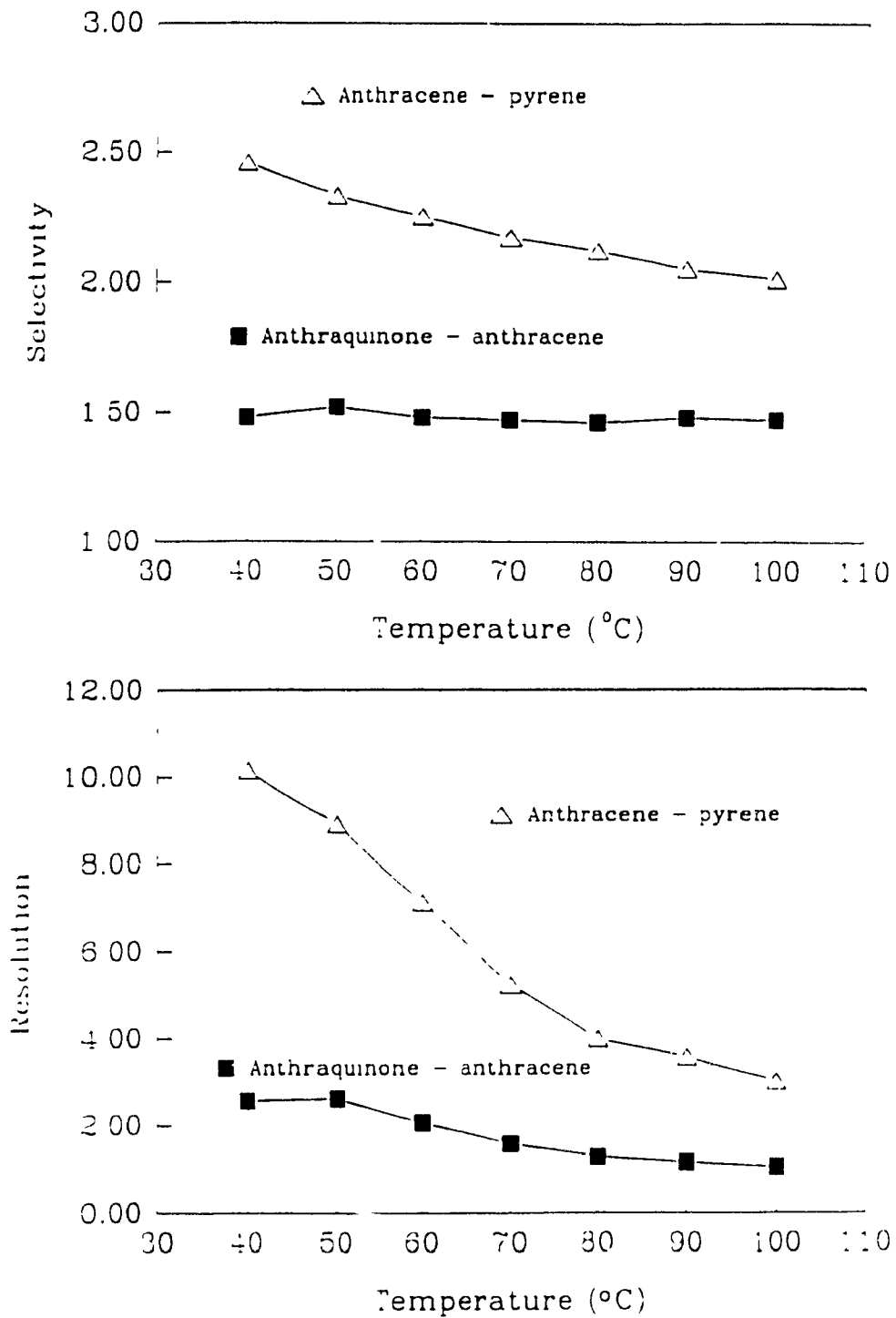


Figure 3.13

Selectivity (a) and resolution (b) as a function of temperature at constant density (0.7 g/ml). Mobile phase: formic acid (1.26 mole%) in carbon dioxide.

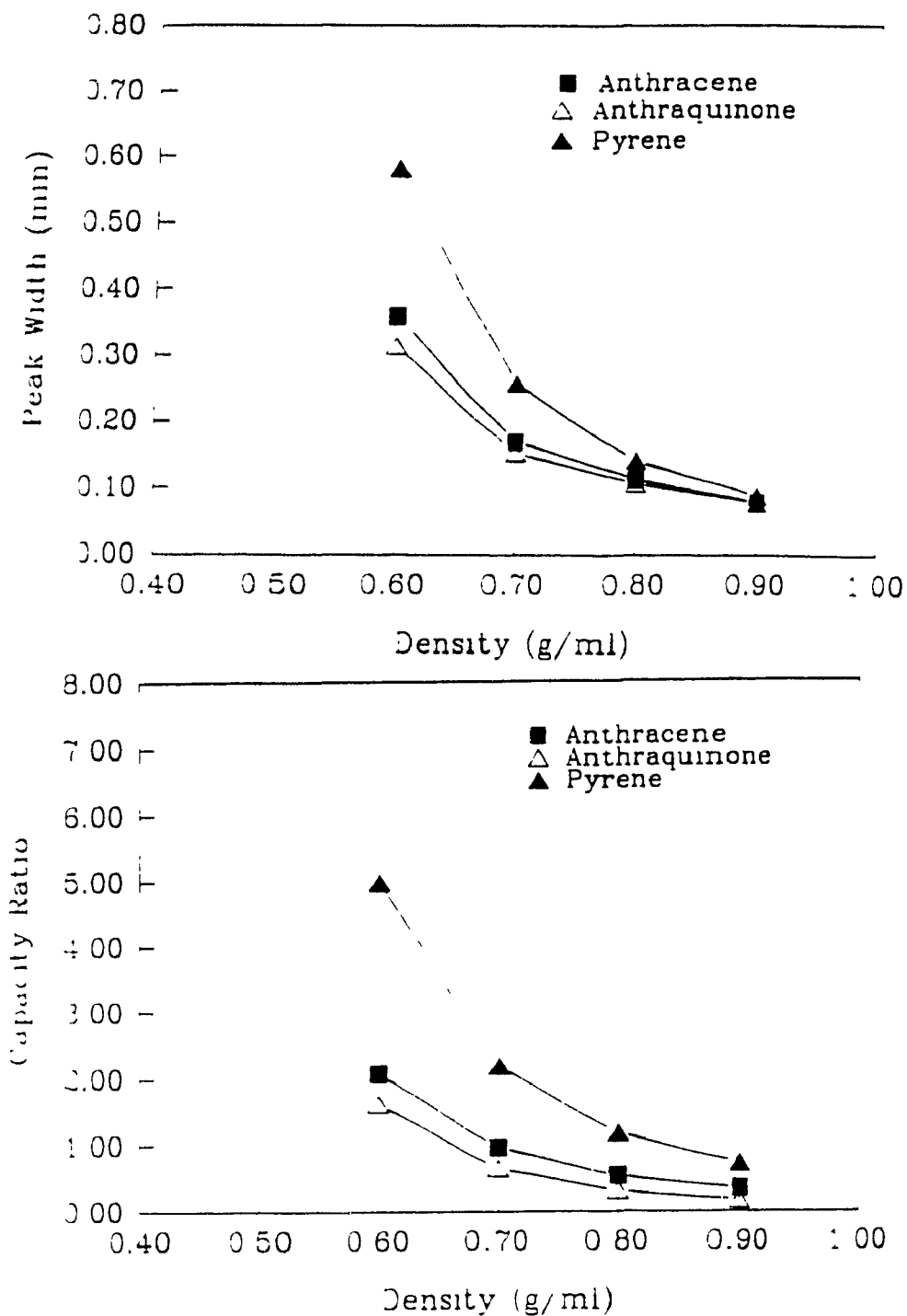


Figure 3.14

Peak widths (a) and capacity ratios (b) as a function of density at constant temperature (60°C). Mobile phase: formic acid (1.26 mole%) in carbon dioxide.

between the two is constant (Figure 3.15). Both the selectivity and resolution for the anthracene/pyrene pair decrease with increasing density. Addition of an increased amount of formic acid essentially has little effect on the chromatographic properties of the solutes.

Since the addition of formic acid decreased both the peak width and capacity factor, it must modify both the stationary phase surface and at least to some extent increase the solubility of the solutes in the mobile phase. Increasing the formic acid content had little effect on retention, indicating its modifying ability is limited.

3.3.2.4 Dichloromethane/formic acid modified carbon dioxide

A third component was added to the formic acid (0.16 mole %) modified mobile phase in order to assess its influence on capacity ratio. Dichloromethane, a solvent in which all the solutes are soluble, was added at a concentration of 0.87 mole % in order to increase the solubility of the compounds in the mobile phase and because of its low response in both FID and UV detection systems and its intrinsic solubility in supercritical carbon dioxide. Dichloromethane was added in an attempt to decrease solute retention times while the formic acid covered up the active sites on the silica support. However, since a decrease in capacity ratios causes peak widths to decrease, it is not possible to distinguish between the two mechanisms

Capacity ratios decreased with an increase in density, in a similar pattern to that obtained with the three previous mobile phases (Figure 3.16a); little change occurred at increasing temperature (Figure 3.16b). For anthraquinone/anthracene both the selectivity and resolution increased with density. Selectivity and resolution for anthracene/pyrene both decreased with increasing density (Figure 3.17)

3.3.2.5 Acetonitrile modified carbon dioxide

Finally the effects of acetonitrile modifiers on the chromatographic performance of the test mixture were investigated. This was carried out for two

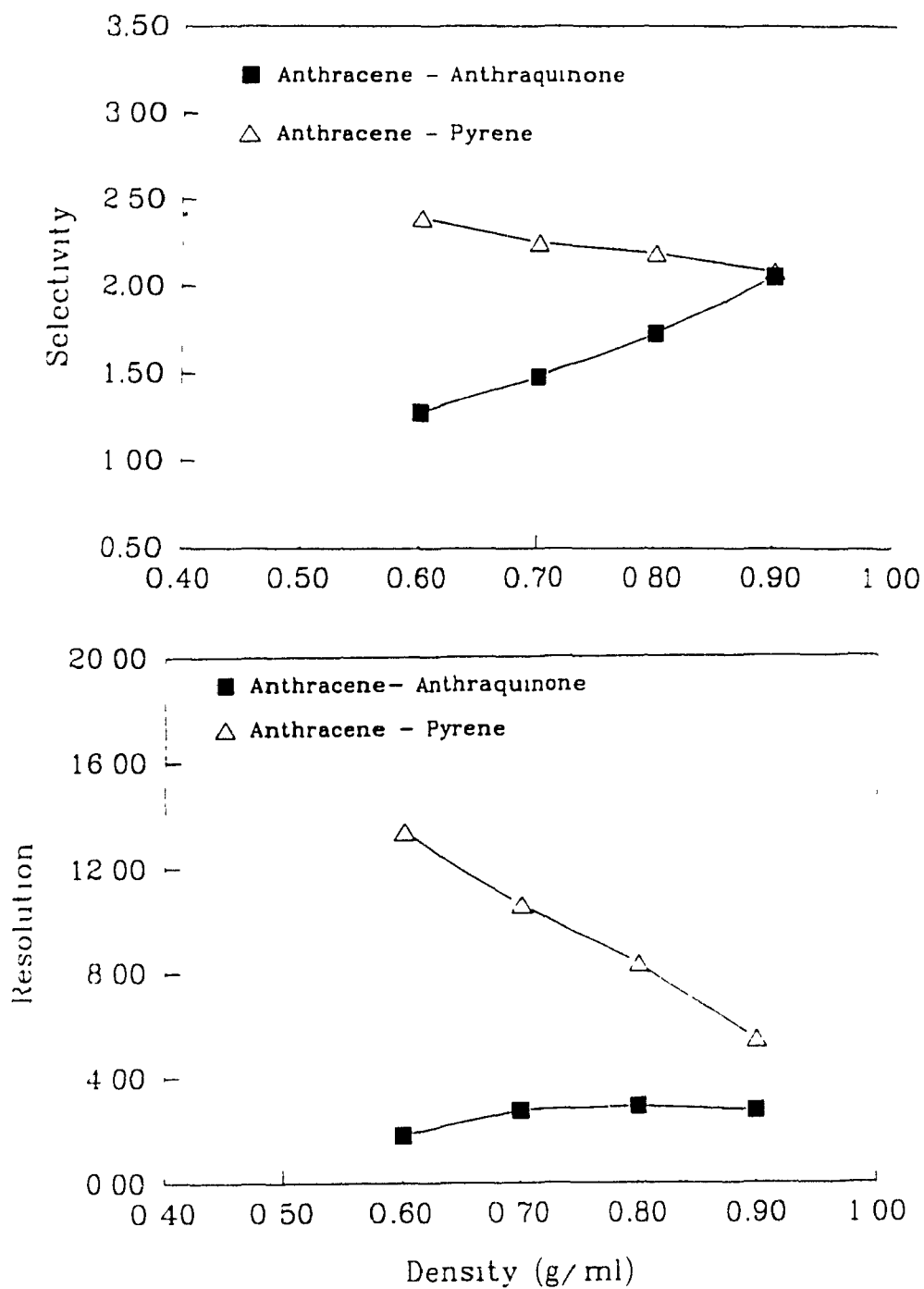


Figure 3.15

Selectivity (a) and resolution (b) as a function of density at constant temperature (60°C). Mobile phase: formic acid (1.26 mole%) in carbon dioxide.

reasons: (i) since acetonitrile increases the polarity of the mobile phase, it extends the range of supercritical CO₂ making it useful for the separation of phenothiazinones (see chapter 4), a series of relatively polar compounds; and (ii) the feasibility of an electrochemical detection system for SFC was also under investigation and acetonitrile/tetrabutyl ammonium salt modified carbon dioxide provided the necessary conductivity to the mobile phase.

Peak widths decreased for anthraquinone, anthracene and pyrene with increasing temperature at constant density. Little change was obtained in capacity ratios for the three compounds with increasing temperature (Figure 3.18). Temperature also had a minimal effect on resolution and selectivity for the three solutes (Figure 3.19). At constant temperature both peak widths and capacity ratios decreased at higher densities (Figure 3.20). Selectivity increased for anthraquinone/anthracene pair with increasing mobile phase density, but remained constant for anthracene/pyrene pair (Figure 3.21a). Resolution between anthracene and pyrene decreased rapidly with increasing density (Figure 3.21b).

3.3.3 Modifier effects.

3.3.3.1 Effects on retention times

The results of the previous investigation indicate that mobile phase density is the main factor controlling retention. Under isobaric conditions, temperature has a minimal effect on retention parameters. Hence comparisons of modifier effects should be made at equivalent densities under isothermal conditions. The capacity ratios for anthraquinone (Figure 3.22a), anthracene (Figure 3.23a) and pyrene (Figure 3.24a) are plotted as a function of density at a constant temperature of 60°C for simple carbon dioxide and three modified CO₂ mobile phases. Capacity ratios were highest for the three compounds in the supercritical carbon dioxide mobile phase. The order of decrease in k' values was dependent on the solute. For anthraquinone, the next highest values were obtained for 0.25 mole% formic acid/CO₂ mixture and the lowest

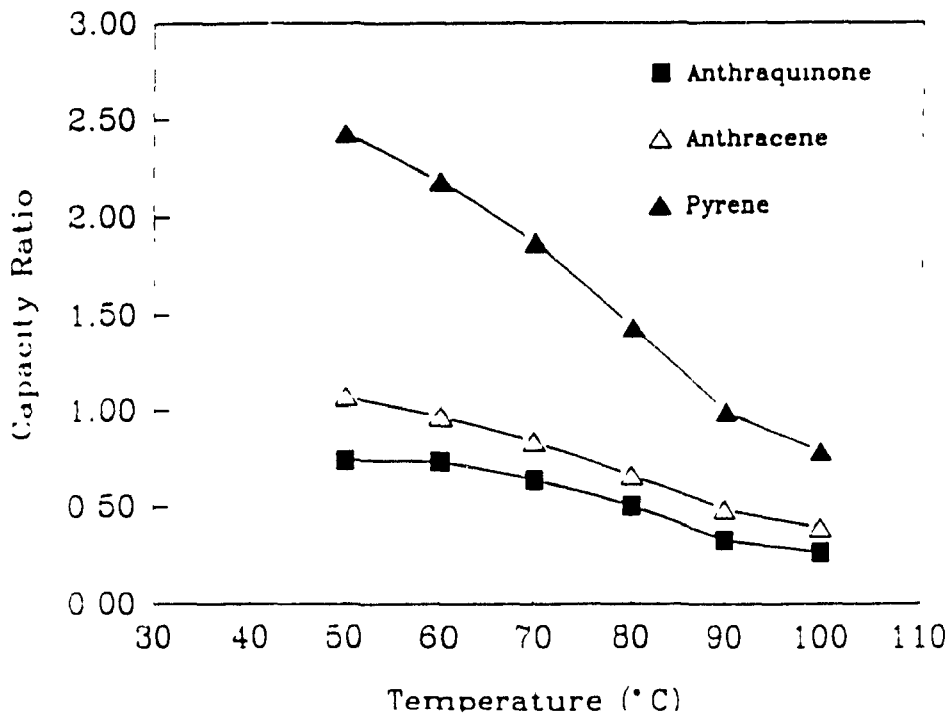
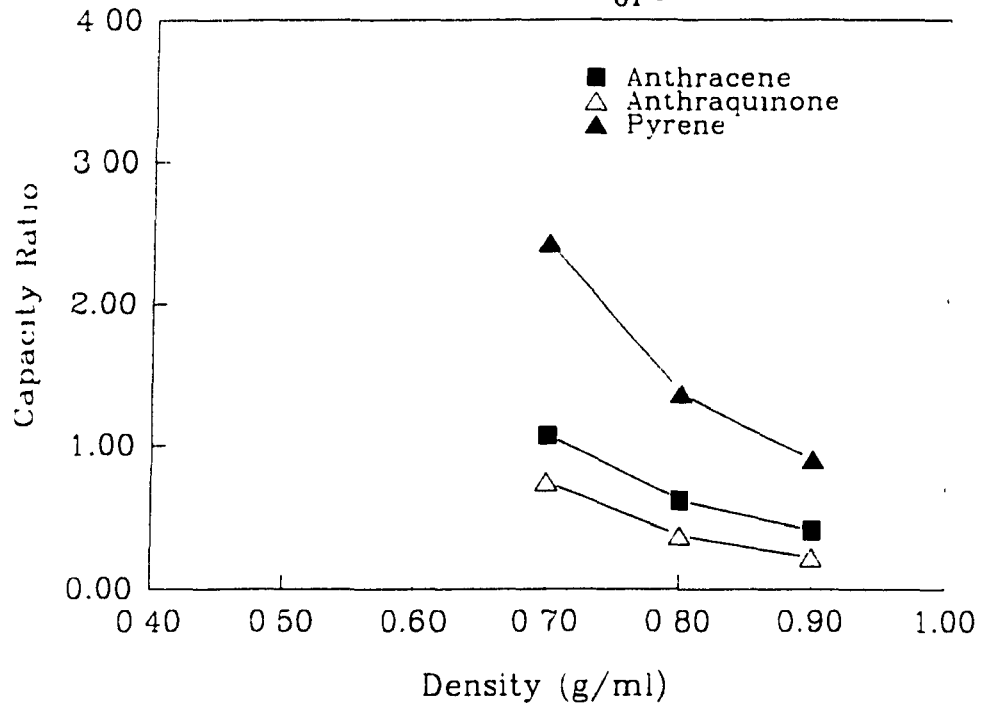


Figure 3.16

k' as a function of density at constant temperature (60°C) and k' as a function of temperature at constant density (0.7g/ml) Mobile phase: 0.87 mole% dichloromethane/0.16 mole% formic acid/carbon dioxide.

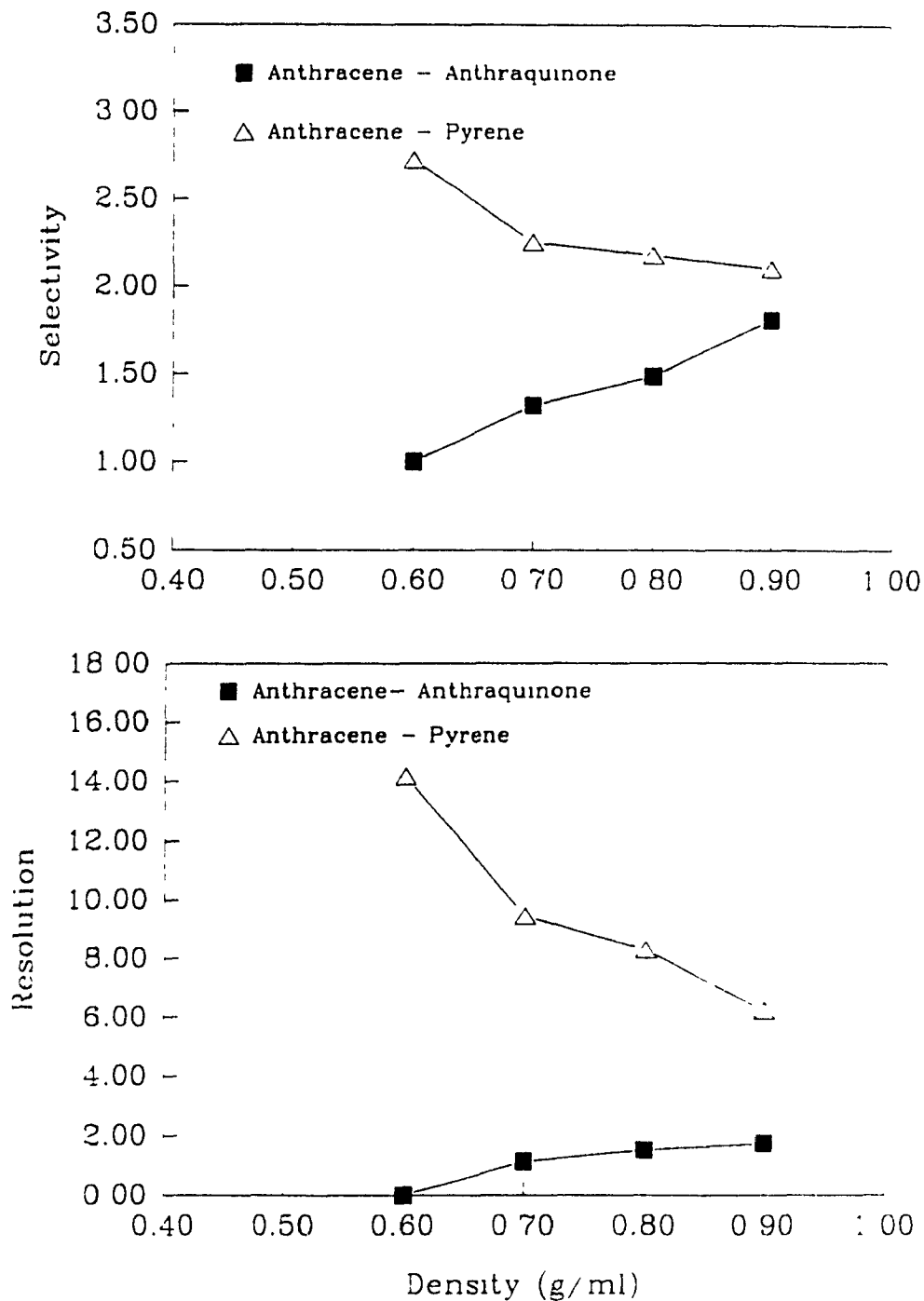


Figure 3.17

Selectivity (a) and resolution (b) as a function of density at constant temperature (60°C). Mobile phase 0.87 mole % dichloromethane/0.16 mole% formic acid/carbon dioxide.

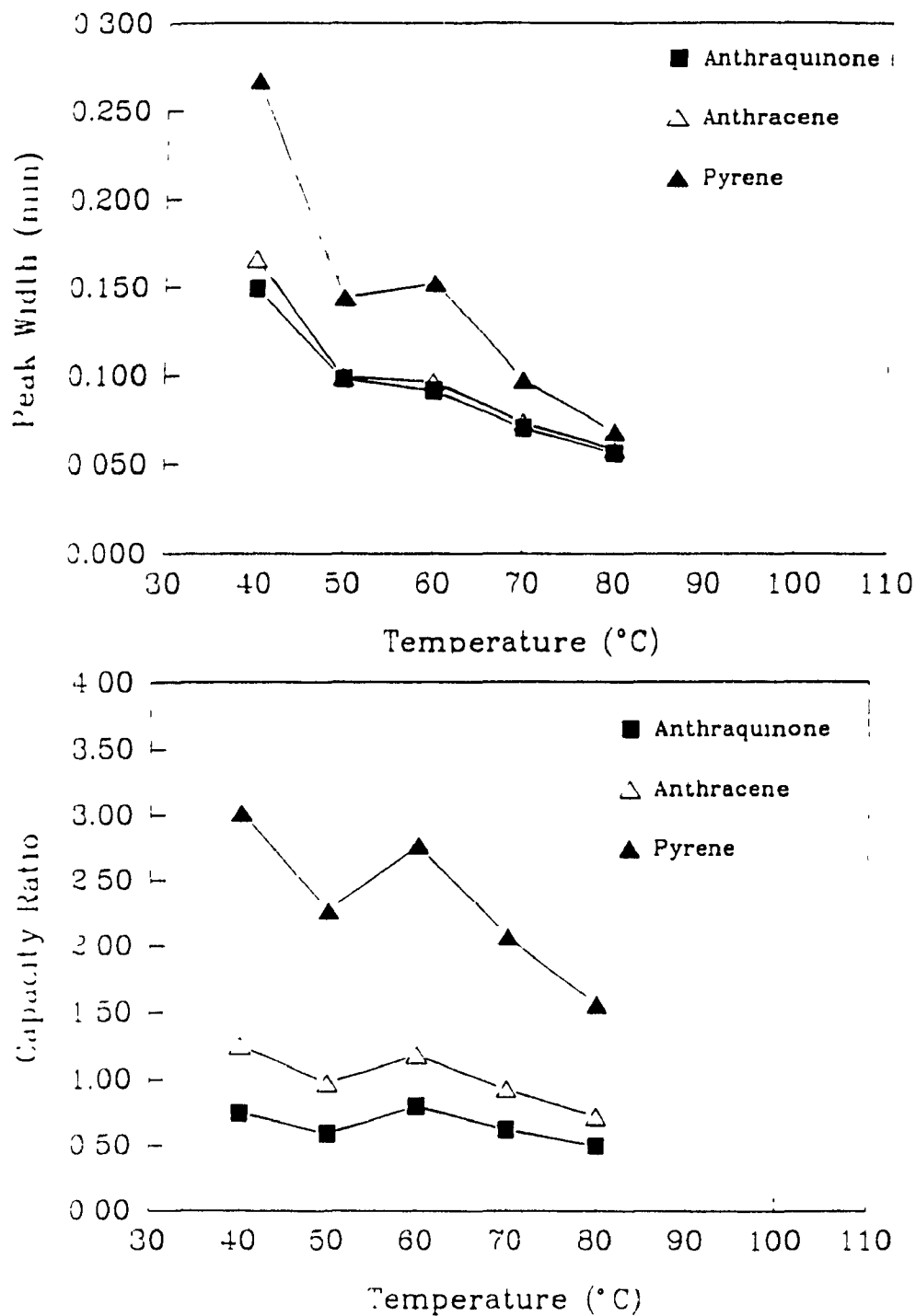


Figure 3.18 Peak widths (a) and capacity ratios (b) plotted against temperature at constant density (0.7 g/ml). Mobile phase: 0.8 mole% acetonitrile in carbon dioxide.

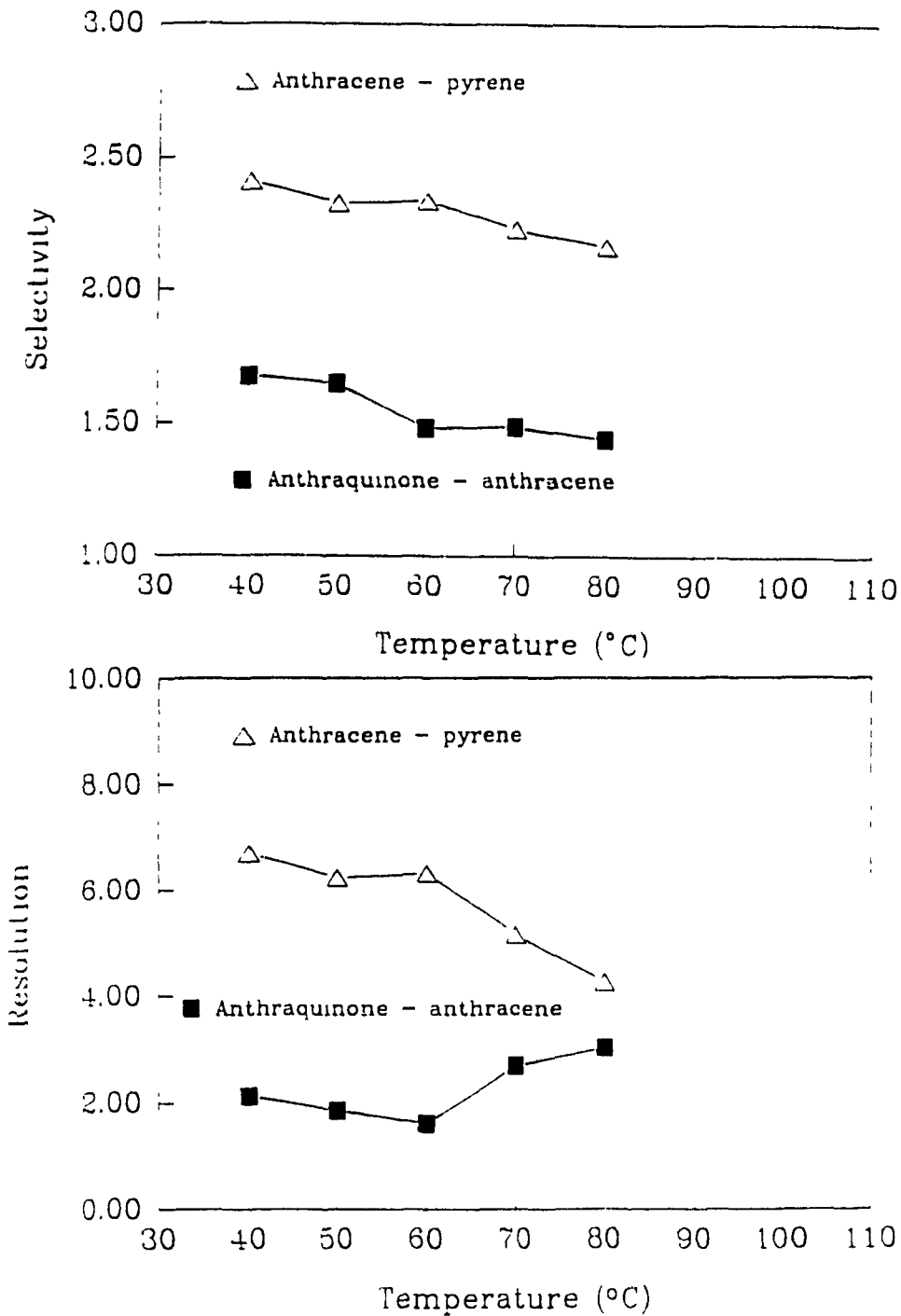


Figure 3.19

Selectivity (a) and resolution (b) as a function of temperature at constant density (0.7 g/ml). Mobile phase 0.8 mole% acetonitrile in carbon dioxide.

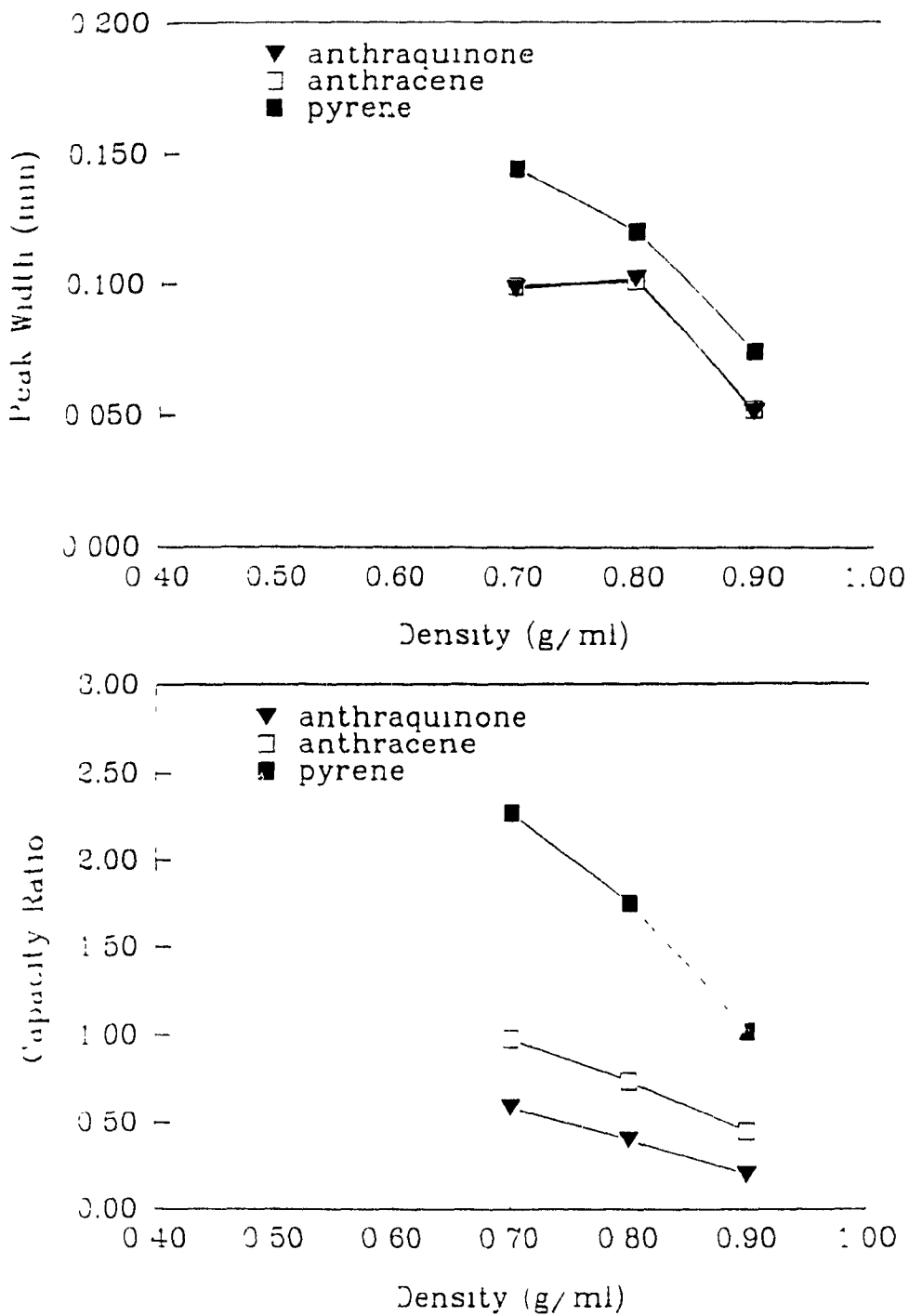


Figure 3.20 Peak widths (a) and capacity ratios (b) as a function of density at 60°C. Mobile phase: 0.8 mole% acetonitrile in carbon dioxide.

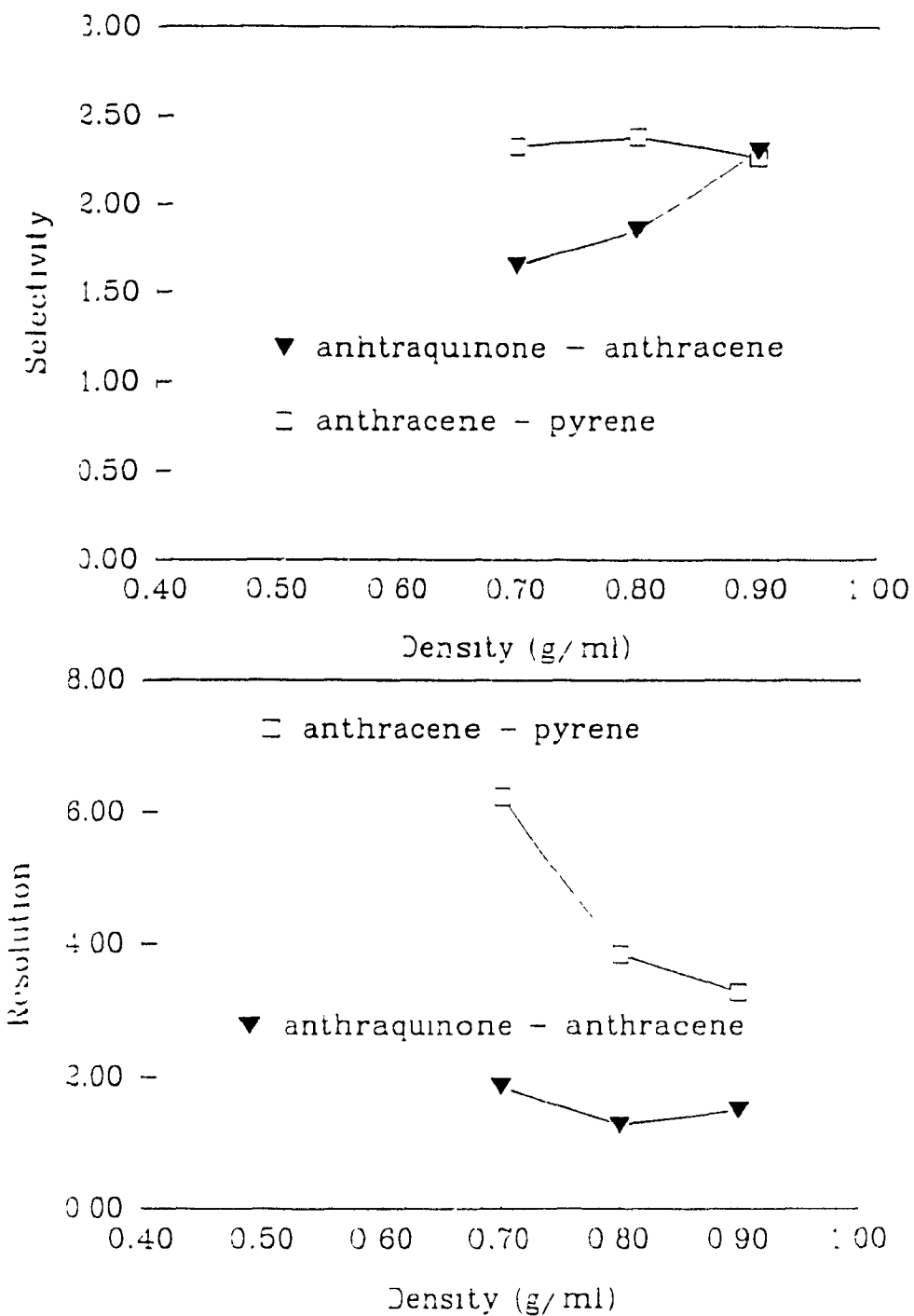


Figure 3.21 Selectivity (a) and resolution (b) as a function of density at constant temperature (60°C). Mobile phase: 0.8 mole% acetonitrile in carbon dioxide.

values for the 1.26 mole% formic acid/carbon dioxide mobile phase. The dichloromethane actually decreases the polarity of the mobile phase as compared to the phase with higher formic acid content, therefore decreasing the solubility of the polar anthraquinone molecule. Anthracene is retained least in the dichloromethane/formic acid/carbon dioxide mobile phase at lower densities, while capacity ratios are equivalent to those in the 1.26% formic acid/CO₂ mobile phase at higher densities. Capacity ratios for pyrene are similar for both CH₂Cl₂/CHO₂H/CO₂ and CHO₂H/CO₂.

Capacity ratio values were compared at equivalent densities (0.7 g/ml) as a function of temperature for the five mobile phases. Anthraquinone (Figure 3.22b), anthracene (Figure 3.23b) and pyrene (Figure 3.24b) showed decreases in k' values with increasing temperature, indicating greater solvation of the solutes at higher temperatures. Only slight changes were obtained with the acetonitrile modified CO₂, suggesting that the k' is affected more by enhancement of solubility by this modifier than temperature. k' values for the dichloromethane/formic acid/ carbon dioxide mobile phase showed only a small decrease with increasing temperature. At constant density much greater changes in k' values were obtained for small changes in density. At 60°C only two densities were investigated for the acetonitrile/carbon dioxide mobile phase.

In this study plate height comparison could not be carried out, since a change in density and/or temperature results in changing linear velocities. Information on peak shape and symmetry is included in plate height and plate number measurements. Peak distortion during the length of time a substrate migrates through the column is dependent on the linear velocity of the eluent. Chromatograms of the test mixture are compared at equivalent densities of 0.7 g/ml and a temperature of 60°C (Figure 3.25). Addition of the modifier has decreased the analysis times, especially for the larger compounds, for each type of modifier. Although dichloromethane was added to the formic acid modified CO₂ to increase the solubility of the compounds in the mobile phase, it had little effect on retention times. Peak shape of some compounds change noticeably; a greater response and sharper peak was obtained for pyrene and a

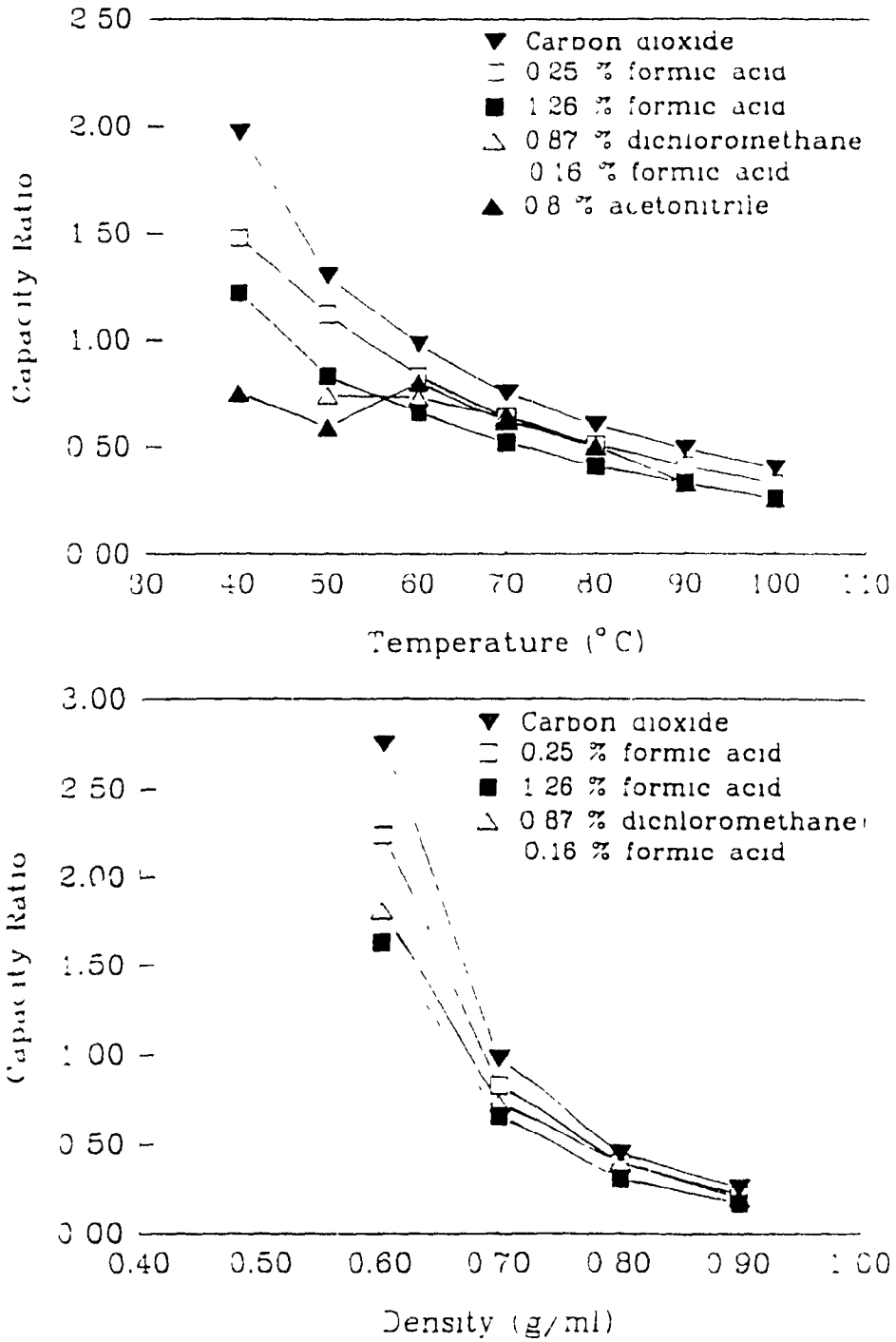


Figure 3.22 Plot of k' versus temperature at constant density (0.7 g/ml) (a) and versus density at constant temperature (60°C) (b) for anthraquinone.

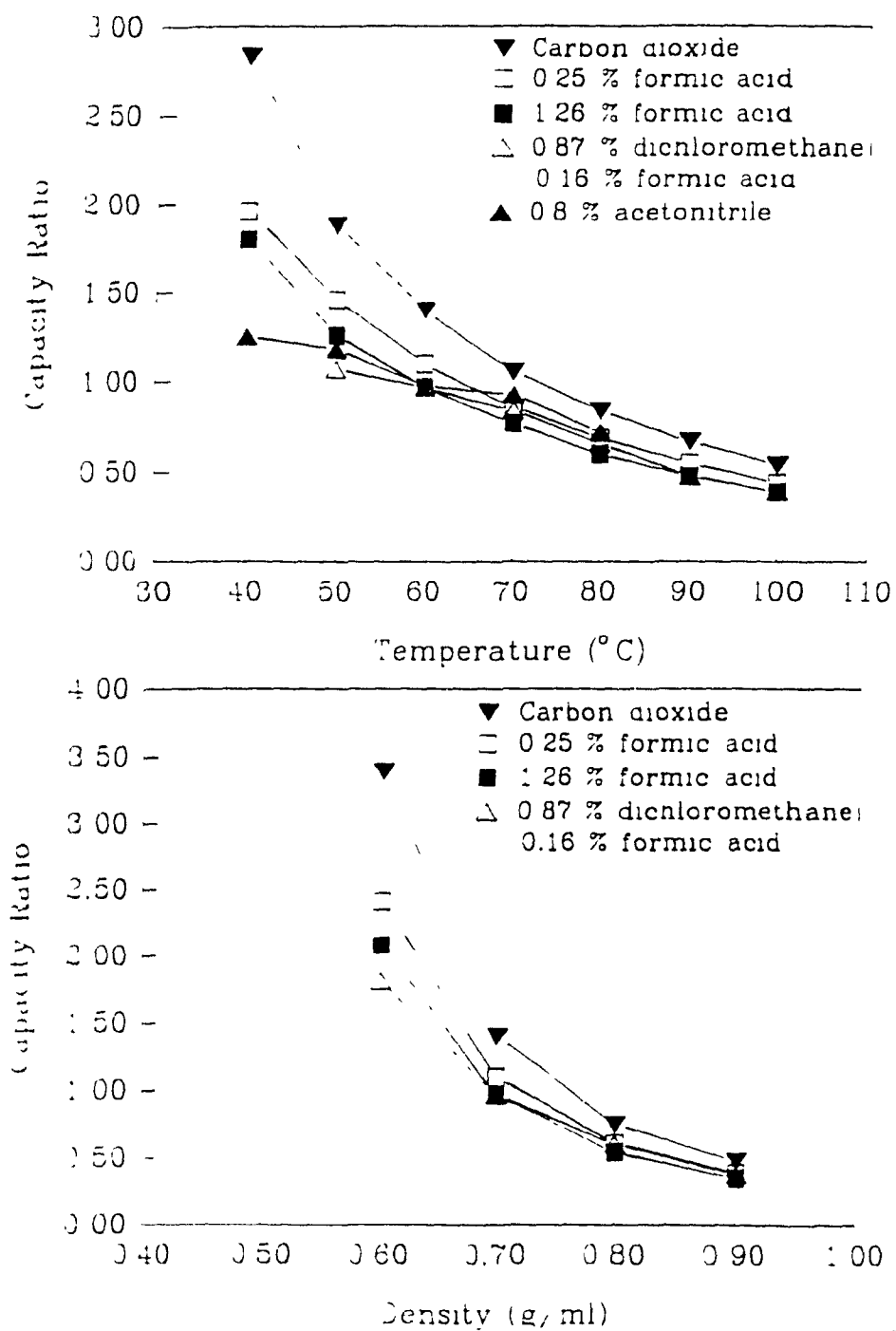


Figure 3.23 Plot of k' versus temperature at constant density (0.7 g/ml) (a) and versus density at constant temperature (60°C) (b) for anthracene.

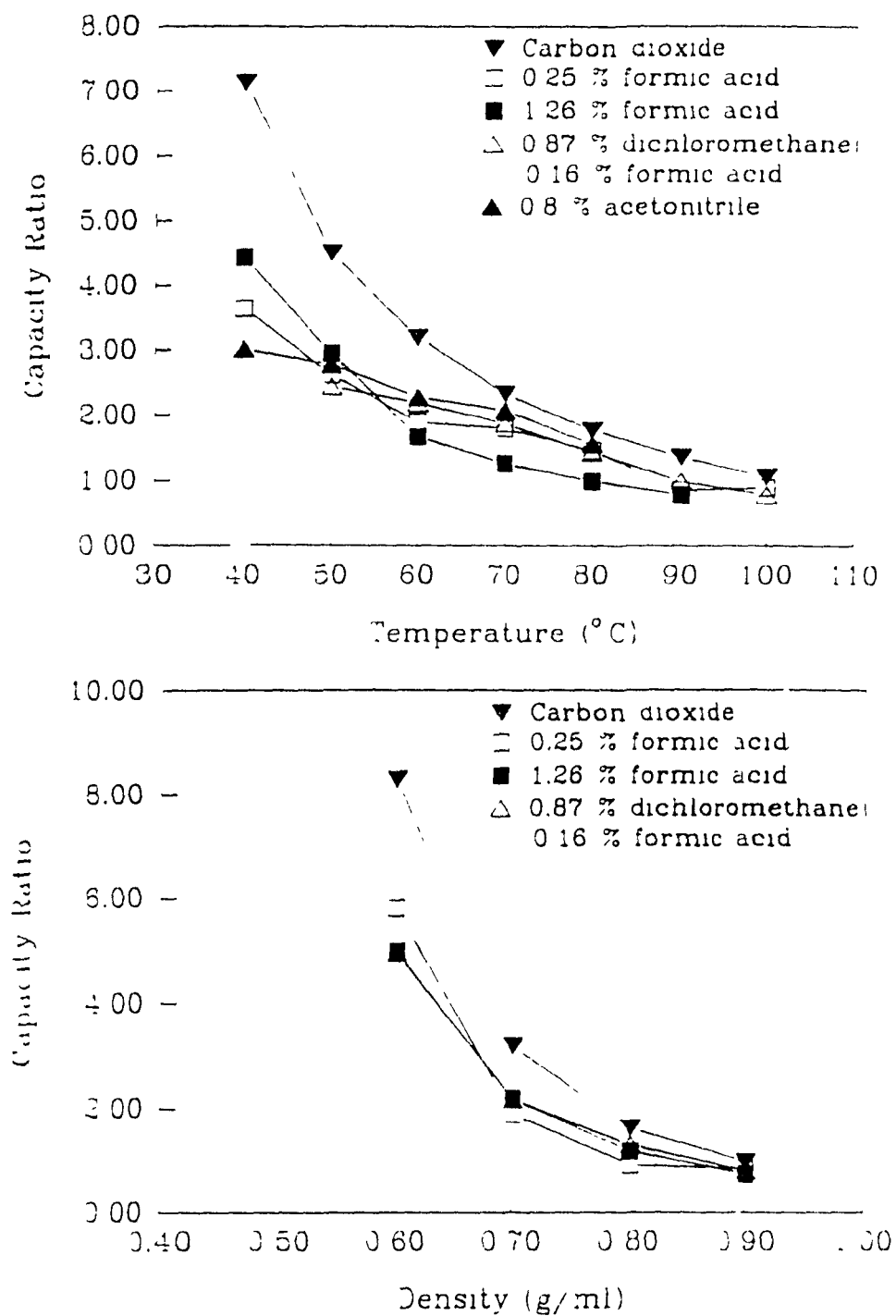


Figure 3.24 Plot of k' versus temperature at constant density (0.7 g/ml) (a) and versus density at constant temperature (60°C) (b) for pyrene.

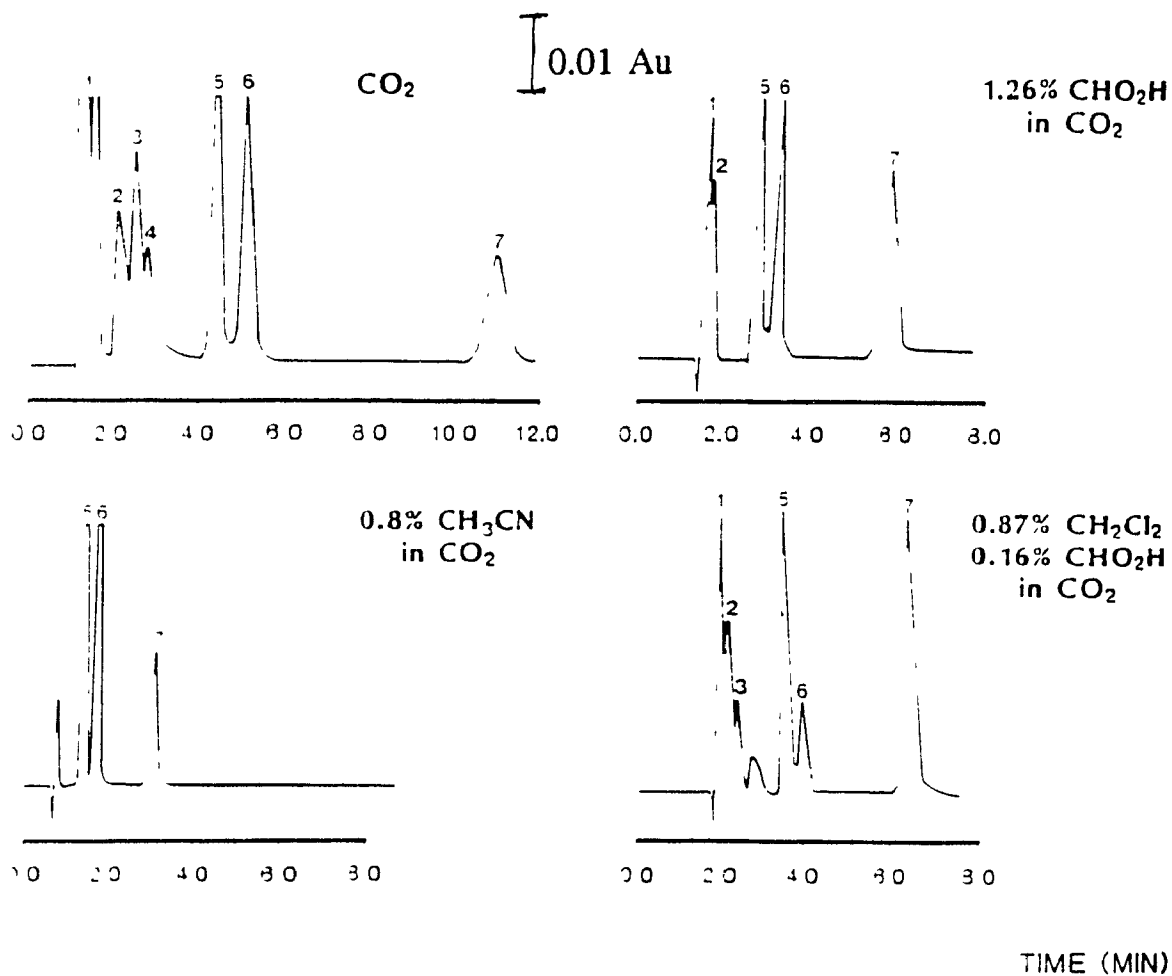


Figure 3.25

Chromatograms of model compounds in three modified and simple carbon dioxide mobile phases at constant temperature (60°C) and equivalent densities (0.7 g/ml).

decreased response for anthracene was recorded. The addition of acetonitrile modifier to the carbon dioxide resulted in better resolution between anthracene and anthraquinone and increased response for the pyrene, anthracene and anthraquinone, indicating greater solubility of these compounds in this mobile phase.

3.3.3.2 Effects on enthalpy of transfer between mobile and stationary phases

At constant pressure, the dependence of capacity ratios on temperature can be calculated by the van't Hoff equation,

$$\left(\frac{\partial \ln k'}{\partial T^{-1}} \right)_P = - \frac{\Delta H}{R} \quad (3.9)$$

where ΔH = enthalpy for the transition of a solute between the mobile and stationary phases.

At constant density, the slope of the plot of $\ln(k')$ as a function of the inverse temperature is equal to the effective enthalpy of solute transfer between the mobile phase and stationary phase, according to the following equation,

$$\left(\frac{\partial \ln k'}{\partial T^{-1}} \right)_\rho = \delta + \Delta H - \Delta H_T \quad (3.10)$$

Plots of $\ln(k')$ as a function of the inverse of temperature (van't Hoff plots) are linear. The slope of these plots represents the transition enthalpy. Figures 3.26 - 3.28 are representative for anthraquinone; enthalpy values are summarized in Table 3.1. A linear dependence of enthalpy with density, where the greatest solvation occurs at higher densities (less negative values) is indicative of a partition-like mechanism. Non-linear behaviour is attributed to solvation or swelling of the bonded phase by the mobile phase. Enthalpy values have been plotted for anthraquinone (Figure 3.29),

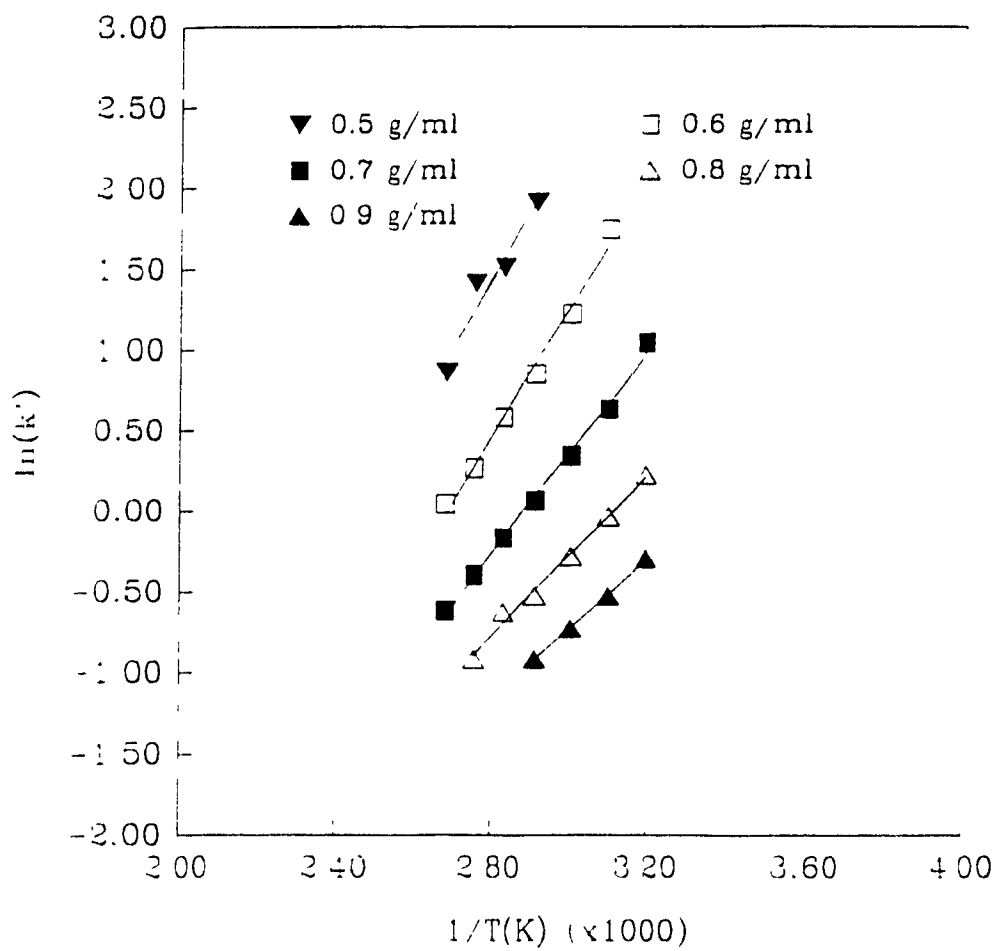


Figure 3.26 van't Hoff plot for anthraquinone in supercritical carbon dioxide.

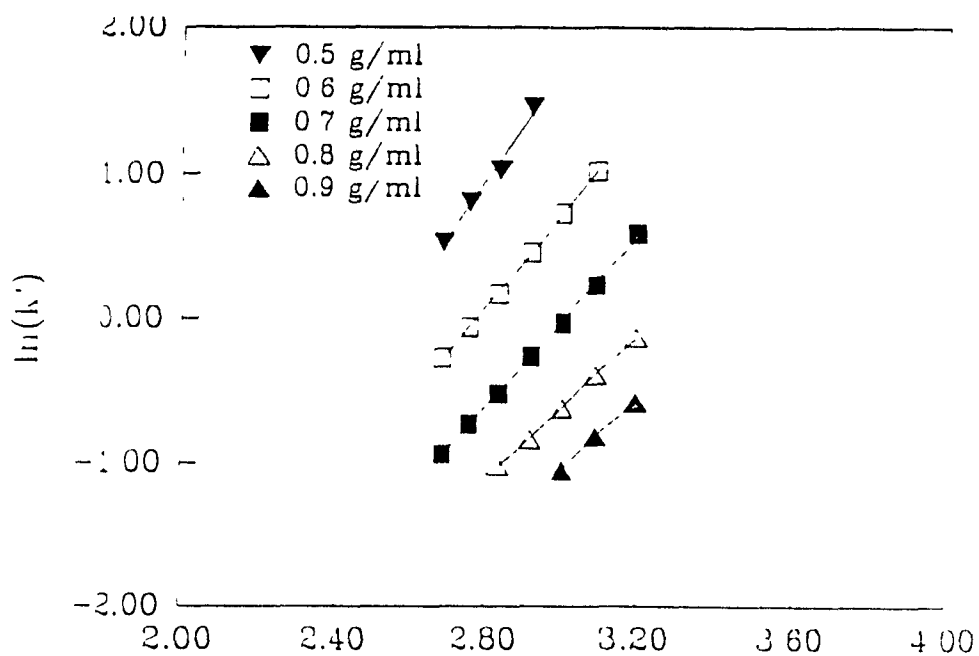
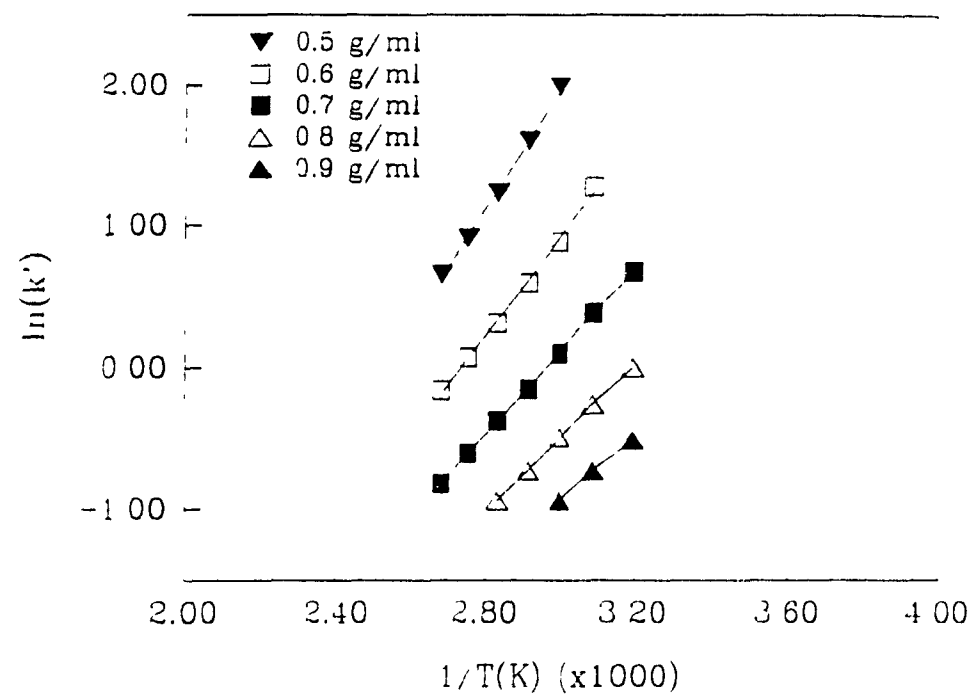


Figure 3.27

van't Hoff plot for anthraquinone in (a) 0.25 mole% and (b) 1.26 mole% formic acid in carbon dioxide.

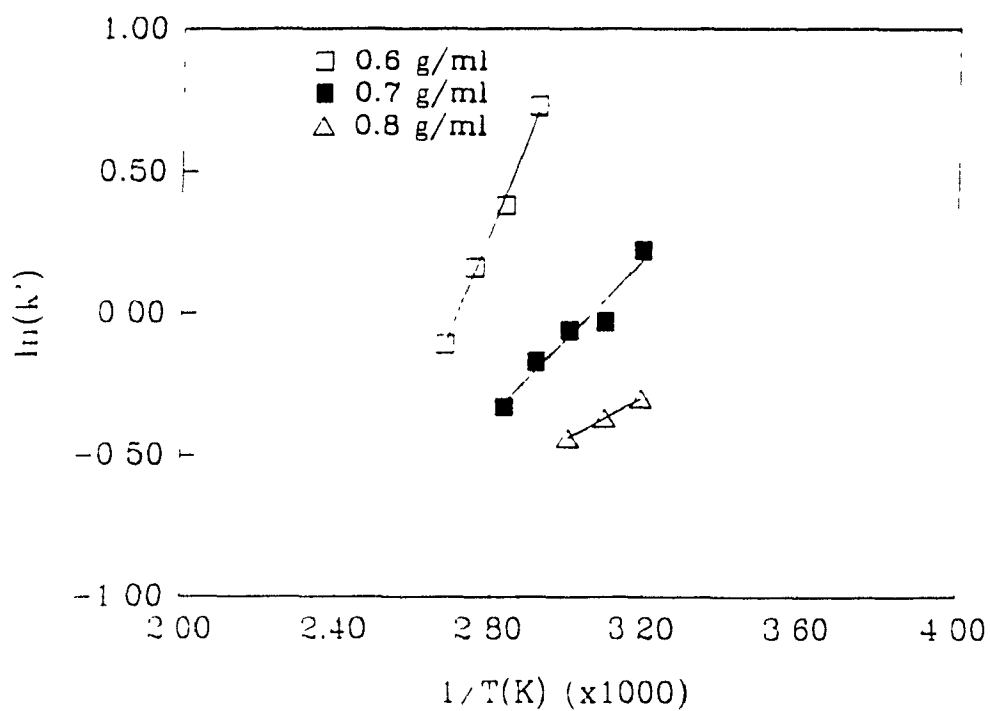
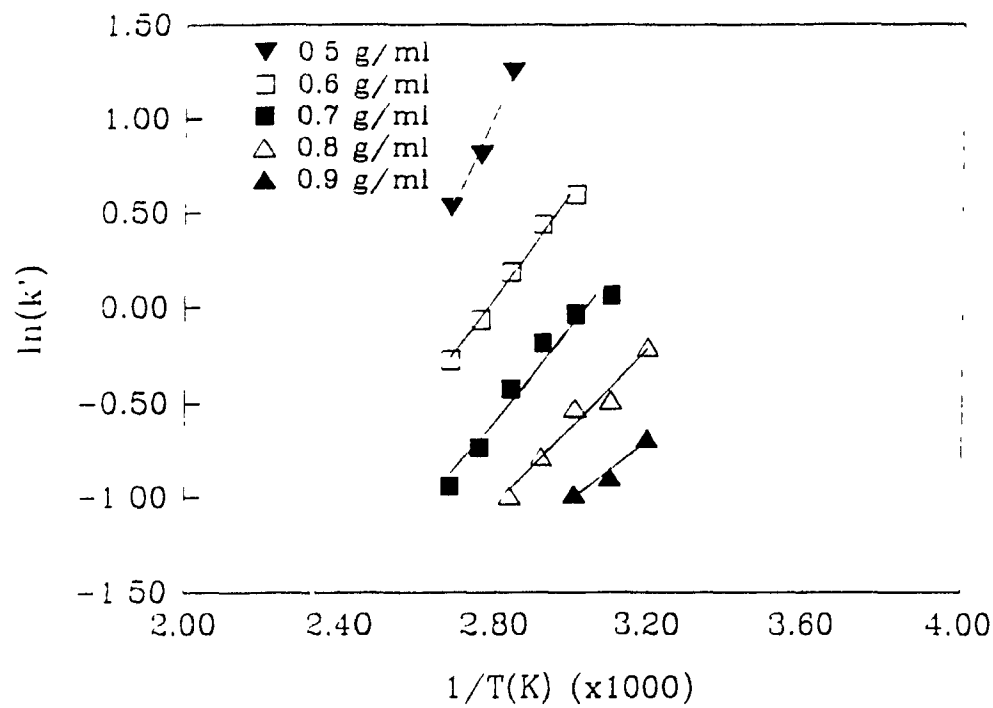


Figure 3.28

van't Hoff plot for anthraquinone in (a) 0.87 mole% $\text{CH}_2\text{Cl}_2/0.16$ mole% $\text{CHO}_2\text{H}/\text{CO}_2$ and (b) 0.8 mole% acetonitrile in carbon dioxide.

Table 3.1 Linear regression of van't Hoff plots

Compound		Anthraquinone		Anthracene		Pyrene	
Mobile phase	ρ	Slope	r^2	Slope	r^2	Slope	r^2
CO ₂	0.5	-10.74	0.9060	-10.17	0.9347	-10.85	0.9258
	0.6	-10.99	0.9865	-10.83	0.9896	-11.54	0.9912
	0.7	-9.09	0.9929	-9.13	0.9960	-9.71	0.9964
	0.8	-7.63	0.9777	-7.80	0.9914	-8.51	0.9988
	0.9	-7.28	0.9938	-7.38	0.9996	-7.92	0.9982
CHO ₂ H (0.25%) in	0.5	-10.63	0.9979	-10.63	0.9978	-10.61	0.9978
	0.6	-9.79	0.9985	-9.31	0.9968	-9.90	0.9964
	0.7	-8.94	0.9995	-8.55	0.9998	-9.17	0.9582
	0.8	-9.16	0.9999	-8.30	0.9998	-7.77	0.9692
	CO ₂	0.9	-6.95	0.9806	-7.67	1.0000	-7.86
CHO ₂ H (1.26%) in	0.5	-10.06	0.9864	-9.83	0.9849	-10.31	0.9878
	0.6	-8.46	0.9932	-8.71	0.9992	-9.12	0.9988
	0.7	-9.09	0.9966	-8.80	0.9982	-9.15	0.9978
	0.8	-8.61	0.9982	-8.40	0.9991	-8.48	0.9996
	CO ₂	0.9	-8.97	0.9997	-8.02	1.0000	-8.75
CH ₂ Cl ₂ (0.87%)	0.5	-13.75	0.9760	-12.23	0.9876	-13.03	0.9860
CHO ₂ H (0.16%) in	0.6	-9.61	0.9542	-7.70	0.9914	-9.41	0.9740
	0.7	-8.83	0.9388	-7.65	0.9586	-7.76	0.9506
	0.8	-6.84	0.9752	-6.83	0.9645	-6.85	0.9655
	0.9	-5.68	0.9423	-5.71	0.9569	-5.91	0.9803
CH ₃ CN (0.8%) in	0.6	-9.75	0.9926	-9.53	0.9942	-9.86	0.9962
	0.7	-4.06	0.9196	-4.21	0.9454	-4.44	0.9561
	CO ₂	0.8	-2.58	0.9997	-2.63	0.9996	-2.90

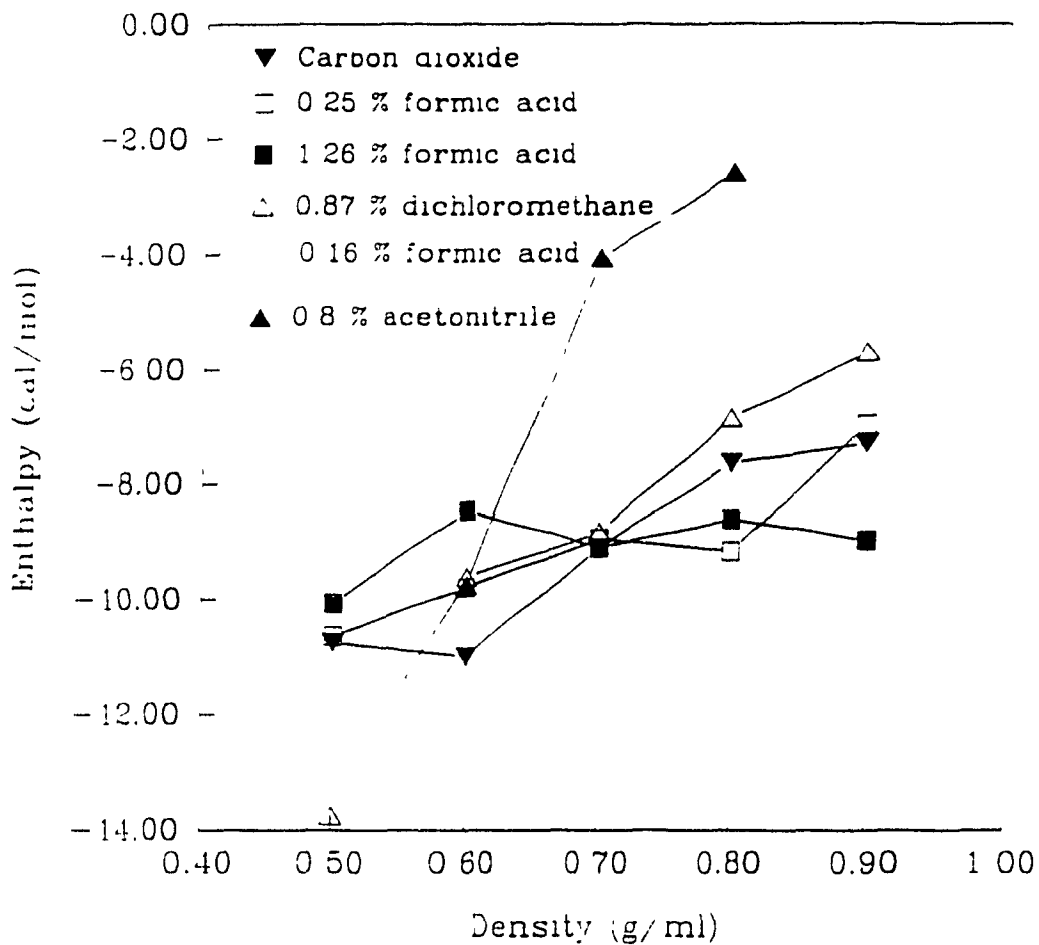


Figure 3.29

Enthalpy as a function of density for anthraquinone for each mobile phase investigated.

anthracene (Figure 3.30) and pyrene (Figure 3.31) as a function of density for each mobile phase investigated. All relationships were linear indicating no solvation of the C-18 bonded phase or the silica support. Enthalpy values become more negative as the density decreases, ultimately approaching the enthalpy values typical for GC. Both formic acid modified phases and the carbon dioxide mobile phase have the lowest enthalpy values which change very little with increasing density. For these mobile phases a change in density is not great enough to significantly change the solvent strength of the mobile phase. Dichloromethane/formic acid modified carbon dioxide gives higher enthalpy values at higher densities, while very low values are obtained at low densities. Acetonitrile modified carbon dioxide reaches less negative enthalpy values rapidly and has the smallest values for all the mobile phase compositions evaluated. This suggests that the greatest enhancement of the solvating power of the mobile phase for these compounds is obtained with the acetonitrile modifier.

The impact of the co-solvent on the retention mechanism in SFC can be also described in terms of the change in enthalpy for solute transfer between the mobile and stationary phases as a function of mobile phase composition (Figure 3.32). Enthalpy values show only small decreases for two concentrations of formic acid modified CO₂ and formic acid/dichloromethane modified carbon dioxide. A dramatic decrease in enthalpy is achieved with acetonitrile modifier, indicating greater solvating ability of this mobile phase.

Recently other investigations into the role of modifiers [10], density [11], temperature [12], pressure [13], linear velocity [14] in retention behaviour have been published. Some researchers [15] have reported a maximum in their plots of k' and resolution as a function of temperature or density, while our studies do not. These studies were conducted from subcritical to supercritical conditions and maxima were obtained at approximately critical conditions. If data from this study are compared to the studies in the literature conducted under supercritical conditions then similar trends are observed.

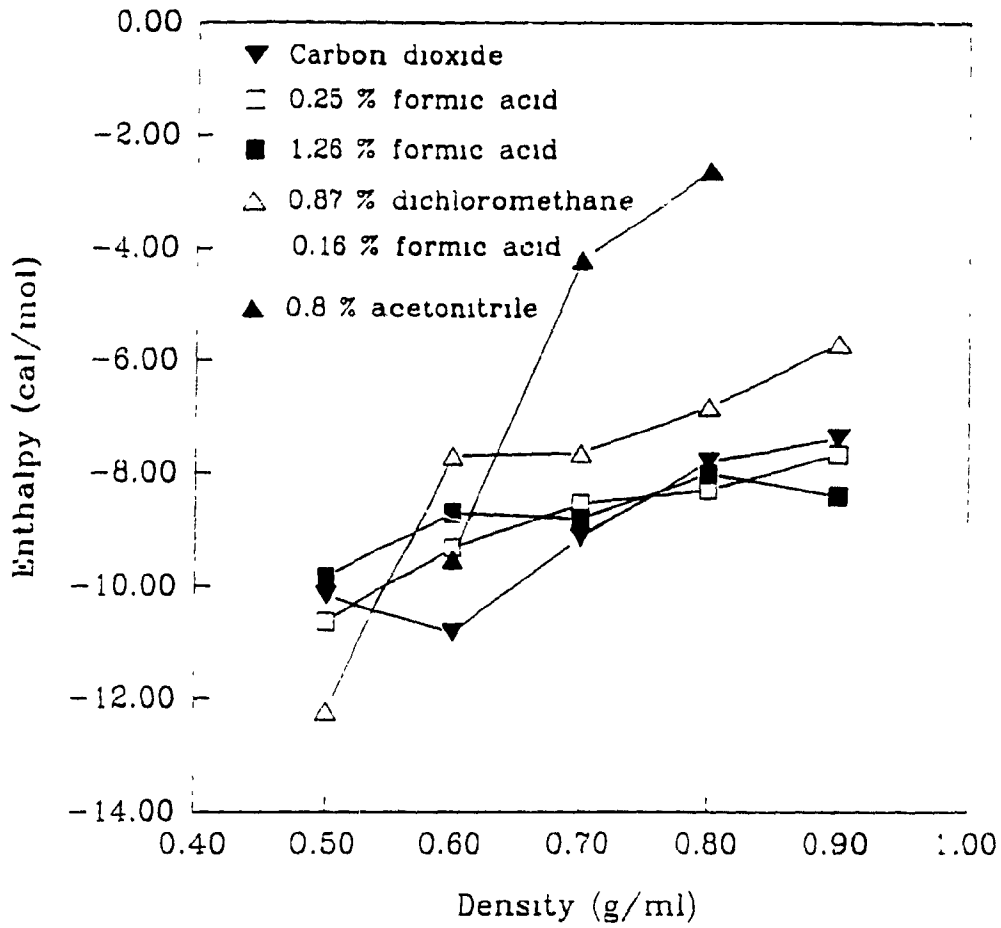


Figure 3.30

Enthalpy as a function of density for anthracene for each mobile phase investigated.

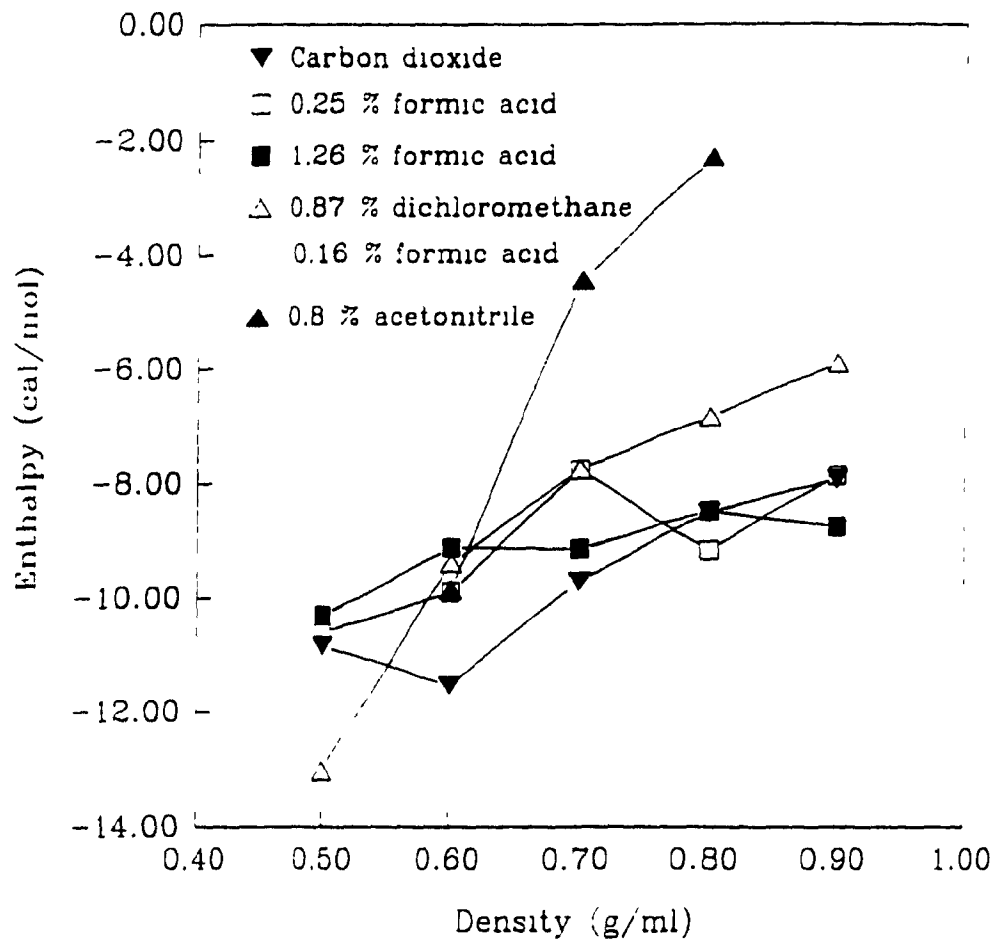


Figure 3.31

Enthalpy as a function of density for pyrene for each mobile phase investigated.

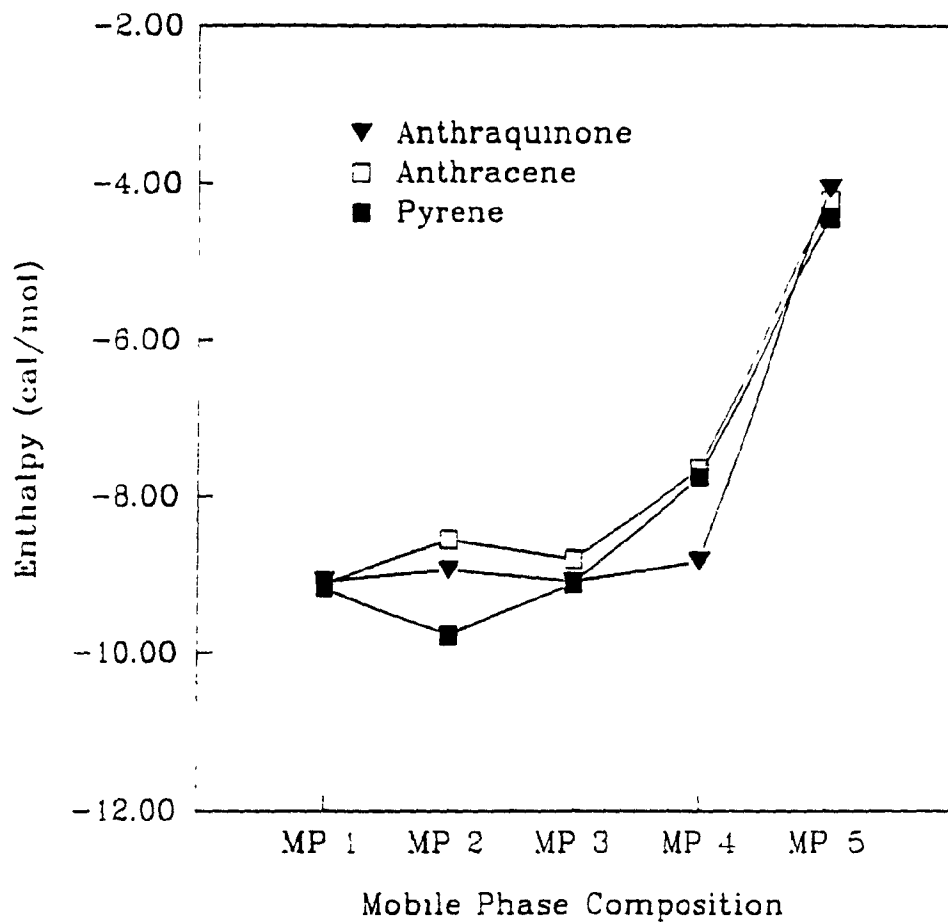


Figure 3.32

Enthalpy as a function of mobile phase composition at a density of 0.7 g/ml.

3.4 Conclusion

A model for the dependence of chromatographic parameters (k' , N , α , R) on temperature, density pressure, linear velocity and mobile phase composition requires instrumentation capable of varying one physical parameter independent of all others. At present this is not possible; studies of changing temperature under constant density conditions results in non-linear pressure changes and changes in density at constant temperature varies the linear velocity of the mobile phase. These studies on the retention behaviour as a function of physical parameters for a given chromatographic system provide a means to determine initial conditions for a particular application. Changes in retention are best understood in terms of changes in density for a particular mobile phase, where the capacity ratio decreases non-linearly with increasing density. At higher densities, the linear velocity also increases causing the solute to elute faster from the column, decreasing analysis times. An increase in temperature leads to a decrease in density with the resulting increase in retention. At constant density retention is only slightly affected by temperature.

The mobile phase modifier can alter the chromatographic process by increasing the solubility of the solutes in the mobile phase and by modifying the stationary phase. Although formic acid was added to supercritical carbon dioxide to cover up the active sites on the silica support, the decrease in both the peak widths and capacity ratios indicate both a modification of the stationary phase surface and the properties of the mobile phase. Dichloromethane modifier slightly increased the solvation of the solutes in the mobile phase. Acetonitrile doped carbon dioxide greatly improved peak shape for later eluting species and decreased analysis times. The less negative enthalpy values for the acetonitrile modified CO_2 demonstrates the greater solvating ability for this modifier.

3.5 References

1. J.C. Giddings, M.N. Myers, L. McLaren, and R.A. Keller, *Science*, **162** (1968) 67.
2. F.P. Schmitz and E. Klesper, *J. Chromatogr.*, **357** (1987) 3.
3. L.M. Bowman Jr., Doctoral Dissertation entitled *Dense Gas Chromatographic Studies*, University of Utah, Salt Lake City (1976).
4. S.M. Fields, K.E. Markides, M.L. Lee, *J. High Resolut. Chromatogr. Chromatogr. Commun.*, **11** (1988) 25.
5. J.M. Levy and W.M. Ritchey, *J. High Resolut. Chromatogr. Chromatogr. Commun.*, **10** (1987) 493.
6. M.E. McNally, J.R. Wheeler, and W.R. Melander, *LC-GC*, **6** (1988) 816.
7. P. Mourier, P. Sassiati, M. Caude, and R. Rosset, *J. Chromatogr.*, **353** (1986) 61.
8. P.R. Sassiati, P. Mourier, M.H. Caude and R.H. Rosset, *Anal. Chem.*, **59** (1987) 1164.
9. K.D. Bartle, Theory and Principles of Supercritical Fluid Chromatography, in *Supercritical Fluid Chromatography*, ed. R.M. Smith, Royal Society of Chemistry Burlington House, London (1988) Chapter 1, p1.
10. F.O. Geiser, S.G. Yocklovich, S.M. Lurcott, J.W. Guthrie and E.J. Levy, *J. Chromatogr.*, **459** (1988) 173.
11. P.J. Schoenmakers, P.E. Rothfusz and F.C.C.J.G. Verhoeven, *J. Chromatogr.*, **395** (1987) 91.
12. D. Leyendecker, F.P. Schmitz and E. Klesper, *J. Chromatogr.*, **315** (1984) 19.
13. R.D. Smith, E.G. Chapman and B.W. Wright, *Anal. Chem.*, **57** (1985) 2829.
14. S.Shah and L.T. Taylor, *Anal. Chem.*, in press.
15. D. Leyendecker, D. Leyendecker, F.P. Schmitz and E. Klesper, *J. Liq. Chromatogr.*, **10(8+9)** (1987) 1917.

Chapter 4

Analysis of Phenothiazinones in Plasma by Packed Column SFC

4.1 Introduction

Leukotrienes are believed to play an important pathophysiological role in the allergic bronchoconstriction of asthma. Under normal physiological conditions leukotrienes and prostaglandins behave as chemical mediators in maintaining homeostasis in their micro-environment. When conditions become so hostile that normal homeostasis cannot be achieved, then full inflammatory response occurs. Arachidonic acid, stored in membrane-bound phospholipids, is then released by phospholipases. Enzymatic conversion of arachidonic acid then proceeds through one of several routes (Figure 4.1). The cyclo-oxygenase pathway produces prostaglandins, prostacyclin and thromboxanes. The formation of leukotrienes is initiated by 5-lipoxygenase and dehydrase producing leukotriene A₄, an epoxide intermediate. Hydrolysis of LTA₄ results in the formation of leukotriene B₄. Leukotriene C₄, formed by the incorporation of glutathione in LTA₄, undergoes further conversion to form leukotriene D₄ and leukotriene E₄.

Leukotriene C₄ and D₄ are peptido-lipid conjugates which collectively account for the biological activity known as the slow reacting substance of anaphylaxis. They have potent smooth muscle contracting activity and high structural affinity for specific receptor sites. In addition these leukotrienes promote mucous production, decrease mucocilliary clearance, modulate vascular permeability changes, are potent inflammatory agents in human skin, and may be involved in the induction of non-specific bronchial hyperactivity. The sulphidopeptide leukotrienes, LTC₄ and LTD₄,

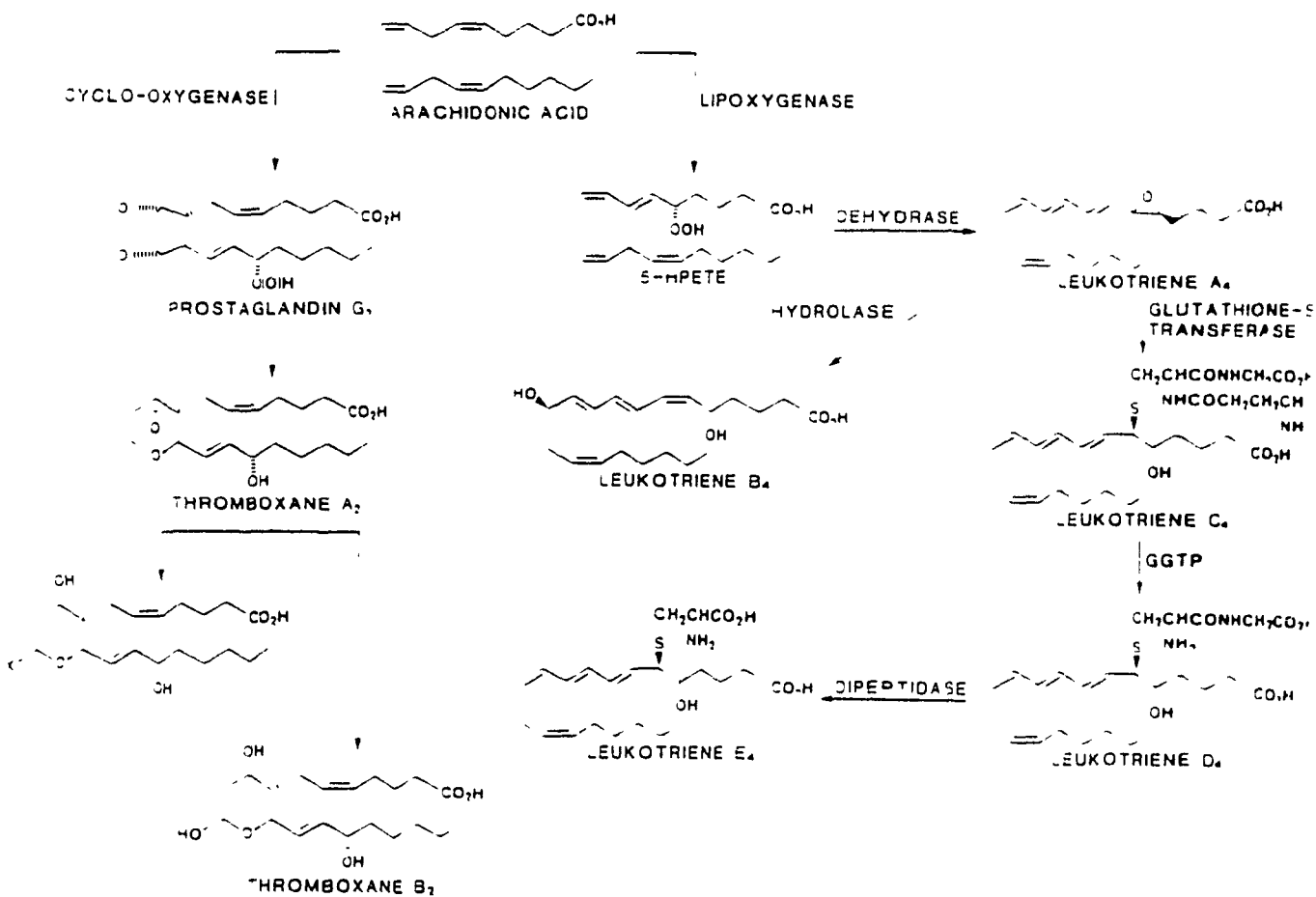


Figure 4.1 Cyclo-oxygenase and 5-lipoxygenase pathways.

are thought to be important mediators of human bronchial asthma and allergic diseases. They are also potent vasoconstrictors for both coronary and cerebral circulation, hence have important cardiovascular implications.

Leukotriene B_4 is a hydroxyecosatetraenoic acid which has a high affinity, structurally specific receptor sites on the neutrophil cell surface. Interaction with these receptor sites leads to induction of neutrophil cell functions including chemotaxis, chemokinesis and aggregation. In addition a subpopulation of both helper and suppressor T-cells have receptor sites for leukotriene B_4 , interaction with which results in an overall immunosuppressive effect. Injection of leukotriene B_4 into animal models or man results in induction of leucocyte accumulation, vascular permeability changes and modulation of pain responses suggesting that this leukotriene is an important mediator of inflammation.

Potential 5-lipoxygenase inhibitors are chosen according to the following criteria. (i) To compete with arachidonic acid for the 5-lipoxygenase enzyme, the inhibitor must have structural similarity with the substrate. In particular, the inhibitor should possess a moiety bearing significant lipophilic and π character, mimicking arachidonic acid; (ii) The generally accepted mechanism of lipoxygenation of fatty acids suggests an electron transfer from a skipped diene (1,4 Z,Z diene) followed by proton abstraction and the trapping of the resulting radical by oxygen to give rise to a hydroperoxy derivative. To functionally mimic the substrate of the enzyme, chemical entities known to favour an electron transfer process must be incorporated in the design of the inhibitor [1].

Studies using aromatic tricyclic derivatives in the alteration of the biological activities of prostanoids [2], combined with their lipophilic and π character, led to the study of tricyclic compounds with a heterocyclic ring, which could potentially permit a facilitated electron transfer. Using these concepts it was found that phenothiazines and their oxidized form, phenothiazinones, were selective inhibitors of the 5-lipoxygenase enzyme. One derivative of phenothiazinone class of compounds L651,392 (4-bromo-2,7-dimethoxy-3H-phenothiazin-3-one) [1] has shown potency as an oral drug for inhibiting leukotriene-mediated allergic responses. Such a compound may prove

useful in elucidating the role of 5-lipoxygenase products in biological and pathological processes both *in vitro* and *in vivo*. The separation and detection of plasma levels of these phenothiazinone compounds (Figure 4.2) are important in their development as drug therapy.

Information from the studies conducted in the previous chapter was used to develop a separation strategy for a series of phenothiazinone compounds. The behaviour of these compounds was investigated under changing conditions of temperature, density and mobile phase composition. An assay for 4-chloro-3H-phenothiazin-3-one (L615,919) in plasma is described. The electrochemical activity of these compounds was also investigated as potential candidates for electrochemical detection in SFC.

4.2 Experimental conditions

For experimental details see sections 2.2.3.1 - 2.2.3.7 in chapter two.

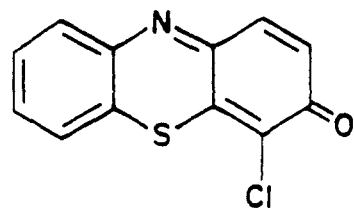
4.3 Results and Discussion

4.3.1 Retention behaviour in supercritical carbon dioxide.

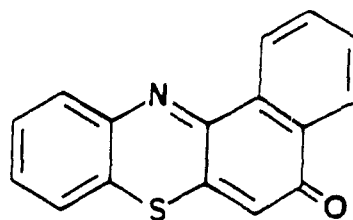
The behaviour of one analog, 4-bromo-2,7-dimethoxy-3H-phenothiazin-3-one (L651,392) was studied under various chromatographic conditions. Initial experiments were conducted on a C-18 bonded phase column with supercritical carbon dioxide as the mobile phase. At a temperature of 40°C and pressures below 3500 psi ($d = 0.85\text{--}0.90\text{ g/ml}$) compound L651,392 does not elute within a run time of 15 minutes. At 3500 psi, the analyte elutes as a very broad peak at $k' = 12.7$, and upon increasing to 4500 psi the front end of the peak begins to sharpen and retention decreases, $k' = 7.11$. Chromatograms obtained at increasing temperatures (60, 80, & 100°C) and constant pressure (4500 psi) showed sharpening of the front end of the analyte peak and a slight reduction in retention time. Improvements in peak tailing were not

observed. Retention of L651,392 is most likely due to more than one mechanism. At higher temperatures the solubility of the compound increases resulting in a sharper peak front. Tailing of L651,392 is probably due to interaction between one or more substituents on the molecule with active sites on the silica support. Two experiments were carried out to elucidate the retention mechanism. (i) A study of the behaviour of similar molecules with various substituents revealed the participating group and (ii) the use of a modifier to cover-up the active sites minimized interaction with the stationary phase, resulting in less peak tailing. A series of phenothiazinone compounds were chromatographed at 4500 psi and 80 °C (Figures 4.3 and 4.4). The peak shape and elution order of the series is very much dependent on the substituent groups on the molecules. L615,919 (4-chloro-3H-phenothiazin-3-one) elutes as a sharp peak at $k' = 1.06$, it is the least retained of the series. L649,991 (1-methyl-2-propylsulfide-phenothiazin-3-one) also elutes as sharp peak at $k' = 1.44$, it has a slightly increased retention due to the large substituents as compared to L615,919. L653,849 (7-methoxy-4-amino-phenothiazin-3-one) shows some tailing and increased retention, suggesting that the methoxy group may interact with active sites on the chromatographic support. L649,927 (benzo(a)-phenothiazin-5-one) elutes with increased retention indicating that the large benzene ring retards its mobility and the lack of peak tailing is supported by the lack of polar groups to interact with active sites on column. The two methoxy groups on L651,392 results in slightly longer retention and a substantial increase in tailing. L653,086 (4-nitro-2,7-dimethoxy-3H-phenothiazin-3-one) which is similar in structure to L651,392 with its bromine replaced by a nitro group, is retained for a very long time resulting in an extremely broad peak. This compound is not very soluble in dichloromethane, therefore its solubility in carbon dioxide may be not great enough to remove the compound from the stationary phase.

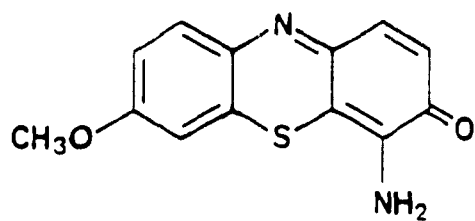
In order to obtain separation of a mixture of the first four compounds with reasonable resolution and an improved peak shape for the individual compounds a density or temperature gradient was necessary. Determining the actual values for such a gradient requires some knowledge of the principal mechanism of retention, therefore



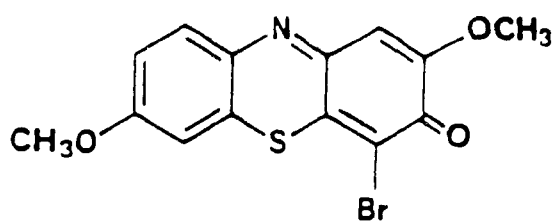
L-615,919



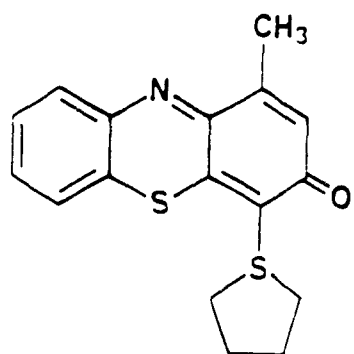
L-649,927



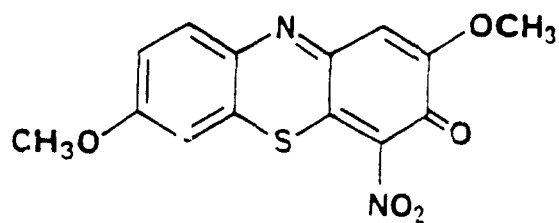
L-653,849



L-651,392



L-649,991



L-653,086

Figure 4.2 Structure of phenothiazinone compounds.

their behaviour was studied under various conditions of temperature, density and mobile phase composition.

4.3.2 Effect of modifiers on retention characteristics.

Chromatographic behaviour is governed by the interaction of the analyte with (i) the bonded stationary phase, including active sites on the chromatographic support; (ii) the mobile phase, including its solubility in the mobile phase or; (iii) the volatility of the species of interest; or (iv) some combination of these effects. As was shown in Chapter 3, modifiers, in the form of organic solvents, in the supercritical mobile phase can alter the stationary phase by covering up active sites, or by altering the solvent strength of the mobile phase. The choice and concentration of the modifier determines its effect. Formic acid (0.25 mole%) was added to the supercritical carbon dioxide mobile phase in order to cover up active sites on the stationary phase. Four analogs L615,919, L649,991, L653,849, and L649,927 were each injected at 100 ng/ μ l under conditions of constant density and varying temperatures for supercritical carbon dioxide with 0.25% formic acid mobile phase. Retention times, peak widths and heights were recorded for the average of four injections. Addition of the formic acid modifier reduced capacity ratio values for all compounds as compared to the values obtained with simple supercritical carbon dioxide mobile phase. At a density of 0.9 g/ml, chromatograms were obtained between 60 - 80°C, higher temperatures required very large pressures not feasible with current instrumentation. Capacity ratios for the four analogs increased from 60 to 70°C and decreased at 80°C to values below those recorded at 60°C (Figure 4.5b). The decreased capacity ratios at 80°C are a result of increased solubility of the analytes at the higher temperature. Peak widths generally increase proportionally with retention time, therefore a plot of peak widths at half height versus temperature should have a similar pattern to that of capacity ratio plots (Figure 4.5a). Although L649,991 is retained slightly longer than L615,919, its peak widths are smaller, suggesting that the lower polarity of the former minimizes its interaction with the silica support and its increase in retention is governed by its increased interaction with the bonded phase. The same compounds were investigated

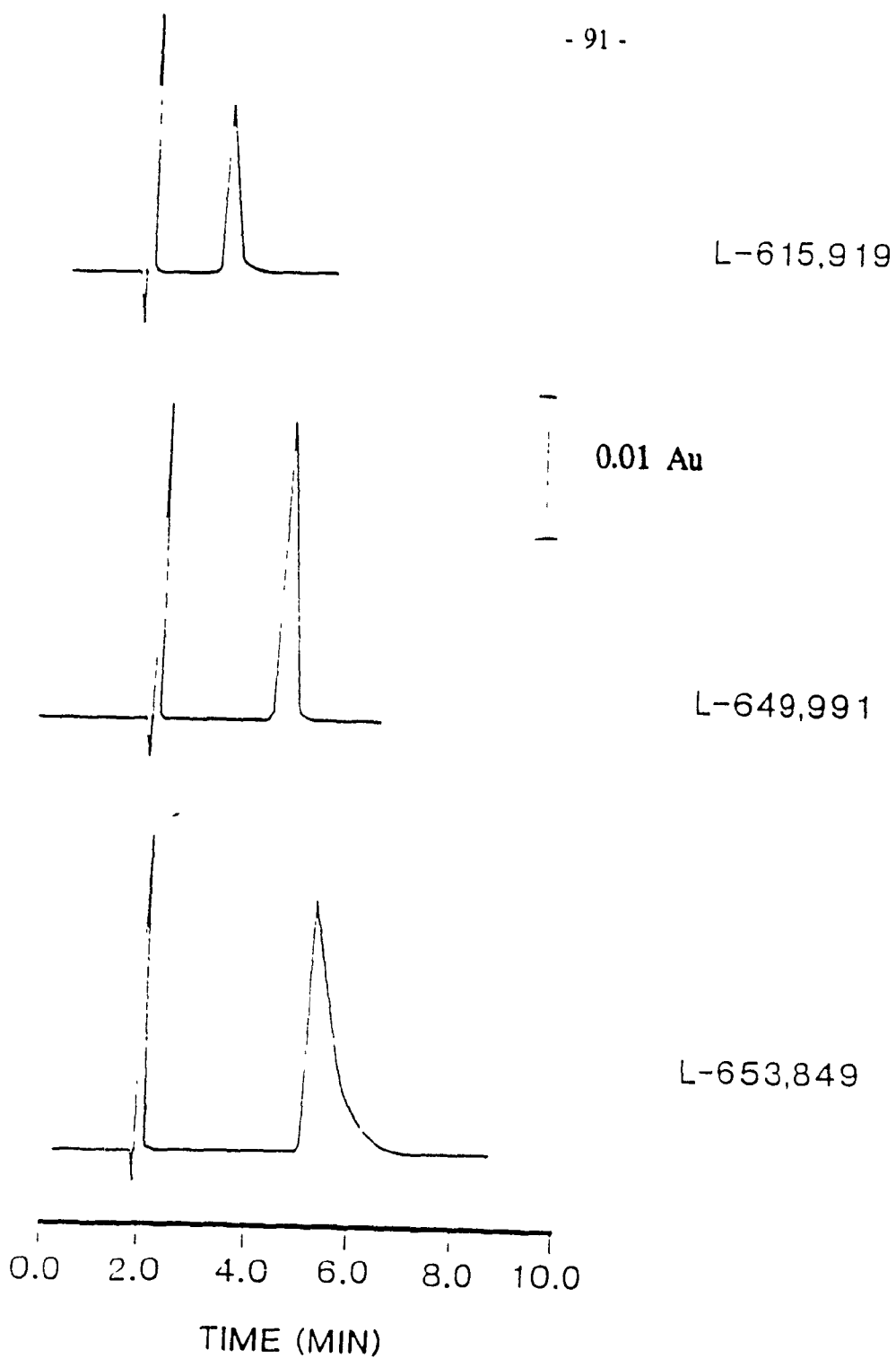


Figure 4.3

Chromatograms of phenothiazinone analogs at 80°C and 4500 psi in supercritical carbon dioxide.

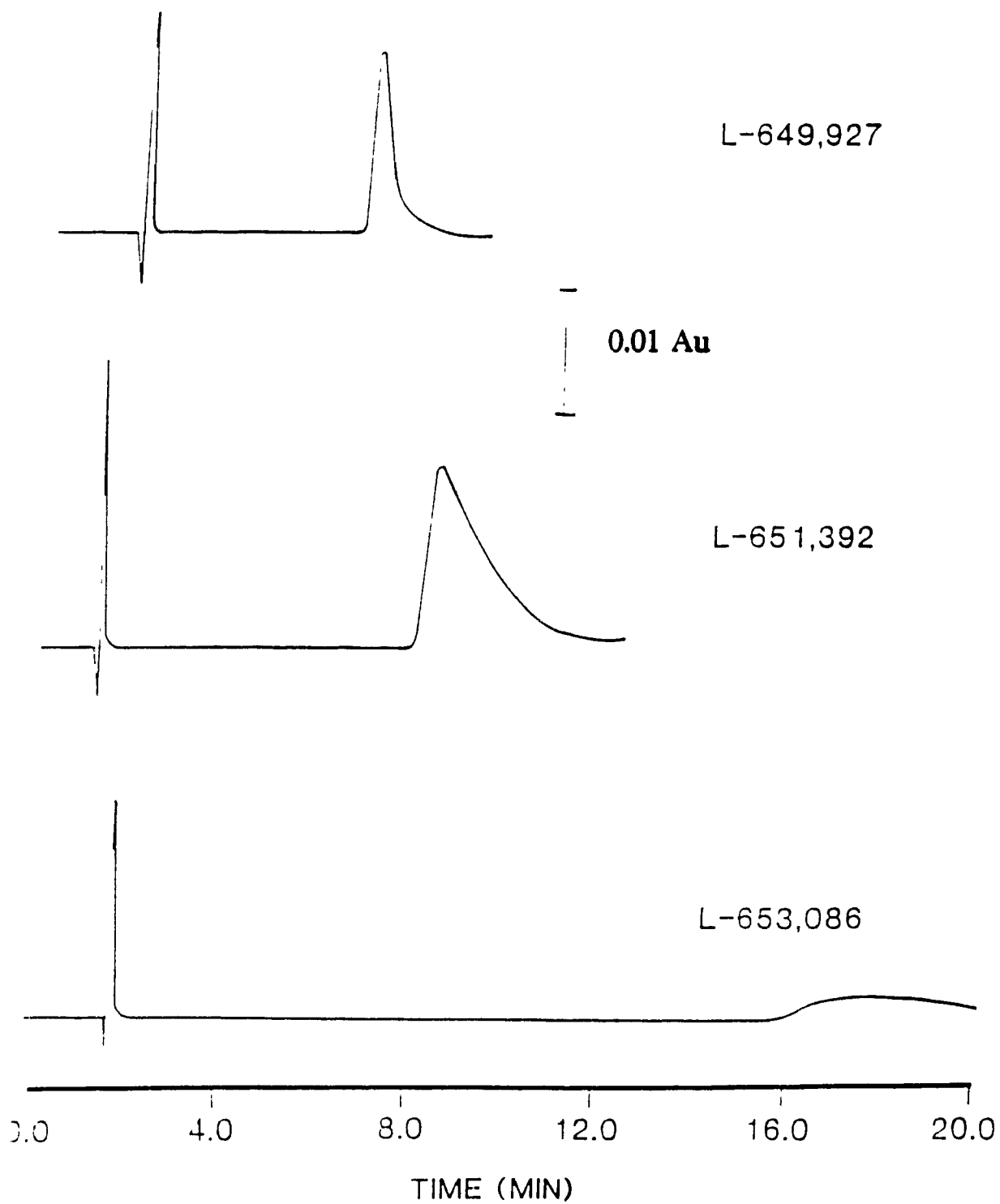


Figure 4.4

Chromatograms of phenothiazinone analogs at 80°C and 4500 psi in supercritical carbon dioxide.

at a lower density (0.7 g/ml) and higher temperatures of 80 to 100°C. Although the density and consequently the solvent strength is decreased the compounds eluted with similar capacity ratio values as those recorded at the higher density (Figure 4.6a). This suggests that the solubility of the analytes is greater at higher temperatures. At 100°C, the capacity ratio decreases considerably suggesting that the increase solubility of the analytes at higher temperatures contributes to the retention mechanism at this temperature. The plots of peak width at half height as a function of temperature reflect the change in capacity ratio (Figure 4.6b).

As with the study of the model compounds in Chapter 3, a further increase in formic acid content resulted in little change in capacity factors, indicating that the original concentration was sufficient to decrease the interaction of the analytes with active sites but a further increase in concentration had no influence on the mobile phase interactions. A third component, dichloromethane, was added to the mobile phase in an attempt to increase the solubility of the phenothiazinone compounds in this phase. It had no visible effects on retention times but did show some differences in peak shape. In Figure 4.7, chromatograms of three compounds of the series are compared at equivalent densities and temperatures for the formic acid and the formic acid/dichloromethane modified supercritical carbon dioxide phases. L615,919, the phenothiazinone with a chlorine substituent, showed an increased peak height and better peak shape in the tertiary mobile phase. Peak height and peak tailing improved more for L653,849, the compound with the one methoxy substituent, upon the addition of dichloromethane to the mobile phase. No difference was observed for L649,927, the phenothiazinone with the large aromatic substituent in binary and tertiary mobile phases. This suggests that the addition of dichloromethane increased the solubility of the more polar compounds in the mobile phase with the improvement decreasing as the molecule becomes less polar.

4.3.3 Separation of phenothiazinone analogs.

Separation of a mixture of the phenothiazinone compounds with reasonable resolution and improved peak shape necessitates the addition of a modifier to the

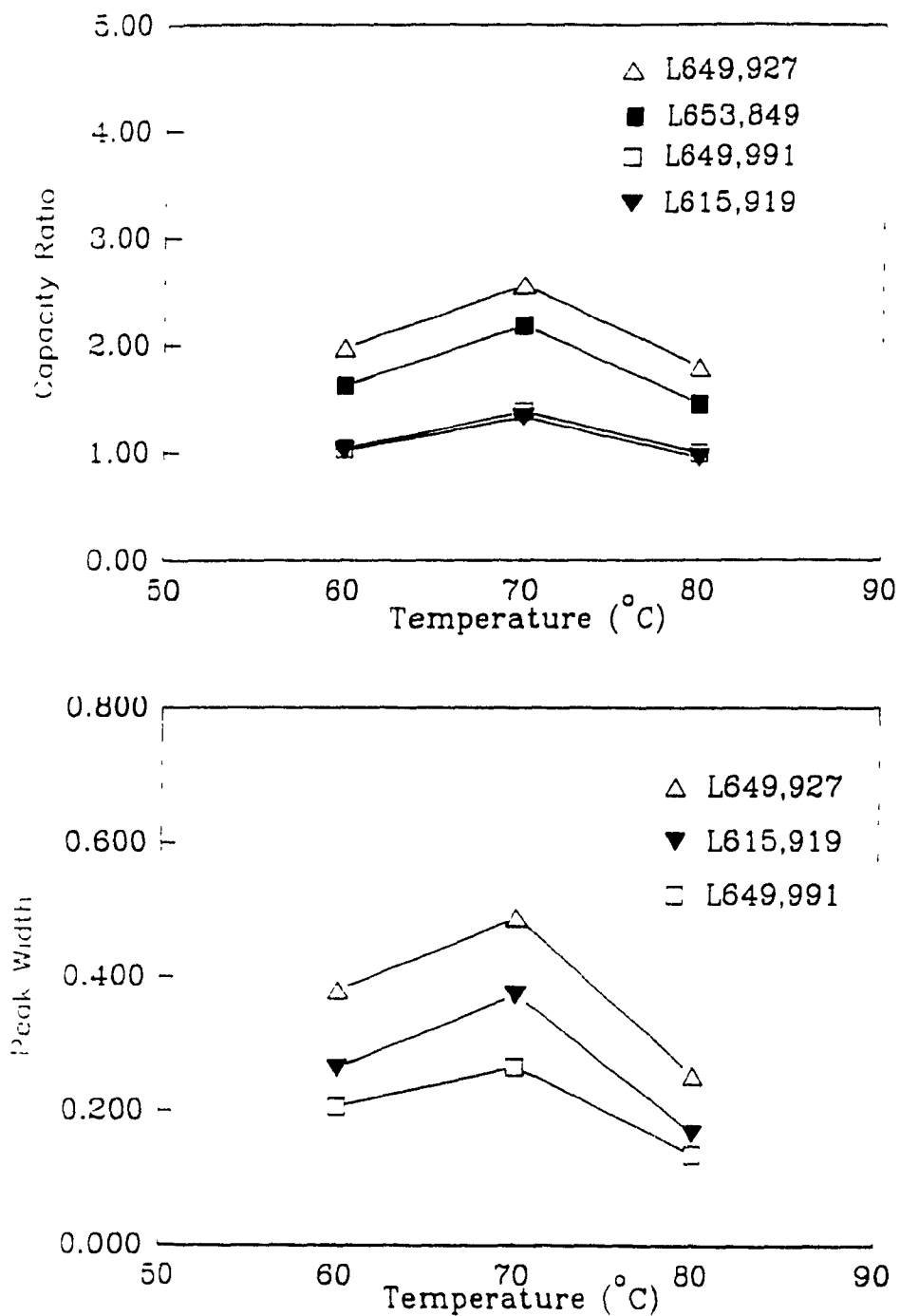


Figure 4.5

Capacity ratios (a) and peak widths (b) as a function of temperature at a density of 0.7 g/ml. Mobile phase: 0.25 mole% formic acid.

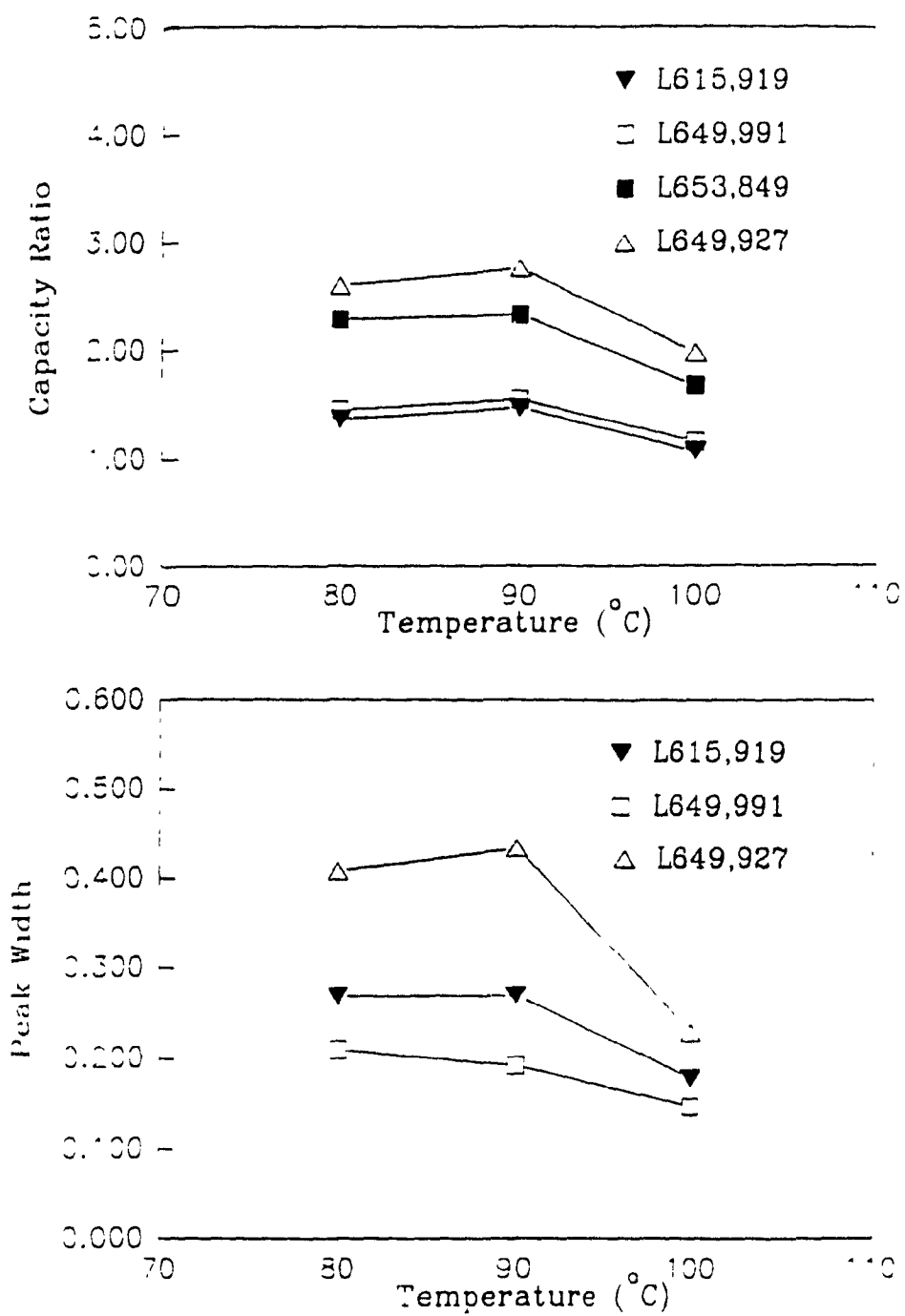


Figure 4.6 Capacity ratios (a) and peak widths (b) as a function of temperature at a density of 0.9 g/ml. Mobile phase: 0.25 mole% formic acid.

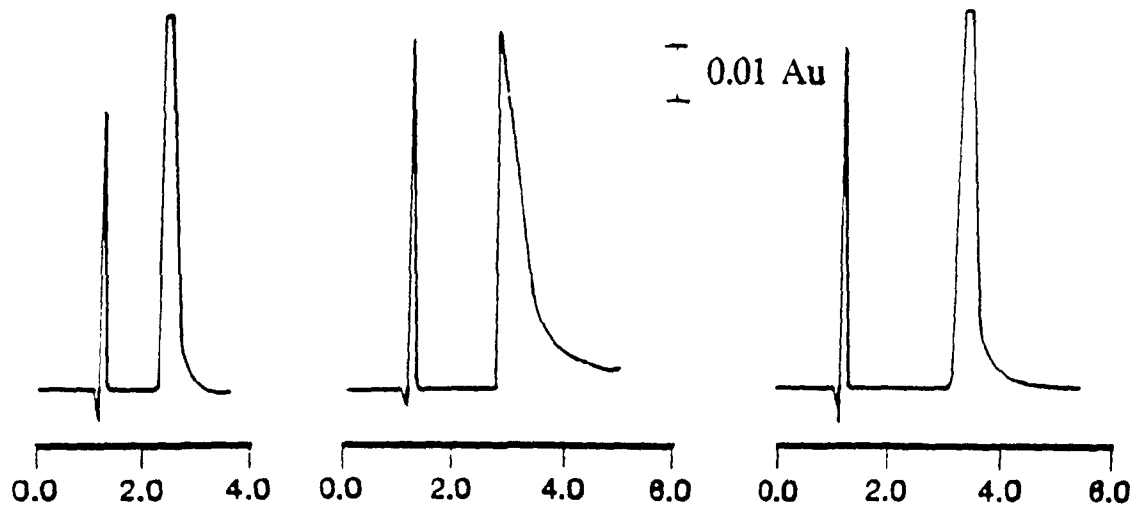
mobile phase and the use of a density gradient. The phenothiazinone analogs are not soluble in aqueous solvents therefore highly polar modifiers cannot be used. An increased solvation power is required to elute the larger, more polar analogs with minimal peak tailing. Acetonitrile is a suitable choice since the phenothiazinone compounds are soluble in this medium and it increases the solvent strength of the mobile phase. The effect of increasing acetonitrile content on retention times, peak widths, resolution, and efficiency at two temperatures was investigated. A solution containing L615,919, L649,991, L649,927, and L651,392 at 100 ng/ul was injected in a mobile phase of varying acetonitrile concentration under conditions of a constant pressure gradient and constant temperature. Capacity ratios for each of the compounds decreased, in a non-linear fashion, with increasing acetonitrile concentration (Figure 4.8a). Peak widths decreased slightly for three of the compounds with acetonitrile concentration, but decreased rapidly for L651,392 from 0.4 to 1.2 mole% (Figure 4.8b). This suggests a reduced interaction with the bonded phase. Increasing the modifier content in the mobile phase increases the solvent strength of the mobile phase, thus increasing the solubility of the analytes. This results in faster analysis times and sharper peaks, but reduced resolution. A much sharper decrease in resolution is observed between L649,927 and L651,392 since the capacity ratios of the latter decreases more rapidly than that for the former (Figure 4.9). Resolution between L615,919 and L649,991 remains constant since their retention times are affected in the same manner with increasing modifier concentration. Figure 4.10 demonstrates the loss of resolution with increasing modifier concentration in the mobile phase, peaks 3 and 4 are not resolved at the higher acetonitrile concentration. Similar studies were carried out at a higher temperature of 80°C. Capacity ratios are generally greater at the higher temperature (Figure 4.11a). Although capacity ratio values decrease with the amount of acetonitrile, little change is observed above a concentration of 1.2 mole%. The higher temperature decreases the density of the mobile phase, but is not high enough for volatility effects to be observed on the retention mechanism. Peak widths decrease slowly with increasing modifier concentration for three of the analytes; values are similar to those obtained at 40°C (Figure 4.11b). For L651,392

L-615,919

L-653,849

L-649,927

A.



B.

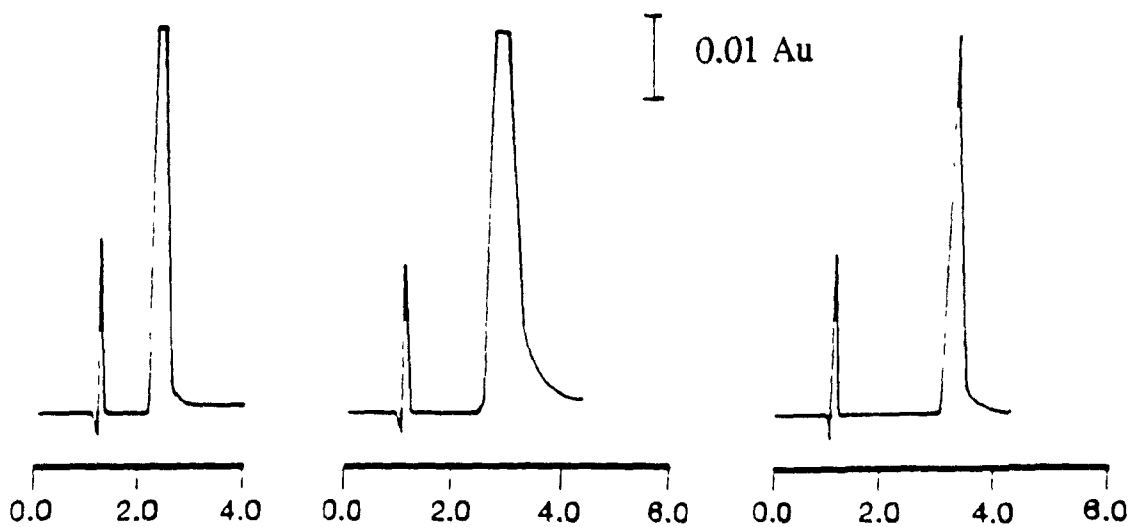


Figure 4.7

Comparison of three phenothiazinone analogs in (A) 0.25 mole% formic acid and (B) 0.87 mole% dichloromethane/0.16 mole% formic acid in carbon dioxide at 80°C and 0.8 g/ml.

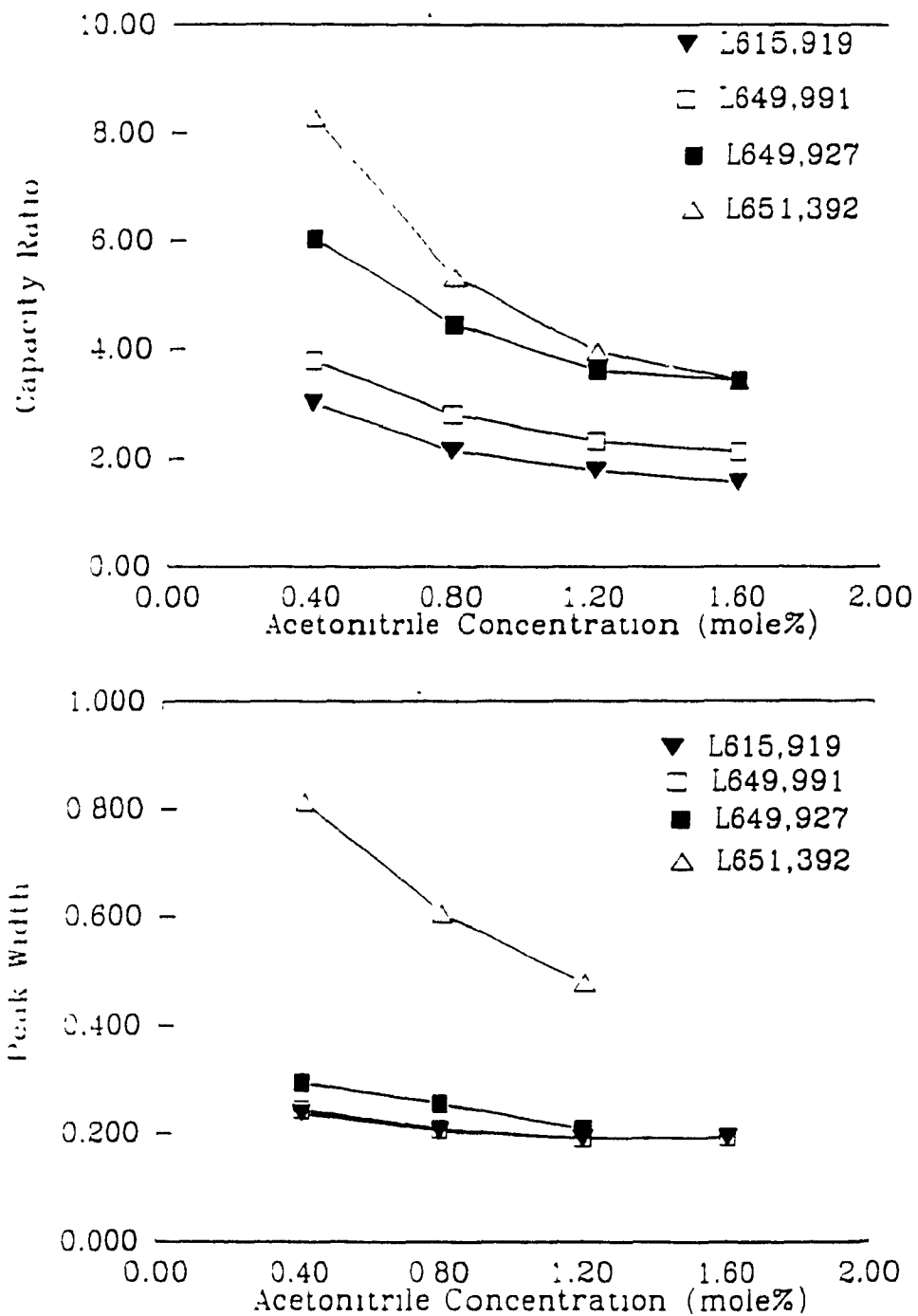


Figure 4.8 Capacity ratios (a) and peak widths (b) as a function acetonitrile concentration in mobile phase. Temperature: 40°C. Density gradient: isodense 0.72 g/ml for 1 min, 0.91 g/ml at 10 min.

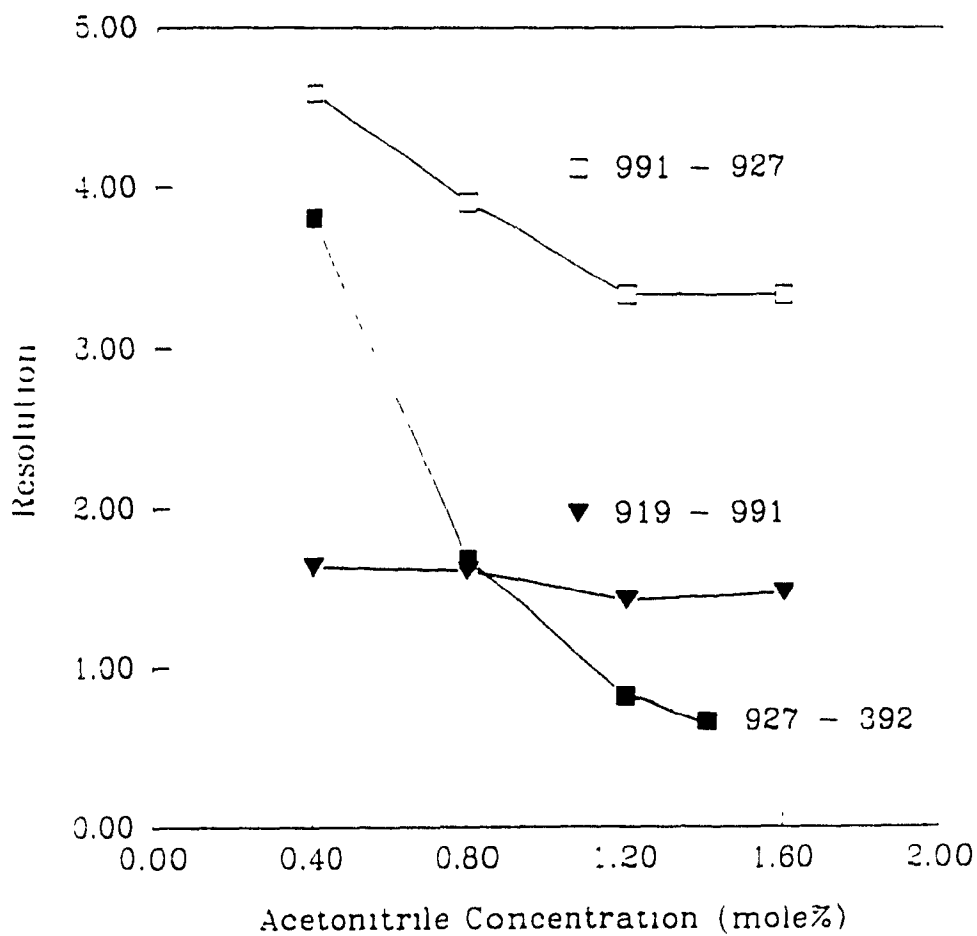


Figure 4.9

Resolution as a function of percent modifier. Temperature: 40°C. Density gradient: isodense 0.72 g/ml for 1 min, 0.91 g/ml at 10 min.

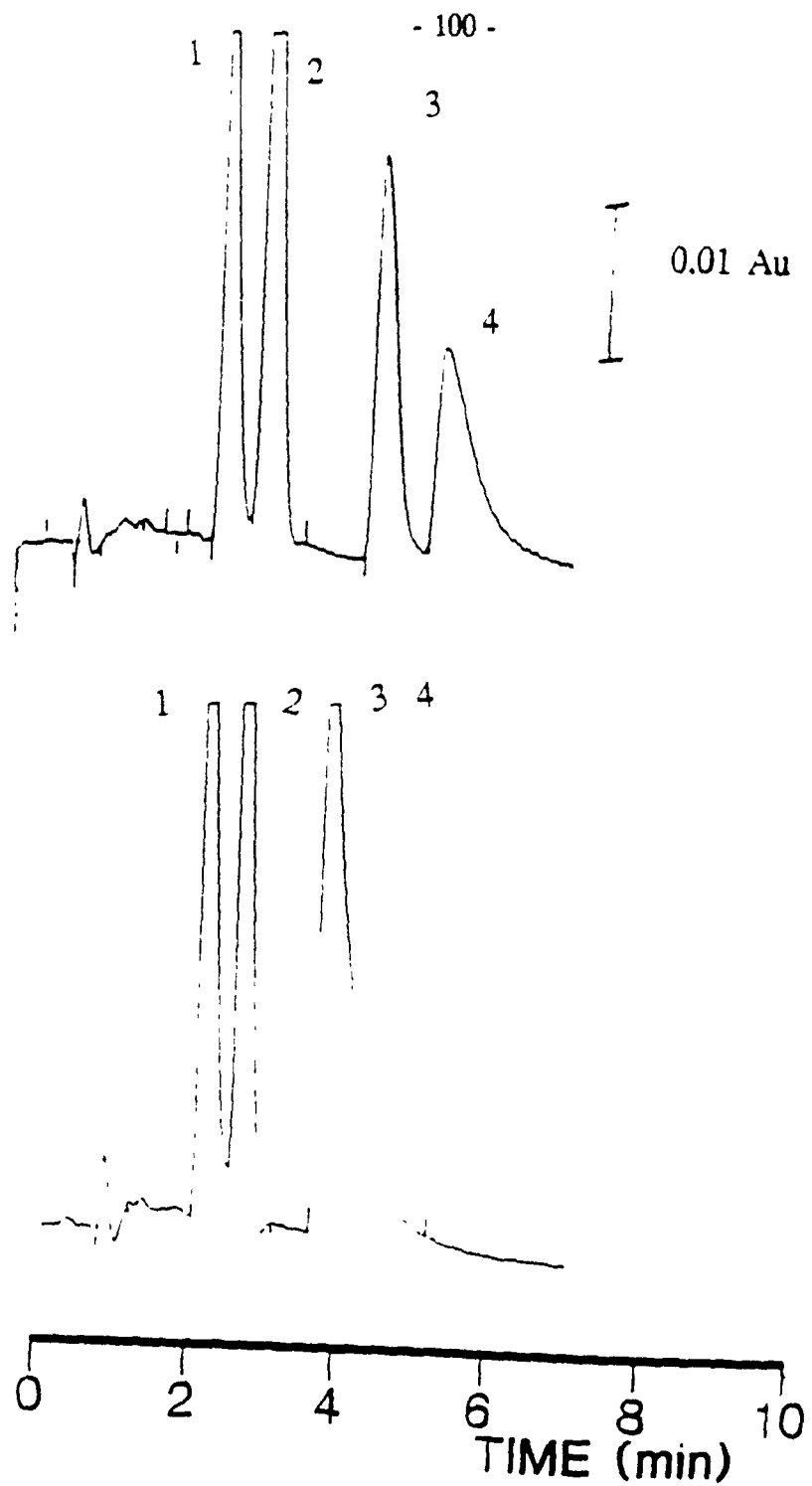


Figure 4.10

Chromatograms of phenothiazinone mixture at 40°C in (a) 0.8 mole% acetonitrile and (b) 1.6 mole% acetonitrile in carbon dioxide. 1. L615,919; 2. L649,991; 3. L649,927; 4. L651,392.

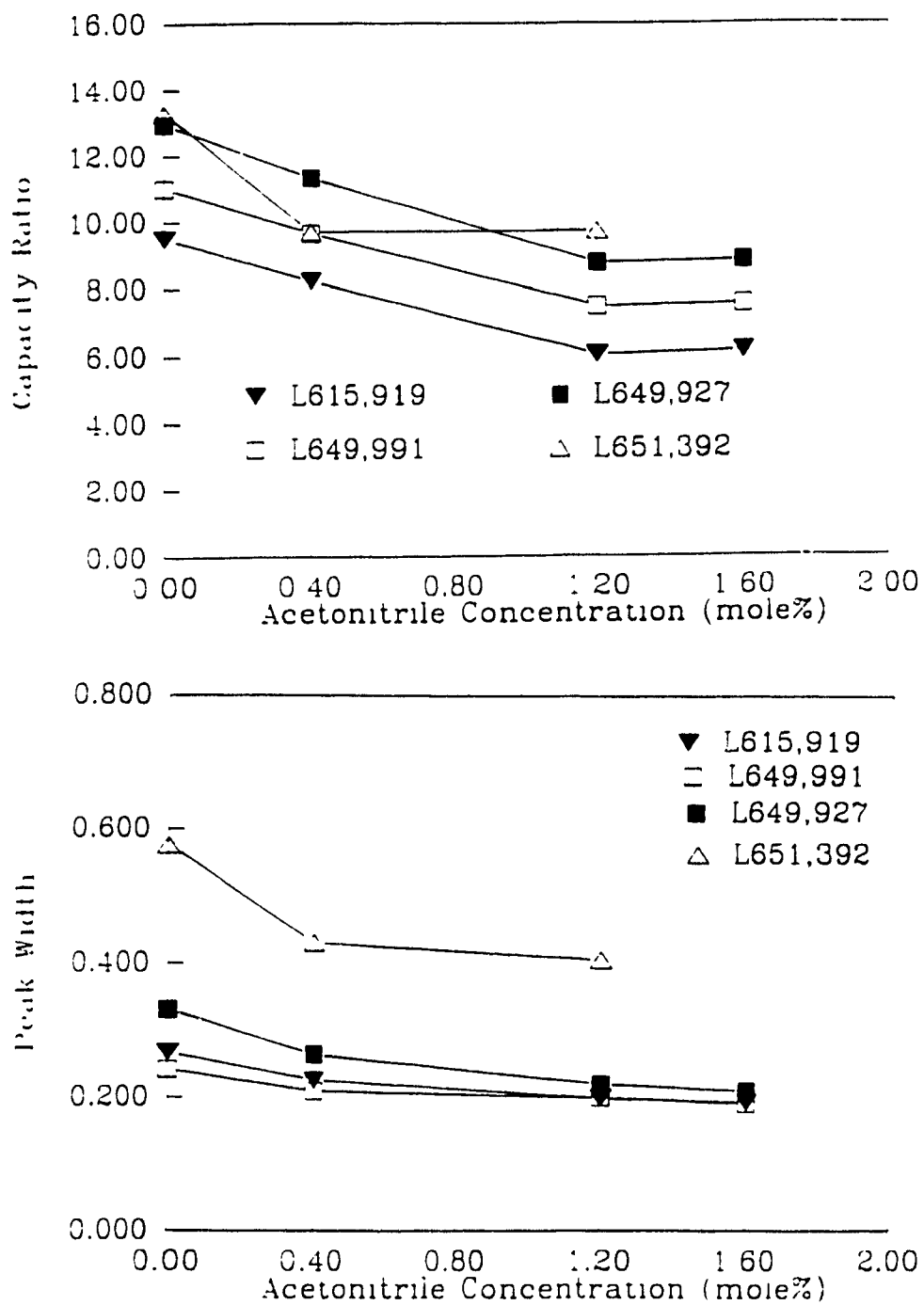


Figure 4.11 Capacity ratios (a) and peak widths (b) as function of modifier (acetonitrile) concentration at 80°C.

peak widths improve at a more rapid rate and actual values are smaller than those recorded at the lower temperature. At 80°C, the increased solubility of L651,392 in the mobile phase therefore reducing the retention time and decreasing peak width.

4.3.4 Assay for L615,919 in plasma.

An optimum set of operating conditions was obtained from these results. After an initial one minute isobaric period, a density gradient ramping from 0.72 g/ml to 0.91 g/ml at a rate of 0.021g/ml at 40°C was used to separate four analogs of this series. Figure 4.12a was obtained for a 1 µl injection of 100 ng of each analog dissolved in acetonitrile. A comparison of this chromatogram with that obtained for the same pressure gradient in simple supercritical carbon dioxide mobile phase clearly demonstrates the need for the modifier (Figure 4.12b). These conditions were then used as a starting point in the development of a method for the analysis of one of the analogs, 4-chloro-3H-phenothiazin-3-one, in plasma.

The drug was initially administered at a dose of 150 mg/kg p.o. as a suspension in 1% Methocel. An internal standard (L649,927) was used for all measurements. Chromatograms of the drug and internal standard as a standard solution and in plasma are represented in Figure 4.13. A calibration curve for peak height ratio of L615,919/L649,927 was linear between 2 and 900 ng injected on column, with a r^2 value of 0.9988 (Figure 4.14a). A plot of the low concentration range, 2 to 100 ng, was also linear at $r^2 = 0.9972$ (Figure 4.14b).

Plasma levels increased up to 2.7 µg/ml at 2 hours following the oral administration, followed by a slow increase to 5.19 µg/ml at 24 hours (Figure 4.15). All points on the plasma profile were obtained with %RSD's between 0.8 and 3.2 %.

A second study was conducted with time points up to 29 hours in an attempt to determine the elimination profile for this drug. Since studies were conducted on different weeks, different restrictors were used resulting in changes in linear velocity. It was, therefore, necessary to prepare calibration curves for each study. A calibration curve was prepared between 1 and 100 ng with $r^2 = 0.9971$ (Figure 4.16). Again a similar plasma profile was obtained (Figure 4.17). The final study was then conducted

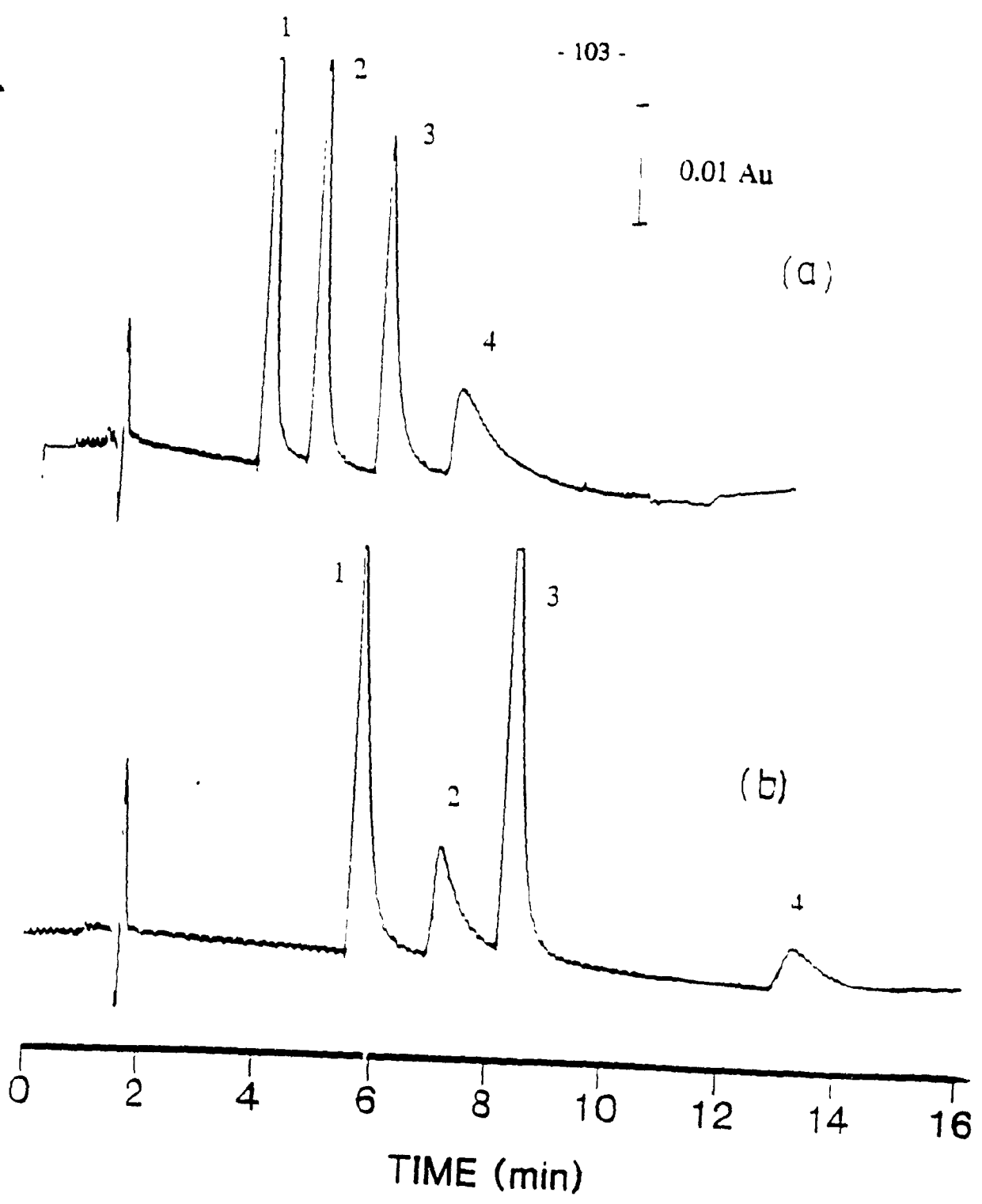


Figure 4.12

Comparison of chromatograms for the phenothiazinone mixture at equivalent density programs and same temperature (40°C) in (a) 0.8 mole% acetonitrile/carbon dioxide and (b) simple carbon dioxide.

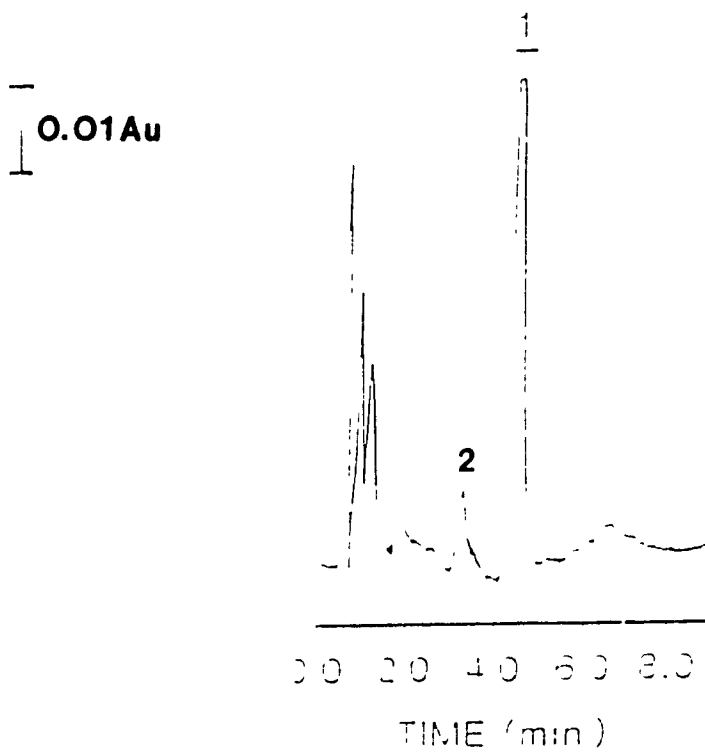
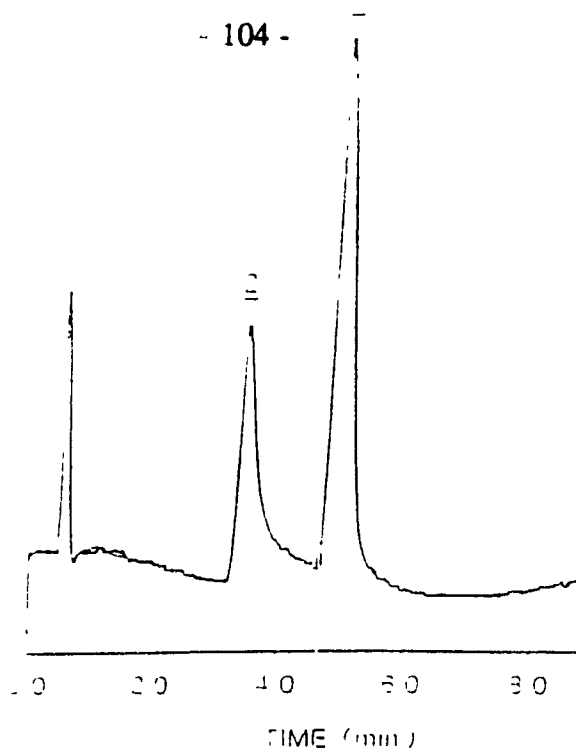


Figure 4.13

Chromatogram of drug (L615,919) 2 and internal standard (L649,927) 1 (a) standard solution and (b) rat plasma.

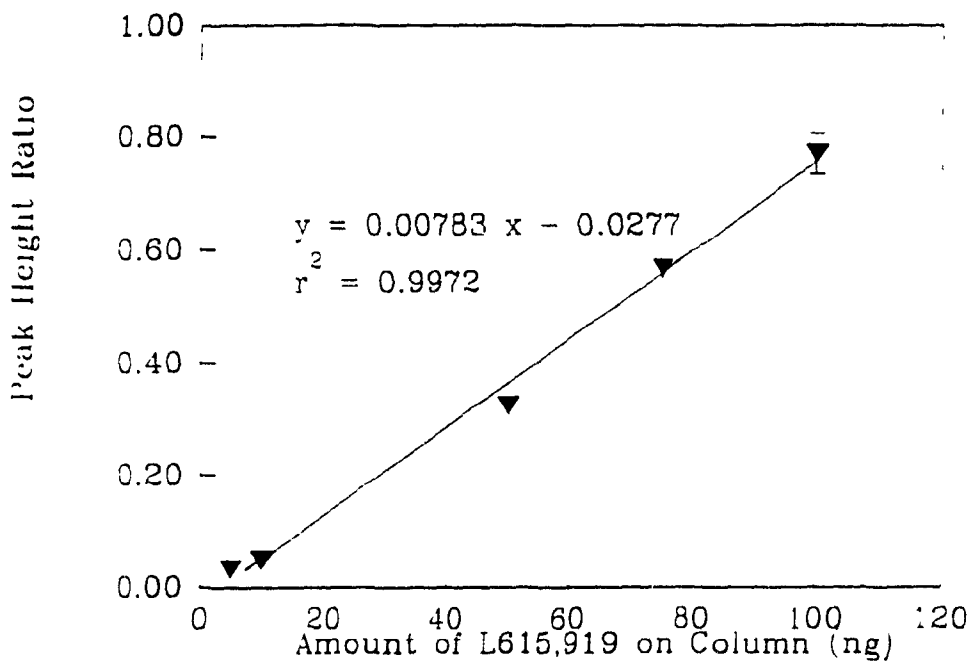
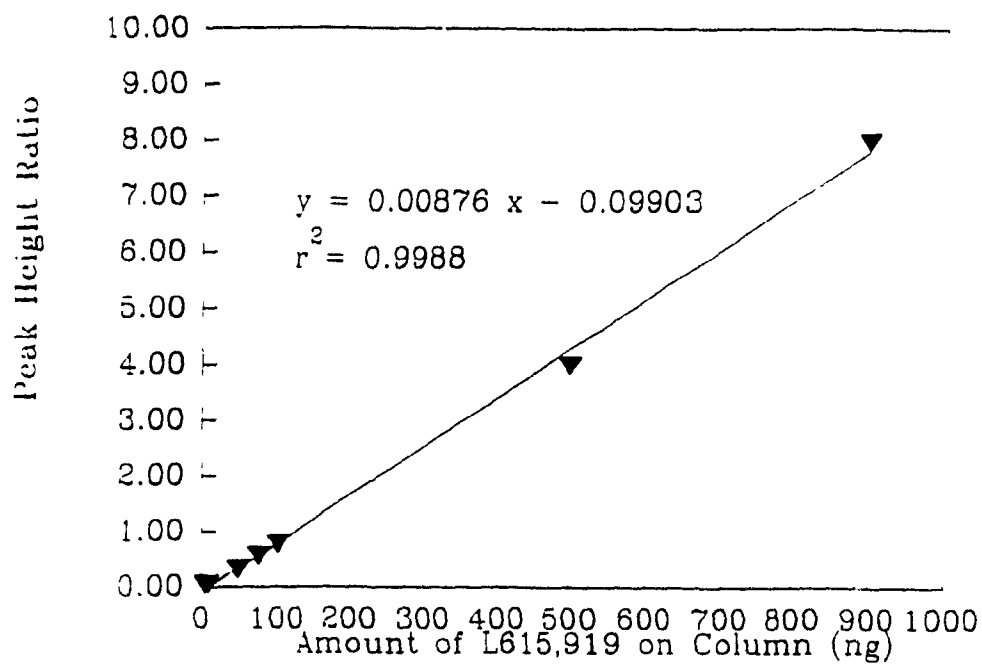


Figure 4.14 Calibration curve for study 1 for an average of 3 injections. (a) full concentration range and (b) low concentration range.

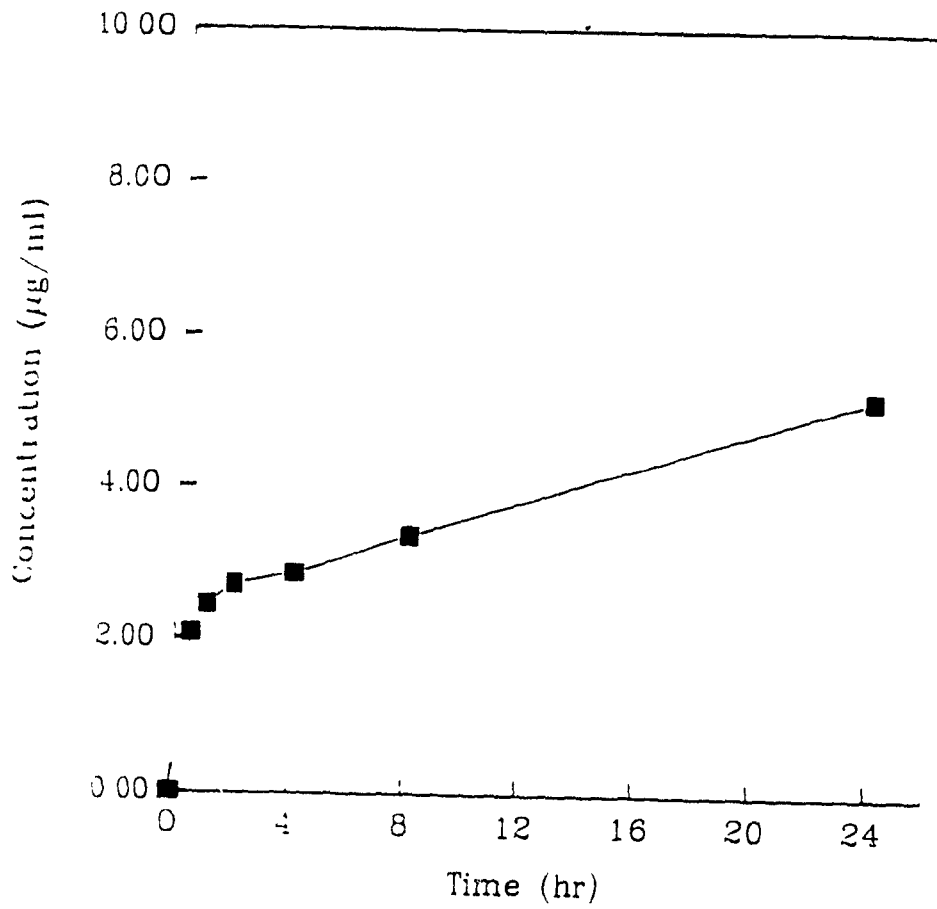


Figure 4.15 Plasma profile for one rat in study 1.

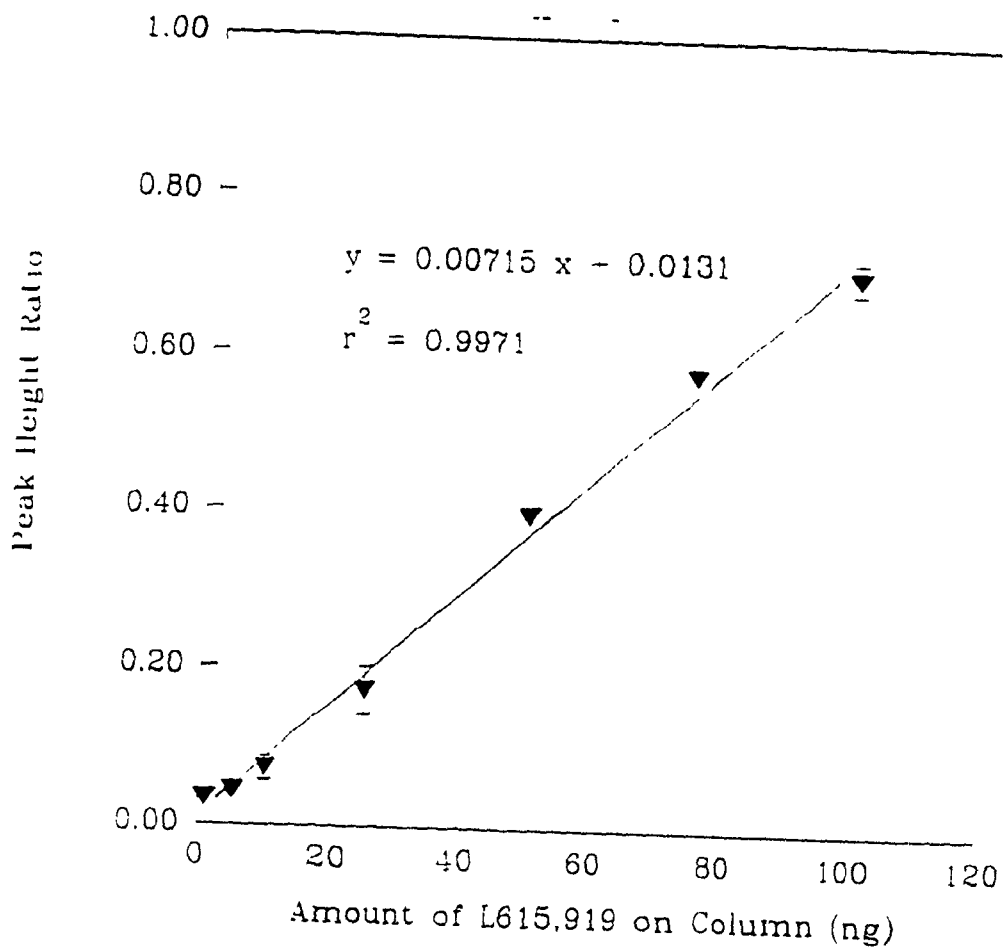


Figure 4.16

Calibration curve for study 2

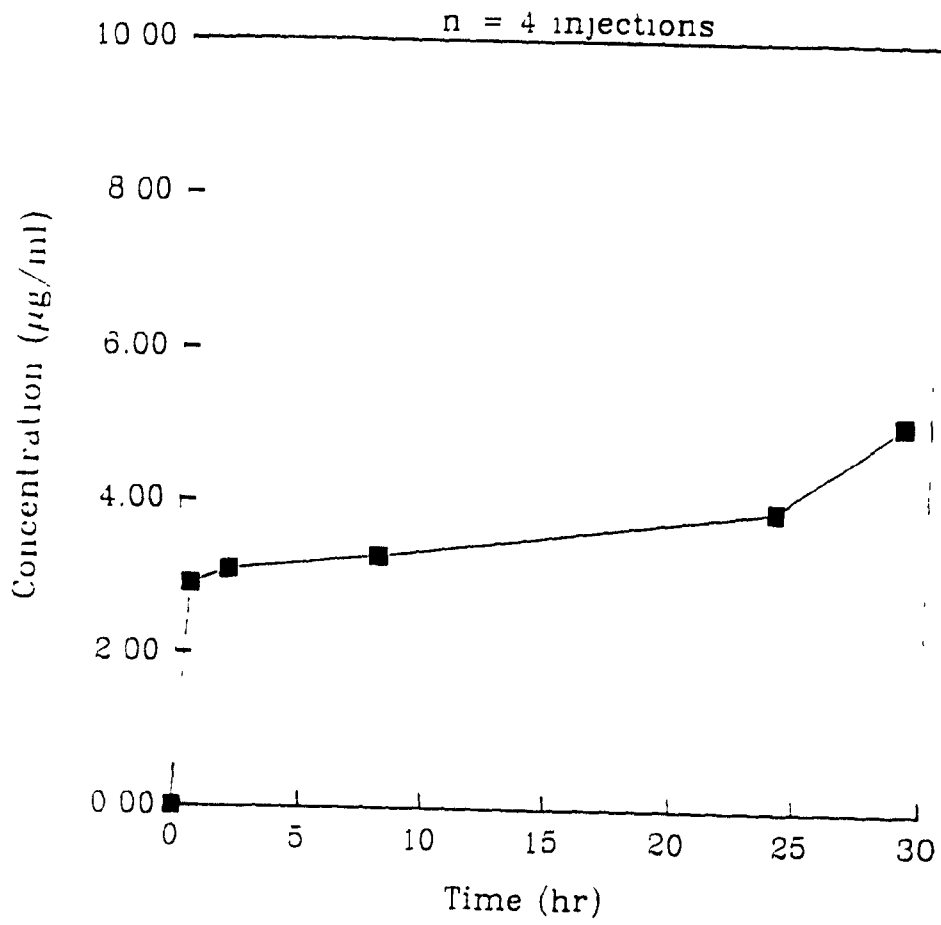


Figure 4.17

Plasma profile study 2

by administering the drug at 150 mg/kg in three rats simultaneously (Figures 4.18). Studies of plasma levels of another analog, L651,392 have shown that at the high dose of 150 mg/kg, maximum peak levels were reached at 30 minutes and maintained after 24 hours. At lower doses of 20 mg/kg, plasma level drop after 5 hours and the drug is completely eliminated by 24 hours. Due to the low bioavailability of these compounds detection limits are consistently a problem.

4.3.5 Electrochemical investigation

The high sensitivity achieved with HPLC/ECD prompted the investigation of SFC/ECD as a viable alternate for this class of compounds. The electrochemical activity of some of the phenothiazine analogs were investigated. Cyclic voltammograms of the phenothiazinone derivatives were obtained in acetonitrile with 0.1M TBA TFB as the supporting electrolyte. A platinum microdisc electrode served as the working electrode, a silver/silver chloride electrode as the reference and a platinum wire as the auxiliary electrode. All voltammograms were obtained for 1 mg/ml concentrations of the analyte. For L615,919 a reversible oxidation is obtained with a half wave potential of 0.4 volts (Figure 4.19a). L649,991 undergoes a first oxidation at $E_{1/2} = 0.16$ volts, which does not reach a steady state response as a second oxidation occurs at $E_{1/2} = 0.38$ volts (Figure 4.19b). On the reverse scan a reduction is obtained at $E_{1/2} = -0.29$ volts. Two well resolved, sigmoidal-shaped red-ox waves are recorded at $E_{1/2} = 0.38$ and 0.91 volts for L653,849 (Figure 4.20a). The cyclic voltammogram for L651,392 has one oxidation at $E_{1/2} = 0.32$ volts (Figure 4.20b).

4.4 Conclusions

The role of physical parameters (temperature, density and mobile phase composition) on the retention behaviour of four phenothiazinone analogs has been investigated. Results obtained demonstrate the need for both an organic modifier (acetonitrile) in the carbon dioxide mobile phase and a density gradient for the elution of each analog with reasonable retention times and resolution. An assay for

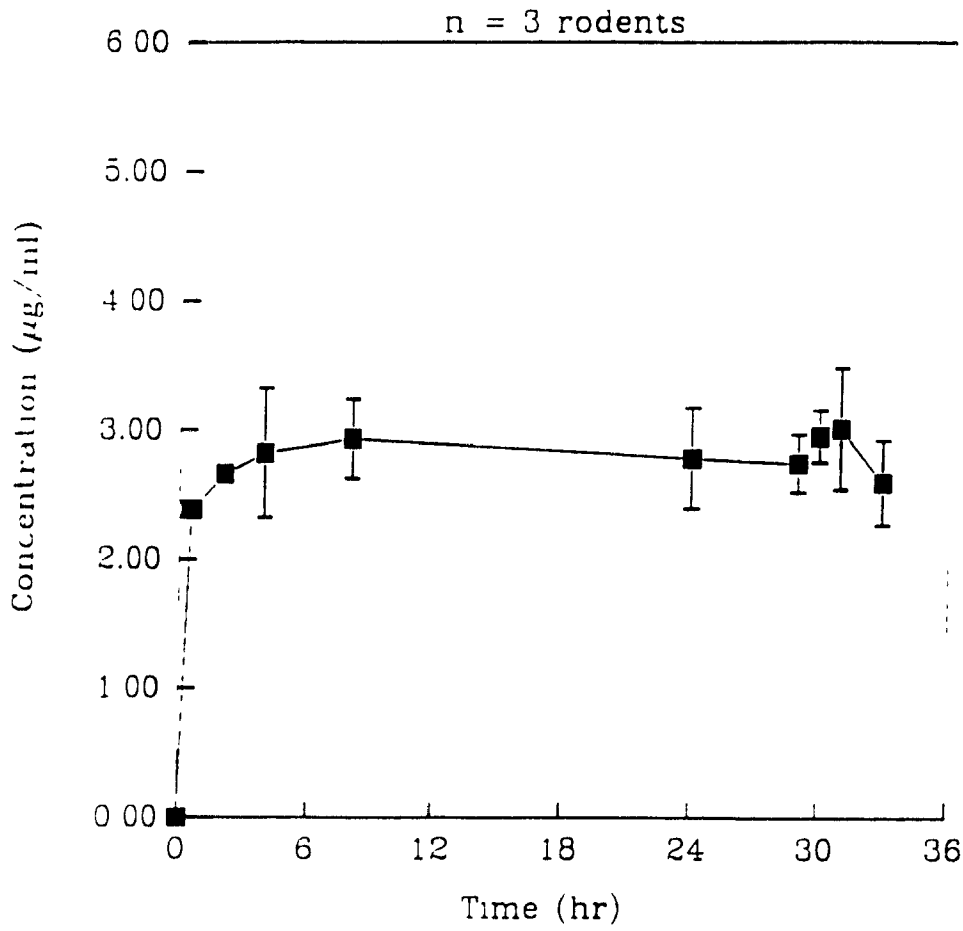


Figure 4.18 Plasma profile for three rodents in a simultaneous study.

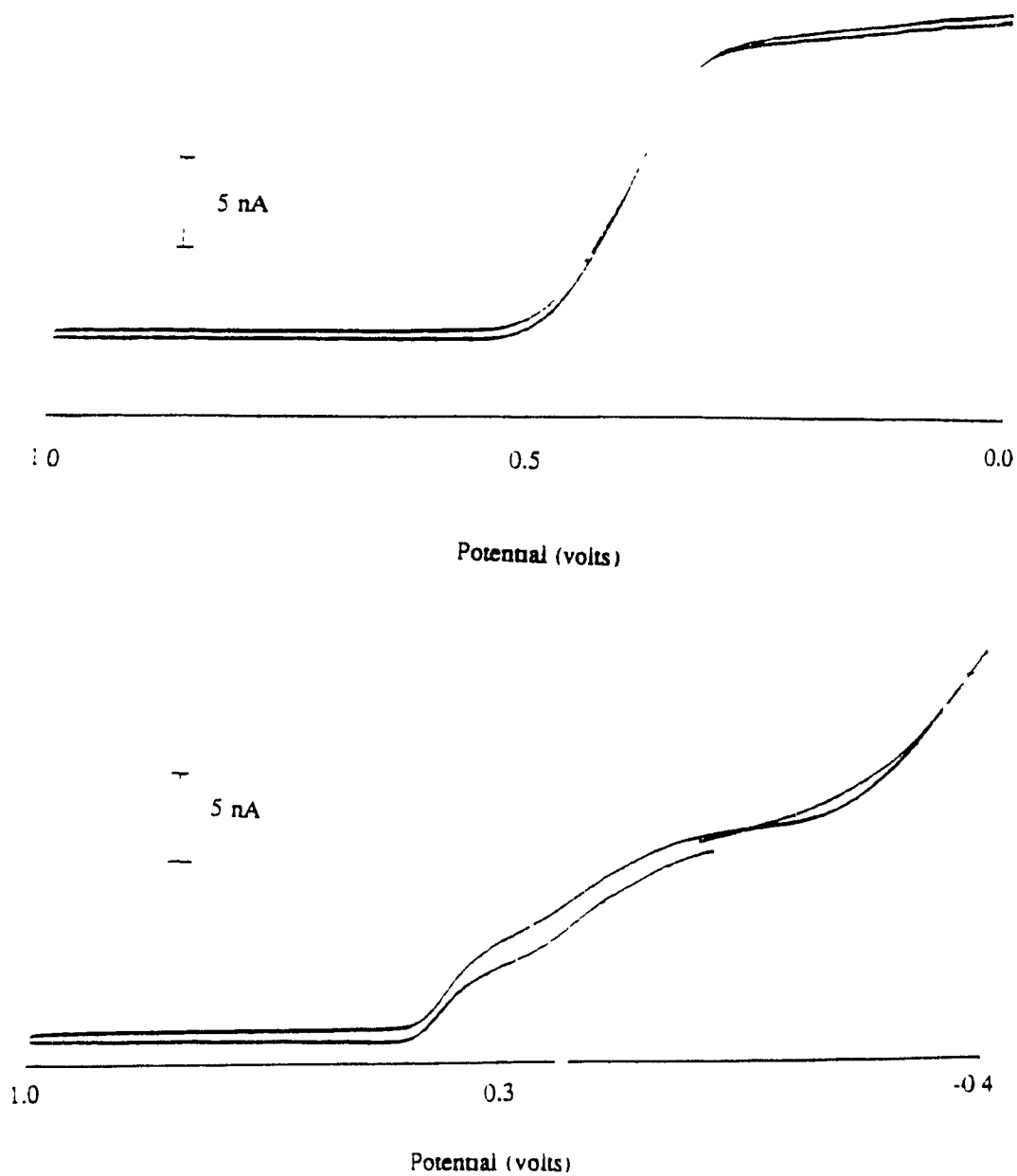


Figure 4.19

Cyclic voltammogram of (a) L615,919 and (b) L649,927 in $\text{CH}_3\text{CN}/0.1\text{M TBA TFB}$. Pt-wire auxiliary and Ag/AgCl reference electrodes and platinum ultramicroelectrode as the working electrode.

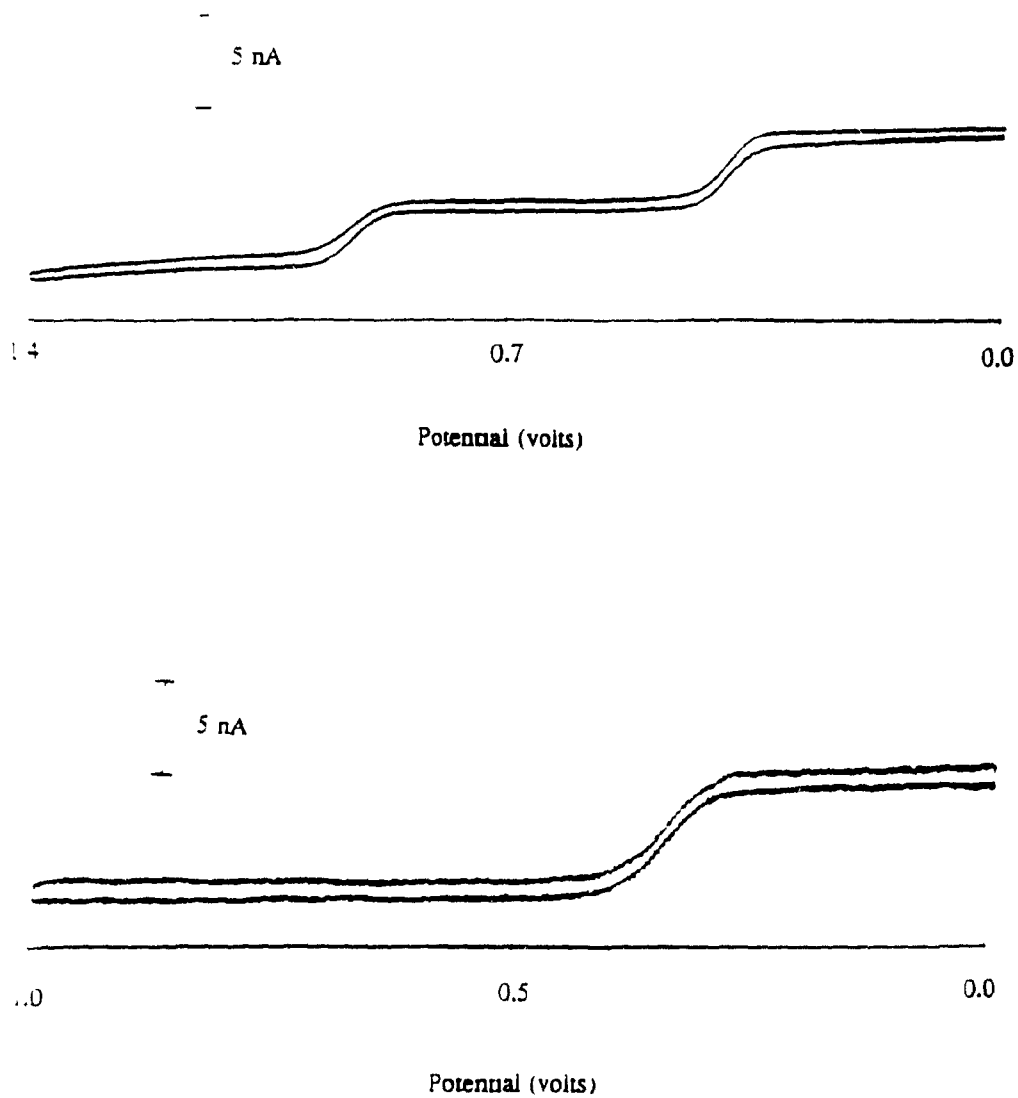


Figure 4.20

Cyclic voltammogram of (a) L653,849 and (b) L651,392 in $\text{CH}_3\text{CN}/0.1\text{M TBA TFB}$. Pt-wire auxiliary and Ag/AgCl reference electrodes and platinum ultramicroelectrode as the working electrode.

determining the plasma profile of L615,919 in rodents was developed. The electrochemical activity of these phenothiazinones were also investigated. The low oxidation potentials of these compounds make them suitable for measurement with amperometric detectors.

4.5 References

1. Y. Guindon, Y. Girard, A. Maycock, A.W. Ford-Hutchinson, J.G. Atkinson, P.C. Bélanger, A. Dallib, D. DeSousa, H. Dougherty, R. Egan, M.M. Goldenberg, E. Ham, R. Fortin, P. Hamel, R. Hamel, C.K. Lau, Y. Leblanc, C.S. McFarlane, H. Piechuta, M. Thérien, C. Yoakim, and J. Rokach, *L-651,392: A Novel, Potent and Selective 5-Lipoxygenase Inhibitor*, in *Advances Prostaglandin, Thromboxane and Leukotriene Research*, ed. B. Samuelsson, R. Poaletti and P.W. Ramwell, Raven Press, New York, 17 (1987) p557.
2. E.J. Cragoe, D. Ethier, A.W. Ford-Hutchinson, Y. Girard, R.A. Hall, P. Hamel, J. Rokach, N.N. Share, C.A. Stone, and P. Yusko, *Br. J. Pharmacol.* 82 (1984) 389.

Chapter 5

An Electrochemical Detection System for Supercritical Fluid Chromatography

5.1 Introduction

Electrochemical detection in liquid chromatography is a highly sensitive and selective technique for the analysis of a wide range of biologically important compounds. The possibility of extending electrochemical detection to supercritical fluid chromatography would greatly broaden the range and scope of analyses currently being carried out by this technique. Electrochemical measurements in supercritical media have, at least in principle, the potential for improving detection limits, since diffusion coefficients in supercritical fluids are approximately an order of magnitude greater than those found in liquids. This advantage, until recently, has been offset by the highly resistive nature of supercritical fluids. The recent development of ultramicroelectrodes with their inherently low residual ohmic effects and reduced requirement for added supporting electrolyte make them ideal candidates for electrodes in supercritical fluid chromatography electrochemical detection systems.

Voltammetric behaviour changes dramatically as the size of the electrode decreases from millimeter to micrometer dimensions. Wightman first reported on the unique properties of these electrodes and the size advantage of microelectrodes for direct measurements of neurotransmitter concentration inside the mammalian brain [1]. Steady-state current responses are obtained at microvoltammetric electrodes and the small currents produced are virtually non-destructive of the species of interest. Other advantages include reduced iR drop, increased mass transport to and from the electrode surface, and rapid response times.

Microelectrodes have been constructed from various materials including carbon,

gold, platinum, and mercury deposited on any of these three substrates. The most widely used geometry is disk-shaped with a diameter of 10 μm , but other geometries include micro-ring, thin-ring, hemisphere, line cylinder, and disk array (Table 5.1).

Table 5.1 Microelectrode Geometries

Geometry	Radius	Width
disk	0.3-50 μm	
micro-ring	1-50 μm	0.01-0.7 μm
thin-ring	> 1 mm	0.01-0.7 μm
hemisphere	2-7 μm	
line		0.005-100 μm
cylinder	5-12.5 μm	1 > 100 μm
disk array	0.375-5 μm	

Although there are many techniques for fabrication of microelectrodes the most common method for disk and cylindrical electrodes uses small wires of the substrate (carbon, platinum, or gold) of diameters between 5 and 20 μm . A glass capillary is pulled around the wire and then heated to seal it. For cylindrical electrodes the wire protrudes from the glass capillary, while for a disk electrode the glass is cut and polished exposing only the cross-sectional area of the wire.

Engstrom and co-workers [2] positioned 10 μm diameter microelectrodes within the diffusion layer of conventional electrodes. Movement of the microelectrode with a micro-positioning device permitted spatial resolution of the electrochemically generated concentrations in three dimensions within the diffusion layer at the macroelectrode surface. The diffusion profile measured with 2 μm resolution perpendicular to the macroelectrode surface agreed well with the theoretical profile. Dispersion in flow injection analysis was measured with microvoltammetric electrodes

by Kristensen, Wilson and Wightman [3]. The results obtained demonstrated that the primary source of dispersion was due to the tubing, while the finite volume of the channel-type detector contributed negligibly to the observed response. This technique has also been used to observe less defined flow situations such as turbulent flow or secondary dispersion effects.

5.1.1 Diffusion characteristics

Microvoltammetric electrodes perform differently from conventional electrodes. One striking difference is the sigmoidal-shaped cyclic voltammogram obtained at microelectrodes as opposed to the peak-shaped voltammograms at macroelectrodes. The current during electrolysis is proportional to the flux of molecules at the electrode surface. Initially, the flux at the electrode surface is due primarily to planar diffusion of the electroactive species to the electrode. The current, which is proportional to the electrode area, decreases with time since the rate at which the species reaches the electrode surface decreases (Figure 5.1). The rate of electrolysis exceeds the rate of diffusion resulting in a peak shaped voltammogram (Figure 5.2). When the diffusion layer thickness approaches the radius of the electrode, the diffusion layer boundary will grow into a hemispherical shape. At this point non-planar or convergent diffusion predominates (Figure 5.3). As the volume of the diffusion layer increases, more of the bulk solution contributes to the flux at the electrode which in-turn counteracts the increase in diffusion time. The rate of mass transport of the analyte to the electrode surface equals the rate of electrolysis and a steady-state current proportional to the radius of the electrode is obtained. The sigmoidal-shaped voltammograms reflect the steady-state character of the redox process at these electrodes. Thus diffusion processes that occur at an ultramicroelectrode can be equated with processes that occur at spherical electrodes.

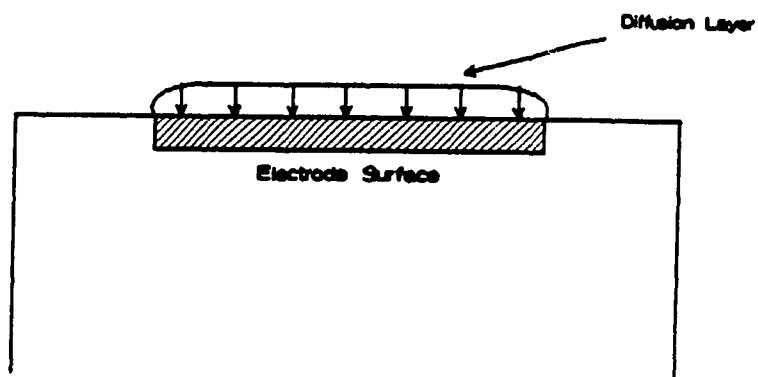


Figure 5.1 Semi-infinite linear diffusion at a macroelectrode.

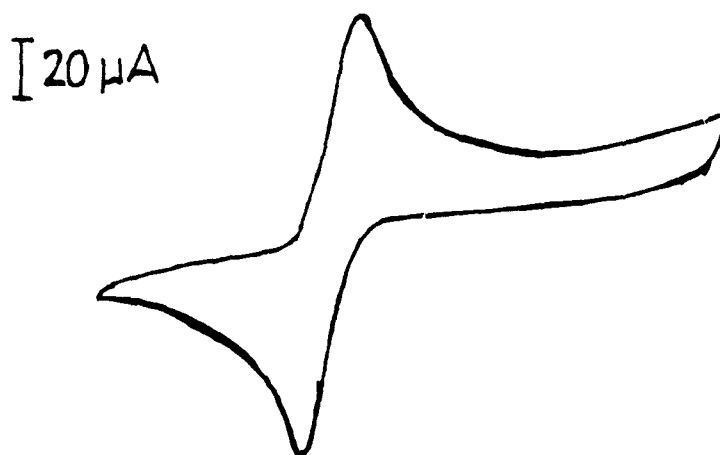


Figure 5.2 Peak-shaped voltammogram at a macroelectrode.

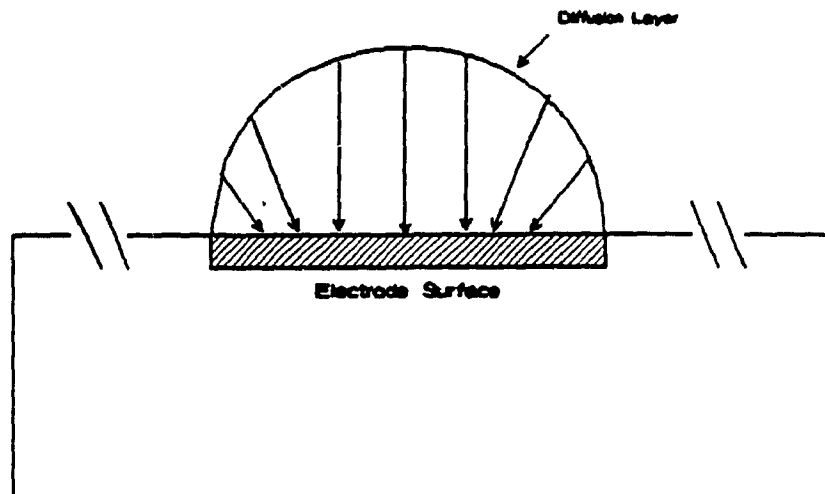


Figure 5.3 Radial diffusion at a microelectrode.

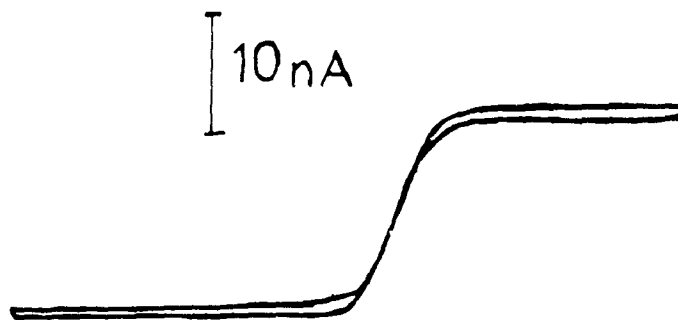


Figure 5.4 Sigmoidal-shaped voltammogram at a microelectrode.

5.1.1.1 Diffusion to a spherical electrode.

In chronoamperometry, the potential is stepped from a value where electrolysis does not occur to a value where an oxidation or reduction takes place and where the current is limited only by diffusion of the analyte to the electrode surface. A chronoamperometric experiment at a spherical electrode with radius r_0 will be considered first.

Working in spherical coordinates, the boundary conditions for reduction of species O are,

$$\lim_{r \rightarrow \infty} C(r,t) = C^* \quad \text{Bulk Concentration} \quad 5.1$$

$$C(r,0) = C^* \quad \text{when } r > r_0 \quad 5.2$$

$$C(r_0,t) = 0 \quad \text{when } t > 0 \quad 5.3$$

The concentration gradient at the electrode surface can be expressed in terms of the Faradaic current (i),

$$i = nFAD \left(\frac{\partial C(r,t)}{\partial r} \right) \quad 5.4$$

where

- n = number of electrons
- F = Faraday constant
- A = electrode area (cm²)
- D = diffusion coefficient (cm²/sec)

From Ficks's second law,

$$\frac{\partial C(r,t)}{\partial t} = D \frac{\partial^2 C(r,t)}{\partial r^2} \quad 5.5$$

Solution of this second order differential equation with the boundary conditions established above, gives the following complimentary error function for the concentration profile [4],

$$C(r,t) = C^* \left(1 - \frac{r_0}{r} \right) \operatorname{erfc} \left(\frac{r - r_0}{(4Dt)^{1/2}} \right) \quad 5.6$$

For large electrodes, where r_0 approaches infinity, the equation for the concentration profile at a large planar electrode is given by:

$$C(r,t) = C^* \operatorname{erf} \left(\frac{r - r_0}{(4Dt)^{1/2}} \right) \quad 5.7$$

At long times, the expression becomes

$$C(r,t \rightarrow \infty) = C^* \left(1 - \frac{r_0}{r} \right) \quad 5.8$$

By plotting C/C^* as a function of $r - r_0$ (the distance from the electrode surface), equation 5.7 predicts that the concentration profile will keep extending into the solution as a function of time. At small spherical electrodes the growth of the diffusion layer is initially similar to that observed at large planar electrodes (as described by equation 5.7), but at longer times the growth rate decreases considerably, as predicted by equation 5.8.

The current at a spherical electrode is obtained by differentiating equation 5.6 with respect to the radius and integrating over the area of the electrode.

$$i = nFADC^* \left(\frac{1}{(\pi Dt)^{1/2}} + \frac{1}{r_0} \right) \quad 5.9$$

I
II

where A = $4\pi r_0^2$ for a sphere
 = $2\pi r_0^2$ for a hemisphere

At short times, term I is significant and the current at a spherical electrode is governed by planar diffusion. However, at long times term I becomes insignificant and term II predominates resulting in a steady-state (or time-independent) current response. To determine the point at which the steady-state response predominates, the expression for the current at a spherical electrode can be divided by the current at a planar electrode, as described by the Cottrell equation.

$$i_{plane} = \frac{nFAD^{1/2}C^*}{(\pi t)^{1/2}} \quad 5.10$$

$$\frac{i_{sphere}}{i_{plane}} = 1 + \frac{(\pi Dt)^{1/2}}{r_0} \quad 5.11$$

The relative amount of the time-independent contribution to the total current can be determined from the dimensionless parameter, Dt/r_0^2 . For a 10% contribution from the steady-state term, Dt/r_0^2 should have a value of 3.2×10^{-3} . For aqueous solutions, where $D \approx 1 \times 10^{-5}$ cm²/sec and a typical ultramicroelectrode diameter radius of 5×10^{-4} , a 10% contribution corresponds to a time of 0.08 msec. Therefore at spherical ultramicroelectrodes, some effect of non-planar diffusion is seen at reasonably short times. Shain and Martin [5] used a hanging mercury drop electrode to experimentally verify the response described by equation 5.9. At large values of Dt/r_0^2 , namely small radii and long times, the limiting current under diffusion controlled conditions will be independent of the potential excitation. In other words,

for cyclic voltammetric experiments at slow scan rates, the current beyond the oxidation (or reduction) potential of the analyte will be constant and given by the second term of equation 5.9.

$$i_l = ar_0 n F D C^* \quad 5.12$$

where a = 4π for a sphere
= 2π for a hemisphere

Under these steady-state conditions a reverse wave is not observed since the electrolysis product has time to leave the diffusion layer. The resulting voltammograms are sigmoidal in shape. For the same experiment at faster scan rates, with small values for Dt/r_0^2 , the voltammograms resemble those observed at planar electrodes, peak-shaped. This has been experimentally verified for the reduction of $\text{Ru}(\text{NH}_3)_6^{3+}$ in aqueous medium at a hemispherical mercury electrode [6].

5.1.1.2 Shape of voltammogram at a spherical electrode.

The shape of a voltammogram can be easily evaluated under steady-state conditions. Consider the following reversible reaction,



Under steady-state conditions, the derivative of the concentration with respect to time is zero and therefore, equation 5.4 can be evaluated linearly,

$$i = nFAD \left(\frac{C_O^* - C_O(r_0)}{\delta} \right) \quad 5.13$$

This is the same equation used in the Nernst diffusion layer concept for hydrodynamic voltammetry [7]. The Nernst or stagnant diffusion layer thickness is given by δ . The concentration of O at the electrode is a function of the applied potential and is given by the Nernst equation.

$$\frac{C_O(r_0)}{C_R(r_0)} = \exp\left(\frac{nF}{RT}(E_{app} - E^0)\right) \quad 5.14$$

where E^0 = formal reduction potential
 E_{app} = applied potential

When the applied potential becomes more negative than the formal potential, all the O getting to the surface is promptly reduced, decreasing its concentration at the electrode surface to zero. The limiting current under this steady state condition is given by equation 5.12. Substituting this in equation 5.13 and with $C_O(r_0) = 0$, then

$$\frac{i_l}{nFA} = \frac{DC_O^*}{\delta} = \frac{DC^*}{r_0} \quad 5.15$$

By assuming that the diffusion coefficient of O is equivalent to that of R, the concentration of R at the electrode surface is equal to the bulk concentration of O minus its concentration at the electrode surface, $C_R(r_0) = C_O^* - C_O(r_0)$. According to equation 5.14,

$$C_R(r_0) = \frac{C_O(r_0)}{\exp\left(\frac{nF}{RT}(E_{app} - E^0)\right)} \quad 5.16$$

Therefore, solving for $C_O(r_0)$ gives the following,

$$C_O(r_0) = C_O^* - \frac{C_O(r_0)}{\exp\left(\frac{nF}{RT}(E_{app} - E^0)\right)} \quad 5.17$$

$$C_o(r_o) = \frac{C_o^*}{1 + \exp\left(-\frac{nF}{RT}(E_{app} - E^{o'})\right)} \quad 5.18$$

The value of δ has been found to be equal to the electrode radius (equation 5.15) and substituting equation 5.18 for the value of $C_o(r_o)$ into equation 5.13, gives an expression for the voltammetric curve at a spherical electrode under steady-state conditions;

$$i = \frac{nFADC_o^*}{r_o \left(1 + \exp\left(-\frac{nF}{RT}(E^{o'} - E_{app})\right)\right)} \quad 5.19$$

5.1.1.3 Diffusion to a disc electrode.

Although there are many ultramicroelectrode geometries, the most easily fabricated electrode is a microdisc. In cyclic voltammetry at conventional electrodes, the current produced is proportional to the flux of analyte molecules to the electrode surface, this flux is controlled by planar diffusion. The diffusion-limited current, in response to a potential step under conditions of semi-infinite linear diffusion, is described by the Cottrell equation (equation 5.10).

The current decreases with time since the length of time required for the species to diffuse to the electrode surface increases as the diffuse layer thickness grows, resulting in rapid depletion of the analyte. This leads to the conventional peak-shaped voltammogram. When the diffusion layer thickness approaches the radius of the electrode it continues to grow in a hemispherical shape. At this point a radial component contributes to the flux at the electrode surface. Deviations from the

Cottrell equation, due to this additional quasi-spherical component, are obtained for disc electrodes of small size and for long analysis times. This increased flux has been referred to as 'edge effects'; with construction of smaller electrodes these effects have become more pronounced. For small electrodes this increased flux to the surface counteracts the increase in time for a molecule to diffuse to the electrode surface and therefore a steady-state current response is achieved. At macroelectrodes the diffusion layer thickness that must be obtained is quite large requiring a long time to grow and because of its size it can be disturbed by convection of analyte solution. At microelectrodes the diffusion layer thickness that must be realised in order to obtain contribution from the radial diffusion is much smaller and therefore established much faster. Soos and Lingane [8] modified the Cottrell equation to quantify this effect:

$$i = nFADC \left(\frac{1}{(\pi Dt)^{1/2}} + \frac{b}{\pi^{1/2} r_0} \right) \quad 5.20$$

Saito [9] first derived an expression for the diffusion limited steady-state current at a disc of radius r_0 .

$$i_l = 4nFDC \cdot r_0 \quad 5.21$$

By substituting this into equation 5.20, the value of b is to equal to $4/\pi^{1/2}$ which agrees with the analytical solution by Oldham [10] and a simulated response by Heinze [11]. The diffusion-limited current at a finite disc electrode is identical to that of a sphere of radius $\pi r_0/4$ [12] or a hemisphere $\pi r_0/2$. Oldham [10] first noted that microdiscs and microhemispheres of equal superficial diameters give identical steady-state voltammograms under reversible conditions. Treating the microdisc electrode as though it were a sphere of radius $\pi r_0/4$, the equations developed for spherical electrodes can be applied. The current, in response to a potential step for a diffusion controlled process at a microelectrode or a spherical electrode, is made up of two components, a transient one proportional to the electrode area which is time

dependent, and a steady-state term proportional to the electrode radius.

$$i = \frac{4nFD^{1/2}C^*r_0^2}{(\pi t)^{1/2}} + 4nFDC^*r_0 \quad 5.22$$

At low scan rates (large t) and electrodes of small radii, the first term becomes insignificant and the second term, corresponding to a steady-state response, predominates resulting in sigmoidal-shaped voltammograms. Unlike spherical electrodes, the current density at microdisc electrodes is not uniform but more concentrated on the edges. Therefore, derivation of expressions for diffusion processes at a disc is more complicated.

The expected current can be predicted by analytical solutions as well as digital simulation procedures [13,14]. Aoki and Osteryoung [13] have described a two-part solution for a chronoamperometric experiment at a finite disc. The current is expressed as a function of a dimensionless time variable, $\tau = 4Dt/r_0^2$,

$$i = 4nFADC^*f(\tau) \quad 5.23$$

At short times the solution takes the following form,

$$\lim_{t \rightarrow 0} f(\tau) = \frac{\pi^{1/2}}{2\tau^{1/2}} + \frac{\pi}{4} - \frac{3\pi\tau}{2^{10}} + \dots \quad 5.24$$

At long times,

$$\lim_{t \rightarrow \infty} f(\tau) = 1 + \frac{4}{\pi^{3/2}\tau^{1/2}} + 32 \left(\frac{\left(\frac{1}{9} - \frac{1}{\pi^2} \right)}{\pi^{3/2}\tau^{3/2}} \right) + \dots \quad 5.25$$

Shoup and Szabo [14] have proposed a simpler form for this function, which is accurate to 0.6% for all times.

$$f(\tau) = 0.7854 + \frac{0.8862}{\tau^{1/2}} + 0.2146 \left(\exp \left(- \frac{0.7832}{\tau^{1/2}} \right) \right) \quad 5.26$$

The chronoamperometric expressions described above were verified by applying them to the oxidation of ferrocyanide in 0.5M K₂SO₄ at a gold disc electrode of radius 1.34x10⁻³cm [15]. It has been shown experimentally that for fast scan rates (small values of Dt/r₀²), cyclic voltammograms at microdisc electrodes are peak-shaped, indicating the predominance of planar diffusion [16]. At slow scan rates (large value for Dt/r₀²), sigmoidal-shaped voltammograms are obtained. Howell and Wightman [17] obtained sigmoidal-shaped voltammograms for ferrocene in acetonitrile at a gold microvoltammetric disc electrode (radius = 6.5x10⁻³ cm) for a 0.1 volt sec⁻¹ scan rate and a conventional peak-shaped curve at a scan rate of 10 V-sec⁻¹.

5.1.1.4 Shape of voltammogram at a disc electrode

As with spherical electrodes, the shape of the voltammogram under steady-state conditions at a microdisc can be derived using the Nernst diffusion layer concept (equation 5.13).

By combining equation 5.21 and equation 5.26, the Nernst diffusion layer thickness for a disc electrode is given by $\delta = \pi r_0/4$, thus,

$$i = 4nFDr_0 [C_O^* - C_O(r_0)] \quad 5.27$$

The concentration of O at the electrode surface is a function only of the applied potential under steady-state conditions. Consequently, the expression for C_O(r₀) is similar to that previously developed for spherical electrodes.

$$C_O^* - C_O(r_0) = \frac{C_O^*}{1 + \exp\left(-\frac{nF}{RT}(E^{0'} - E_{app})\right)} \quad 5.28$$

Therefore, the forward scan of the voltammetric curve at a microdisc electrode, under steady-state conditions, is described by the following expression;

$$i = \frac{4nFD C_O^* r_0}{1 + \exp\left(-\frac{nF}{RT}(E^{0'} - E_{app})\right)} \quad 5.29$$

Again, this is identical to that obtained for the spherical electrode case, if $r_{\text{sphere}} = 4r_{\text{disc}}/\pi$. Since the products formed at the electrode rapidly diffuse away from the diffusion layer and the mass transport of O to the electrode is time-independent, the current on the reverse scan is identical to that on the forward scan. As shown above there are similarities between the current observed at microdisc and at spherical electrodes and this presents an approximate way to obtain solutions for the more complicated geometry [18].

5.1.2 Ohmic drop at ultramicroelectrodes.

Ohmic drop, caused by current through the uncompensated solution resistance, reduces the potential at the electrode-solution interface. In practice, voltammetry with macroelectrodes in highly resistive solutions results in non-linear change in potential with time. The current through the electrolyte solution actually generates a potential that opposes the applied potential. With conventional electrodes the ohmic drop generated is subtracted from the applied potential difference between the working and reference electrode by the use of a three-electrode potentiostat. However, this method to minimize distortion from iR drop requires accurate and reproducible placement of the reference electrode tip relative to the working electrode. Other techniques to reduce ohmic drop such as semi-integral analysis [19] or derivative methods [20]

are often difficult to implement. Severe ohmic drop has precluded voltammetric measurements in highly resistive media such as supercritical fluids until the advent of microelectrodes.

The total resistance for a working microdisc electrode with a large reference electrode placed an infinite distance away is given by the following [21]:

$$R = \frac{\rho}{4r_0} \quad 5.30$$

where ρ = conductivity of the electrolyte

Although the cell resistance increases as the radius of the microelectrode is made smaller, the resistance per unit area of the electrode surface is low and becomes lower with decreasing radius. As will be shown later, the capacitive current is directly proportional to the electrode area and the resistance is inversely proportional to the electrode radius, therefore ohmic drop caused by charging current and by Faradaic current decreases with decreasing electrode area. For some voltammetric processes the observed ohmic drop at microdisc electrodes of small diameter is actually less than that predicted by combining the equations for resistance and Faradaic current [22]. This may be due to a change in the conductance at the electrode surface. As electrolysis occurs a charged species is produced which is at its highest concentration in the diffusion layer, thus generating a less resistive medium in this region. The reduced iR drop at ultramicroelectrodes allows measurements to be obtained in solutions of highly resistive nature not previously explored. Howell and Wightman [17] obtained undistorted voltammograms for ferrocene in acetonitrile with low concentrations of supporting electrolyte (0.01M TBAP) utilizing a two-electrode cell. If the current is maintained at a low value, as with microelectrodes, the potential of the working electrode can be controlled in a two-electrode cell by passing the current between the working electrode and a reference electrode of much larger area [21]. Studies have been performed with microelectrodes in other resistive media. Bond, Fleischmann and Robinson [23] were the first to report on the voltammetry of

ferrocene at the liquid-glass transition temperature of acetonitrile. Electrochemical measurements have been made in chlorobenzene, benzene, tetrahydrofuran, and 1,2-dimethoxyethane [24,25]. Ghoroghchian et al. [26] demonstrated that microelectrodes can be used as sensitive electrochemical detectors or sensors in the gas phase. In their system, the charge required for the double layer is supplied from the free carrier charge at the surface of an insulator in contact with the working microelectrode. Undistorted voltammograms for ferrocene have been achieved in supercritical carbon dioxide with added water and tetrahexylammonium hexafluorophosphate [27]. By eliminating the supporting electrolyte, Cassidy and co-workers [28] have extended the positive potential limit of acetonitrile from 2.4 volts to 4.3 volts, and were able to observe the oxidation of methane and other short-chain alkanes. Electrochemical measurements can be used to predict the feasibility of homogeneous electron-transfer reactions. With conventional electrodes these measurements have been restricted to conductive solutions which often are different from the medium in which the homogeneous reaction takes place. Microelectrodes can now be used to determine thermodynamic and kinetic parameters for heterogeneous electron-transfer reactions in the highly resistive media of the homogeneous reactions.

5.1.3 Cell time constant.

The cell time constant (RC) of an electrochemical cell determines the maximum rate of potential change. The capacitative nature of the impedance of an electrochemical cell with macroelectrodes precludes rapid changes in potential. The interest in fast electrochemical measurements stems from the desire to determine rapid heterogeneous or homogeneous reaction rates. The double layer capacitance (C) is directly proportional to the area of the electrode surface. The solution resistance (R), as shown previously, is inversely proportional to the radius, therefore the RC time constant is directly proportional to the radius of the microdisc. With reduced ohmic drop and the small cell time constant at microelectrodes, voltammetric measurements can be made in the sub-microsecond domain. As the electrode is made smaller, faster

scan rates may be used while still retaining the sigmoidal shape. At very fast scan rates with microelectrodes, current is primarily due to planar diffusion and the electrode response can be treated as a conventional electrode. A decrease in electrode radius allows faster scan rates to be used before non-planar diffusion becomes insignificant.

Robinson and co-workers [29,30] first demonstrated that the reduced values of resistance and capacitance at microelectrodes lower the time constant of the cell and therefore are useful in spectroelectrochemical measurements. At these very fast time scales planar diffusion predominates at the microelectrodes and therefore current is uniformly distributed across the electrode surface. Although background subtraction is necessary, voltammograms with useful electrochemical information can be obtained at scan rates greater than $100\ 000\ \text{volts sec}^{-1}$ with microdisc electrodes [31,32]. Fast scan cyclic voltammetry has been used to detect and characterize transient species generated electrochemically. Howell and Wightman [25] studied the doubly charged cation of diphenylanthracene which is only stable on a microsecond time scale in acetonitrile. Ultrafast cyclic voltammetry with microelectrodes has been used for the study of a fast chemical step in an electrode reaction [33]. Structural changes similar to the thermochromic conversion of bianthrone were induced by electrochemical reduction of bianthrone and the rate constant for conversion determined. Andrieux and co-workers [34] have shown that the use of fast scan cyclic voltammetry at microelectrodes allows kinetic characterization of electrochemically generated intermediates having lifetimes in the microsecond range. Double potential step chronoamperometry has been used to accurately determine the rate constant for the dimerization of the radical obtained from the reduction of 1-methyl-4-*tert*-butyl pyridinium cation [35]. The low capacitive charging current and low ohmic drop at microelectrodes permits rapid measurement of Faradaic current after an initial potential step. Fast scan cyclic voltammetry can also be used to determine the standard oxidation potential for an electrochemical oxidation generating a chemically reactive species. With macroelectrodes, upon reversing the potential sweep no reverse wave is present because of the follow-up chemical reaction. By

increasing the scan rate, the ensuing chemical reaction can be out run and a reverse wave observed. A scan rate of 10 000 volts sec⁻¹ with microelectrodes allows direct electrochemical observation of species with half-lives of 1.0 μsec [25].

5.1.4 Capacitative current at ultramicroelectrodes

In the absence of electrolysis, a two-electrode electrochemical cell behaves similar to a resistor-capacitor series network. The electrolyte solution has a finite resistance, while the working electrode behaves as a capacitor. Charge cannot cross the solution-electrode interface unless electrolysis is taking place and consequently, a capacitance (C) arises from the order of the ions in the double layer. Upon application of a potential step ΔE, current will flow as the capacitor is charged or discharged. With no electroactive species in solution, this current is equal to the charging current and is given by [36];

$$i_c = \frac{\Delta E}{R} \exp\left(\frac{-t}{RC}\right) \quad 5.31$$

The current produced as a result of the oxidation or reduction of an electroactive species in solution is actually a combination of the Faradaic current, given by the equations described previously, and the charging current. Information about the species undergoing electrolysis is contained in the Faradaic portion of the current, therefore most favourable electroanalytical techniques are those that minimize the effect of charging currents. Large capacitative currents have also precluded electrochemical measurements under a variety of conditions. Most common techniques that discriminate against capacitative current use pulsed waveforms. Upon application of a potential step, the capacitative current will decay exponentially with time, while Faradaic current decay is inversely proportional to the square-root of time. In pulsed methods, the charging current is allowed to decay before measurements are made. For long times at ultramicroelectrodes the Faradaic current rapidly converges to a steady-state value as the charging current continues to fall. As shown previously,

the RC time constant at microvoltammetric electrodes is small, and combined with long analysis times, the capacitive current at these electrodes is also reduced. Consequently, ultramicroelectrodes are better suited for pulsed voltammetric techniques. On the reverse step of a pulse a small amount of Faradaic current is produced since the product of electrolysis rapidly diffuses away from the diffusion layer. Thus, the current produced on the reverse step can be subtracted from the current measured at the pulse to obtain only the Faradaic current response. Ewing et al. [37] and Ponchon et al. [38] used normal pulse voltammetry for the *in vivo* determination of dopamine in the rat neostriatum. The pulsed waveform minimizes electrode response deterioration caused by filming of the electrode surface by electrogenerated products.

5.1.5 Small size advantages of ultramicroelectrodes

The most obvious advantage of microelectrodes is their small size. Ponchon and co-workers [38] were first to use carbon fibre electrodes *in vivo* to study the release of dopamine in the rat neostriatum. Microvoltammetric electrodes can be used to provide reproducible results in an extremely complex medium such as the mammalian brain. Nerve terminals have diameters in the 1 μm range, therefore microelectrodes are necessary in order not to destroy the region where measurements are being made. The electrode must be implanted in the brain and monitored for a minimum of 8 hours for most experiments; this does not permit any electrode resurfacing in the interim. Ewing, Dayton, and Wightman [37] have demonstrated that stable voltammograms can be obtained with ultramicroelectrodes using pulse potential waveform. Voltammograms of dopamine are sigmoidal, but dihydroxyphenylacetate, a major dopamine metabolite, and ascorbic acid both give drawn out voltammograms due to their slow rate of charge transfer at carbon fibre electrodes [39]. Although these three compounds have very similar formal potentials, the difference in charge transfer rates make the carbon fibre electrode more sensitive to dopamine. In the presence of ascorbic acid, the oxidation of dopamine is followed by the catalytic regeneration of the reductant. At microelectrodes the product of the oxidation will

diffuse a distance, given by $(Dt)^{1/2}$, greater than the radius from the microelectrode; the regenerated dopamine is far removed from the electrode surface and therefore a minimal catalytic contribution to the current is observed. The increased rate of mass transport due to non-planar diffusion eliminates the need for forced convection during the preconcentration stage of stripping analysis, thus minimizing a source of error. A static solution gives higher precision and the lower iR drop eliminates the need for high concentrations of supporting electrolyte, which interferes with the Faradaic current. Baranski and Quon [40] described the use of anodic stripping voltammetry with ultramicro mercury electrodes for cadmium and lead in 5.0 μl volumes. Very sharp peaks are obtained for anodic stripping analysis at ultramicroelectrodes since the analyte concentrated at the electrode is completely stripped during the scan.

5.1.6 Steady state current response.

Reactions following an initial electron transfer (ECE mechanism) are less apparent at microvoltammetric electrodes because of the steady-state nature of the current. The product formed during the chemical reaction following the initial electron transfer can diffuse away from the electrode surface. Since the diffusion layer thickness is considerably reduced at ultramicroelectrodes, the product is not available to undergo the second electron transfer at the electrode. This has been demonstrated experimentally for the intra-cyclization of dopamine-o-quinone, an ECE reaction [41]. The pseudo first order and second order rate constants for the catalytic regeneration of ferrocyanide following its oxidation in the presence of amidopyrine (EC' mechanism) have been determined by plotting steady-state currents as a function of electrode radius [42]. In the same paper, a rate constant for the dissociation reaction near the diffusion limit for the reduction of protons in a solution of acetic acid (CE mechanism) has been determined from the linear dependence of the inverse of the current density on electrode radius. Similarly, steady-state measurements at microelectrodes have been used to obtain kinetic data for ECE and DISP 1 (first order disproportionation reaction) type reactions [43].

5.1.7 Ultramicroelectrodes in hydrodynamic systems.

Amperometric detection in liquid chromatography and flow injection analysis is capable of detecting nanomolar concentrations of electroactive species [44].

Variations in the path of the solvent flow due to incomplete wetting of the electrode surface and fluctuations in the applied potential are two major sources of noise. Since both these sources are proportional to the electrode area (A) and the Faradaic current in a channel electrode is proportional to $A^{2/3}$, Weber and Purdy [45] have proposed a reduction in electrode area to reduce noise levels. Fluctuations in flow rate lead to a changes in the size of the stagnant layer. At macroelectrodes the diffusion layer thickness is determined by the thickness of the stagnant layer, therefore a change in flow rate results in a change in the current response of the electrode [46]. Under steady-state conditions, the small diffusion layer at an ultramicroelectrode is much smaller than the stagnant layer next to the electrode surface in a flow stream. Changes in flow rate do not effect the diffusion layer at these electrodes.

As a result of their small size, small currents are produced at microvoltammetric electrodes. To increase the magnitude of the current, an array of microdisc electrodes has been employed, where the total current is equal to the sum of the individual currents. Caudill and co-workers [47], using an array of 100 5 μm carbon disc electrodes as a detection system for liquid chromatography, have found a significant increase in the signal-to-noise ratio as well as a flow rate independent response. Since ultramicroelectrodes can be easily used in resistive media, they are particularly suited for normal phase chromatography where non-polar mobile phases are used. The ability to use ultramicroelectrodes at low electrolyte concentrations with high analytical sensitivity provides new areas for electrochemical detection for both high performance liquid chromatography and flow injection analysis. Bixler and Bond [48] used 5 μm carbon and 50 μm platinum microdisc electrodes in a wall-jet electrochemical cell for a flow injection system with micromolar concentrations of supporting electrolyte. Good sensitivity has been obtained for the detection of four catecholamines, after separation by an LC system, at a platinum thin ring electrode in the absence of a supporting electrolyte [49]. Caudill and co-workers [50]

combined rapid scanning pulse voltammetry with a microelectrode array channel-type detector for use with flow injection analysis and high performance liquid chromatography. The background corrected voltammograms obtained in the flowing stream were characteristic of the particular analyte and therefore used to identify each eluting peak.

High separation efficiencies can be achieved with open-tubular capillary column liquid chromatography. Jorgenson and co-workers [51,52] have successfully used carbon-fibre cylindrical electrodes as chromatographic detectors with open tubular capillary columns.

5.1.8 Electrochemical measurements in supercritical fluids.

Recently Bard et al., using macroelectrodes, have investigated electrochemical processes in polar supercritical fluids including ammonia [53], water [54], and acetonitrile [55]. The high critical temperatures of both acetonitrile and water and the highly corrosive nature of ammonia make them inappropriate as mobile phases for SFC at this time. Supercritical carbon dioxide, a non-polar solvent, is the most commonly used mobile phase for SFC because of its moderate critical pressure and temperature. However, electrochemical measurements in supercritical carbon dioxide using conventional electrodes are difficult at best due to the non-conductive, non polar nature of the media. Philips et al. [27] first demonstrated that voltammetry with surface modified microelectrodes is possible in near-critical carbon dioxide with small amounts of supporting electrolyte.

A two-electrode amperometric detector design using a platinum microelectrode working electrode based on the wall-jet principle has been developed. The electrochemical cell has been investigated as a detection system for SFC and the factors influencing its performance are discussed.

5.2 Experimental

For details on experimental procedures see sections 2.2.4.1. - 2.2.4.2 in chapter 2.

5.3 Results and Discussion

5.3.1 High pressure conditions.

Operation of an electrochemical detector in a flowing stream of supercritical media places strict requirements on both the electrode system and the cell. The electrochemical cell must be placed before fluid decompression in order to make measurements while the mobile phase is in the supercritical state. This means that under conventional SFC operating conditions the detector must withstand pressures up to 5000 psi.

5.3.2 Flow rate dependency.

The current response of amperometric detectors employing conventional electrodes in laminar flow streams is proportional to 1/3 power of the flow rate [56]. In liquid chromatographic systems where analyses are conducted under conditions of constant flow, this does not present a problem. However in SFC, pressure or density are controlled as opposed to flow; this results in varying flow rates throughout the chromatographic run. This precludes the use of conventional sized electrodes in SFC detectors. Under steady-state conditions, the small diffusion layer at an ultramicroelectrode is well within the stagnant layer next to the electrode surface in a flowing stream. Changes in flow rate will affect only the stagnant layer and leave the diffusion layer undisturbed at micro-amperometric detectors.

These unique properties of microelectrodes overcome some of the difficulties presented by electrochemical determinations in a supercritical flowing system and they were therefore investigated further.

5.3.3 Design of electrochemical cell.

The preliminary design employs a high pressure stainless steel tee-union as the electrochemical cell (Figure 5.5). Two ports are 1/16" diameter where fused silica tubing is swaged and the third port is 1/8" diameter for the working electrode. All

components are swaged into the cell using graphite ferrules. The small currents at microelectrodes permit the use of two-electrode systems with the cell body acting as a quasi-reference electrode. A platinum wire (10 μm) sealed in soft glass functions as the working microdisc electrode (Figure 5.6). About two centimetres of the electrode body was ground such that it slides easily into the cell compartment and provides a rough surface for swaging. A new ferrule was necessary for the electrode port each time the cell was disassembled. The restrictor is placed through the sidearm such that decompression is well removed from the working electrode. Re-sealing the electrode with the same ferrule causes failure of the fitting upon pressurization. The column eluent enters the cell through a fused silica capillary threaded into the swagelok union positioned directly above the working electrode in a wall-jet geometry. This is so since decompression near the electrode may cause precipitation of either analyte or the electrolyte modifier causing fouling of the electrode surface. This problem with decompression has been noted in other cell designs [57].

5.3.4 Characterization of electrochemical cell.

Voltammetric data obtained in resistive media cannot be directly compared to that obtained in conventional solutions. For this reason initial cell characterizations were carried out using ferrocene since (i) this redox couple has been widely used in the characterization of electrochemical systems, thus providing means for comparison and (ii) ferrocene is soluble in supercritical carbon dioxide [58]. The voltammetric behaviour of ferrocene was examined in all cases with a platinum microvoltammetric working electrode in both a three- and two-electrode system. Cyclic voltammograms of ferrocene in acetonitrile and supporting electrolyte were carried out using the 10- μm platinum working electrode in a conventional three-electrode mode. The cyclic voltammogram shown in Figure 5.7 was recorded for 5mM solution of ferrocene in acetonitrile with 0.01 M tetrabutylammonium tetrafluoroborate as the supporting electrolyte. A sigmoidal shaped voltammogram characteristic of ultramicroelectrodes was obtained with a half-wave potential of 0.42 volts vs Ag/AgCl reference electrode. This established the performance of the electrode under normal operating conditions.

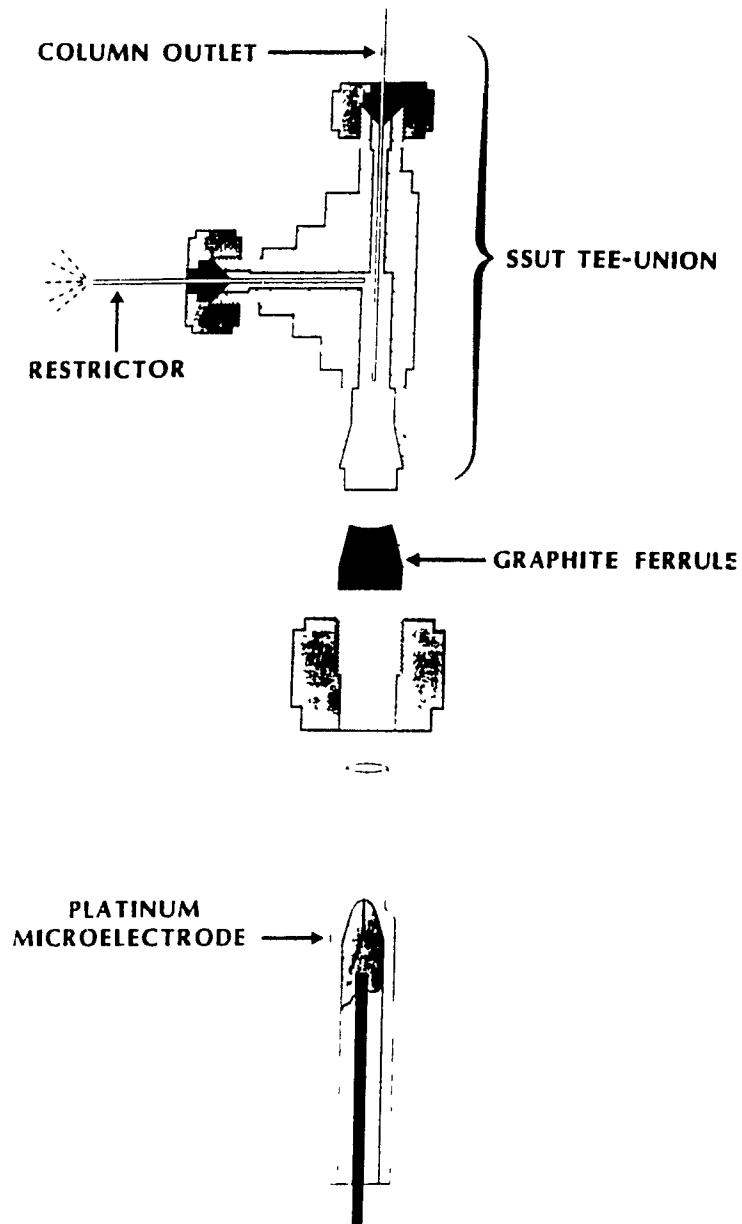


Figure 5.5 High pressure electrochemical cell.

The platinum working electrode was then incorporated into the flow cell, the flow cell was then filled with the same ferrocene/acetonitrile/supporting electrolyte mixture and a cyclic voltammogram carried out under static conditions using a two-electrode mode, where the cell body is used as a quasi-reference electrode. This established the performance of the working electrode in the cell operating in the two-electrode mode. As can be seen in Figure 5.8 the cyclic voltammogram has retained its characteristic sigmoidal shape but the half-wave potential has shifted negatively by 140 millivolts. This is due to the lack of a true reference electrode.

The electrode performance was then evaluated under more realistic operating conditions, though still in the static mode. A solution of ferrocene/acetonitrile/supporting electrolyte (50 μ l) was placed in the cell, the system was then sealed and pressurised with carbon dioxide from a syringe pump to 2000 psi at 40°C. Again the sigmoidal shape of the cyclic voltammogram is maintained but the half-wave potential shifted more negatively by about 220 millivolts (Figure 5.9), again due to the lack of a true reference electrode. This established the performance of the detector using carbon dioxide/acetonitrile/supporting electrolyte mixtures under supercritical but static conditions.

5.3.5 Hydrodynamic performance of cell.

The next evaluation was to establish the performance of the electrochemical cell in a flowing stream under normal operating conditions. Due to interference from injection solvents and turbulence generated by the injection process it was necessary to develop a chromatographic procedure so that the ferrocene signal is well removed from the void volume signals. Separations were achieved on a reversed phase column at 40°C using a variety of mobile phases from simple carbon dioxide to mixtures of carbon dioxide/acetonitrile/tetrabutylammonium tetrafluoroborate. An ultraviolet absorbance detector was positioned before the electrochemical detector, providing a dual-detection system (Figure 5.10). Ferrocene/acetonitrile solutions were then injected onto the column and the detector response monitored under a variety of operating conditions. No faradaic response was obtained from the electrochemical

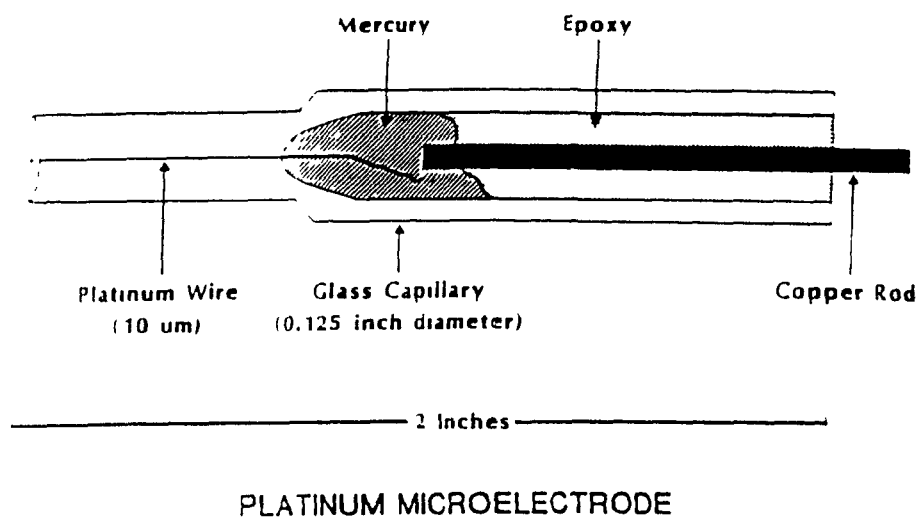


Figure 5.6 Platinum Microelectrode.

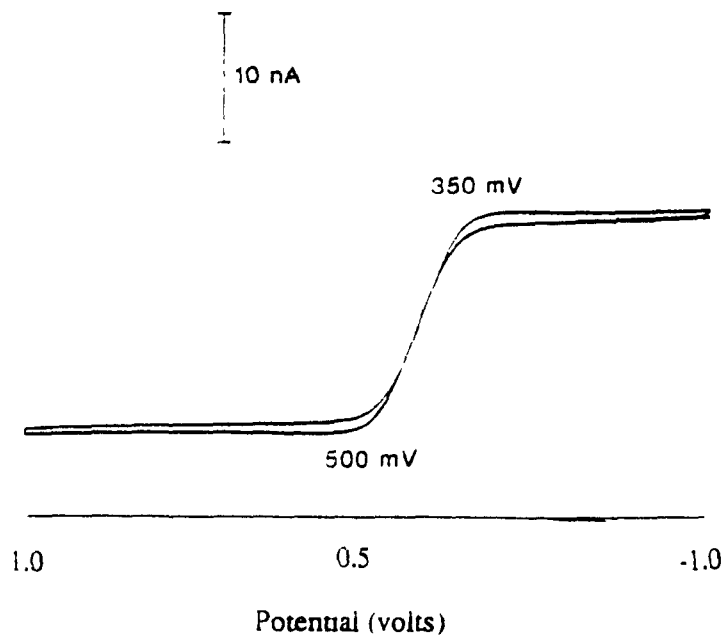


Figure 5.7 Cyclic voltammogram of ferrocene (5mM) in $\text{CH}_3\text{CN}/0.1\text{M}$ TBA TFB in three-electrode cell. Reference electrode: Ag/AgCl . Auxiliary electrode: platinum wire.

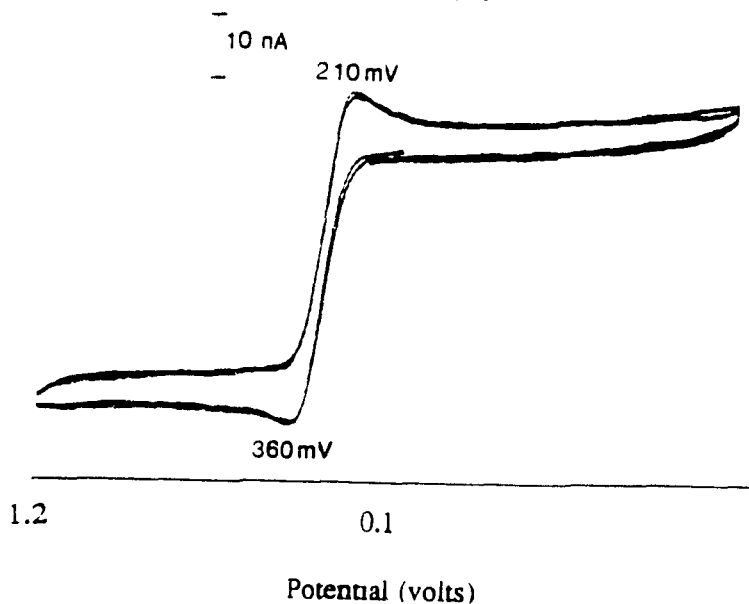


Figure 5.8 Cyclic voltammogram of ferrocene (5mM) in $\text{CH}_3\text{CN}/0.1\text{M}$ TBA TFB in electrochemical cell. Stainless steel quasi-reference electrode.

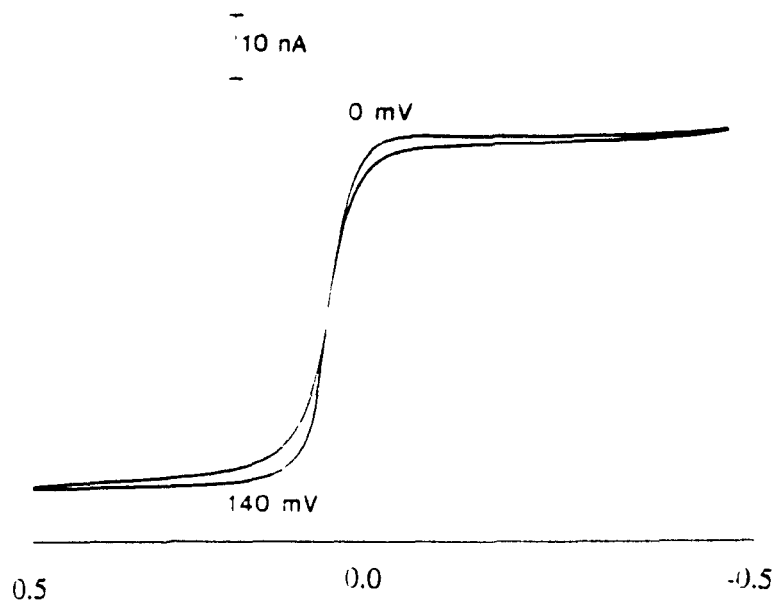


Figure 5.9 Cyclic voltammogram of ferrocene (5 mM) in $\text{CH}_3\text{CN}/0.1\text{M}$ TBA TFB in electrochemical cell pressurized to 2000 psi with CO_2 . Stainless steel quasi-reference electrode.

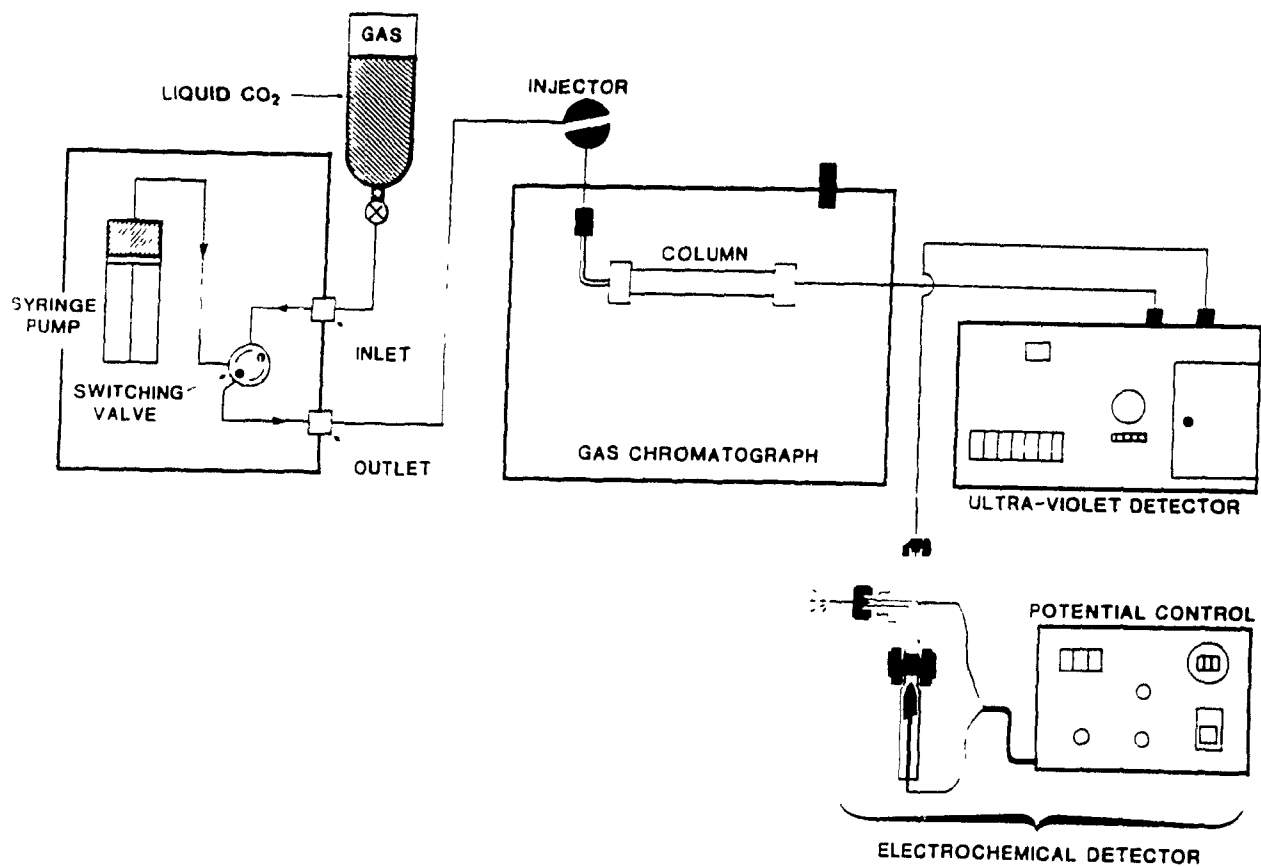


Figure 5.10 Schematic of complete SFC/ECD system.

detector at applied potentials up to 1.2 volts with simple carbon dioxide mobile phases. Acetonitrile modifier was then added to the carbon dioxide up to 1.6 mole%, at 0.4 mole% intervals. Again no faradaic response was detected at applied potentials ranging from 0.0 to 1.2 volts. Although the positive potential limit of this medium has not been determined, low noise backgrounds were recorded at applied potentials as high as 1.4 volts.

Tetrabutylammonium tetrafluoroborate (TBA TFB) at 0.05 mole% was then added to the acetonitrile modified supercritical carbon dioxide and a faradaic response was observed from the electrochemical detector. Figure 5.11 and Figure 5.12 represent chromatograms obtained for a 1- μ l injection of acetonitrile and ferrocene in acetonitrile (10 μ g/ml), respectively, with 1.6 mole% acetonitrile and 0.05 mole% TBA TFB modified supercritical carbon dioxide mobile phase under isobaric conditions at 2200 psi and 40°C. The addition of the electrolyte has either increased the conductivity of the mobile phase or, as predicted by Niehaus et al. [59], the electrolyte has formed a conducting layer on the electrode surfaces. The latter is unlikely as *in situ* formation of a conducting layer would tend to give irreproducible current responses, at least initially, and this was not observed. The high solubility of TBA TFB in acetonitrile and the low concentration of the electrolyte in the mobile phase also precludes the precipitation of the salt at the electrode surface.

Formal redox potential tables or potentials obtained from cyclic voltammograms obtained under static conditions are insufficient for determining the optimal operating potential for detecting the same species in a flowing stream. This is due to the increased iR drop in these systems. The optimum operating potential for the detection of ferrocene was established by injecting 10 μ g of ferrocene on column and measuring the current response at applied potentials between 0.0 and 1.1 volts. The reduced capacitive currents at microelectrodes led to rapid equilibration after changes in the applied potential. Unlike liquid chromatographic systems, chromatograms were recorded within fifteen minutes of a change in applied potential. A hydrodynamic voltammogram (Figure 5.13) plotted for ferrocene in this system shows an optimal applied potential of 0.9 volts. Beyond this potential there is a drop

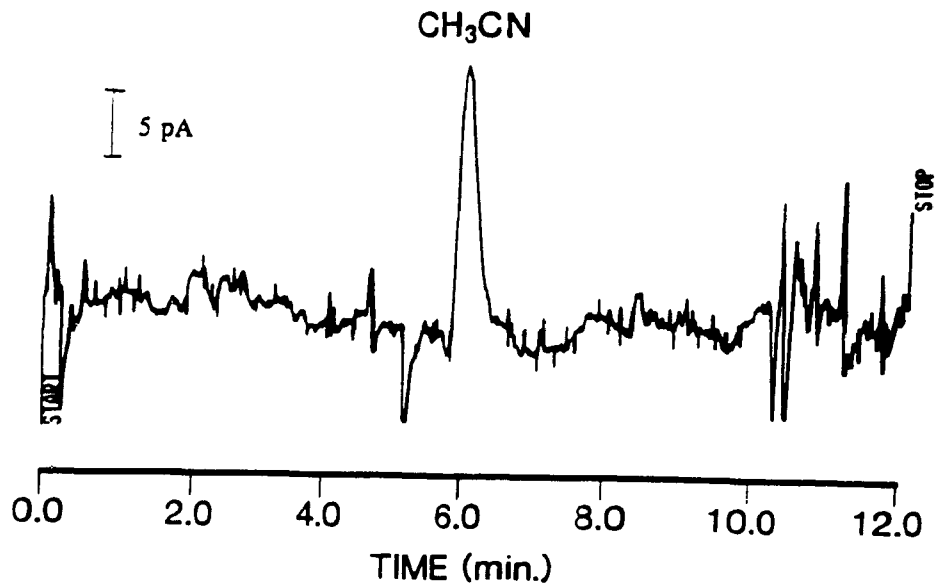


Figure 5.11 Response of electrochemical detector for the solvent (acetonitrile) injected on column. Applied potential set at 0.8 volts. Isobaric at 2200 psi and 40°C.

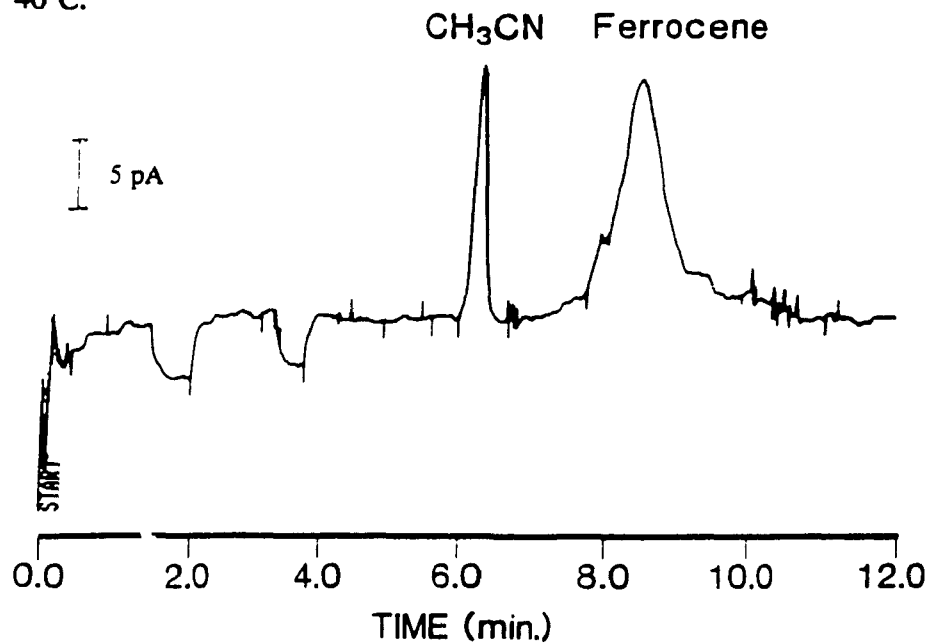


Figure 5.12 Response of electrochemical detector for 10 μ g of ferrocene injected on column. Applied potential set at 0.8 volts. Isobaric at 2200 psi and 40°C.

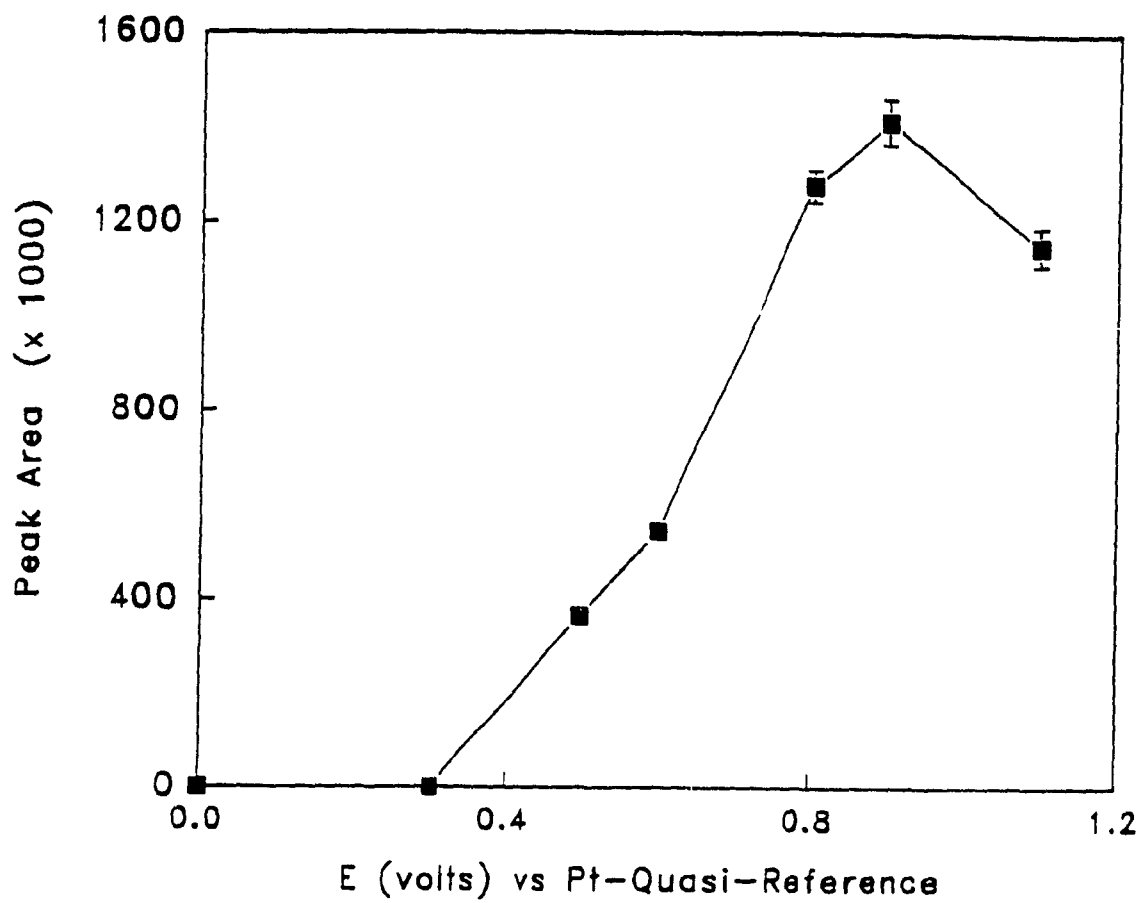


Figure 5.13 Hydrodynamic voltammogram for ferrocene, average of three injections.

in the current response that may be due to the effects of increased iR drop at higher applied potentials. The relative standard deviations are less than 5% indicating good reproducibility for this electrochemical detection system.

Although the preliminary electrochemical cell has functioned well, some problems were encountered. The hairlike thickness of the platinum fibre and the fragility of the glass capillary require specialized equipment, such as micromanipulators and microbunsen burners, for fabrication of the microelectrode. While attempting to construct the electrodes in-house, it became apparent that a perfect seal between the glass body and the platinum fibre is essential. The high pressure encountered in an SFC system tend to push the wire out of the glass capillary sleeve causing fluid build-up around and behind the fibre which eventually shatters the glass. An attempt was made to enhance the seal by using non-conducting epoxy, but supercritical carbon dioxide is able to dissolve the epoxy. These problem were overcome by using slightly modified commercially available microelectrodes from BioAnalytical Systems. Eventually after a period of use, hairline cracks were observed on the glass surrounding the electrode, resulting in erratic response. Although it is necessary to add an electrolyte to the mobile phase for detection, anticipated problems of precipitation of the tetraalkylammonium salt at the restrictor were not encountered.

The results reported above have shown the feasibility of developing an electrochemical detection strategy for SFC. According to two recent reports [58,60], voltammetry in supercritical carbon dioxide is possible only with a thin film of conducting phase, either in the form of an ion-exchange polymer or a molten salt layer, on both the surfaces of the working and quasi-reference electrodes. We have demonstrated that this conducting phase is not necessary and that electroactive species can be detected at a bare platinum microdisc working electrode of an SFC/ECD system.

5.4 Conclusion

The application of an electrochemical detection strategy in supercritical fluid chromatography would extend both the sensitivity and selectivity of the technique. The advantages of increased diffusion coefficients in supercritical fluids and low ohmic drop, fast RC time constants and flow-rate independent response at microelectrodes has led to the design and use of an electrochemical cell in an SFC method. The cell design is simple and inexpensive; the cell casing is a commercially available stainless steel tee-union and the working electrode is a slightly modified commercial microdisc platinum electrode. The cell can be easily disassembled for cleaning while maintaining high pressures when the ports are swaged. Potential is controlled with a simple three-electrode potentiostat by shorting the reference and auxiliary electrode leads. The current produced was recorded with a chromatographic integrator with no modification. The conductivity of the supercritical mobile phase was increased with the addition of tetrabutylammonium tetrafluoroborate (0.05 mole%) in acetonitrile; the electrolyte had no detrimental effect on the chromatographic behaviour. A hydrodynamic voltammogram plotted for ferrocene in this system shows an optimal applied potential of 0.9 volts. The relative standard deviation calculated for three replicate injections at each applied potential is less than 5% indicating good reproducibility for this electrochemical detection system. Further modification and complete characterization of the cell is required in order to develop a method for the separation and detection of the electroactive phenothiazinone compounds investigated in the previous chapter.

5.5 References

1. R.M. Wightman, *Anal. Chem.* **53** (1981) 1125A.
2. R.C. Engstrom, M. Weber, D.J. Wander, R. Burgess, S. Winquist, *Anal. Chem.* **58** (1986) 844.
3. E.W. Kristensen, R.L. Wilson, and R.M. Wightman, *Anal. Chem.* **58** (1986) 986.
4. P. Delahay, *New Instrumental Methods in Electrochemistry*, Interscience, New York, (1954).
5. I. Shain and K.J. Martin, *J. Phys. Chem.*, **65** (1961) 254.
6. K.R. Wehmeyer and R.M. Wightman, *Anal. Chem.*, **57** (1985) 1989.
7. *Laboratory Techniques in Electroanalytical Chemistry*, P.T. Kissinger and W.R. Heineman ed., Marcel Dekker, New York, (1984), Chapter 3.
8. Z.G. Soos and P.J. Lingane, *J. Phys. Chem.* **68** (1964) 3821.
9. Y. Saito, *Rev. Polagr. Jpn.*, **15** (1968) 177.
10. K.B. Oldham, *J. Electroanal. Chem.*, **122** (1981) 1.
11. J. Heinze, *J. Electroanal. Chem.*, **124** (1981) 73.
12. J.R. Delmastro and D.E. Smith, *J. Phys. Chem.*, **71** (1967) 2138.
13. K. Aoki and J. Osteryoung, *J. Electroanal. Chem.*, **122** (1981) 19.
14. D. Shoup and A Szabo, *J. Electroanal. Chem.*, **140** (1982) 237.
15. T. Hepel, W. Plot, and J. Osteryoung, *J. Phys. Chem.*, **87** (1983) 1278.
16. T. Galus, J.O. Schenk, and R.N. Adams, *J. Electroanal. Chem.*, **135** (1982) 1.
17. J.O. Howell and R.M. Wightman, *Anal. Chem.*, **56** (1984) 524.
18. M.A. Dayton, A.G. Ewing, and R.M. Wightman, *Anal. Chem.*, **52** (1980) 2392.
19. M.W. Vandenberg and D.M. Evans, *Anal. Chem.*, **46** (1974) 643.
20. E. Ahlberg and V.D. Parker, *J. Electroanal. Chem.*, **121** (1981) 57.

21. B. Scharifker and G. Hills, *J. Electroanal. Chem.*, **130** (1981) 81.
22. A.M. Bond, M. Fleischmann, and J. Robinson, *J. Electroanal. Chem.*, **172** (1984) 11.
23. A.M. Bond, M. Fleischmann, and J. Robinson, *J. Electroanal. Chem.*, **180** (1984) 257.
24. R. Lines and V.D. Parker, *Acta. Chem. Scand. B.*, **31** (1977) 369.
25. J.O Howell and R.M. Wightman, *J. Phys. Chem.*, **88** (1984) 3915.
26. J. Ghoroghchian, F. Sarfarazi, T. Dibble, J. Cassidy, J.J. Smith, A. Russel, G. Dunmore, M. Fleischmann, and S. Pons, *Anal. Chem.*, **58** (1986) 2278.
27. M.E. Phillips, M.R. Deakin, M.V. Novotny, and R.M. Wightman, *J Phys. Chem.*, **91** (1987) 3934.
28. J. Cassidy, S.B. Khoo, S. Pons, and M. Fleischmann, *J. Phys. Chem.*, **89** (1985), 3933.
29. R.S. Robinson and R.L. McCreery, *Anal. Chem.*, **53** (1981) 997.
30. R.S. Robinson, C.W. McCurdy, and R.L. McCreery, *Anal. Chem*, **54** (1982) 2356.
31. D.O. Wipf, E.W. Kristensen, M.R. Deakin, and R.M. Wightman, *Anal. Chem.*, **60** (1988) 306.
32. M.I. Montenegro and D. Pletcher, *J. Electroanal. Chem.*, **88** (1986) 371.
33. A. Fitch and D.H. Evans, *J. Electroanal. Chem.*, **202** (1986) 83.
34. C.P. Andrieux, P. Hapiot, and J-M. Saveant, *J. Phys. Chem*, **92** (1988) 5987.
35. C.P. Andrieux, P. Hapiot, and J-M. Saveant, *J. Phys Chem*, **92** (1988) 5992.
36. A.J. Bard and L.R. Faulkner, *Electrochemical Methods*, Wiley, New York, (1980) p384.
37. A.G. Ewing, M.A. Dayton, and R.M. Wightman, *Anal Chem*, **53** (1981) 1842.
38. J-L. Ponchon, R. Cespuglio, F. Gonon, M. Jouvet, and J-F. Pujol, *Anal Chem*, **51** (1979) 1483.
39. M.A. Dayton, A G. Ewing, and R.M. Wightman, *Anal Chem*, **52** (1980) 2392.
40. A.S. Baranski and H. Quon, *Anal. Chem.*, **58** (1986) 407.

41. M.A. Dayton, J.C. Brown, K.J. Stutts, and R.M. Wightman, *Anal. Chem.*, **52** (1980) 946.
42. M. Fleischmann, F. Lasserre, J. Robinson, and D. Swan, *J. Electroanal. Chem.*, **177** (1984) 97.
43. M. Fleischmann, F. Lasserre, and J. Robinson, *J. Electroanal. Chem.*, **177** (1984) 115.
44. P.T. Kissinger, *Anal. Chem.*, **49** (1977) 447A.
45. S.G. Weber and W.C. Purdy, *Anal. Chim. Acta*, **100** (1978) 531.
46. D.G. Swartzfager, *Anal. Chem.*, **48** (1976) 2189.
47. W.L. Caudill, J.O. Howell, and R.M. Wightman, *Anal. Chem.*, **54** (1982) 2532.
48. J.W. Bixler and A.M. Bond, *Anal. Chem.*, **58** (1986) 2859.
49. S.B. Khoo, H. Gunasingham, K.P. Ang, and B.T. Tay, *J. Electroanal. Chem.*, **216** (1987) 115.
50. W.L. Caudill, A.G. Ewing, S. Jones, and R.M. Wightman, *Anal. Chem.*, **55** (1983) 1877.
51. L. A. Knecht, E.J. Guthrie, and J.W. Jorgenson, *Anal. Chem.*, **56** (1984) 479.
52. J.G. White and J.W. Jorgenson, *Anal. Chem.*, **58** (1986) 2992.
53. R.M. Crooks and A.J. Bard, *J. Phys. Chem.*, **91** (1987) 1274.
54. W.M. Flarsheim, Y-M. Tsou, I. Trachtenberg, K.P. Johnston, and A.J. Bard, *J. Phys. Chem.*, **90** (1986) 3857.
55. R.M. Crooks and A.J. Bard, *J. Electroanal. Chem.*, **243** (1987) 117.
56. L.R. Snyder and J.J. Kirkland, *Introduction to Modern Liquid Chromatography*, John Wiley & Sons, Inc., New York, 1979, pp.153-8.
57. A.C. Michael and R.M. Wightman, *Anal. Chem.*, **61** (1989) 2193.
58. R.E. Jentoft and T.H. Gouw, *Anal. Chem.*, **44** (1972) 681.
59. D. Niehaus, M. Philips, A.C. Michael, and R.M. Wightman, *J. Phys. Chem.*, **93** (1989) 6232.
60. A.C. Michael and R.M. Wightman, *Anal. Chem.*, **61** (1989) 270.

Chapter 6

Determination of Sorbitan Trioleate in Metered-dose Inhalers by Supercritical Fluid Chromatography

6.1 Introduction

Supercritical fluid chromatography can be interfaced with both specific and universal detection systems. Although GC techniques can provide universal detection, the solutes must be thermally stable and have an appreciable volatility for migration. HPLC is suitable for the analysis of thermally labile, non-volatile solutes, but common LC detection systems require that the analyte have a chromophore. By combining the elution power of liquid-like densities, low critical temperature mobile phases and universal detection systems, SFC is capable of analyzing many compounds not amenable to either GC or HPLC techniques. The analysis of sorbitan trioleate, a high molecular weight, thermally labile surfactant by supercritical fluid chromatography with flame-ionization detection was carried out to demonstrate the unique capabilities of this technique.

Metered-dose inhalers are compact, pressurized aerosol dispensers specially designed for the oral inhalation delivery of multiple doses of a finely dispersed drug to the lung. Metered-dose inhalers typically discharge several hundred accurately metered shots, each with a drug concentration between 50 µg and 5 mg, generally delivered in a metered liquid volume between 25 and 100 µl as a finely atomized spray. The basic metered-dose inhaler consists of five essential components 1. container (aluminum); 2. metering valve; 3. propellant; 4. actuator and, 5. drug in suspension form (Figure 6.1). The metering valve is the most crucial component in terms of design and manufacturing quality, since it must accurately meter many

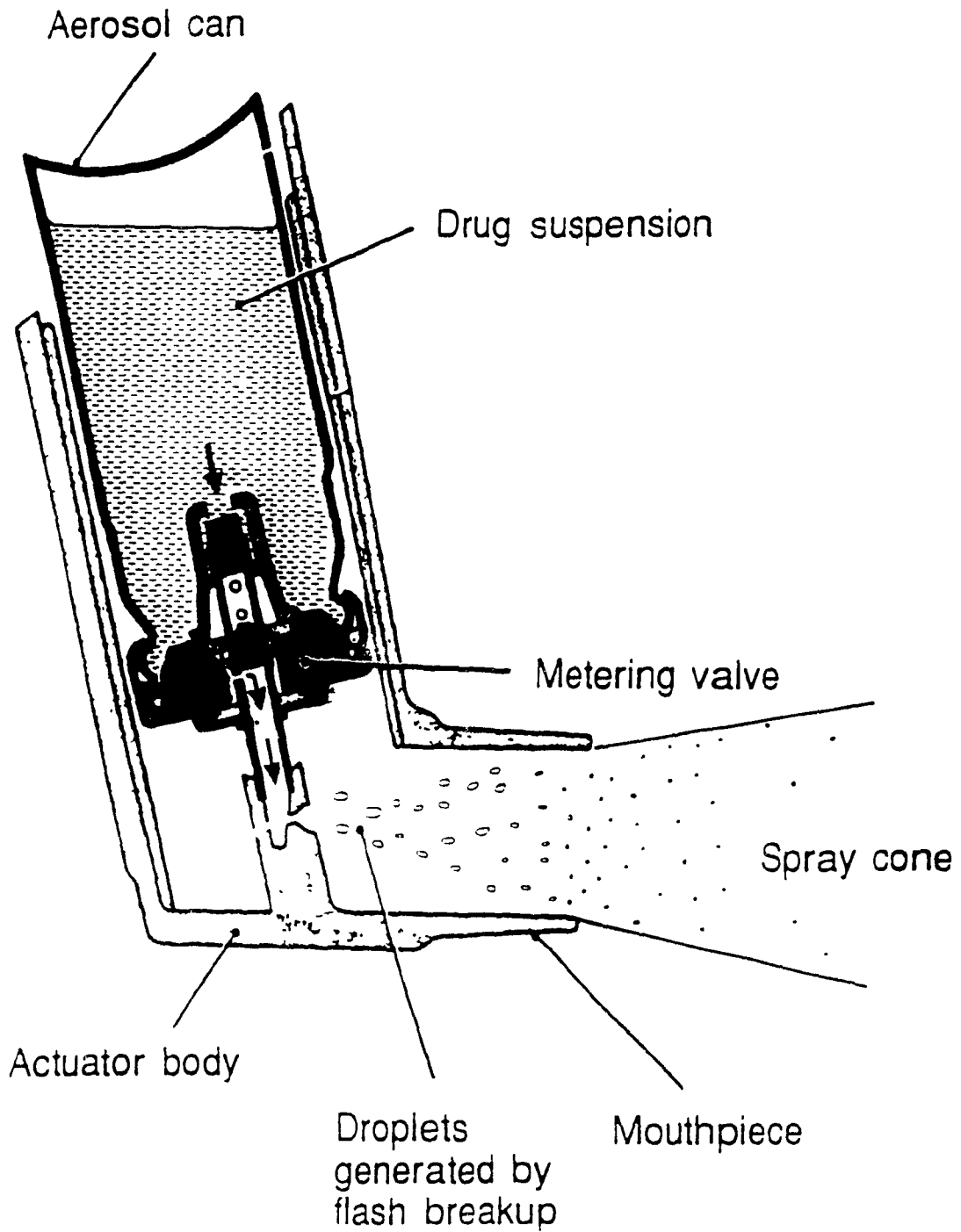


Figure 6.1 Schematic of a metered-dose inhaler.

successive doses of a liquid formulation while maintaining a proper vapour seal during the lifetime of the aerosol product. The drug is usually present in a suspension formulation because of the greater chemical stability and lower impactational deposition of droplets in the throat. The particle size of the drug powder is critical in determining the pulmonary deposition, suspension stability and metering valve function. The propellant is a blend of approved liquefied gas chlorofluorocarbons, capable of producing an aerosol cloud of suitably fine drug particles. The liquefied gas propellants must also maintain a steady vapour pressure during emptying in order to give uniform particle dispersion during the use of the whole contents. Excipients used in the propellant blend are typically surfactants which presumably reduce the flash breakup and volatility of the droplets, resulting in greater delivery efficiency. The concentration of the surfactant does not affect the concentration of the drug released per dose, but does influence the aerosol flumes (Figure 6.2). The addition of increasing amounts of sorbitan trioleate, a surfactant, to the propellant blend causes a progressive increase in the persistence of the flumes. This is a direct result of the reduced rate of volatilization and reduced flash break up of the droplets. There are considerable constraints on selection of surfactants which are toxicologically satisfactory for inhalation use.

Sorbitan esters are nonionic surface active agents used in the preparation of various pharmaceutical formulations and as additives in foods, beverages, drugs, textiles, and plastics. Sorbitan trioleate (SPAN 85®) (Figure 6.3), a partial ester of oleic acid derived from sorbitol, is commonly used in many drug products. It is used in metered-dose inhalers to keep the drug dispersed in the propellant and to lubricate the actuator valve. SPAN 85 is presently used in the preparation of an in-house aerosol formulation, up to approximately 5% by weight. There has been some concern as to the possible toxicity by inhalation of sorbitan trioleate. Published oral and dermal toxicity studies label sorbitan trioleate as relatively non-toxic by oral administration and causes slight irritation when administered topically [1,2]. However, good product design dictates that the amount of sorbitan trioleate used be compatible with achieving optimum performance characteristics and be within the

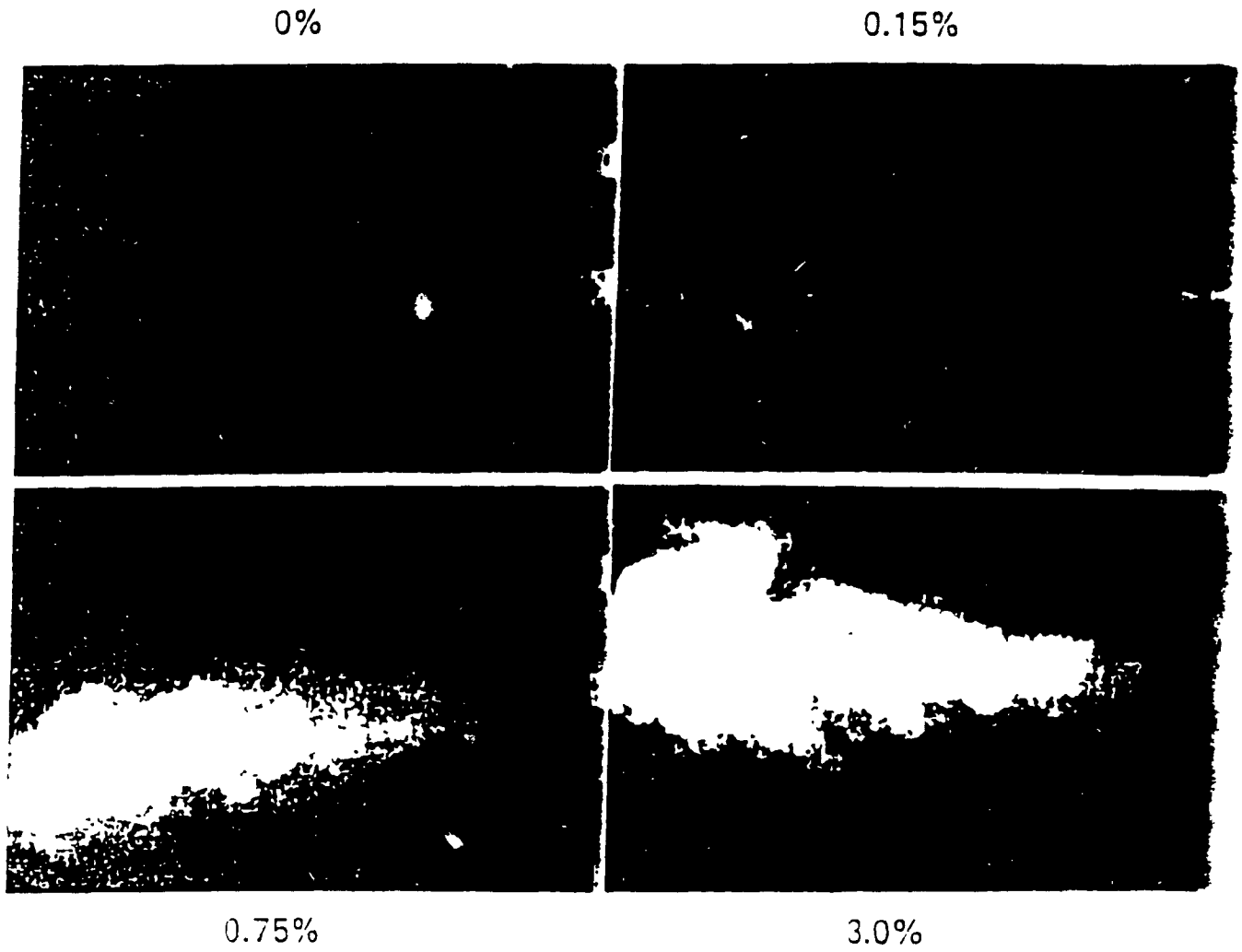


Figure 6.2 Effect of SPAN 85 concentration on aerosol plumes.

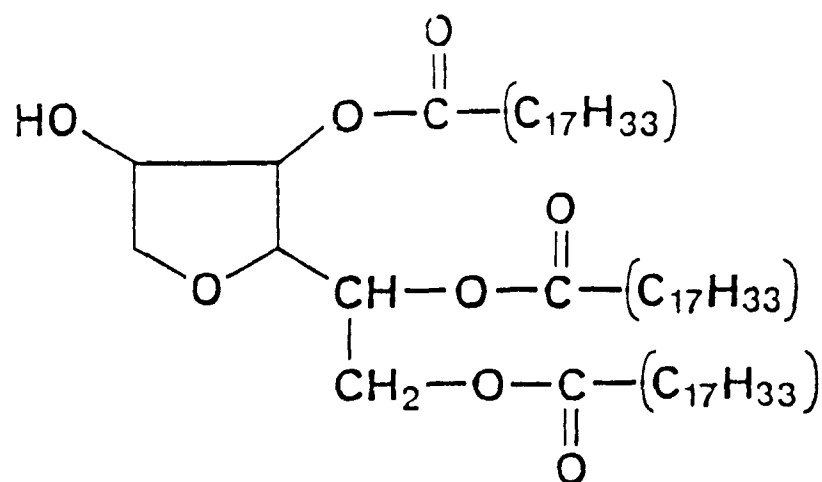


Figure 6.3 Structure of sorbitan trioleate.

industry-accepted quantities. Although listed as an ingredient in several commercially available aerosol formulations, the level in each dose is not reported. Consequently an assay procedure for the measurement of sorbitan trioleate in four marketed aerosol preparations and an experimental formulation was developed.

6.2 Experimental

For experimental details see sections 2.2.5.1 - 2.2.5.2 in chapter 2.

6.3 Results and Discussion

6.3.1 Restrictor placement

When supercritical carbon dioxide is used as the mobile phase, flame-ionization detection can be readily interfaced to SFC to provide a detection method with universal and sensitive response characteristics. The low critical temperature of

carbon dioxide also permits the analysis of thermally labile compounds. The effluent from the column is introduced into the flame ionization detector after it has expanded to ambient pressure. High flow rates, typical for packed columns, causes cooling which can result in decreased ionization efficiency in the flame or it can extinguish it entirely. This is a result of a large Joule-Thompson cooling effect which occurs due to the adiabatic expansion of the supercritical fluid mobile phase [3]. FID spiking is controlled by postponing decompression as long as possible (this allows less time for nucleation) while heating the mobile phase at the restrictor outlet where the cooling effect of the expanding fluid is greatest [3]. When using packed columns, the end of the restrictor is placed about 1 to 2 cm below the FID jet (Figure 6.4), permitting higher flows to be introduced into the flame while keeping the flame stable during pressure or density programming. For a given set of chromatographic parameters the effect of the restrictor tip position for two flow rates was investigated. Using a reversed column (250 X 1.0 mm) at 60°C, supercritical carbon dioxide mobile phase, a pressure program from 1800 psi to 2800 psi at 65 psi per minute, and the flame ionization detector set at 350°C, a test solution of tetradecane, pentadecane and hexadecane (0.03% w/w) in hexane was injected for various restrictor positions. The restrictor outlet gas flow rate was measured using a flow-meter with the restrictor tip flush with the jet head (heated to 350°C) and a carbon dioxide inlet pressure of 1800 psi. At a gas flow rate of 30 ml per minute, the restrictor must be placed at least 0.5 cm away to keep the flame lit.

Four injections of the standard solution were averaged for each set of conditions, the data collected have been summarized in Table 6.1. The peak to peak noise in the base line was determined by multiplying the noise level measured from the chromatogram by the range setting on the gas chromatogram and dividing by the attenuation setting on the integrator. The noise level was measured at a constant mobile phase pressure of 1800 psi. Peak areas generally decreased at the higher flow rate, as would be expected for a mass sensitive detector. Peak areas are smaller for the later eluting peaks as the restrictor tip is placed further from the jet head. The later eluting peaks were chromatographed at higher pressures, indicating that the

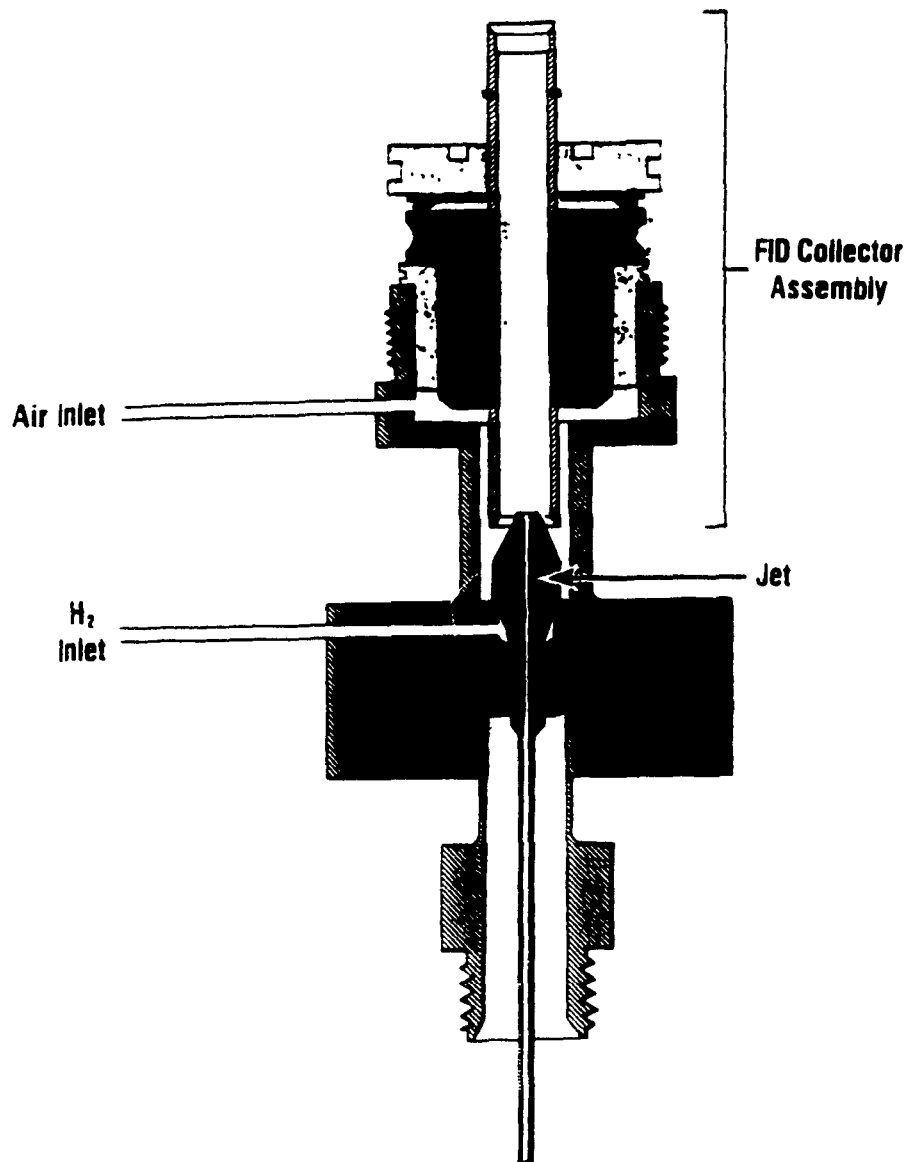


Figure 6.4 Schematic of flame-ionization detector.

Table 6.1 Effect of Restrictor Position

Position (cm)	Background Signal (pA)	Noise _{p-p} (pA)	Peak Area (pA)	RSD%
Flow rate = 17 ml/min				
0.5	48	1.74	441832500	4.49
			12508725	7.75
			1540950	9.90
			1670625	9.44
1.0	57	3.48	383920000	2.70
			9740620	4.84
			1229340	8.86
			1454700	5.12
1.5	54	1.84	382825000	0.67
			9347540	6.97
			1159050	2.86
			1223000	2.21
2.0	44	2.56	381700000	1.35
			8645000	9.43
			949360	8.36
			977375	3.97
Flow rate = 30 ml/min				
0.5	62	1.04	481293333	2.95
			8610833	4.95
			1156867	6.86
			1200487	9.10
1.0	48	2.80	353298000	0.82
			6387880	2.93
			939680	5.55
			1113290	5.34
1.5	56	1.74	355985000	1.46
			6591733	2.50
			957333	1.03
			1024300	0.95
2.0	52	3.48	353506667	0.55
			6541977	3.27
			832371	6.03
			923053	1.93

position of the restrictor is more critical at the higher densities (i.e. higher flow rates). The restrictor should, therefore, be placed as close to the jet head as possible without extinguishing the flame. For the all experiments a 30 ml/min restrictor was placed 0.5 cm from the flame jet head.

6.3.2 Chromatographic separation

The separation of sorbitan trioleate was achieved on a C_{18} column with supercritical carbon dioxide mobile phase at comparatively low temperature and pressure. The capacity ratio for the surfactant decreased with increasing pressure at constant temperature, suggesting that the retention mechanism is governed by the analyte solubility in the supercritical fluid phase. Under isobaric and isothermal conditions, sorbitan trioleate elutes as one major and two minor components (Figure 6.5). The larger peak with a capacity ratio of 1.7 was used to quantitate sorbitan trioleate. For both standards and samples, four injections were averaged and pyrene (2 mg/ml) was used as the internal standard for all solutions. A calibration curve was prepared by injecting serial dilutions of a stock solution (16.4 mg/ml) of sorbitan trioleate in dichloromethane. A linear response was obtained for a plot of peak height ratio between 0.5 - 16 ug injected on column (Figure 6.6).

6.3.3 Concentration of SPAN 85 in each formulation

Five canisters of each product were analyzed. RSD values for retention times were less than 0.5 % and peak height ratios measurements had RSD's between 1.0 and 2.0 %. The amount per dose was calculated by dividing the total weight of sorbitan trioleate per canister by the label claim number of bursts (Table 6.2). The sorbitan trioleate is well separated from other components of all the formulations tested. Figures 6.7 to 6.11 are representative chromatograms for each of the four marketed aerosols and the in-house formulation. The in-house formulation is designed to deliver 120 μ g of sorbitan trioleate per dose which agrees well with the amount found, 123 μ g/burst. The detection limit calculated as three times the peak-to-peak baseline noise

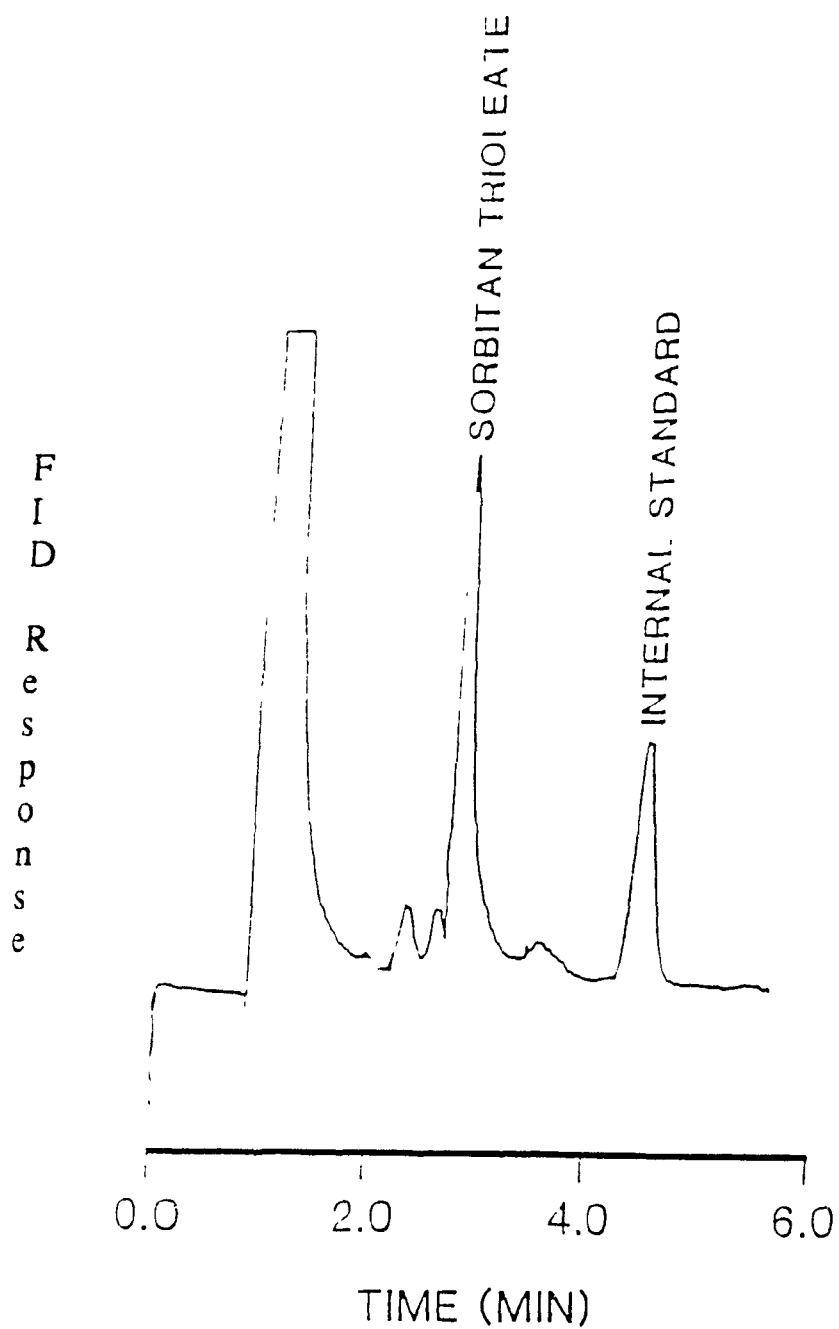


Figure 6.5 Chromatogram of sorbitan trioleate standard (3.2 μg). Column: 2.1x100 mm ODS (5 μm). Mobile phase: supercritical CO_2 . Isobaric at 2400 psi, 40°C.

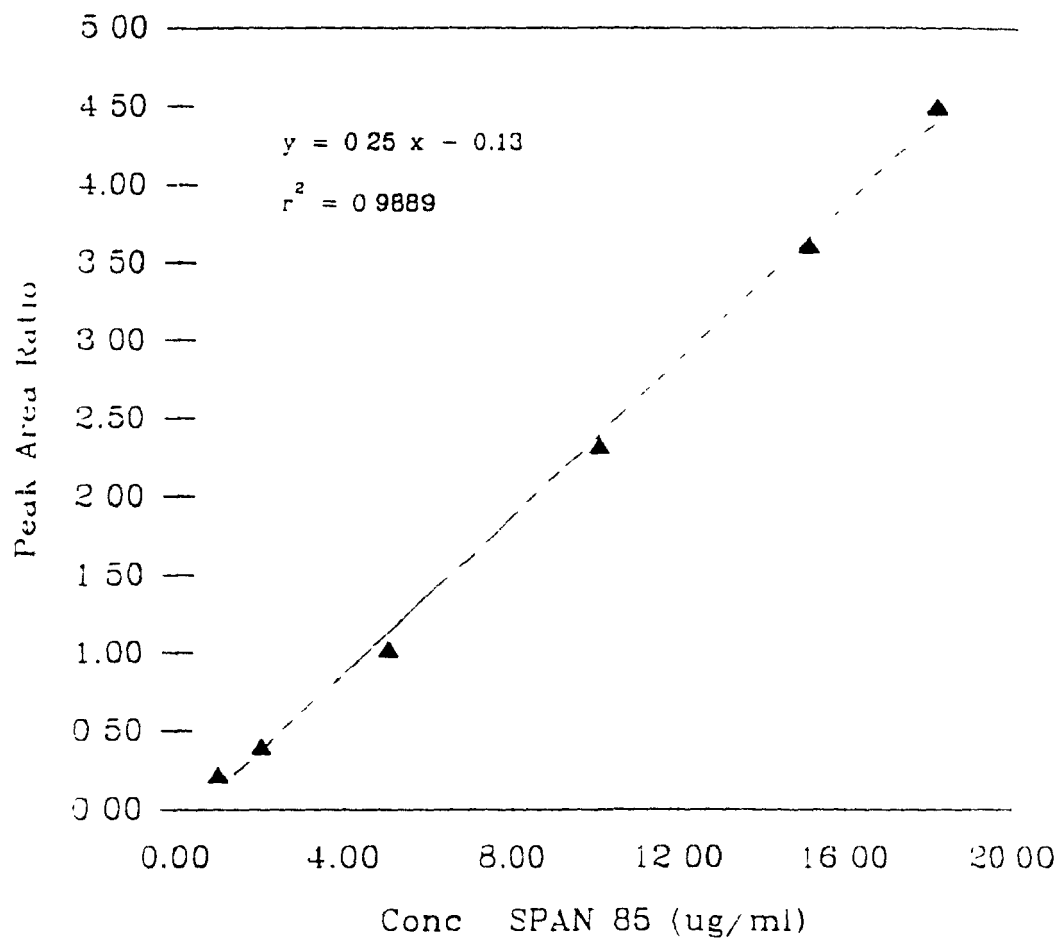


Figure 6.6 Calibration curve for sorbitan trioleate with pyrene as the internal standard.

Table 6.2 SPAN 85 in Drug Products.

Product	Amount per Dose	RSD%
Experimental	123 μg	1.4
Duo-Medihaler [®]	214 μg	1.6
Medihaler ISO [®]	267 μg	1.7
Medihaler EPI [®]	160 μg	1.2
Alupent [®]	212 μg	1.8

was 50 ng per injected volume. This method is currently being used to determine sorbitan trioleate droplet size and distribution in metered-dose inhaler plumes.

6.4 Conclusion

An assay has been developed for the determination of sorbitan trioleate in metered-dose inhalers. Analysis by conventional GC or HPLC methods is not possible because of SPAN 85's thermal instability and lack of a chromophore. Supercritical fluid chromatography with flame-ionization detection was used to separate and detect sorbitan trioleate in aerosol formulations. This method is being used to study effects of surfactant concentration on the formulation performance.

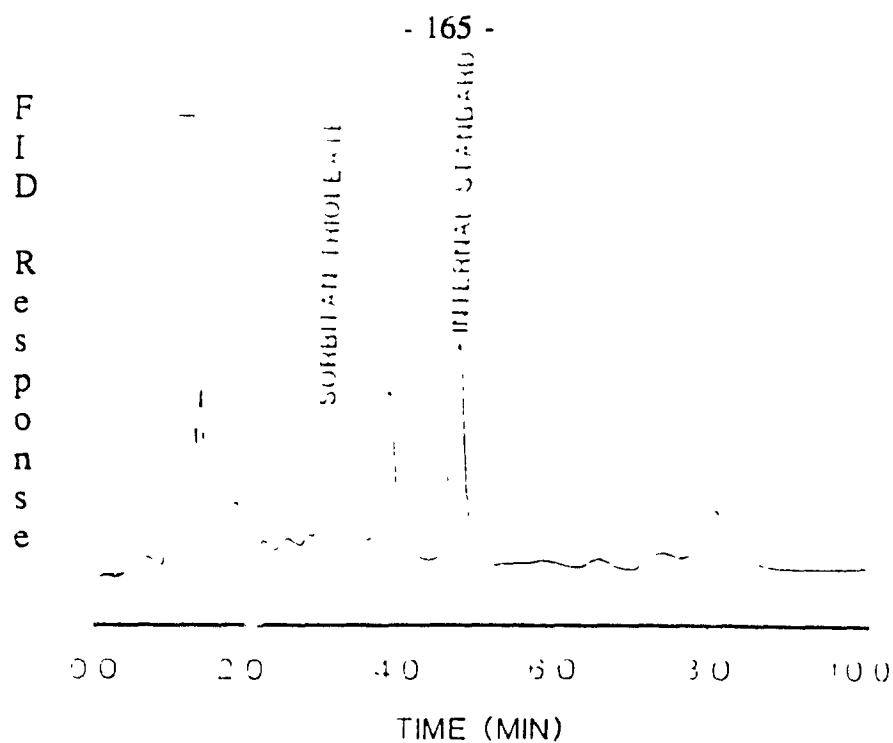


Figure 6.7

Chromatogram of Medihaler ISO® sample (0.95 µg). See Figure 6.6 for chromatographic conditions.

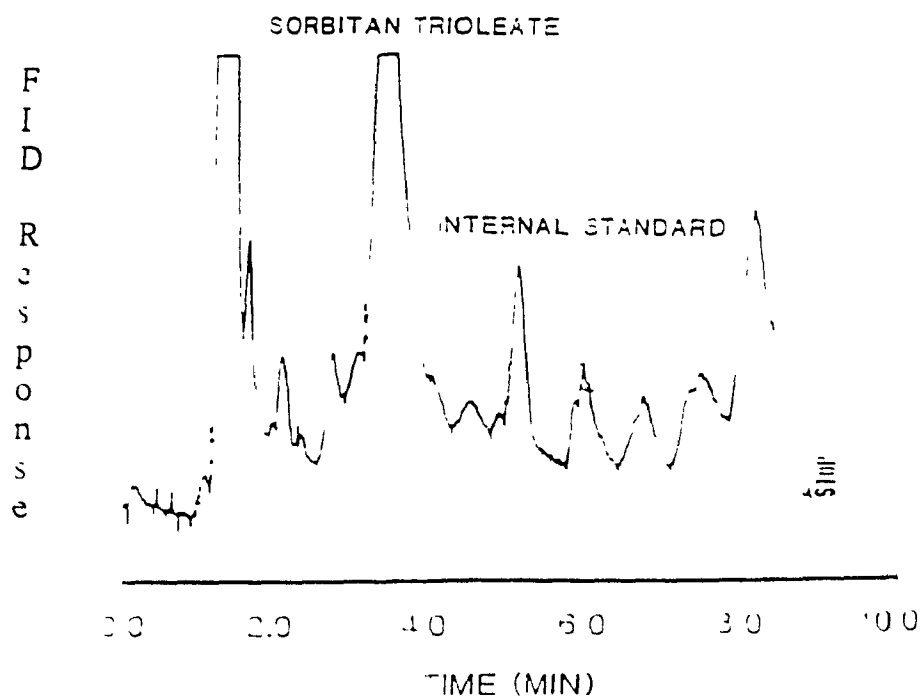


Figure 6.8

Chromatogram of Medihaler EPI® sample (1.5 µg). See Figure 6.6 for chromatographic conditions.

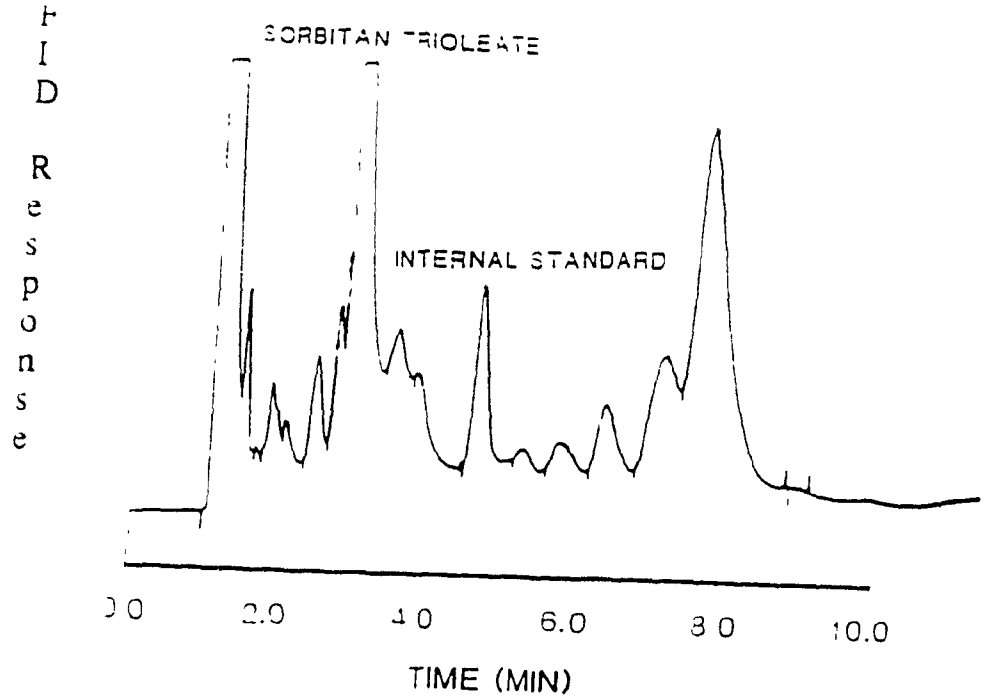


Figure 6.9

Chromatogram of Duo-Medihaler® sample (3.1 µg). See Figure 6.6 for chromatographic conditions.

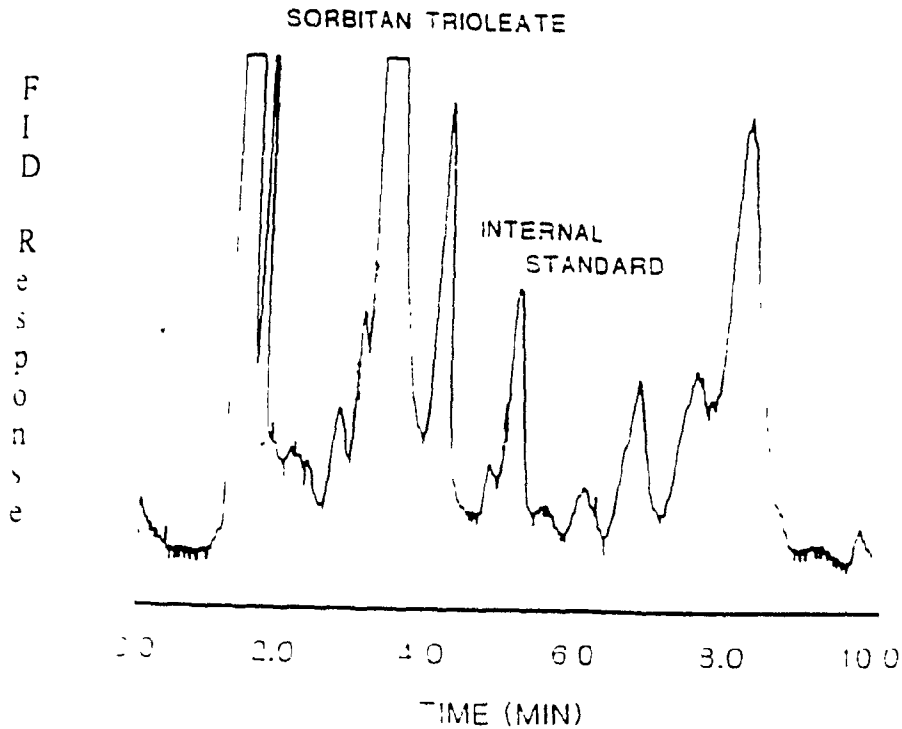


Figure 6.10

Chromatogram of Alupent® sample (2.0 µg). See Figure 6.6 for chromatographic conditions.

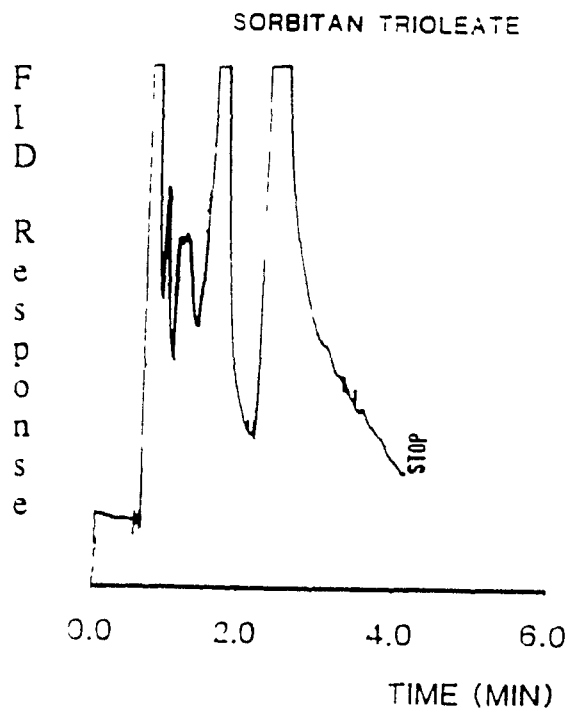


Figure 6.11

Chromatogram of in-house formulation (0.40 μ g). See Figure 6.6 for chromatographic conditions.

6.5 References

1. Cosmetic, Toiletry and Fragrance Assoc., J. Am. Coll. Toxicol., 3(5), **1-82**, (1984).
2. Yamamoto, H.; Tsutsui, K.; Shimadu, K.; Imai, S., J. Toxicol. Sci., 8(4), **301-310**, (1983).
3. T.L. Chester, *Microbore Column Chromatography: A Unified Approach to Chromatography.*, New York, (1989) Chapter 11, 369.

Contributions to Original Knowledge

In this work the following contributions to original knowledge are claimed.

1. The importance of the influence of density on chromatographic behaviour in simple supercritical carbon dioxide and modified carbon dioxide mobile phases was demonstrated.
2. A technique to subdivide gases was modified for the preparation of mixed supercritical mobile phases.
3. It was demonstrated that certain mobile phase modifiers alter the chromatographic process by increasing the solubility of the solutes in the mobile phase and/or by modifying the stationary phase surface.
4. The information gained from mobile phase modifier studies was used to develop methodology for the separation and detection of a series of phenothiazinone compounds.
5. A simple and rapid assay for L-615,919 in plasma was developed.
6. The determination of sorbitan trioleate in metered-dose inhalers by supercritical fluid chromatography with flame-ionization detection was achieved.
7. An electrochemical detector incorporating a platinum ultramicro working electrode and a high pressure stainless steel cell was designed and constructed.
8. The feasibility of this electrochemical system as a detector for SFC was demonstrated.

Appendix A

Pascal Program to Calculate Operating Pressure

Program Pressure;

{Program to calculate pressure at a given density and temperature for pure and for modified supercritical carbon dioxide, using the Peng-Robinson Equation of state.}

const

r = 0.082054;
TC = 304.2;
PC = 72.8;
WC = 0.225;
KC = 0.70798;
MC = 44.02;

var

G, CHOICE, T, D : INTEGER;
XI, XJ, PA, V, TA, KA, Z : REAL;
AT, BT, MA, MW, VP, W, AI, AJ, AC, PRESS : REAL;
I, J, K, PRES, Z1, LL, LINE : INTEGER;
RESULT : ARRAY[1..63,1..4] OF INTEGER,
HIGH : BOOLEAN;

PROCEDURE VPRESSURE(A,B,T: REAL; VAR VP :REAL);
{Calculates the vapour pressure of each component of mixture}
VAR
T7, LP : REAL;
BEGIN
T7 := 0.7*T - 273.15;
LP := A - (B/(T7 + 230));
VP := EXP(LP*2.3026)/760;
END; {VPRESSURE}

```
PROCEDURE ACENTRIC(VP,P :REAL; VAR W :REAL);  
  {Calculates the acentric factor for each component}  
  VAR  
    PR : REAL;  
  BEGIN  
    PR := VP/P;  
    W := -LN(PR)/2.3026 - 1;  
  END; {ACENTRIC}
```

```
PROCEDURE AITERM(CT,CP,K,TT :REAL; VAR AI: REAL);  
  {Determines constant (a) in Peng-Robinson Equation of State}  
  VAR  
    TR, L ,M : REAL;  
  BEGIN  
    TR := TT/CT;  
    L := SQR(1 + K*(1 - SQR(TR)));  
    M := (0.45724 * SQR(R) * SQR(CT))/CP;  
    AI := L * M;  
  END; {AITERM}
```

```
PROCEDURE PENG(VAR PRESS : REAL);
VAR
  D, T : INTEGER;
  A, B : REAL;

BEGIN
  D := 500;
  I := 1;
  WRITELN(LST);
  WRJTELN(LST, ' TEMPERATURE ', ' DENSITY ', 'PRESSURE ', 'Z ');
  WRITELN(LST);
  WHILE D <= 900 DO
    BEGIN
      T := 313;
      WHILE T <= 373 DO
        BEGIN
          MW := XI*MC + XJ*MA;
          AITERM(TC,PC,KC,T, AI);
          AC := AI;
          IF XJ > 0 THEN
            BEGIN
              AITERM(TA,PA,KA,T, AD);
              AJ := AI;
            END;
          A := XI*XI*AC + XJ*XJ*AJ;
          B := XI*0.0778*R*TC/PC;
          PRESS := (R*T/(MW/D - B)) - (A/((MW/D)*(MW/D+B) +
            B*(MW/D-B)));
          Z := PRESS*(MW/D)/(R*T);
          PRESS := INT(PRESS * 14.696);
          PRES := ROUND(PRESS);
          Z1 :=ROUND(Z*1000);
          RESULT[I,1] := D;
          RESULT[I,2] := T;
          RESULT[I,3] := PRES;
          RESULT[I,4] := Z1;
          T := T + 10;
          I := I + 1;
        END;
      D := D + 50;
    END;
  END;
```

```
K := 1;
I := 1;
LL := 4;
WHILE K <= 7 DO
  BEGIN
    I := K;
    WHILE I <= 63 DO
      BEGIN
        HIGH := FALSE;
        IF RESULT[I,3] >5500 THEN HIGH := TRUE;
        IF HIGH = FALSE THEN
          WRITELN(LST,RESULT[I,2]-273:8,
            RESULT[I,1]/1000:15:2,  RESULT[I,3]:13,
            RESULT[I,4]/1000:13:3);
        I := I + 7;
        LL := LL + 1;
        IF (LL >= 73) and (I <= 63) THEN
          BEGIN
            writeln(lst);
            WRITELN(LST);
            WRITELN(LST,'TEMPERATURE','DENSITY','PRESSURE','Z');
            WRITELN(LST);
            LL := 4;
          END;
        END;
        WRITELN(LST);
        LL := LL + 1;
        K := K + 1;
      END;
    END;
  END;
  (PENG)
```

BEGIN

{Generates a screen menu for selection of mobile phase mixtures}

ClrScr;

GOTOXY(5,10);

WRITELN('MOBILE PHASES');

WRITELN(' 1. CARBON DIOXIDE');

WRITELN(' 2. ACETONITRILE');

WRITELN(' 3. METHANOL');

WRITELN(' 4. DICHLOROMETHANE');

WRITELN(' 5. FORMIC ACID');

WRITELN(' 6. QUIT');

WRITELN;

WRITELN;

WRITELN;

WRITE('SELECT MOBILE PHASE (1-6. '); READLN(CHOICE);

WRITELN;

WRITELN;

CASE CHOICE OF

1 : BEGIN {CARBON DIOXIDE}

WRITELN(LST);

WRITELN(LST, 'SUPERCRITICAL CARBON DIOXIDE');

XJ := 0;

XI := 1 - XJ;

PENG(PRESS);

END;

2 : BEGIN {ACETONITRILE}

WRITE('ENTER MOLE FRACTION OF MODIFIER: ');

READLN(XJ);

writeln(LST);

WRITELN(LST, XJ*100:5:2, 'MOLE% ACETONITRILE IN
CARBON DIOXIDE');

II := 1; ,

XI := 1 - XJ;

TA := 547.85;

PA := 47.7;

AT := 7.12578;

BT := 1322.74;

MA := 41.06;

VPRESSURE(AT,BT,TA, VP);

ACENTRIC(VP,PA, W);

KA := 0.37464 + 1.54226*W - 0.26992*SQR(W);

PENG(PRESS);

END;

```
3: BEGIN {METHANOL}
  WRITE('ENTER MOLE FRACTION OF MODIFIER: ');
  READLN(XJ);
  WRITELN(LST, XJ*100:5:2, ' MOLE% METHANOL IN
    CARBON DIOXIDE');
  XI := 1 - XJ;
  TA := 512.6;
  PA := 78.2;
  AT := 8.23608;
  BT := 1580.6;
  MA := 32.04;
  VPRESSURE(AT,BT,TA, VP);
  ACENTRIC(VP,PA, W);
  KA := 0.37464 + 1.54226*W - 0.26992*SQR(W);
  PENG(PRESS);
END;

4: BEGIN {DICHLOROMETHANE}
  WRITE('ENTER MOLE FRACTION OF MODIFIER: ');
  READLN(XJ);
  WRITELN(LST, XJ*100:5:2, ' MOLE%
    DICHLOROMETHANE IN CARBON DIOXIDE');
  XI := 1 - XJ;
  TA := 510.2;
  PA := 60;
  AT := 6.91821;
  BT := 1090.1;
  MA := 84.93;
  VPRESSURE(AT,BT,TA, VP);
  ACENTRIC(VP,PA, W);
  KA := 0.37464 + 1.54226*W - 0.26992*SQR(W);
  PENG(PRESS);
END;

5: BEGIN {FORMIC ACID}
  WRITE ('ENTER MOLE FRACTION OF MODIFIER: ');
  READLN (XJ);
  WRITELN(LST, XJ*100:5:2, ' MOLE% FORMIC ACID IN
    CARBON DIOXIDE');
  XI := 1 - XJ;
  TA := 487.0;
  PA := 59.2;
```

```
AT := 7.15563;  
BT := 1413.9;  
MA := 60.05;  
VPRESSURE(AT,BT,TA, VP);  
ACENTRIC (VP, PA, W);  
KA := 0.37464 + 1.54226*W - 0.26992*SQR(W);  
PENG(PRESS);  
END;
```

```
6: END;      {QUIT};  
END.
```

```
END.
```

Appendix B

Retention Data for Modifiers Studies in Chapter 3.

Mobile Phase: Supercritical carbon dioxide

Compound	Temp	Density	t ₀	t _r	W _{with}
isobutyl benzene	40	0.7	1.77	2.22	0.141
isobutyl benzene	40	0.8	1.43	1.62	0.1
isobutyl benzene	40	0.9	1.04	1.14	0.064
phenyl acetic acid	40	0.7	1.77	3.28	0.303
phenyl acetic acid	40	0.8	1.43	2.01	0.186
phenyl acetic acid	40	0.9	1.04	1.27	0.096
anthraquinone	40	0.7	1.77	5.25	0.297
anthraquinone	40	0.8	1.43	2.49	0.127
anthraquinone	40	0.9	1.04	1.44	0.074
anthracene	40	0.7	1.77	6.78	0.33
anthracene	40	0.8	1.43	3.21	0.149
anthracene	40	0.9	1.04	1.81	0.084
pyrene	40	0.7	1.77	14.39	0.766
pyrene	40	0.8	1.43	5.62	0.249
pyrene	40	0.9	1.04	2.76	0.112
isobutyl benzene	50	0.6	1.48	2.16	0.162
isobutyl benzene	50	0.7	1.35	1.61	0.095
isobutyl benzene	50	0.8	1.11	1.23	0.101
isobutyl benzene	50	0.9	0.82	0.82	0.091
phenyl acetic acid	50	0.6	1.48	3.56	0.571
phenyl acetic acid	50	0.7	1.35	2	0.115
phenyl acetic acid	50	0.8	1.11	1.41	0.151
phenyl acetic acid	50	0.9	0.82	0.95	0.065
anthraquinone	50	0.6	1.48	8.48	0.502
anthraquinone	50	0.7	1.35	3.11	0.177
anthraquinone	50	0.8	1.11	1.76	0.113
anthraquinone	50	0.9	0.82	1.08	0.056
anthracene	50	0.6	1.48	9.96	0.565

Compound	Temp	Density	to	tr	Width
anthracene	50	0.7	1.35	3.89	0.201
anthracene	50	0.8	1.11	2.18	0.117
anthracene	50	0.9	0.82	1.3	0.056
pyrene	50	0.6	1.48	23.32	1.24
pyrene	50	0.7	1.35	7.42	0.365
pyrene	50	0.8	1.11	3.49	0.164
pyrene	50	0.9	0.82	1.85	0.075
isobutyl benzene	60	0.6	1.22	2.24	0.265
isobutyl benzene	60	0.7	1.1	1.27	0.103
isobutyl benzene	60	0.8	0.91	0.99	0.054
isobutyl benzene	60	0.9	0.69	0.69	0.047
phenyl acetic acid	60	0.6	1.22	2.62	0.261
phenyl acetic acid	60	0.7	1.1	1.55	0.233
phenyl acetic acid	60	0.8	0.91	1.08	0.104
phenyl acetic acid	60	0.9	0.69	0.69	0.091
anthraquinone	60	0.6	1.22	4.57	0.266
anthraquinone	60	0.7	1.1	2.18	0.131
anthraquinone	60	0.8	0.91	1.32	0.07
anthraquinone	60	0.9	0.69	0.87	0.06
anthracene	60	0.6	1.22	5.35	0.294
anthracene	60	0.7	1.1	2.64	0.139
anthracene	60	0.8	0.91	1.59	0.071
anthracene	60	0.9	0.69	1.02	0.057
pyrene	60	0.6	1.22	11.33	0.532
pyrene	60	0.7	1.1	4.61	0.22
pyrene	60	0.8	0.91	2.38	0.101
pyrene	60	0.9	0.69	1.36	0.065
isobutyl benzene	70	0.5	1.08	1.66	0.1

Compound	Temp	Density	to	tr	Width
isobutyl benzene	70	0.6	1.04	1.59	0.136
isobutyl benzene	70	0.7	0.93	1.04	0.072
isobutyl benzene	70	0.8	0.78	0.86	0.067
isobutyl benzene	70	0.9	0.58	0.58	0.049
phenyl acenc acid	70	0.5	1.08	2.62	0.48
phenyl acenc acid	70	0.6	1.04	1.79	0.165
phenyl acetic acid	70	0.7	0.93	1.18	0.115
phenyl acenc acid	70	0.8	0.78	0.86	0.09
phenyl acenc acid	70	0.9	0.58	0.58	0.051
anthraquinone	70	0.5	1.08	8.36	0.74
anthraquinone	70	0.6	1.04	3.02	0.161
anthraquinone	70	0.7	0.93	1.63	0.083
anthraquinone	70	0.8	0.78	1.06	0.07
anthraquinone	70	0.9	0.58	0.58	0.042
anthracene	70	0.5	1.08	8.36	0.74
anthracene	70	0.6	1.04	3.48	0.176
anthracene	70	0.7	0.93	1.92	0.089
anthracene	70	0.8	0.78	1.24	0.068
anthracene	70	0.9	0.58	0.81	0.078
pyrene	70	0.5	1.08	20.15	0.92
pyrene	70	0.6	1.04	6.76	0.311
pyrene	70	0.7	0.93	3.09	0.137
pyrene	70	0.8	0.78	1.73	0.08
pyrene	70	0.9	0.58	1.04	0.077
isobutyl benzene	80	0.5	0.95	1.33	0.079
isobutyl benzene	80	0.6	0.9	1.08	0.098
isobutyl benzene	80	0.7	0.81	0.81	0.089
isobutyl benzene	80	0.8	0.66	0.66	0.058
phenyl acenc acid	80	0.5	0.95	1.8	0.277
phenyl acenc acid	80	0.6	0.9	1.28	0.103

Compound	Temp	Density	to	τ	Width
phenyl acetic acid	80	0.7	0.81	0.81	0.097
phenyl acetic acid	80	0.8	0.66	0.66	0.088
anthraquinone	80	0.5	0.95	5	0.244
anthraquinone	80	0.6	0.9	2.21	0.144
anthraquinone	80	0.7	0.81	1.3	0.094
anthraquinone	80	0.8	0.66	0.89	0.08
anthracene	80	0.5	0.95	5.24	0.273
anthracene	80	0.6	0.9	2.5	0.15
anthracene	80	0.7	0.81	1.49	0.093
anthracene	80	0.8	0.66	1.01	0.083
pyrene	80	0.5	0.95	11.48	0.568
pyrene	80	0.6	0.9	4.45	0.212
pyrene	80	0.7	0.81	2.24	0.12
pyrene	80	0.8	0.66	1.32	0.084
isobutyl benzene	90	0.5	0.87	1.2	0.114
isobutyl benzene	90	0.6	0.8	0.92	0.076
isobutyl benzene	90	0.7	0.7	0.76	0.065
isobutyl benzene	90	0.8	0.58	0.58	0.054
phenyl acetic acid	90	0.5	0.87	1.56	0.252
phenyl acetic acid	90	0.6	0.8	1.01	0.063
phenyl acetic acid	90	0.7	0.7	0.76	0.065
phenyl acetic acid	90	0.8	0.58	0.58	0.054
anthraquinone	90	0.5	0.87	4.42	0.278
anthraquinone	90	0.6	0.8	1.65	0.1
anthraquinone	90	0.7	0.7	1.04	0.101
anthraquinone	90	0.8	0.58	0.73	0.058
anthracene	90	0.5	0.87	4.42	0.278
anthracene	90	0.6	0.8	1.84	0.1
anthracene	90	0.7	0.7	1.17	0.067

Compound	Temp	Density	τ_0	τ	Width
anthracene	90	0.8	0.58	0.81	0.057
pyrene	90	0.5	0.87	9.61	0.474
pyrene	90	0.6	0.8	3.03	0.135
pyrene	90	0.7	0.7	1.65	0.076
pyrene	90	0.8	0.58	1.03	0.059
isobutyl benzene	100	0.5	0.77	0.96	
isobutyl benzene	100	0.6	0.71	0.71	
isobutyl benzene	100	0.7	0.63	0.63	
phenyl acetic acid	100	0.5	0.77	1.12	
phenyl acetic acid	100	0.6	0.71	0.79	
phenyl acetic acid	100	0.7	0.63	0.63	
anthraquinone	100	0.5	0.77	2.47	0.12
anthraquinone	100	0.6	0.71	1.32	0.083
anthraquinone	100	0.7	0.63	0.88	0.067
anthracene	100	0.5	0.77	2.59	0.153
anthracene	100	0.6	0.71	1.45	0.08
anthracene	100	0.7	0.63	0.97	0.06
pyrene	100	0.5	0.77	4.87	0.22
pyrene	100	0.6	0.71	2.25	0.102
pyrene	100	0.7	0.63	1.3	0.065

Mobile phase: 0.25 mole% formic acid in supercritical carbon dioxide

Compound	Temp	Density	Height	Width	k'
isobutyl benzene	40.00	0.70	25986	0.158	0.17
anthraquinone	40.00	0.70	32141	0.242	1.48
		0.80	54884	0.118	0.67
		0.90	65226	0.076	0.34
anthracene		0.70	71706	0.251	1.96
		0.80	63132	0.125	1.00
		0.90	141500	0.078	0.60
pyrene		0.70	22943	0.411	3.64
		0.80	45222	0.188	2.37
		0.90	64746	0.094	1.38
isobutyl benzene	50.00	0.60	41106	0.263	0.29
		0.70	67977	0.193	0.13
		0.80			
anthraquinone		0.60	77543	0.719	3.20
		0.70	87914	0.230	1.12
		0.80	66724	0.148	0.51
		0.90	60696	0.075	0.20
anthracene		0.60	77543	0.719	3.57
		0.70	172897	0.327	1.46
		0.80	124864	0.165	0.77
		0.90	115669	0.076	0.48
pyrene		0.60	5140	0.451	9.17
		0.70	63769	0.513	2.61
		0.80	56726	0.243	1.74
		0.90	55122	0.093	0.4
isobutyl benzene	60.00	0.50	71989	0.216	0.09
		0.60	56549	0.220	0.22

Compound	Temp	Density	Height	Width	k'
		0.70	73801	0.181	0.10
anthraquinone		0.50	65215	1.181	7.35
		0.60	55867	0.360	2.24
		0.70	97562	0.177	0.83
		0.80	58266	0.076	0.40
		0.90	162528	0.088	0.22
anthracene		0.50	65215	1.180	7.35
		0.60	117547	0.437	2.41
		0.70	192387	0.201	1.10
		0.80	121911	0.086	0.61
		0.90	317859	0.085	0.39
pyrene		0.60	40893	0.349	5.81
		0.70	75584	0.328	1.89
		0.80	51540	0.115	0.91
		0.90	154972	0.093	0.84
isobutyl benzene	70.00	0.50	29560	0.270	0.38
		0.60	34194	0.174	0.16
		0.70	62045	0.142	0.07
anthraquinone		0.50	55442	0.790	4.94
		0.60	41359	0.252	1.55
		0.70	68315	0.149	0.64
		0.80	87819	0.104	0.31
anthracene		0.50	55442	0.786	4.93
		0.60	86451	0.302	1.80
		0.70	128511	0.159	0.86
		0.80	156368	0.103	0.48
pyrene		0.50	9118	1.380	12.48
		0.60	31077	0.530	4.21
		0.70	55090	0.225	1.89

Compound	Temp	Density	Height	Width	k'
		0.80	76716	0.121	1.02
isobutyl benzene	80.00	0.50	31273	0.211	0.28
		0.60	39627	0.141	0.12
		0.70	25986	0.158	0.16
anthraquinone		0.50	79033	0.610	3.42
		0.60	51008	0.180	1.17
		0.70	70470	0.109	0.51
		0.80	89888	0.091	0.25
anthracene		0.50	79033	0.483	3.42
		0.60	104984	0.219	1.37
		0.70	142075	0.125	0.69
		0.80	170551	0.091	0.39
pyrene		0.50	17533	0.890	8.37
		0.60	40480	0.363	3.08
		0.70	66559	0.164	1.46
		0.80	87079	0.098	0.81
isobutyl benzene	90.00	0.50	35678	0.175	0.22
		0.60	44739	0.116	0.09
anthraquinone		0.50	101970	0.343	2.49
		0.60	60284	0.136	0.91
		0.70	74064	0.090	0.41
anthracene		0.50	101970	0.343	2.49
		0.60	120442	0.165	1.07
		0.70	140927	0.104	0.55
pyrene		0.50	25690	0.619	5.80
		0.60	51099	0.260	2.31
		0.70	74434	0.125	0.85

Compound	Temp	Density	Height	Width	k'
isobutyl benzene	100.00	0.50	45937	0.177	0.17
anthraquinone		0.50	117464	0.260	1.92
		0.60	65791	0.117	0.72
		0.70	75553	0.076	0.33
anthracene		0.50	117464	0.260	1.92
		0.60	128341	0.134	0.85
		0.70	171939	0.092	0.44
pyrene		0.50	31731	0.409	4.33
		0.60	56487	0.178	1.79
		0.70	77358	0.101	0.89

Mobile phase: 1.26 mole% formic acid in supercritical carbon dioxide

Compound	Temp	Density	to	tr	Height	Width
isobutyl benzene	40	0.7	2.02	2.28	39845	0.194
		0.8	1.56	1.69	49235	0.152
phenyl acetic acid	40	0.7	2.02	2.59	23406	0.25
anthraquinone	40	0.7	2.01	4.47	45655	0.267
		0.8	1.57	2.38	75370	0.122
		0.9	1.13	1.44	92785	0.078
anthracene	40	0.7	2.01	5.63	48832	0.307
		0.8	1.57	2.97	84489	0.141
		0.9	1.13	1.76	113448	0.084
pyrene	40	0.7	2.01	10.92	28113	0.547
		0.8	1.57	4.85	58451	0.22
		0.9	1.13	2.56	84415	0.109
isobutyl benzene	50	0.6	1.99	2.4	32776	0.249
		0.7	1.7	1.86	39089	0.143
phenyl acetic acid	50	0.6	1.99	2.95	15823	0.23
		0.7	1.7	2.02	25376	0.147
anthraquinone	50	0.6	1.99	6.29	33086	0.363
		0.7	1.7	3.13	55939	0.165
		0.8	1.37	1.9	81393	0.101
		0.9	1.17	1.42	103392	0.088
anthracene	50	0.6	1.99	7.52	32612	0.418
		0.7	1.7	3.86	45722	0.19
		0.8	1.37	2.29	79086	0.111
		0.9	1.17	1.68	105083	0.084
pyrene	50	0.6	1.99	15.85	20346	0.654
		0.7	1.7	6.74	34522	0.309
		0.8	1.37	3.47	71263	0.156

Compound	Temp	Density	to	tr	Height	Width
		0.9	1.17	2.3	96783	0.102
isobutyl benzene	60	0.6	1.91	2.23	37973	0.203
phenylacetic acid	60	0.6	1.91	2.62	21305	0.207
anthraquinone	60	0.6	1.91	5.01	43888	0.313
		0.7	1.68	2.78	74278	0.152
		0.8	1.4	1.84	94260	0.106
		0.9	1	1.15	105318	0.077
anthracene	60	0.6	1.91	5.86	42513	0.358
		0.7	1.68	3.31	68124	0.169
		0.8	1.4	2.16	93180	0.112
		0.9	1	1.33	108958	0.078
pyrene	60	0.6	1.91	11.39	26376	0.581
		0.7	1.68	5.37	55978	0.257
		0.8	1.4	3.06	85795	0.14
		0.9	1	1.75	98448	0.087
isobutyl benzene	70	0.5	2.07	2.38	44798	0.204
		0.6	1.98	2.26	45118	0.186
phenylacetic acid	70	0.5	2.07	2.76	25971	0.387
		0.6	1.98	2.56	27116	0.228
anthraquinone	70	0.5	2.07	10.11	21527	0.602
		0.6	1.98	4.46	58094	0.27
		0.7	1.96	2.99	85689	0.18
		0.8	1.8	2.25	9326	0.141
anthracene	70	0.5	2.07	10.61	23978	0.58
		0.6	1.98	5.12	53917	0.322

Compound	Temp	Density	to	tr	Height	Width
		0.7	1.96	3.48	75892	0.199
		0.8	1.8	2.58	102887	0.148
pyrene	70	0.5	2.07	25.18	12058	1.311
		0.6	1.98	9.35	37984	0.529
		0.7	1.96	5.31	65907	0.276
		0.8	1.8	3.44	93626	0.168
isobutyl benzene	80	0.5	2.45	3.02	38786	0.415
		0.6	2.32	2.56	44289	0.194
phenylacetic acid	80	0.5	2.45	3.91	13437	0.343
		0.6	2.32	2.82	28719	0.226
anthraquinone	80	0.5	2.45	8.97	36317	0.549
		0.6	2.32	4.49	62370	0.28
		0.7	2.12	2.98	92292	0.183
		0.8	1.58	1.91	115036	0.119
anthracene	80	0.5	2.45	9.5	35142	0.612
		0.6	2.32	5.08	57382	0.333
		0.7	2.12	3.39	85913	0.209
		0.8	1.58	2.15	108702	0.127
pyrene	80	0.5	2.45	19.17	18497	1.131
		0.7	2.32	3.41	43374	0.524
		0.7	2.12	4.8	75365	0.263
		0.8	1.58	2.74	96223	0.137
isobutyl benzene	90	0.5	1.46	1.77	48306	0.216
		0.6	1.37	1.48	57678	0.103
phenylacetic acid	90	0.5	1.46	2.19	26116	0.213
		0.6	1.37	1.6	41389	0.14

Compound	Temp	Density	to	r	Height	Width
anthraquinone	90	0.5	1.46	4.49	50862	0.238
		0.6	1.37	2.39	86085	0.136
		0.7	1.22	1.62	107001	0.097
anthracene	90	0.5	1.46	4.74	49003	0.298
		0.6	1.37	2.66	71486	0.156
		0.7	1.22	1.81	90032	0.102
pyrene	90	0.5	1.46	8.97	32102	0.508
		0.6	1.37	4.13	65852	0.219
		0.7	1.22	2.43	95549	0.117
isobutyl benzene	100	0.5	1.41	1.64	53529	0.163
phenylacetic acid	100	0.5	1.41	1.94	30991	0.21
anthraquinone	100	0.5	1.41	3.63	63083	0.187
		0.6	1.32	2.18	101259	0.122
		0.7	1.24	1.57	112183	0.087
anthracene	100	0.5	1.41	3.82	60613	0.241
		0.6	1.32	2.33	84186	0.136
		0.7	1.24	1.73	90920	0.096
pyrene	100	0.5	1.41	6.76	41027	0.398
		0.6	1.32	3.41	66855	0.176
		0.7	1.24	2.22	100892	0.108

Mobile phase: 0.87 mole% dichloromethane/0.16 mole% formic acid in CO₂

Compound	Temp	Density	to	tr	Height	Width
isobutyl benzene	40	0.8	1.95	2.08	51736	0.254
anthraquinone	40	0.8	1.95	2.93	79347	0.158
anthraquinone	40	0.9	1.34	1.69	100498	0.101
anthracene	40	0.8	1.95	3.54	38938	0.182
anthracene	40	0.9	1.34	2.01	36846	0.138
pyrene	40	0.8	1.95	5.64	58006	0.279
pyrene	40	0.9	1.34	2.84	78855	0.124
isobutyl benzene	50	0.7	2.34	2.55	45958	0.165
	50	0.8	1.85	1.96	64869	0.18
phenyl acetic acid	50	0.7	2.34	2.74	33073	0.195
anthraquinone	50	0.7	2.34	4.08	67915	0.244
anthraquinone	50	0.8	1.85	2.54	94471	0.137
anthraquinone	50	0.9	1.33	1.62	100835	0.089
anthracene	50	0.7	2.34	4.85	22582	0.27
anthracene	50	0.8	1.85	2.99	33761	0.145
anthracene	50	0.9	1.33	1.88	25432	0.086
pyrene	50	0.7	2.34	3.03	45370	0.415
pyrene	50	0.8	1.85	4.37	70234	0.215
pyrene	50	0.9	1.33	2.51	97954	0.11
isobutyl benzene	60	0.6	2.25	2.69	33643	0.256
	60	0.7	2.01	2.18	49039	0.145
phenylacetic acid	60	0.6	2.25	3.26	13312	0.199
	60	0.7	2.01	2.35	33524	0.189
anthraquinone	60	0.6	2.25	5.46	36163	0.443

Compound	Temp	Density	to	π	Height	Width
anthraquinone	60	0.7	2.01	3.48	76749	0.249
anthraquinone	60	0.8	1.6	2.24	94902	0.146
anthraquinone	60	0.9	1.12	1.35	106770	0.087
anthracene	60	0.6	2.25	6.46	36163	0.443
anthracene	60	0.7	2.01	3.96	23326	0.323
anthracene	60	0.8	1.6	2.55	23713	0.18
anthracene	60	0.9	1.12	1.54	31435	0.115
pyrene	60	0.6	2.25	13.55	26234	0.805
pyrene	60	0.7	2.01	6.39	54682	0.342
pyrene	60	0.8	1.6	3.68	78689	0.174
pyrene	60	0.9	1.12	2	104092	0.092
isobutyl benzene	70	0.6	1.89	2.16	46512	0.197
phenylacetic acid	70	0.5	1.89	2.55	26275	0.253
anthraquinone	70	0.6	1.89	4.84	47101	0.362
anthraquinone	70	0.7	1.64	2.69	86306	0.185
anthraquinone	70	0.8	1.34	1.75	107871	0.109
anthracene	70	0.6	1.89	4.84	47101	0.362
anthracene	70	0.7	1.64	3.02	25000	0.23
anthracene	70	0.8	1.34	1.96	27226	0.169
pyrene	70	0.6	1.89	9.82	33619	0.538
pyrene	70	0.7	1.64	4.7	64638	0.242
pyrene	70	0.8	1.34	2.68	90412	0.129
isobutyl benzene	80	0.5	1.7	2.18	36812	0.213
	80	0.6	1.61	1.8	51273	0.153
phenylacetic acid	80	0.5	1.7	3.04	11948	0.187
	80	0.6	1.61	2.05	27840	0.189

Compound	Temp	Density	to	tr	Height	Width
anthraquinone	80	0.5	1.7	7.62	34317	0.55
anthraquinone	80	0.6	1.61	3.53	60320	0.266
anthraquinone	80	0.7	1.41	2.11	95311	0.116
anthraquinone	80	0.8	1.15	1.42	105509	0.088
anthracene	80	0.5	1.7	7.62	34317	0.55
anthracene	80	0.6	1.61	3.53	60320	0.266
anthracene	80	0.7	1.41	2.33	23235	0.155
anthracene	80	0.8	1.15	1.58	33120	0.107
pyrene	80	0.5	1.7	16.17	18312	0.957
pyrene	80	0.6	1.61	6.57	44850	0.365
pyrene	80	0.7	1.41	3.39	76360	0.167
pyrene	80	0.8	1.15	2.03	97771	0.094
isobutyl benzene	90	0.5	1.46	1.77	48306	0.216
	90	0.6	1.37	1.48	57678	0.103
phenylacetic acid	90	0.5	1.46	2.19	26116	0.213
	90	0.6	1.37	1.6	41389	0.14
anthraquinone	90	0.5	1.46	4.49	50862	0.238
anthraquinone	90	0.6	1.37	2.39	86085	0.136
anthraquinone	90	0.7	1.22	1.62	107001	0.097
anthracene	90	0.5	1.46	4.74	49003	0.298
anthracene	90	0.6	1.37	2.66	71486	0.156
anthracene	90	0.7	1.22	1.81	90032	0.102
pyrene	90	0.5	1.46	8.97	32102	0.508
pyrene	90	0.6	1.37	4.13	65852	0.219
pyrene	90	0.7	1.22	2.43	95549	0.117
isobutyl benzene	100	0.5	1.41	1.64	53529	0.163

Compound	Temp	Density	to	tr	Height	Width
phenylacetic acid	100	0.5	1.41	1.94	30991	0.21
anthraquinone	100	0.5	1.41	3.63	63083	0.187
anthraquinone	100	0.6	1.32	2.18	101259	0.122
anthraquinone	100	0.7	1.24	1.57	112183	0.087
anthracene	100	0.5	1.41	3.82	60613	0.241
anthracene	100	0.6	1.32	2.33	84186	0.136
anthracene	100	0.7	1.24	1.73	90920	0.096
pyrene	100	0.5	1.41	6.76	41027	0.398
pyrene	100	0.6	1.32	3.41	66855	0.176
pyrene	100	0.7	1.24	2.22	100892	0.108

Mobile phase: 0.80 mole% acetonitrile in supercritical carbon dioxide

Compound	Temp	Density	t ₀	t _r	area	width
anthraquinone	40	0.7	1.07	1.87	669037	0.149
anthraquinone	40	0.8	0.78	1.06	479302	0.095
anthraquinone	40	0.9	0.57	0.69	272017	0.073
anthracene	40	0.7	1.07	2.41	1188200	0.166
anthracene	40	0.8	0.78	1.32	846582	0.101
anthracene	40	0.9	0.57	0.84	443513	0.074
pyrene	40	0.7	1.07	4.3	279880	0.267
pyrene	40	0.8	0.78	2.07	194875	0.126
pyrene	40	0.9	0.57	1.18	101927	0.078
anthraquinone	50	0.7	0.81	1.29	391815	0.098
anthraquinone	50	0.8	0.65	0.91	465720	0.102
anthraquinone	50	0.9	0.51	0.61		0.051
anthracene	50	0.7	0.81	1.6	927440	0.099
anthracene	50	0.8	0.65	1.13	870340	0.101
anthracene	50	0.9	0.51	0.74		0.052
pyrene	50	0.7	0.81	2.65	266440	0.144
pyrene	50	0.8	0.65	1.79	167772	0.12
pyrene	50	0.9	0.51	1.03		0.074
anthraquinone	60	0.7	0.65	1.17	481395	0.091
anthraquinone	60	0.8	0.53	0.73	251675	0.054
anthracene	60	0.7	0.65	1.42	341662	0.096
anthracene	60	0.8	0.53	0.87	439495	0.057
pyrene	60	0.7	0.65	2.45	208623	0.152
pyrene	60	0.8	0.53	1.28	96116	0.062
anthraquinone	70	0.6	0.64	1.72	549153	0.133

Compound	Temp	Density	to	tr	area	width
anthraquinone	70	0.7	0.56	0.91	429330	0.07
anthracene	70	0.6	0.64	1.97	888710	0.14
anthracene	70	0.7	0.56	1.08	695120	0.073
pyrene	70	0.6	0.64	3.79	215930	0.24
pyrene	70	0.7	0.56	1.72	161945	0.097
anthraquinone	80	0.6	0.58	1.26	503992	0.099
anthraquinone	80	0.7	0.5	0.75		0.056
anthracene	80	0.6	0.58	1.43	894920	0.102
anthracene	80	0.7	0.5	0.86		0.058
pyrene	80	0.6	0.58	2.53	209728	0.155
pyrene	80	0.7	0.5	1.28		0.068
anthraquinone	90	0.6	0.51	0.99	433242	0.075
anthracene	90	0.6	0.51	1.11	730315	0.075
pyrene	90	0.6	0.51	1.82	169427	0.097
anthraquinone	100	0.6	0.47	0.81		0.069
anthracene	100	0.6	0.47	0.89		0.07
pyrene	100	0.6	0.47	1.38		0.082